



**Investigation of (super)hydrophilic coatings for marine
antifouling applications**

Jan Henryk Kardela

A thesis submitted to Newcastle University in candidature for the
Degree of Doctor of Philosophy

School of Natural and Environmental Sciences

September 2019

Abstract

The undesirable colonization of artificial structures at sea, termed marine biofouling, has significant economic and environmental impacts.

The marine antifouling (AF) market is currently dominated by biocidal coatings that release toxic heavy metals or organic biocides, limiting the attachment and growth of fouling organisms. The central aim of this thesis was to explore the potential of environmentally inert, (super)hydrophilic surfaces as next-generation AF coatings. In contrast to previous research in this area, the coatings presented here were prepared as industrially relevant copolymers and tested in the laboratory against two major fouling species; cypris larvae of the barnacle *Balanus improvisus* and cells of the diatom *Navicula incerta*, as well as a multispecies biofilm and field testing in temperate and tropical locations.

The laboratory assays revealed that, in general, barnacles settled in lower numbers on bulk polymers containing ionic functionalities. The surfaces containing zwitterionic sulfobetaine methacrylate (SBMA) and anionic 3-sulfopropyl methacrylate (SPMA) were found to not only inhibit cyprid settlement but also promote high removal of juvenile barnacles, diatom cells and biofilm. The exceptional AF and fouling-release performance of these two chemistries was explained by the large degree of swelling when hydrated and presence of nonfreezable water at the interface. The surfaces presented showed limited AF efficacy when subjected to the real-world marine environment. Using behavioural analysis and imaging surface plasmon resonance (iSPR) experiments, it was shown that barnacle cyprids explored all surfaces. However, in the case of SBMA, the exploratory events were very short and the amount of retained temporary adhesive was low.

In conclusion, this work demonstrates the potential of bulk hydrophilic copolymers as a starting point for the development of next-generation, green AF coatings. It is hoped that the findings of this work will encourage greater industrial participation in the development of fouling-control technologies that function via non-biocidal means.

Acknowledgments

This dissertation would not have been possible without the guidance and the help of a number of people who in one way or another contributed and extended their valuable assistance in the preparation and completion of this study.

I would like to thank Prof. Tony Clare for creating an opportunity for me to join the Marine Biofouling Research Laboratory group, for his supervision and guidance during the preparation and completion of the project. I owe a great debt of gratitude to my second supervisor, Dr Nick Aldred, for his sustained interest, tremendous support, creative suggestions and constructive criticism throughout the entire course of this work.

My thanks go to my industrial supervisors from International Paint (IP): Dr Ian Millichamp, Dr James Ferguson, Dr Alison Parry and Dr Kevin Reynolds for their support, guidance and understanding during my work at the IP laboratory. I would like to also thank Sam Allen-Marley, Jindra Purmová and John Sellers from IP / AkzoNobel for their help with SEC and GC-MS measurements.

I am very grateful to Prof. David Fulton from School of Chemistry for his support, for inviting me to work in the Chemical Nanoscience Laboratory. I have been fortunate to work with Dr Luke Dixon, who helped me enormously with the preparation of polymer brushes and taught me the RAFT polymerization technique. I would like to also thank other colleagues from the Chemical Nanoscience Laboratory for their help and advice: Dr Gema Dura, Dr Osama El-Zubir, Dr Milene Dalmina and Patrick Higgs.

I am truly grateful to Prof. Thomas Ederth from Linköping University for supplying me with gold substrates, for hosting me for a month at the Department of Physics, Chemistry and Biology (IFM). During my stay at IFM, I was able to carry out iSPR experiments and characterize the prepared polymer brushes in an exceptionally hospitable and inspirational academic environment. I would like to thank COST Action CA15216 for the financial support during my stay at IFM.

I am also grateful to Dr John Finlay for his friendship, help and inspiring talks.

I would like to thank my parents, to whom I dedicate this work, for their outstanding support. Special thanks to all my family and friends who supported me during this PhD journey.

Finally, this research would not have been possible without the financial support from AkzoNobel, Marine and Protective Coatings (International Paint).

Table of contents

Chapter 1. Biofouling and different antifouling strategies	1
1.1 Introduction	1
1.2 A brief history of the marine antifouling technologies	3
1.3 Biocidal antifouling paints	4
1.3.1 Insoluble matrix (contact leaching).....	5
1.3.2 Soluble matrix or controlled depletion paints (CPDs)	5
1.3.3 Self-polishing copolymer paints (SPCs)	5
1.4 Fouling-release coatings (FRCs)	6
1.5 Novel non-fouling technologies	7
1.5.1 Design principles of (super)hydrophilic surfaces	7
1.5.2 Poly(ethylene glycol) (PEG) as source of hydrophilicity	8
1.5.3 Zwitterions – an ultra-low fouling alternative to PEG.....	9
1.5.4 Other sources of hydrophilicity.....	11
1.5.5 Amphiphilic surfaces	12
1.6 Examples of marine fouling organisms used in AF laboratory testing	14
1.6.1 Barnacles	14
1.6.2 Diatoms	15
1.7 Scope of the thesis and research question	16
Chapter 2. Nonfreezable water and polymer swelling control the marine antifouling performance of polymers with limited hydrophilic content	18
2.1 Introduction	18
2.2 Experimental section	19
2.2.1 Materials.....	19
2.2.2 Preparation of bulk polymers	19
2.2.3 Polymer characterization.....	21
2.2.4 Underwater contact angle measurements and surface energy calculations	22
2.2.5 Determination of Equilibrium Water Content (EWC).....	23
2.2.6 Determination of forms of water present in the swollen polymers	23
2.2.7 Barnacle culturing	24
2.2.8 Settlement assay using cypris larvae of <i>B. improvisus</i>	24
2.2.9 Attachment strength of juvenile barnacles	25
2.2.10 Removal of diatom cells	25

2.2.11	Biofilm growth and release testing	26
2.3	Results	26
2.3.1	Sample preparation and characterization	26
2.3.2	Wettability of polymers	27
2.3.3	Determination of swelling and water states in experimental polymers	28
2.3.4	Settlement and removal of barnacle cyprids	30
2.3.5	Attachment strength of the diatom, <i>N. incerta</i> , and a multispecies biofilm	32
2.4	Discussion	33
Chapter 3. Analysis of the settlement behaviour of barnacle cyprids, <i>Balanus improvisus</i> , on different hydrophilic polymer brushes.....		39
3.1	Introduction	39
3.2	Materials and methods.....	41
3.2.1	Materials.....	41
3.2.2	Preparation of polymer brushes on glass substrates using grafting-from approach (SI-RAFT)	41
3.2.3	Direct grafting of polymers to gold using a grafting-to approach	43
3.2.4	Preparation of polymer brushes on gold substrates using SI-RAFT from a chemisorbed CPAD SAM.....	44
3.2.5	Preparation of polymer brushes on gold substrates using SI-RAFT from a stabilized gold surface.....	45
3.2.6	Characterization of polymer brush solutions	47
3.2.7	Characterization of polymer brushes attached to glass and gold	48
3.2.8	Underwater contact angle measurements and surface energy calculations of polymer brushes on glass	48
3.2.9	Culturing of barnacles	48
3.2.10	Settlement assay using cypris larvae of <i>B. improvisus</i>	49
3.2.11	Tracking experiments.....	49
3.2.12	Imaging surface plasmon resonance (iSPR)	50
3.3	Results	51
3.3.1	Sample preparation and characterization	51
3.3.2	Grafting of polymer Z-L to gold using two experimental SI-RAFT methods.....	55
3.3.3	Wettability of polymer brushes.....	57
3.3.4	Settlement of barnacles	58
3.3.5	Tracking experiments: analysis of cyprid behaviour on various surfaces	59
3.3.6	Visualization of deposition of barnacle footprints in-situ using iSPR.....	61
3.4	Discussion	64

Chapter 4. Development of hybrid coating incorporating both fouling-resistant and fouling-release properties.....	69
4.1 Introduction	69
4.2 Materials and methods.....	70
4.2.1 Materials.....	70
4.2.2 Synthesis of copolymer Z-GL (pBMA- <i>co</i> -SBMA- <i>co</i> -GMA)	71
4.2.3 Grafting of copolymer Z-GL to PDMS substrate	71
4.2.4 Characterization of Z-GL copolymer in the solution and grafted to PDMS.....	72
4.2.5 Wettability measurements.....	73
4.2.6 Attachment and removal of <i>N. incerta</i> diatom cells	73
4.2.7 Settlement and removal of <i>U. linza</i> zoospores.....	73
4.3 Results and discussion.....	74
4.3.1 Synthesis and chemical characterization of copolymer Z-GL and grafting it to the PDMS	74
4.3.2 Wettability.....	76
4.3.3 Attachment and removal of diatom cells and zoospores.....	77
Chapter 5. Long-term stability of selected bulk polymer coatings	81
5.1 Introduction	81
5.2 Materials and methods.....	84
5.2.1 Preparation and storage of panels used in the laboratory-based assays	84
5.2.2 Polymer characterization after long-term storage in water	84
5.2.3 Wettability measurements	85
5.2.4 Determination of swelling and water states	85
5.2.5 Settlement assays using cypris larvae	85
5.2.6 Attachment strength of juvenile barnacles.....	85
5.2.7 Removal of diatom cells	85
5.2.8 Field testing.....	85
5.3 Results and Discussion.....	86
5.3.1 Chemical stability of polymers after immersion in DIW and ASW	86
5.3.2 Wettability.....	94
5.3.3 Determination of swelling and water states in aged polymer samples	97
Chapter 6. Discussion	111
6.1 General discussion and conclusions	111

6.1.1	Production of industrially relevant bulk hydrophilic coatings for marine antifouling applications	111
6.1.2	Determination of the mechanism of action of hydrophilic coatings against barnacle larvae	112
6.1.3	Incorporation of zwitterionic moiety into silicone elastomer for improved fouling resistance.....	112
6.1.4	Long-term stability of selected bulk polymer coatings.....	113
6.2	Future research and recommendations	113
Appendix A. Preparation of bulk polymers		117
Appendix B. Bulk polymer composition determination by ^1H NMR.....		122
Appendix C. SEC traces of bulk polymers		136
Appendix D. Surface energy derivations for underwater contact angle measurements		139
Appendix E. Single settlement experiment using barnacle cypris larvae and comparison with meta-analysis approach		142
Appendix F. Biofilm growth and removal data		144
Appendix G. Preparation and characterization of polymer brushes		145
Appendix H. Polymer brush solution composition determination by ^1H NMR		147
Appendix I. SEC traces of polymer brush solutions		153
Appendix J. Comparison of settlement of barnacle cypris larvae on bulk polymers and polymer brushes		158
Appendix K. Long-term tracking experiments		158
References.....		164

List of Tables

Table 2.1 Chemical structures of prepared bulk polymers together with their abbreviations used in the text.....	20
Table 2.2 Amounts of materials used in grams in polymer preparation together with final coating concentrations and dry coating thicknesses.	21
Table 2.3 Copolymer compositions and characteristic data for prepared polymers.	27
Table 2.4 Initial underwater measured angles within the air bubble (θ_m) and silicone oil (ϕ_m) and calculated surface energies of hydrated polymers together with results after six weeks of leaching in deionized water. Errors are 95% CIs.	28
Table 3.1 Characteristic data of polymer brush solutions remaining after grafting-from reactions on glass.....	52
Table 3.2 Characteristic data of polymer brushes attached to glass using grafting-from method. ...	53
Table 3.3 Thicknesses of polymers grafted-to gold as measured by ellipsometry.....	55
Table 3.4 Characteristic data of polymer Z-L prepared on gold using various grafting-from methods with different [M]:[CPAD]:[I] ratios; ^a Thickness determined by ellipsometry; ^b Conversion determined after 18 h; ^c Number average molecular weight (M_n) determined by end-group analysis with ¹ H NMR.	57
Table 3.5 Initial underwater contact angles measured inside the air bubble (θ_m) and silicone oil (ϕ_m) and calculated surface energies of hydrated polymer brushes together with results after six weeks of leaching in deionized water. Errors are 95% CIs.....	58
Table 4.1 Copolymer composition and characteristic data for polymer Z-GL.	74
Table 4.2 Measured contact angles of sessile droplets of DIW and CH ₂ I ₂ in air and corresponding surface energies determined using the Owens-Wendt method.	77
Table 5.1 Initial copolymer compositions and after six months of storage in DIW and ASW as determined by ¹ H NMR experiments.....	87
Table 5.2 Underwater contact angles within the air bubble (θ_m) and silicone oil droplet (ϕ_m) and calculated surface energies of coatings before and after storage in DIW for six weeks and six months. Crossed out values do not have a physical meaning and should be ignored. Errors are 95% CIs.....	96

List of Figures

Figure 1.1 Schematic representation of a successional marine fouling processes (Lejars <i>et al.</i> , 2012).	1
Figure 1.2 Comparison of succession and dynamic model (Rittschof, 2010).	2
Figure 1.3 Schematic illustration of mechanisms of action of biocidal antifouling paint in seawater, (A) insoluble matrix paint, (B) soluble matrix paint, (C) self-polishing copolymer paint (Lejars <i>et al.</i> , 2012).	6
Figure 1.4 Schematic structure of amphiphilic coating comprising of hyperbranched fluoropolymer (HPFP) and PEG (Gudipati <i>et al.</i> , 2005).	12
Figure 1.5 Life cycle of a typical thoracican barnacle (Khandeparker and Anil, 2007).	15
Figure 2.1 DSC thermograms at the heating rate of 10 °C·min ⁻¹ for copolymers of n-BMA with different hydrophilic functionalities.	29
Figure 2.2 (A) EWC (%) in swollen polymers after six-week immersion in deionized water. (B) Mass ratio of freezable water to the mass of polymer ($W_{\text{freezable}}$). (C) Mass ratio of nonfreezable to the mass of polymer ($W_{\text{nonfreezable}}$). (D) Number of nonfreezable water molecules (N_w) per repeating copolymer unit. Error bars are 95% CIs.	29
Figure 2.3 Forest plot of barnacle <i>B. improvisus</i> combined settlement with polymer H-0 selected as a control treatment. Individual points show summary effect sizes (raw mean differences) and 95% CIs. Vertical dotted line indicates effect size of zero and similar performance to polymer H-0. The effect sizes for the nonionic/ionic polymers together with corresponding statistics were generated using separate subgroup analysis.	31
Figure 2.4 Mean removal of four-day-old juvenile barnacles, <i>B. improvisus</i> , together with corresponding 95% CIs. Each point represents the mean from four replicate slides. Letters indicate Tukey's pairwise comparisons and bars that do not share a letter are significantly different.	32
Figure 2.5 (A) Percent removal of <i>N. incerta</i> cells. Each point represents the mean from 90 counts on three replicate slides. Error bars are 95% CIs from arcsine transformed data. (B) Percentage removal of biomass. Each point represents the mean from three replicate slides. Error bars represent SEs of the mean. Letters indicate Tukey's pairwise comparisons and points that do not share a letter are significantly different.	33
Figure 3.1 Schematic illustration of preparation of polymer brushes on glass using grafting-from approach. The inset table presents the monomers used in the synthesis of specific polymers.	43
Figure 3.2 Schematic illustration of preparation of polymer brushes on gold using a grafting-to approach.	44
Figure 3.3 Schematic illustration of preparation of polymer brushes on gold using grafting-from approach using chemisorbed CPAD.	45
Figure 3.4 Schematic illustration of preparation of polymer brushes on gold using grafting-from approach from stabilized gold surface.	47
Figure 3.5 Cartoon image showing the iSPR experimental setup. Cyprids are showed touching the surface with their antennules and leaving the footprints behind (Andersson <i>et al.</i> , 2009).	51
Figure 3.6 XPS survey spectra of polymer brushes attached to glass using grafting-from method.	53
Figure 3.7 XPS C 1S core level spectra of polymer brushes attached to glass using grafting-from method.	54

Figure 3.8 Infrared reflection-absorption spectra of polymers attached to gold using grafting-to approach.	55
Figure 3.9 Infrared reflection-absorption spectra of polymers attached to gold using two different grafting-from methods.	56
Figure 3.10 Mean percent settlement of three-day old cyprids of <i>B. improvisus</i> on polymer brushes after 24 h, together with corresponding 95% CIs. Letters represent Tukey's pairwise comparisons and bars that do not share a letter are significantly different.	58
Figure 3.11 Data collected from short-term tracking experiments. Bars represent means from three replicate experiments and error bars are standard error of the mean. (A) Total nodes (one-way ANOVA $F_{4,10} = 0.37$, $p = 0.822$), Total movement (one-way ANOVA $F_{4,10} = 1.433$, $p = 0.293$); (B) Movements per node (one-way ANOVA $F_{4,10} = 1.642$, $p = 0.239$); (C) Number of steps (Kruskal-Wallis $H = 3.5$, $df = 4$, $p = 0.477$); (D) Total walking period (Kruskal-Wallis $H = 5.58$, $df = 4$, $p = 0.233$); (E) Number of walking periods (Kruskal-Wallis $H = 6.51$, $df = 4$, $p = 0.164$); (F) Steps per minute (Kruskal-Wallis $H = 10.82$, $df = 4$, $p = 0.029$). Letters represent Dunn's pairwise comparisons and bars that do not share a letter are significantly different.	60
Figure 3.12 (A) Mean number of touchdowns and deposited footprints on each tested surface. Bars that do not share a letter are significantly different. (B) Likelihood of footprint deposition calculated as a ratio of touchdowns events and persistent footprints. Error bars represent standard error of the mean.	62
Figure 3.13 The illustrative SPR wavelength maps (2D and 3D) generated for polymer H-0. Yellow colored areas depict shifts in SPR wavelength due to deposition of footprints.	62
Figure 3.14 (A) Image of actual deposited footprint. (B) the reflectivity curves showing shift in SPR wavelength. The curves were acquired before (blue line) and after (red line) the experiment.	63
Figure 3.15 SPR wavelength shifts generated by the deposited footprints together with their corresponding standard errors of the mean. Bars that do not share a letter are significantly different.	63
Figure 4.1 Schematic illustration of the grafting procedure of the Z-GL copolymer to PDMS substrate.	72
Figure 4.2 ^1H NMR spectrum of Z-GL copolymer (pBMA- <i>co</i> -SBMA- <i>co</i> -GMA) in CdCl_3	75
Figure 4.3 ATR-IR spectrum of virgin PDMS (red line) and PDMS with grafted polymer Z-GL (green line).	76
Figure 4.4 (A) Density of <i>N. incerta</i> cells. Pre-flow counts are the number of cells before exposure to 31 Pa wall shear stress in the calibrated water channel. Post-flow counts are the number of diatom cells remaining after exposure to flow. Each point represents the mean from 90 counts on three replicate slides. Error bars are 95% CIs. Letters/symbols indicate Tukey's corresponding pairwise comparisons between surfaces before and after flow, and points that do not share a letter/symbol are significantly different. (B) Same data presented as percentage removal. Error bars are 95% CIs from arc-sine transformed data. Letters/symbols indicate Tukey's corresponding pairwise comparisons, and points that do not share a letter/symbol are significantly different.	79
Figure 4.5 (A) Density of <i>U. linza</i> spores. Pre-flow counts are the number of spores before exposure to 52 Pa wall shear stress in the calibrated water channel. Post-flow counts are the number of spores remaining after exposure to flow. Each point represents the mean from 90 counts on three replicate slides. Error bars are 95% CIs. Letters/symbols indicate Tukey's corresponding pairwise comparisons between surfaces before and after flow, and points that do not share a letter/symbol are significantly different. (B) Same data presented as percentage removal of spores. Error bars are 95% CIs from arc-	

sine transformed data. Letters/symbols indicate Tukey's corresponding pairwise comparisons, and points that do not share a letter/symbol are significantly different.	79
Figure 5.1 Schematic illustration of surface and bulk erosion in polymers.	82
Figure 5.2 Diagram of processes involved in hydrolytic degradation of bulk eroding polymers (Farrar, 2008).	82
Figure 5.3 ^1H NMR spectrum of H-0 homopolymer (pBMA) in CdCl_3 . (A) initial (B) after six months in DIW (C) after six months in ASW.	88
Figure 5.4 ^1H NMR spectrum of E-L copolymer (pBMA- <i>co</i> -IBoMA- <i>co</i> -mPEG350MA) in CdCl_3 . (A) initial (B) after six months in DIW (C) after six months in ASW.	89
Figure 5.5 ^1H NMR spectrum of Z-L20 copolymer (pBMA- <i>co</i> -SBMA _{20mol%}) in CdCl_3 . (A) initial (B) after six months in DIW (C) after six months in ASW.	90
Figure 5.6 ^1H NMR spectrum of A-L copolymer (pBMA- <i>co</i> -SPMA) in CdCl_3 . (A) initial (B) after six months in DIW (C) after six months in ASW.	91
Figure 5.7 The GC-MS spectra of polymer leachates after six months of storage in DIW.	92
Figure 5.8 ATR-IR spectrum of polymer H-0 (pBMA) before (red line) and after (green line) immersion in DIW for six months.	93
Figure 5.9 ATR-IR spectrum of polymer E-L (pBMA- <i>co</i> -IBoMA- <i>co</i> -mPEG350MA) before (red line) and after (green line) immersion in DIW for six months.	93
Figure 5.10 ATR-IR spectrum of polymer Z-L20 (pBMA- <i>co</i> -SBMA _{20mol%}) before (red line) and after (green line) immersion in DIW for six months.	94
Figure 5.11 ATR-IR spectrum of polymer A-L (pBMA- <i>co</i> -SPMA) before (red line) and after (green line) immersion in DIW for six months.	94
Figure 5.12 Changes in total surface energy (SFE) of polymers together with corresponding polar and dispersive contributions after storage in DIW. Errors bars are 95% CIs.	97
Figure 5.13 Changes in interfacial energy polymer/water (IFE) after storage in DIW. Errors bars are 95% CIs.	97
Figure 5.14 Equilibrium water content (EWC) of polymers stored for six weeks in DIW and six months in DIW and ASW. Error bars are 95% CIs.	98
Figure 5.15 DSC heating thermograms of samples stored for six months in DIW (A) and ASW (B) at the heating rate of $10\text{ }^\circ\text{C}\cdot\text{min}^{-1}$	99
Figure 5.16 Mass ratio of freezable water to the mass of polymer ($W_{\text{freezable}}$) after six weeks and six months of storage in DIW and ASW. Error bars are 95% CIs.	99
Figure 5.17 Mass ratio of nonfreezable water to the mass of polymer ($W_{\text{nonfreezable}}$) after six weeks and six months of storage in DIW and ASW. Error bars are 95% CIs.	100
Figure 5.18 Number of nonfreezable water molecules (N_w) per repeating copolymer unit after six weeks and six months of storage in DIW and ASW. Error bars are 95% CIs.	100
Figure 5.19 Mean percent settlement of cyprids of <i>B. improvisus</i> (A) initial (B) after six months of storage in DIW. Error bars are 95% CIs. Letters represent Tukey's pairwise comparisons and bars that do not share a letter are significantly different.	101
Figure 5.20 Removal results of four-day-old juveniles barnacles, <i>B. improvisus</i> . (A) Initial using the water channel; (B) After six months of storage in DIW using the water jet. Error bars are 95% CIs. Letters represent Tukey's pairwise comparisons and bars that do not share a letter are significantly different.	102

Figure 5.21 Percent removal of <i>N. incerta</i> cells (A) initially, and (B) after six months of storage in DIW. Each point represents the mean from 90 counts on three replicate slides. Error bars are 95% CIs from arc-sine transformed data. Letters represent Tukey's pairwise comparisons and bars that do not share a letter are significantly different.	103
Figure 5.22 Layout of the panels deployed in Hartlepool and Changi.	103
Figure 5.23 Image of the panel deployed at Hartlepool Marina after immersion for two months.	105
Figure 5.24 Percentage coverage of total biofouling divided into four categories after immersion for two months in Hartlepool Marina. Error bars represent SEs of the total sample biofouling from three replicates. Bars that do not share a letter are significantly different.	105
Figure 5.25 Image of the panel deployed at Hartlepool Marina after immersion for four months.	106
Figure 5.26 Percentage coverage of total biofouling divided into four categories after immersion for four months in Hartlepool Marina. Error bars represent SEs of the total sample biofouling from three replicates.	106
Figure 5.27 Image of the panel deployed at Changi after immersion for two weeks.	108
Figure 5.28 Percentage coverage of total biofouling divided into four categories after immersion for two weeks in Changi. Error bars represent SEs of the total sample biofouling from three replicates. Points that do not share a letter are significantly different.	108
Figure 5.29 Image of the panel deployed at Changi after immersion for two months.	109
Figure 5.30 Percentage coverage of total biofouling divided into four categories after immersion for two months in Changi. Error bars represent SEs of the total sample biofouling from three replicates.	109
Figure A.1 Schematic representation of preparation of hydrophilic bulk copolymers using the dual-feed technique.	121
Figure B.1 ¹ H NMR spectrum of bulk H-0 homopolymer (pBMA) in CdCl ₃	125
Figure B.2 ¹ H NMR spectrum of bulk E-L copolymer (pBMA- <i>co</i> -IBoMA- <i>co</i> -mPEG350MA) in CdCl ₃	126
Figure B.3 ¹ H NMR spectrum of bulk H-L copolymer (pBMA- <i>co</i> -HEMA) in CdCl ₃	127
Figure B.4 ¹ H NMR spectrum of bulk G-L copolymer (pBMA- <i>co</i> -DHPMA) in CdCl ₃	128
Figure B.5 ¹ H NMR spectrum of bulk M-L copolymer (pBMA- <i>co</i> -MAA) in CdCl ₃	129
Figure B.6 ¹ H NMR spectrum of bulk Z-L copolymer (pBMA- <i>co</i> -SBMA _{10mol%}) in CdCl ₃	130
Figure B.7 ¹ H NMR spectrum of bulk Z-L20 copolymer (pBMA- <i>co</i> -SBMA _{20mol%}) in CdCl ₃	131
Figure B.8 ¹ H NMR spectrum of bulk A-L copolymer (pBMA- <i>co</i> -SPMA) in CdCl ₃	132
Figure B.9 ¹ H NMR spectrum of bulk C-L copolymer (pBMA- <i>co</i> -METAC) in CdCl ₃	133
Figure B.10 ¹ H NMR spectrum of bulk P-L10 copolymer (pBMA- <i>co</i> -SPMA _{5mol%} - <i>co</i> -METAC _{5mol%}) in CdCl ₃	134
Figure B.11 ¹ H NMR spectrum of bulk P-L20 copolymer (pBMA- <i>co</i> -SPMA _{10mol%} - <i>co</i> -METAC _{10mol%}) in CdCl ₃	135
Figure C.1 SEC traces of bulk polymers H-0, H-L, G-L, M-L. Refractive index (mV) vs Retention volume (mL).	136
Figure C.2 SEC traces of bulk polymers G-L, H-0, H-L, M-L. Light scattering (mV) vs Retention volume (mL).	136

Figure C.3 SEC traces of bulk polymers Z-L, Z-L20, A-L, C-L, P-L20. Refractive index (mV) vs Retention volume (mL).	137
Figure C.4 SEC traces of bulk polymers Z-L, Z-L20, A-L, C-L, P-L20. Light scattering (mV) vs Retention volume (mL).	137
Figure C.5 SEC traces of bulk polymers E-L, P-L10. Refractive index (mV) vs Time (min).	138
Figure C.6 SEC traces of bulk polymers E-L, P-L10. Light scattering (mV) vs Time (min).	138
Figure D.1 Schematic representation of underwater contact angles measurements using air bubble (A) and silicone oil droplet (B). θ_m , ϕ_m in degrees is the measured angle between the polymer surface and the air bubble/oil droplet inside the probing liquid. Larger measured angle inside the bubble/droplet corresponds to higher surface wettability. The actual contact angles used in surface energy calculations are expressed as $\theta = 180^\circ - \theta_m$ for air bubble and $\phi = 180^\circ - \phi_m$ for oil droplet.	139
Figure E.1 Mean percent settlement with 95% CIs of <i>B. improvisus</i> after 72 h. Letters represent pairwise comparisons and bars that do not share a letter are significantly different.	143
Figure E.2 (A) Box plot presenting single settlement experiment results of cyprids larvae of <i>B. improvisus</i> . (B) Box plot presenting settlement results from four independent studies combined using meta-analysis. Black squares inside the boxes together with attached labels represent the mean settlement or summary effect sizes. Outliers are presented with asterisks. Letters indicate pairwise comparisons and boxes that do not share a letter are significantly different.	143
Figure F.1 Biomass generated by multispecies biofilm after 14 days of immersion in the slime farm quantified as relative fluorescence units (RFUs) using fluorescence plate reader. Mean RFUs were calculated from three slides using square root transformed data. Error bars represent SEs of the mean. Letters indicate Tukey's pairwise comparisons and points that do not share a letter are significantly different.	144
Figure F.2 Amount of remaining biomass after removal in the water channel quantified as relative fluorescence units (RFUs) using fluorescence plate reader. Mean RFUs were determined from three replicates after exposure to flow (8.2 Pa) and were calculated using square root transformed data. Letters indicate Tukey's pairwise comparisons and points that do not share a letter are significantly different.	145
Figure H.1 ^1H NMR spectrum of H-0 polymer brush solution (pBMA) in CdCl_3	148
Figure H.2 ^1H NMR spectrum of E-L polymer brush solution (pBMA-co-IBoMA-co-mPEG350MA) in CdCl_3	149
Figure H.3 ^1H NMR spectrum of Z-L polymer brush solution (pBMA-co-SBMA _{10mol%}) in CdCl_3	150
Figure H.4 ^1H NMR spectrum of A-L polymer brush solution (pBMA-co-SPMA) in CdCl_3	151
Figure H.5 ^1H NMR spectrum of P-L10 polymer brush solution (pBMA-co-SPMA _{5mol%} -co-METAC _{5mol%}) in CdCl_3	152
Figure I.1 SEC traces of H-0 polymer brush solutions. Refractive index (mV) vs Time (min).	153
Figure I.2 SEC traces of H-0 polymer brush solutions. Light scattering (mV) vs Time (min).	153
Figure I.3 SEC traces of E-L polymer brush solutions. Refractive index (mV) vs Time (min).	154
Figure I.4 SEC traces of E-L polymer brush solutions. Light scattering (mV) vs Time (min).	154
Figure I.5 SEC traces of Z-L polymer brush solutions. Refractive index (mV) vs Time (min).	155
Figure I.6 SEC traces of Z-L polymer brush solutions. Light scattering (mV) vs Time (min).	155
Figure I.7 SEC traces of A-L polymer brush solutions. Refractive index (mV) vs Time (min). ...	156

Figure I.8 SEC traces of A-L polymer brush solutions. Light scattering (mV) vs Time (min).....	156
Figure I.9 SEC traces of P-L10 polymer brush solutions. Refractive index (mV) vs Time (min). 157	
Figure I.10 SEC traces of P-L10 polymer brush solutions. Light scattering (mV) vs Time (min).157	
Figure J.1 Mean percent settlement of three-day-old <i>B. improvisus</i> cyprids on bulk polymers and polymer brushes after 24 h. Error bars are 95% CIs. The difference in settlement was statistically significant (Welch ANOVA $F_{9,60} = 22.54$, $p \leq 0.001$ with Games-Howell tests). Letters represent pairwise comparisons and bars that do not share a letter are significantly different.	158
Figure K.1 Independent tracks of cyprid walking (blue) and inspection (red) behaviours in the polymer brush H-0 tracking tube. The cumulative inspection movements and walking stretches vs time are presented alongside, with letters corresponding to the cyprid trajectory in the tube.....	159
Figure K.2 Independent tracks of cyprid walking (blue) and inspection (red) behaviours in the polymer brush E-L tracking tube. The cumulative inspection movements and walking stretches vs time are presented alongside, with letters corresponding to the cyprid trajectory in the tube.....	160
Figure K.3 Independent tracks of cyprid walking (blue) and inspection (red) behaviours in the polymer brush Z-L tracking tube. The cumulative inspection movements and walking stretches vs time are presented alongside, with letters corresponding to the cyprid trajectory in the tube.....	161
Figure K.4 Independent tracks of cyprid walking (blue) and inspection (red) behaviours in the polymer brush A-L tracking tube. The cumulative inspection movements and walking stretches vs time are presented alongside, with letters corresponding to the cyprid trajectory in the tube.....	162
Figure K.5 Independent tracks of cyprid walking (blue) and inspection (red) behaviours in the polymer brush P-L10 tracking tube. The cumulative inspection movements and walking stretches vs time are presented alongside, with letters corresponding to the cyprid trajectory in the tube.....	163

Chapter 1. Biofouling and different antifouling strategies

1.1 Introduction

The undesirable colonization of artificial structures such as ships' hulls, aquaculture equipment, pipelines and heat exchangers by marine organisms, termed biofouling, has significant economic and environmental impacts. Fouling of any surface in the marine environment starts immediately after immersing it in the seawater due to the adsorption of organic matter (e.g. proteins, polysaccharides, lipids) which often acts a conditioning layer for fouling organisms. Traditionally, the biofouling process is described by the linear successional model (Figure 1.1). Once the organic conditioning layer is formed, primary colonization starts with the settlement and growth of bacteria (e.g. *Cobetia marina*) and diatoms (e.g. *Navicula incerta*). Next, secondary colonizers settle which comprise of spores of macroalgae, protozoa and fungi. This microbial film acts as a nutrient source and adhesion promoter for the settlement of macrofouling organisms such as barnacles (e.g. *Balanus amphitrite*), tubeworms (e.g. *Ficopomatus enigmaticus*), tunicates (e.g. *Ciona intestinalis*) and bryozoans (e.g. *Watersipora subtorquata*).

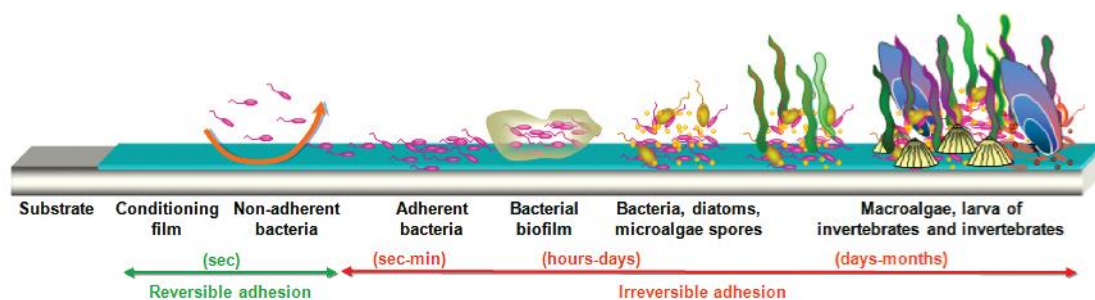


Figure 1.1 Schematic representation of a successional marine fouling processes (Lejars *et al.*, 2012).

In reality, this successional model is oversimplified since different colonisation phases can overlap and/or occur in parallel (Maki and Mitchell, 2002). Additionally, some macrofouling species such as zoospores of *Ulva linza* and cypris larvae of the barnacle *B. amphitrite* can explore virgin surfaces and settle on them without the presence of a microbial film (Callow and Callow, 2011). In a different model proposed by Clare *et al.* (1992), fouling is a dynamic process highly dependent on the abundance and type of fouling organisms in the water column, and the physical, molecular and behavioural interactions between specific fouling organisms. Furthermore, according to the dynamic model, the settlement of macrofouling organisms cannot simply be eliminated by reducing the

formation of biofilm on the surface. A successful fouling-control technology must, therefore, be effective against a wide range of fouling colonizers.

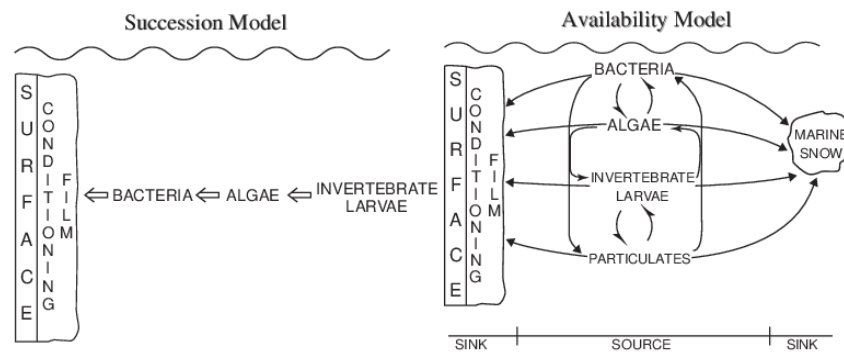


Figure 1.2 Comparison of succession and dynamic model (Rittschof, 2010).

It is estimated that there are over 4000 different marine fouling species worldwide (Yebra *et al.*, 2004). In general, the fouling organisms can be roughly divided into microfoulers such as bacteria, diatoms and algal spores, and macrofoulers such as barnacles, mussels, tubeworms, bryozoans and macroalgae. The presence of particular fouling community can be seasonal, and vary geographically. In addition, various environmental parameters such as water temperature, pH, salinity and intensity of solar radiation can affect the composition and growth of a biofouling community (Yebra *et al.*, 2004). The water temperature is among the most important factors, as it influences the fouling level via growth rate and reproduction of fouling species (Lejars *et al.*, 2012). Furthermore, the intensity of solar radiation not only affects the water temperature and salinity but also stimulates photosynthesis, which boosts the nutrient levels available in the water column (WHOI, 1952). In general, tropical and sub-tropical waters present similarly high fouling challenge throughout the year, while the fouling in temperate waters such as the North Sea is seasonal, with high fouling levels in the summer and relatively low in the winter.

From time immemorial man has dealt with the problem ship hull fouling but the issue has gained particular significance over the last 50 years, with increased marine cargo shipping. It is estimated that between 2005 and 2010 alone, the number of vessels with at least 1,000 gross register tons increased by 26% (CIA, 2005; 2010), thus the importance of effective antifouling (AF) solutions comes into focus. In the case of commercial shipping, the most direct effect of fouling on performance is the increased frictional resistance of the hull through the water (70-90% of ship's total resistance (MAN Diesel & Turbo, 2011)) which, in a heavily fouled condition, can increase powering penalties by up to 86% (Schultz, 2007). This penalty, in turn, requires increased fuel consumption of ~10% for

ships with a simple slime-layer and up to 20% for hulls with small hard-fouling organisms attached, such as juvenile barnacles (Schultz *et al.*, 2011). The Third IMO GHG Study 2014 (Smith *et al.*, 2015) highlighted international shipping as being responsible for around 3% of total global greenhouse gas emissions (GHGs), equivalent to the total emissions from a developed nation such as Germany. CO₂ emissions are the main contributor to this figure. As well as increasing the final cost of maritime cargo, which comprises most of the world's transported goods, marine biofouling is therefore also a contributor to anthropogenic climate change.

Another environmental consequence of marine shipping fouling is the introduction of nonindigenous species (NIS) to ecosystems, where they often displace naturally occurring inhabitants (Reise *et al.*, 1998; Brancato, 1999). In a study by Williams *et al.* (2013) different vectors contributing to introduction of NIS were assessed. The authors stated that ballast waters and ship hull fouling were the most common ones. Chan *et al.* (2015) examined these two vectors as potential transfer routes of nonindigenous species to the Canadian Arctic and concluded that the ship hull fouling presented a higher risk of an introduction event. Although significant efforts have been made to reduce the risk of marine invasions, such as introduction of strict ballast water regulations, biofouling-induced invasions are still a major, unresolved problem. One of the examples of a recent successful invasions is the introduction of acorn barnacle *Megabalanus coccopoma* in several non-native regions. This species, native to the eastern Pacific, has been recorded invading the western Atlantic, North Sea and Indian Ocean, and quite recently Japan (Yamaguchi *et al.*, 2009) and West African waters (Kerckhof *et al.*, 2010). In the last two cases it was speculated that the main translocation vector was hull fouling, thus, the development of an effective AF technology that does not rely on toxic biocides but that prevents the initial attachment of fouling species is of significant importance.

1.2 A brief history of the marine antifouling technologies

The first references to combating marine biofouling date back to ancient times when Phoenicians and Carthaginians used copper and pitch on the bottoms of ships' hulls (WHOI, 1952). Other materials presumably used by Romans and Greeks were tar, wax and even lead (WHOI, 1952). Pitch was the main material used to coat wooden ships in the medieval period until it was widely replaced by lead in the 15th century (WHOI, 1952). However, due to the galvanic corrosion caused by the more noble lead on the iron-based ship elements, lead was replaced with copper. With the industrial revolution in the 19th century, and introduction of iron hulls, copper sheathing was no longer effective both due to high cost and corrosion. Different attempts were made to reduce galvanic corrosion by separating metals with different isolators like rubber, ebonite, cork or glass (WHOI, 1952). However, none of

the above proved to be successful in the long term. Concurrently, with attempts to improve the sheathings of iron hulls with different non-conductive materials, the first solvent-borne paints were introduced with copper oxide, mercury oxide and arsenic as toxic biocides (WHOI, 1952). These biocides were initially incorporated into simple binders such as tar or linseed oil, but due to the low abrasion resistance of binders and uncontrollable release rate of biocides these coatings had short lifespans.

With the development of more durable resins in the late 1940s and the discovery of new highly-effective biocides based on organotin compounds in the mid 1950s (Gitlitz, 1981), the problem of ship hull fouling appeared to be resolved. These organotins, mainly tributyltin (TBT), were regarded as more effective and eco-friendly alternatives to mercury and arsenic based compounds. The TBT-based AF paints had several advantages over the previously available systems such as reduced corrosion effects, high toxicity over a wide range of fouling organisms and lack of colour (Yebra *et al.*, 2004). The real breakthrough in AF technology came in the 1960s with the invention of a new acrylic binder consisting of methyl methacrylate and TBT-acrylate which became known as the TBT-SPC paint. The SPC abbreviation stands for self-polishing copolymer. This new resin facilitated more controlled leaching of biocides such as copper oxide, which led to longer coating lifespan. The environmental friendliness of TBT-SPC coatings was however questioned in the 1980s, when several reports showed significant impacts of TBT-based systems on aquatic life (Goldberg, 1986; Alzieu *et al.*, 1989). It was reported that several marine species including fish, seals and ducks (Evans *et al.*, 1995; Strand and Jacobsen, 2005) had high levels of tin accumulated in their organs. Finally, the extinction of marine organisms in certain areas (e.g. *Nucella*), and thickening of oysters shells (Alzieu, 1991), led to a complete ban of the TBT-SPC in 2008.

1.3 Biocidal antifouling paints

According to Lindholdt *et al.* (2015), over 90% of the AF paint market is dominated by biocide-based coatings. Based on the reaction of the polymeric matrix with seawater, these AF coatings are generally divided into insoluble matrix (contact leaching paints), soluble matrix or controlled depletion paints (CPDs) and self-polishing copolymer coatings (SPC). The above technologies work on the principle of releasing biocides directly to the water and although they are highly effective in preventing attachment of macroorganisms, such as barnacles, tubeworms, mussels and macroalgae, they are susceptible to biofilm formation.

1.3.1 Insoluble matrix (contact leaching)

This technology, also known as contact leaching, is based on insoluble binders that contain high levels of biocidal pigments. Resins that are used to formulate those paints include acrylics, epoxies, vinyl polymers and chlorinated rubber (Yebra *et al.*, 2004). Owing to the high glass transition temperature and high molecular weight of the polymers, these paints are both durable and very stable in the marine environment. With immersion in seawater, only biocides (soluble pigment ions) are dissolved, leaving behind empty pores in the binder that are immediately penetrated by seawater, thus enabling further pigment dissolution (Figure 1.3A). The contact leaching paints present short lifetimes, no longer than 18 months (Yebra *et al.*, 2004), which can be attributed to insoluble binder that creates a diffusion barrier for some deeply embedded pigments. For the reasons presented above, insoluble matrix paints currently have very limited application.

1.3.2 Soluble matrix or controlled depletion paints (CPDs)

The soluble matrix (Figure 1.3B), also called erodible or ablative paints, consist of soluble binders with incorporated biocides, mainly oxides of copper, iron or zinc (Almeida *et al.*, 2007). Initially, soluble matrix paints were based on rosin binders, which had high dissolution rates and thus exhibited low lifespans comparable to insoluble matrix paints (Lejars *et al.*, 2012). Due to the oxidation of rosin, these paints are not suitable for long dry-docking periods, and because of low release rates of biocides they are not recommended for slower moving vessels (Berendsen, 1989). To overcome these issues, controlled depletion paints (CDPs) were developed. In these paints the rosin binder is mixed with plasticisers and more durable resins to produce a system that has reduced erosion rates and higher overall durability giving up to three years of antifouling protection (Almeida *et al.*, 2007).

1.3.3 Self-polishing copolymer paints (SPCs)

Contrary to the AF systems described above that rely on dissolution of the binder, SPCs are formulated of resins such as (meth)acrylates that hydrolyse in seawater (Lejars *et al.*, 2012). Early SPC paints were based on TBT copolymers, which through the hydrolysis of the carboxyl-TBT bond, released the TBT groups, causing a slow, controlled binder erosion and gradual release of co-biocides such as copper oxide. After the ban on organotins, new tin-free SPC systems based on copper or zinc (meth)acrylates were developed. The general mechanism of action of the SPC paints is as follows (Bressy *et al.*, 2009): (1) The soluble pigment particles in the coating are dissolved, creating pores that fill with seawater. (2) The ester groups in acrylics undergo hydrolysis which allow slow coating erosion and reveal more pigment particles available to dissolution. (3) As more pigment particles are

dissolved, the brittle polymer is more exposed to seawater and it can more easily erode revealing new surface untouched by the seawater (Figure 1.3C). This effect, called self-polishing, can render a stable erosion rate of a coating of 5 – 20 $\mu\text{m}/\text{year}$ (Almeida *et al.*, 2007), which, in turn, increases the protection period to five years and reduces the roughness of a hull.

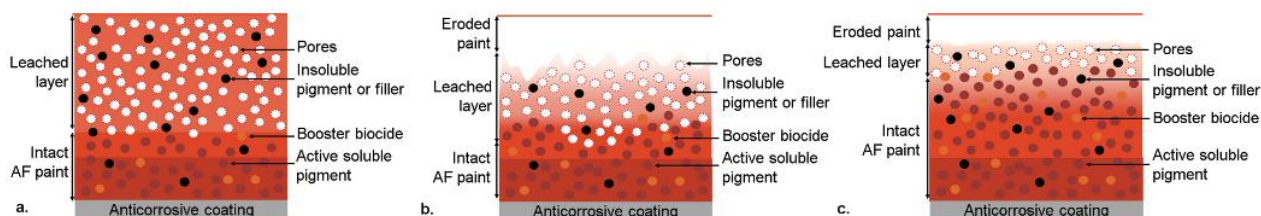


Figure 1.3 Schematic illustration of mechanisms of action of biocidal antifouling paint in seawater, (A) insoluble matrix paint, (B) soluble matrix paint, (C) self-polishing copolymer paint (Lejars *et al.*, 2012).

1.4 Fouling-release coatings (FRCs)

The ban of TBT and alarming reports of increased copper concentrations in coastal areas (Matthiessen *et al.*, 1999), resulted in greater awareness of the detrimental effects of heavy metals in aquatic environments (Daehne *et al.*, 2017) and a more strict regulatory regime for biocides, which in Europe is described within the European Union Biocides Regulation 528/2012 (European Union, 2012). In addition, with growing concern over the translocation of NIS, significant attention was directed toward technologies that do not rely on biocides, although these have yet to gain a significant market share.

Fouling-release coatings (FRCs) are an example of such a technology, where the main objective of the coating is to reduce the adhesion strength between the surface and fouling species so that during the vessel's navigation or dock cleaning the fouling organisms can be easily removed from the ship's hull (Schultz *et al.*, 1999; Brady, 2005). According to Brady (2000), the highest fouling-release (FR) performance is achieved when following conditions are met: (1) flexible polymer backbone, (2) presence of functional groups with low surface energy that allow polymer backbone mobility, (3) smooth surface which precludes any mechanical interlocking, (4) lack of heteroatoms that could facilitate ionic or dipolar interactions with bioadhesives, (5) physical and chemical stability in the seawater and (6) sufficient coating thickness for fracture mechanics control. There are two classes of materials that fulfil most of the above conditions, the silicones and fluoropolymers fulfil, but the silicones are more commonly used as binders for FRCs, as the more flexible siloxane backbone offers

both higher surface mobility and lower elastic modulus, which results in better FR properties (Yebra *et al.*, 2004).

While FRCs have proven to be very effective when applied appropriately to the hulls of fast cruising vessels (Holland *et al.*, 2004), they suffer from slime build-up on slower moving ships and those moored dockside for prolonged periods. In such circumstances, subsequent accumulation of hard fouling can damage the soft FRCs leading to wider failure of the coating system. These issues have limited the widespread application of FRCs and driven development of improved FRC systems (e.g. silicones with enhanced cross-linking density and/or addition of fillers for increased durability) and encouraged the research on new materials that can prevent slime formation, are mechanically robust and/or capable of self-healing. The new FRCs are often designed as hybrid coatings, meaning that they incorporate various hydrophilic and hydrophobic functionalities providing chemical, morphological and mechanical ambiguity (Lejars *et al.*, 2012). Intersleek[®] 1100SR is an example of successful commercialization of this concept, where the amphiphilic tri-block PEG-PFPE-PEG copolymer is blended into PDMS for increased slime resistance.

1.5 Novel non-fouling technologies

1.5.1 Design principles of (super)hydrophilic surfaces

From a thermodynamic perspective, surface conditioning - the process of initial adhesion of biogenic macromolecules free in the water column, or released by animals/plants for attachment - is driven by the loss of Gibbs free energy ΔG_{ads} ($\Delta G_{\text{ads}} < 0$) (Estephan *et al.*, 2011). Gibbs free energy, at constant temperature and pressure, can be defined as $\Delta G_{\text{ads}} = \Delta H_{\text{ads}} - T \cdot \Delta S_{\text{ads}}$, where ΔH_{ads} and ΔS_{ads} denote adsorption enthalpy and entropy respectively. To minimize the loss of Gibbs free energy and thus reduce adsorption at the surface-water interface, a putative fouling-resistant coating should minimize the increase of entropy whilst still providing a high enthalpy component. Based on this principle, research in recent years has focused on the development of novel hydrophilic materials including (super)hydrophilic surfaces on which water spreads completely, and that exhibit close to zero contact angle (Drelich and Chibowski, 2010). Hydrophilic surfaces are known for their fouling-resistant properties, which are exploited in the biomedical field to protect surfaces from cell adhesion and the non-specific adsorption of proteins (Chen *et al.*, 2010). A less-explored application of hydrophilic surfaces concerns their use in the prevention of marine biofouling. These materials are designed to manifest tightly bound water layers at the surface, providing high enthalpy of hydration (Rosenhahn *et al.*, 2010) to physically and energetically interfere with the adsorption of biomolecules (Chen *et al.*, 2010; Schlenoff, 2014). Additionally, Ostuni *et al.* (2001a) surveyed different functional groups

for their resistance to protein adsorption and concluded that the best performing chemistries should not only be well-hydrated, but also neutrally charged and capable of accepting hydrogen bonds.

1.5.2 Poly(ethylene glycol) (PEG) as source of hydrophilicity

One of the more successful approaches in commercialization of low fouling, hydrophilic surfaces that are inherently neutral and well-hydrated has been the use of ethylene glycol and its derivatives, such as poly(ethylene glycol) (PEG) / oligo(ethylene glycol) (OEG). The bound water layer at a PEG surface is believed to form through hydrogen bonding between ethylene glycol units and water molecules. Understanding the mechanism of fouling-resistance by PEG / OEG has been the subject of numerous studies. One of the first models explaining the resistive properties of PEG was proposed by Jeon *et al.* (1991) who argued that not only the tightly bound water layer at the polymer interface but also steric repulsion of the long PEG chains might play a vital role in protein resistance, due to unfavourable entropy reduction. Subsequent studies by Wang *et al.* (1997) and Harder *et al.* (1998) revealed that in the case of short OEGs where steric repulsion is minimal, it is the molecular conformation of the polymeric chains that affects protein adsorption. In a later study by Li *et al.* (2005), the high fouling resistance of OEG was also related to the packing density and the number of EG units available in OEG-self-assembled monolayers (SAMs). The authors reported that less dense OEG-SAMs are more mobile and can bind more water molecules, which improves the protein resistance of those structures.

Among various hydrophilic functionalities, PEG and its derivatives was one of the first chemistries that was explored in the marine antifouling field as potential candidate for novel non-biocidal coatings. Several studies reported its encouraging performance in short-term laboratory assays with marine fouling organisms, such as bacteria (Lundberg *et al.*, 2010), diatom cells (Statz *et al.*, 2006), zoospores of macroalgae (Finlay *et al.*, 2008b; Rosenhahn *et al.*, 2010) and barnacle cyprids (Ekblad *et al.*, 2008). Despite the promising results of PEG in the laboratory, it is susceptible to oxidation to aldehydes and acids in seawater (Ostuni *et al.*, 2001b; Li *et al.*, 2007). Ekblad *et al.* (2008) attempted to stabilize the PEG functionality by copolymerizing a 10-unit PEG with (hydroxyethyl)methacrylate (HEMA), producing a HEMA/PEG₁₀MA hydrogel. They reported only 5% loss of initial hydrogel thickness and similarly small changes in IR spectra after six months of storage in artificial seawater (ASW). The long-term fouling resistance of these coatings also remained unchanged. In a later study (Yandi *et al.*, 2014), polymer brushes of poly(HEMA-*co*-PEG₁₀MA) with different thicknesses were prepared and tested in static-immersion field tests in the temperate waters of a British marina. Despite encouraging results initially, after two months of exposure all poly(HEMA-*co*-PEG₁₀MA) brushes

were fully covered by fouling. Authors hypothesized that the reason behind this compromised long-term AF performance was limited mechanical and physicochemical stability of these model surfaces in the seawater. According to Quintana *et al.* (2013) the relatively low long-term performance of highly hydrated polymer brushes grown from the silicone oxide surfaces could be attributed to limited hydrolytic stability of the anchoring siloxane bonds (Si-O-Si) in the seawater.

The limited stability of PEG and its derivatives has resulted in increased interest in a new, bioinspired group of materials called polyzwitterions.

1.5.3 Zwitterions – an ultra-low fouling alternative to PEG

Zwitterions are naturally occurring compounds that can be found in osmolytes (Yancey, 2005), proteins and on the extracellular side of mammalian cell membranes (Bretscher and Raff, 1975), where they reportedly help to resist adsorption of globular proteins. The earliest information on zwitterionic materials dates back to the 1950s, however it was not until the 1980s when they were rediscovered as biomimetic materials (Laschewsky, 2014). Polyzwitterions are ionic materials carrying positively and negatively charged functional groups on the same monomer, giving overall neutral charge, for example poly(sulfobetaine methacrylate) (pSBMA), poly(carboxybetaine methacrylate) (pCBMA) and 2-methacryloyloxyethyl phosphorylcholine (pMPC). Polyzwitterions are a special subgroup of materials called polyampholytes. Polyampholytes also consist of oppositely charged species, but the functional groups can be randomly distributed on different monomers resulting in overall positive or negative charge, with only a limited pH range where the overall charge is zero. Controlling the surface charge of any polymeric material in seawater is difficult and goes beyond producing a surface with initial zero charge. Due to the slightly basic pH of seawater, different surface functional groups are susceptible to protonation or deprotonation, ionizing the surface and promoting electrostatic interactions or adsorption of counterions from seawater. This is almost always detrimental to the antifouling properties of the surface (Guo *et al.*, 2015), and has to be considered during the selection of materials as potential AF agents.

Contrary to PEG materials that maintain their hydration layer via hydrogen bond, it is believed that zwitterionic materials bind water molecules mainly using electrostatic interactions. With the growing interest in application of zwitterions as antifouling agents, a number of studies were devoted to understanding their unique hydration properties. For instance, Shao *et al.* (2010) compared the hydration properties of sulfobetaine (SB), carboxybetaine (CB) and OEG₄ functionalities using a free energy perturbation method and reported that both zwitterionic moieties have lower hydration energy than OEG₄. He *et al.* (2008) compared the phosphorylcholine (PC) and OEG-SAMs through

molecular simulation studies and showed that water molecules around the PC group present reduced mobility and similar dipole distribution to the bulk water, which means that it is more difficult to repel water molecules from zwitterionic materials than it is from EG-based materials. The water structures present at the surface of hydrophilic materials were also studied experimentally. For instance, Leng *et al.* (2015) used (sum frequency generation) vibrational spectroscopy to probe the surface hydration of pSBMA and pOEG and revealed that in pSBMA not only electrostatic interactions are involved in forming hydration layer but also strong hydrogen bonding. In the case of pOEG, the interfacial water at the surface was bound using only hydrogen bonds, some of which were weak. It was argued that the structure and stability of interfacial water is important from the antifouling point of view. In order to further understand the structure-property relationships, Jiang's group performed various simulation and modelling studies (Shao and Jiang, 2013; Shao and Jiang, 2014; Shao *et al.*, 2014; Shao and Jiang, 2015). It was shown that the design of non-fouling zwitterionic materials requires careful consideration of the following parameters: selection of anionic/cationic group, self-associations, hydration, ion-interactions and biomolecular interactions.

One of the first reports of zwitterionic SBMA being used for marine antifouling was presented by Zhang *et al.* (2009) who grafted sulfobetaine methacrylate (SBMA) from glass, producing a polymer brush, which reduced the settlement and adhesion strength of both green seaweed *Ulva* and unicellular diatoms of *Navicula*. Aldred *et al.* (2010a) studied the effect of two different betaines, pCBMA and pSBMA on settlement and the pre-settlement behavioural response of barnacle cyprids (*B. amphitrite*). No settlement was reported on either betaine after three days of testing and while cyprids on pSBMA were active on the surface, those on pCBMA spent most of their time swimming. It was hypothesized that the difference in the response of cyprids was a result of differences in surface hydration of the betaines. Indeed, in a paper by Shao *et al.* (2010), hydration properties of both CBMA and SBMA were investigated and it was concluded that water molecules around the COO⁻ group in CBMA were more tightly bound than those associated with the SO₃⁻ group of SBMA. The strong interactions of carboxybetaine with water molecules presumably hindered the exploratory behaviour of cyprids by reducing electrostatic interactions between the surface and cyprids' attachment discs or, possibly, produced a surface that was indistinguishable from water to the exploring larva (Aldred *et al.*, 2010a).

Although, zwitterionic polymer brushes have proved to be highly effective in laboratory based assays, their antifouling efficacy and mechanical stability may reduce in seawater over time (Quintana *et al.*, 2013). In order to address these issues, Xie *et al.* (2018b) prepared a hydrolysable zwitterionic polymer using a ring-opening reaction of 2-methylene-1,3-dioxepane (MDO), tertiary carboxybetaine

ester (TCB), and 7-methacryloyloxy-4-methylcoumarin (MAMC), and subsequently performed photo-crosslinking for improved mechanical resistance. This unique polymer creates a dynamic surface that can remove weakly attached microorganisms (e.g. dead bacteria) and renew itself through hydrolysis of the side chains providing new zwitterionic moieties for constant antifouling protection. The good mechanical properties of the coating were confirmed by adhesion measurements where no coating degradation was observed after one month of immersion in seawater. Though no marine biofouling data were presented, the concept of a hydrolysable zwitterionic copolymer is an interesting avenue for the development of biodegradable, eco-friendly, SPC coatings.

Although SBMA and CBMA are the two most commonly tested zwitterionic materials, advances in organic synthesis in the last decade have allowed chemists to prepare various zwitterionic molecules with different chemical structures (Laschewsky, 2014). The importance of the chemical nature of the zwitterionic functionality on the antifouling performance of surfaces was recently studied by Koc *et al.* (2019a). Various zwitterionic hydrogels were prepared using a set of sulfa-/sulfobetaine based chemistries with different polymer connections and/or number of spacer units. They were tested in the laboratory for protein adsorption resistance and attachment strength of *N. incerta* cells and *U. linza* spores. The antifouling assays confirmed that precise modulation of the chemical structure of zwitterions is necessary to achieve high fouling resistance.

1.5.4 Other sources of hydrophilicity

PEG and zwitterions are not the only materials to have gained recent attention as potential AF agents. Anionic 3-sulfopropyl methacrylate potassium salt (SPMA) and cationic 2-(methacryloyloxy)ethyltrimethylammonium chloride (METAC) are single charged monomers that, although less explored in the AF field, showed encouraging initial results. Wan *et al.* (2012) prepared polymer brushes of SPMA, METAC and SBMA on silicon wafers and reported equally low settlement of two non-motile microalgae, *Chlorella* and *Nannochloropsis maritima* on all three surfaces. Moreover, the SPMA was grafted from a micropatterned silicone elastomer (Sylgard 184) and both AF and FR properties of the modified, patterned silicone were improved. Yandi *et al.* (2016) synthesized various charged polymer brushes, including pSBMA and pSPMA, and found low settlement and attachment strength of spores of macroalgae *U. linza* to both polymers, but reported high settlement of *B. improvisus* and *B. amphitrite* on pSPMA.

1.5.5 Amphiphilic surfaces

With the diverse suite of fouling organisms in nature, the development of a successful non-biocidal coating based on a single fouling inhibition strategy is highly unlikely. Non-biocidal approaches will probably require a combination of several different strategies, such as incorporation of hydrophilic fouling-resistance functionalities and hydrophobic fouling-release chemistries. On one hand the hydrophilic segments, such as those comprising of PEG or zwitterions, could provide an energetic or physical barrier that would be difficult to overcome by fouling species. On the other hand, the hydrophobic segments, such as PDMS or PTFE, could help to release weakly adhered organisms. This novel approach was presented for the first time by Gudipati *et al.* (2005) who prepared a set of hyperbranched fluoropolymers (HBPF) cross-linked with PEG. By changing the PEG content in the formulation, it was possible to fine tune the surface properties and produce coatings with different compositional, morphological and topographical characteristics (Figure 1.4). The authors hypothesized that the surface complexity had a profound effect on the degree of fouling and coatings with higher compositional and morphological heterogeneity were more resistant to marine biofouling. It was speculated that the surface heterogeneity would deter settling larvae or would interfere with the process of adhesion (Callow and Callow, 2011).

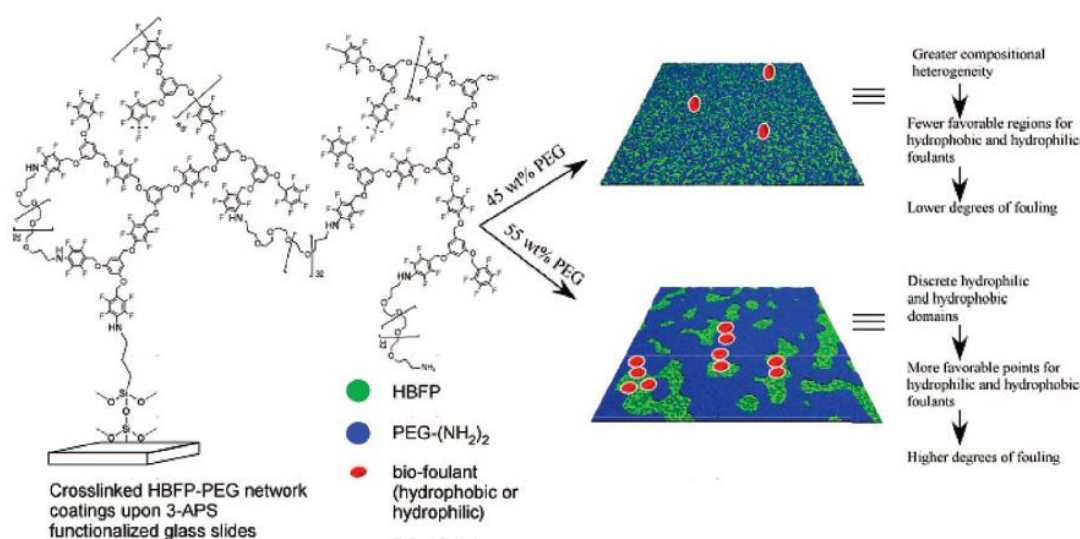


Figure 1.4 Schematic structure of amphiphilic coating comprising of hyperbranched fluoropolymer (HBFP) and PEG (Gudipati *et al.*, 2005).

Assays with spores of *U. linza* showed significantly lower settlement and attachment strength on amphiphilic HBPF-PEG coatings when compared to a glass control. In addition, experiments with young *Ulva* plants (sporelings) revealed smaller biomass growth and higher removal rate from the HBPF-PEG surfaces. In a different approach presented by Wang *et al.* (2011), amphiphilic coatings

were prepared by photo-crosslinking perfluoropolyether (PFPE) with PEG. The PFPE-PEG coatings were tested against spores and sporelings of *Ulva*, cells of *Navicula* and cyprids of *B. amphitrite*, and it was found that PFPE with the longest PEG chain (PEG1100) presented the best AF and FR properties. Contrary to the study by Gudipati *et al.* (2005), where the amphiphilicity of the HBFP-PEG coatings was achieved by nano-segregation, in the PFPE-PEG1100 coating the surface ambiguity was accomplished through macro-segregation of flexible PEG chains in contact with water.

Another widely used approach in the production of surfaces with amphiphilic properties is the use of a multilayer coating based on thermoplastic elastomers, e.g., polystyrene-block-poly-(ethylene-random-butylene)-block-polystyrene (SEBS; Krishnan *et al.* (2006)). This primary layer, also known as block copolymer precursor, is commonly modified with different surface-active block copolymers (SABC) for additional functionality. For instance, Krishnan *et al.* (2006) prepared a coating comprising of SEBS and a top layer of SABC with ethoxylated fluoroalkyl side chains. The experiments with cells of *Navicula*, *Ulva* spores and sporelings revealed excellent FR properties against diatom cells and comparable release of sporelings to that of the PDMS standard. It was hypothesized that upon immersion in water the surface undergoes reconstruction, revealing a larger number of PEG groups that render the surface hydrophilic. As for the *Ulva* assay, it was speculated that the ingress of water between the amphiphilic surface and attached sporeling had a profound effect on its attachment strength and the resulting FR properties. The usefulness of SEBS as a platform for developing amphiphilic coatings was further confirmed in a report by Martinelli *et al.* (2008) who assayed SEBS modified with various amphiphilic fluorinated polystyrene-based block copolymers against cells of *Navicula*, *Ulva* spores and sporelings. It was shown that the hydrophilic and hydrophobic segments were responsive towards water/air forming nanodomains of different shape and size, giving the surface amphiphilic character. The AF performance of coatings was highly dependent on the formulation and type of fouling organism, and it was speculated that the changes in surface morphology and topography after immersion in water played a key role in determining coating performance. Weinman *et al.* (2009) examined the effect of elastic modulus of SEBS with tethered amphiphilic SABC triblock copolymer possessing ethoxylated fluoroalkyl side chains on the removal of sporelings of *Ulva*. They found that the SABC tethered to low-modulus SEBS increased the removal of plants by 70% when compared to the SABC coated on the high-modulus SEBS.

1.6 Examples of marine fouling organisms used in AF laboratory testing

1.6.1 Barnacles

Barnacles are a subclass of marine crustaceans (Cirripedia), many of which colonize a range of habitats along the intertidal zones of temperate and tropical waters. Their settlement-stage larva, the cyprid, is able to settle on a vast array of substrates ranging from man-made structures (e.g. ships' hulls, aquaculture equipment, pipelines) and natural hard surfaces, to the bodies of other marine animals (corals, sponges, turtles, whales). Due to their worldwide distribution, high fecundity and unique ability to attach to various substrates, barnacles are regarded among the most problematic fouling species. This is especially true for the marine shipping industry, where a ship hull with heavy calcareous fouling, formed for instance of barnacles, could develop a powering penalty as high as 86% (Schultz, 2007). In addition, the hard calcareous plates of adult barnacles can damage AF coatings, often resulting in wider coating failure.

Two most commonly used barnacle species in AF testing are the tropical *B. amphitrite* and temperate water *B. improvisus*. These barnacles are simultaneous hermaphrodites and are equipped with both male and female reproduction systems, which means that they can self-fertilise whenever cross-fertilization is not possible (Anderson, 1993; Desai *et al.*, 2006). Obviously, in order to keep the barnacle community in good health, and with high genetic diversity, cross-fertilization is preferred (Aldred and Clare, 2008). The life cycle of a typical barnacle is presented in Figure 1.5. Nauplius larvae hatch within the mantle cavity of the adult, where egg-masses are brooded, and are released into the water column. Once nauplii reach stage two (usually within a few hours of release) they start to feed on phytoplankton. After five more moults, they finally metamorphose into the lecithotrophic (non-feeding) cypris larva, or cyprid which is specialised for surface selection and settlement, and widely used in the laboratory testing of AF coatings (Holm, 2012).

In order to find a suitable spot for settlement, the cyprid uses a pair of highly specialized attachment organs called antennules, with which it probes surfaces and may leave behind a proteinaceous material termed a 'footprint'. Cyprids are known for their highly discriminatory exploratory behaviour and can respond to various surface parameters such as wettability (Finlay *et al.*, 2010; Di Fino *et al.*, 2014), surface charge (Petrone *et al.*, 2011) and texture (Schumacher *et al.*, 2007). In addition, cyprids are known to respond to environmental cues such as local hydrodynamics (Koehl, 2007; Larsson *et al.*, 2016) or surface colour (Yule and Walker, 1984). The selection of a suitable surface/location plays a key role in survival and reproduction, thus the increased interest in

understanding cyprid behaviour and attachment mechanisms. Chapter 3 covers in more detail the settlement behaviour of cyprids and the mechanism of temporary adhesion.

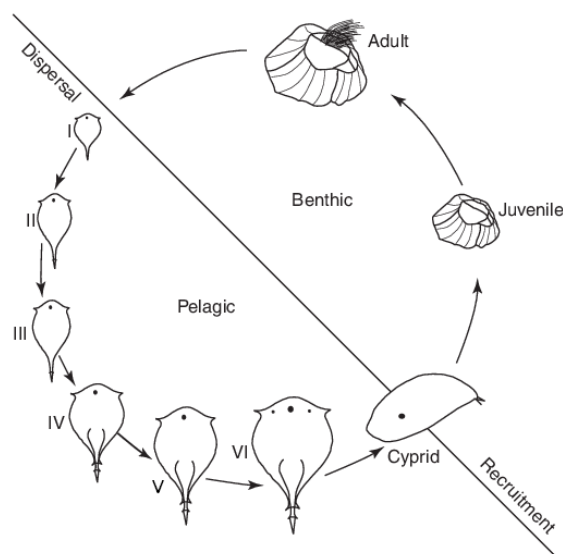


Figure 1.5 Life cycle of a typical thoracican barnacle (Khandeparker and Anil, 2007).

1.6.2 Diatoms

Diatoms are large and diverse group of unicellular algae that can adhere to natural or man-made structures through deposition of adhesive mucilage. Diatoms have an ornamented silica cell wall termed a frustule which is made of overlapping valves. Based on the cell symmetry they can be divided into centric and pennate types. The raphid diatoms attach to surfaces through extracellular polymeric substances (EPS), which are secreted via the raphe(s), and together with bacteria, and other diatoms they form biofilms. The EPS secreted by diatoms serves several functions such as biofilm formation and stabilization, sessile adhesion and motility (Hoagland *et al.*, 1993). After settling on a surface, raphid diatoms move in accordance with different environmental cues such as nutrient levels, light availability and tidal fluctuations (Molino and Wetherbee, 2008). Raphid diatoms move (glide) across surfaces and position themselves using an adhesive complex (AC) that connects the adhesive mucilage through the raphe with an actin-myosin system inside the cell (Molino and Wetherbee, 2008). With the movement of the cell, the adhesive strands are cut, leaving behind a trail of adhesive.

According to Wetherbee *et al.* (1998), benthic diatoms can experience primary and secondary adhesion stages. Primary adhesion takes place on contact with the surface during which the cell re-orientates itself and produces EPS to assist in general adhesion and motility. Interestingly, Lachnit *et al.* (2019) observed with time-lapse video microscopy in combination with immunofluorescence that

not all moving cells deposit permanent trails on the surface, but they could potentially use temporary adhesion for gliding, and as a result leave no adhesion trails behind. Once a suitable place has been found, secondary adhesion takes place and more complex adhesion structures may be produced (i.e. stalks, pads, tubes, films). Both primary and secondary adhesion are reversible processes (Wetherbee *et al.*, 1998).

Until recently the diatom adhesive was not very well characterized, and it was believed that it consisted of proteins, proteoglycans and carbohydrates (Wetherbee *et al.*, 1998). Poulsen *et al.* (2014) isolated and determined the partial composition of the adhesive material from two raphid pennate diatoms *Craspedostauros australis* and *Amphora coffeaeformis* and revealed that adhesives consist of highly hydrophilic proteins, carbohydrate moieties and uronic acids. Based on the low solubility of both secreted adhesives it was proposed that the curing mechanism was through covalent and/or ionic cross-linking. In a recent study, Lachnit *et al.* (2019) conducted a proteomics analysis of the isolated diatom adhesive of *A. coffeaeformis* and identified 21 proteins, however their functions were not determined. It was speculated that the adhesive strands could be composed of multiprotein complexes that could assist in the adhesion and gliding by performing additional tasks such as: (1) substrate adhesion, (2) strand cohesion, (3) connection of adhesive to the cell wall, (4) transduction of force from cell to substrate.

As described earlier, diatom-dominated biofilms are a particular problem on FR coatings to which they adhere strongly (Holland *et al.*, 2004). It is estimated that there are over 10,000 different diatom species present in the oceans (Molino and Wetherbee, 2008), however, it is the genera *Amphora*, *Navicula*, *Nitzschia*, *Cocconeis*, *Craspedostauros*, *Toxarium*, *Licmophora* and *Achnanthes* that are mainly responsible for slime formation on ocean-going ships (Molino and Wetherbee, 2008).

1.7 Scope of the thesis and research question

This thesis examines different surface chemistries that are regarded as (super)hydrophilic for their effectiveness against marine biofouling. To this date the majority of work on novel hydrophilic surfaces was limited to only few chemistries (i.e. PEG, SBMA) and one of the aims of this work was to explore other hydrophilic chemistries that could be used in the next generation of non-biocidal marine coatings. In this work, emphasis was placed on translation of the (super)hydrophilic AF technology from model surfaces to more industrially relevant ‘bulk’ coatings. An important part of this research was to determine what physicochemical properties of (super)hydrophilic surfaces make them effective against marine biofouling as well as the mechanism behind the rejection of those surfaces by fouling species. To assess the usefulness of prepared surfaces as practical marine AF

coatings, stability tests were performed followed by field tests at two different locations. It was hoped that conclusions drawn from this work would provide guidelines in developing more tailored non-fouling solutions that could be industrially applicable.

In this thesis four experimental chapters are presented which cover following topics: the roles of nonfreezable water and polymer swelling in the antifouling performance of polymers; the settlement behaviour of barnacle cyprids on different hydrophilic surfaces; hybrid coating incorporating fouling-resistance and fouling-release properties; long-term stability of hydrophilic polymers.

Chapter 2. Nonfreezable water and polymer swelling control the marine antifouling performance of polymers with limited hydrophilic content

This chapter is based on the following publication:

Kardela J.H, Millichamp I.S., Ferguson J., Parry A.L., Reynolds, K.J., Aldred N. and Clare A.S. (2019) 'Nonfreezable water and polymer swelling control the marine antifouling performance of polymers with limited hydrophilic content', *ACS Applied Materials & Interfaces*, 11(33), pp. 29477-29489.

2.1 Introduction

The majority of published research on low-fouling hydrophilic chemistries such as PEG, zwitterions, and other ionic functionalities has now been limited to well-defined laboratory-scale SAMs, polymer brushes or delicate hydrogels. While laboratory evaluations of various model surfaces have demonstrated that the efficacy requirements are in the realm of the achievable, these model formulations are not, however, suitable for practical fouling-control applications. A successful fouling-resistant coating has to be produced at scale (the global marine fouling control paint market was 42 million liters in 2014), applied in variable environmental conditions and present long-term fouling resistance.

It is presently unknown if a uniform film of hydrophilic functionality is required to elicit non-fouling character via the binding of interfacial water, or if the incorporation of hydrophilic functionality into a more practical bulk polymer system will suffice. To translate this technology to practical marine coatings, the unique surface hydration properties that control adhesion of fouling species must be maintained even at low incorporation levels. Intuitively, the reduction of the hydrophilic functionality in the polymer could potentially decrease final surface hydration and cause reduction of antifouling performance of the coating, but this has never been investigated in the literature.

In this chapter the effect of various hydrophilic functionalities on the AF and FR performance of bulk polymer coatings was investigated. Polymers were prepared by copolymerizing n-butyl methacrylate with relatively small amounts (10-20 mol%) of hydrophilic comonomers such as sulfobetaine methacrylate (SBMA), 3-sulfopropyl methacrylate potassium salt (SPMA), 2-(methacryloyloxy)ethyltrimethylammonium chloride (METAC), methoxy PEG methacrylate (mPEG350MA), hydroxyethyl methacrylate (HEMA), methacrylic acid (MAA) and 2,3-

dihydroxypropyl methacrylate (DHPMA). In addition, polymers bearing mixed charged functionalities (SPMA and METAC), the so-called polyampholytes, were also prepared.

Coatings were tested in the laboratory against model fouling organisms, the cyprid of *B. improvisus* and the slime-forming diatom *N. incerta*. In case of barnacle settlement experiment, a novel experimental design was introduced called meta-analysis, which is a statistical procedure that integrates results from several independent studies. Additionally, the resistance of coatings to biofilm formation was assessed by immersion in a multispecies biofilm culturing reactor. Finally, in order to confirm that the hydrophilicity of the monomers is sustained in the bulk copolymers contact angle measurements, swelling, and water states experiments were performed.

2.2 Experimental section

2.2.1 Materials

N-(2-methacryloyloxyethyl)-N,N-dimethyl-N-(3-sulfopropyl)ammoniumbetaine (SBMA) was supplied by Raschig GmbH under trade name Ralumer SPE. 3-Sulfopropyl methacrylate potassium salt (SPMA, 98%), 2-(methacryloyloxy)ethyltrimethylammonium chloride (METAC) solution (80% in H₂O), isobornyl methacrylate (IBoMA), hydroxyethyl methacrylate (HEMA), 2,3-dihydroxypropyl methacrylate (DHPMA), methacrylic acid (MAA) were purchased from Sigma-Aldrich. Methoxy PEG methacrylate (mPEG350MA) was supplied by GEO Specialty Chemicals. n-Butyl methacrylate (n-BMA, 99%) was obtained from Acros Organics. Methylated spirit, xylene, tetrahydrofuran (THF), dichloromethane (DCM) and methanol (MeOH) were purchased from Fisher Scientific. The 2,2'-azobis(2-methylbutyronitrile) (AMBN) initiator was supplied by AkzoNobel Chemicals B.V. as Perkadox AMBN-gr.

2.2.2 Preparation of bulk polymers

All polymers were synthesized using noncontrolled free radical polymerization (Table 2.1). In order to successfully copolymerize hydrophilic comonomers such as SBMA with hydrophobic n-BMA, a dual-feed technique was used as described by Millichamp (2017). Typically, the first feed constituted of a hydrophilic monomer (e.g. SBMA) (25.89 g, 93 mmol), which was added to methylated spirit (120 g) and preheated to 70 °C on a magnetic stirrer. In the second flask first lot of AMBN initiator (4.46 g, 23 mmol) was dissolved in n-BMA (118.59 g, 834 mmol) and this made up the second feed. The main reaction vessel which contained a small amount of methylated spirit (22.5 g), was equipped with mechanical stirrer and was heated to 75 °C. Both feeds were gradually added to the main reactor using Watson Marlow 101 U/R peristaltic pumps over 4 h. When necessary, the first feed line was

heated to remove blocking derived from crystallization of the hydrophilic moiety. One hour after feeding was complete, a small amount of AMBN (1.06 g, 6 mmol), dissolved in methylated spirit (7.5 g), was added directly to the reaction mixture to ensure full conversion of residual monomer. The main vessel was stirred for another hour, cooled down and left overnight for subsequent post-processing. The next day the polymerization flask was fitted with a condenser, heated to 85 °C and methylated spirit (100 g) was distilled with a simultaneous feed of xylene (131 g). After the distillation, the polymer solution was allowed to cool down to room temperature. In case of polymers Z-L, Z-L20, A-L, C-L, P-L20 additional amount of xylene was added (20-30 m/m%) to reduce the polymer viscosity and ease the final coating application. Specific amounts of materials used in polymerizations and in final coatings preparation are presented in Table 2.2. Detailed descriptions of polymerization procedures for each polymer are presented in Appendix A.

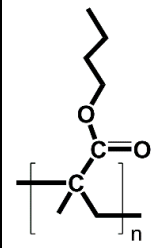
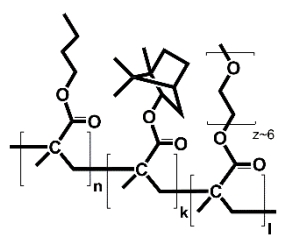
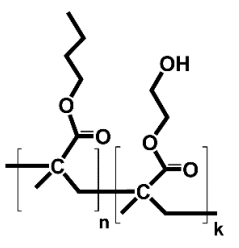
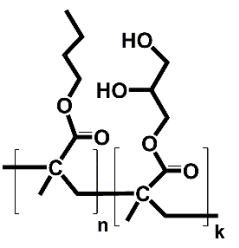
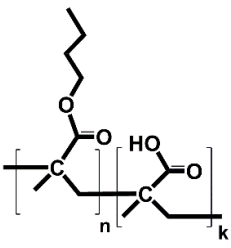
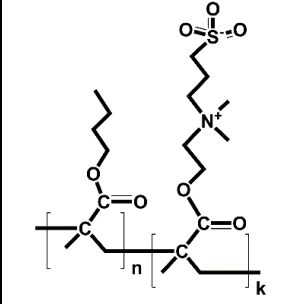
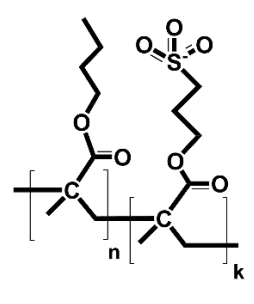
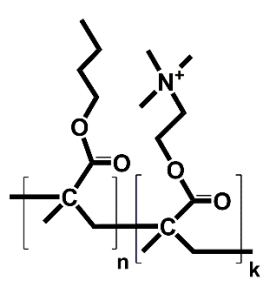
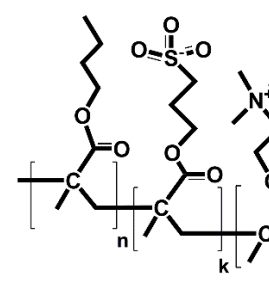

Nonionic polymers					
H-0	E-L		H-L	G-L	M-L
					
Ionic polymers					
Z-L	Z-L20	A-L	C-L	P-L10	P-L20
					

Table 2.1 Chemical structures of prepared bulk polymers together with their abbreviations used in the text.

	H-0	E-L	H-L	G-L	M-L	Z-L	Z-L20	A-L	C-L	P-L10	P-L20
POLYMERIZATION STEP											
n-BMA	143.96	59.78	130.63	128.01	134.67	118.59	97.18	121.06	124.08	122.7	103.46
AMBN	6.04	4.4	6.09	5.96	6.27	5.52	5.09	5.64	5.78	5.53	5.25
Methylated spirit	150	150	150	150	150	150	150	150	150	150	150
IBoMA		54.11									
mPEG350MA		31.71									
HEMA			13.28								
DHPMA				16.03							
MAA					9.06						
SBMA						25.89	47.73				
SPMA								23.3		11.81	22.4
METAC (* = dry)									25.18 *20.14	12.45 *9.96	23.61 *18.89
POSTPROCESSING STEP											
Methylated spirit distilled	100	100	100	100	100	100	100	100	100	100	100
Xylene added	131	131	131	131	131	131	131	131	131	131	131
FINAL VISCOSITY ADJUSTMENT											
Xylene added						60	60	60	60		90
POLYMER CONCENTRATION AND COATING THICKNESS											
Concentration (wt %)	45	45	45	45	45	38	41	38	38	45	36
Dry coating thickness \pm SD (μ m)	20 \pm 3	24 \pm 6	21 \pm 3	28 \pm 3	35 \pm 2	28 \pm 5	30 \pm 3	22 \pm 3	22 \pm 3	26 \pm 6	30 \pm 3

Table 2.2 Amounts of materials used in grams in polymer preparation together with final coating concentrations and dry coating thicknesses.

The prepared polymer solutions were applied to polyvinyl chloride (PVC) substrates. Slides for barnacle testing were coated with polymer solutions using a Sheen 100 μ m cubic applicator, whereas slides for diatom and slime-farm experiments were applied using a regular paint brush. In order to determine final coating thicknesses, polymer solutions were applied onto aluminum panels and Elcometer 456 thickness gauge was used to determine the dry film thickness. Five measurements were made on each panel and average value was calculated. The measured thicknesses ranged between 20 and 35 μ m.

2.2.3 Polymer characterization

Polymer compositions were determined with ^1H NMR experiments using Bruker Avance II 400 MHz NMR spectrometer and CDCl_3 as a solvent. Prior to running NMR experiments the samples were purified twice with dialysis (Spectrum Spectra/Por 3, molecular weight cutoff 3.5 kDa) using a mixture of MeOH and DCM (1:2). The average molecular weights and polydispersity indices (PDIs) were analyzed by size exclusion chromatography (SEC). The SEC system used for analysis consisted of Knauer Smartline 1000 pump equipped with Spark Optimas autosampler and was combined with two PSS PFG linear XL 7 μ m, 300 x 8 mm columns and a Viscotek TDA 302 tetra detector array as

a detector. Dried polymer samples were dissolved in hexafluoroisopropanol (HFIP) to a concentration of 5 mg/mL. Eluent used in the system was HFIP with 0.02 M potassium trifluoroacetate and the flow rate was set at 0.6 mL/min at 303 K. The injection volume of sample was 50 μ l. The SEC system was calibrated using narrow distributed PMMA standards. Glass-transition temperature (T_g) measurements were performed using Netzsch DSC 200 F3 differential scanning calorimeter with autosampler. Dried polymer material, weighing around 10 mg was placed in an aluminium crucible with a pierced lid. Samples were first cooled down to -125 $^{\circ}$ C and then heated to 150 $^{\circ}$ C at 10 K \cdot min $^{-1}$ in order to remove any residual solvent and erase thermal history of the polymer. The T_g of a polymer was determined from a second heating cycle using earlier established parameters. Detailed characterization data including NMR spectra with peak assignments, copolymer composition determination and SEC traces are available in Appendix B and C.

2.2.4 Underwater contact angle measurements and surface energy calculations

Captive bubble contact angles were recorded using a DataPhysics OCA 35 goniometer equipped with a custom-made glass cell filled with deionized water (Milli-Q water, ≥ 18.2 M Ω \cdot cm, Merck Millipore) and U-shape microsyringe. Before performing the measurements, all surfaces were equilibrated in deionized water for 20 min. A 3 μ L air bubble or drop of silicone oil (viscosity 5 cSt, Sigma-Aldrich) was automatically dispensed beneath the surfaces to be tested and the resulting contact angle at the polymer-water-air bubble/silicone oil interface was determined after 3 min using the Young-Laplace fitting method. At least three measurements were made on each surface in different regions and the obtained contact angles were averaged. All measurements were made at ambient temperature (298 K). Surface energy (SFE, γ_{pa}^{TOT}) of hydrated polymers was determined using a two-component model originally developed by Fowkes (1964) and later modified by Hamilton (1972) for underwater contact angle measurements. In this approach, the SFE of a polymer is divided into polar (γ_{pa}^p) and dispersive (γ_{pa}^d) contributions, which represent specific interactions at the hydrated polymer interface. Ultimately by combining Young's equation with Wu's interfacial energy estimate (Wu, 1971) and measuring underwater contact angles of both probing liquids (with earlier established polar and dispersive contributions), the surface energy and interfacial energy at the polymer/water interface (IFE, γ_{pw}) were calculated. Detailed derivations of the equations are available in the Appendix D.

2.2.5 Determination of Equilibrium Water Content (EWC)

Polymers were dried in an oven at 105 °C for 1 h and subsequently transferred to a vacuum oven at 120 °C for another 5 h. Dried samples were then put in vials, and 20 mL of deionized water (Milli-Q water) was added. The vials were then sealed and kept at room temperature for six weeks. The wet polymer samples were then removed and gently blotted with tissue, and the amount of water in the swollen polymers was measured with a thermogravimetric analyzer (TGA, Perkin Elmer TGA 7). The samples were first heated to 100 °C with a heating rate of 10 °C·min⁻¹ and then kept at 100 °C until the weight remained constant. The percentage weight loss calculated from thermogravimetric curves corresponded directly to EWC. A minimum of three thermogravimetric measurements (TGAs) were made for each polymer to assess the reproducibility of the analysis.

2.2.6 Determination of forms of water present in the swollen polymers

Different states of water in the swollen polymer were determined using differential scanning calorimetry (DSC, Netzsch DSC 200 F3). Based on the structure and interaction of water molecules with polymers chains, the water in the polymer matrix can be classified as: nonfreezable, freezable bound water and free water. The nonfreezable water is the type of water that is tightly bound to a surface, followed by freezable water, which has moderate mobility, and free water that has highest mobility and resembles the mobility and structure of bulk water (Tanaka *et al.*, 2013). A six-week period was allowed for swelling of polymer samples prior to measurements. Around 5-10 mg of material was placed in an aluminium pan, which was hermetically sealed to ensure no moisture evaporation during the heating cycle. An empty closed pan was used as the reference. The samples were initially cooled down to -40 °C and then reheated to 40 °C at a rate of 10 °C·min⁻¹. The endothermic peaks present in the heating cycles of calorimetric analysis represent the melting of freezable water inside polymer matrices. By determining the peak area, it is possible to estimate the enthalpy change (ΔH_f) during melting, which in turn can be used to calculate the mass ratio of freezable and nonfreezable water to the mass of polymer and number of nonfreezable water molecules around each repeating unit of copolymer.

To estimate the $W_{\text{freezable}}$, which is the ratio of the mass of the freezable water to the mass of polymer the following equation was used:

$$W_{\text{freezable}} = \frac{1}{w_{\text{polymer}}} \cdot \left(\frac{\Delta H_f}{\Delta H_w} \cdot 100 \right) \quad (1)$$

where the w_{polymer} is the weight percent of the polymer in the swollen polymer matrix, the ΔH_f is the enthalpy change in the heating trace that corresponds to the melting of freezable water in the polymer, and ΔH_w is the enthalpy change of bulk water which is 333.5 J/g.

The $W_{\text{nonfreezable}}$, which is the ratio of the mass of the nonfreezable water to the mass of polymer was calculated using equation:

$$W_{\text{nonfreezable}} = EWC - W_{\text{freezable}} \quad (2)$$

Finally, the number of water molecules per copolymer repeating unit was determined using following equation:

$$N_w = W_{\text{nonfreezable}} \cdot \frac{M_{\text{copolymer unit}}}{M_w} \quad (3)$$

where $M_{\text{copolymer unit}}$ is the average molecular weight of one copolymeric repeating unit based on the NMR composition data (Table 2.3). For example, for polymer Z-L, $M_{\text{copolymer}} = 0.93 \text{ mol} \cdot M_{\text{BMA}} + 0.07 \text{ mol} \cdot M_{\text{SBMA}} = 151.8 \text{ g/mol}$. M_w is the molecular weight of water (18 g/mol).

2.2.7 Barnacle culturing

Adult barnacles of *B. improvisus* were allowed to release stage one nauplii which were attracted to a light source and collected with a plastic pipette to a solution of *Tetraselmis suecica*. After collecting sufficient nauplii they were transferred to a 10 L plastic bucket containing 22 ppt artificial seawater (ASW; Tropic Marin) with 35.6 mg·L⁻¹ of streptomycin sulphate and 21.9 mg·L⁻¹ of penicillin G and kept in the incubator at 28 °C. Larvae was fed every two-three days using *T. suecica* and *Thalassiosira pseudonana* until metamorphosis to the cyprid stage and subsequently filtered using a 250 µm mesh. Filtered cyprids were transferred to a petri dish containing 22 ppt ASW and used immediately for leaching and settlement experiments.

2.2.8 Settlement assay using cypris larvae of *B. improvisus*

Prior to settlement assays, PVC slides coated with polymers were immersed in deionized water for six weeks in order to remove any unreacted monomers and solvent residues that could be leaching out from coatings and be toxic towards larvae. After conducting a leachate toxicity test (data not presented) and confirming that all tested surfaces were nontoxic, samples were transferred to quadriPERM[®] dishes (Sarstedt), and 0.5 mL of ASW (Tropic Marin; 22 ppt) was dropped onto each slide, followed by addition of 20 ± 2 freshly filtered larvae in a minimal volume of ASW. The dishes

were then wrapped with wet paper towel, covered with aluminum foil and placed in an incubator at 28 °C in the dark. After 72 h, dishes were carefully removed from the incubator and the number of settled cyprids was enumerated using a dissection microscope. Because of the large number of formulations tested simultaneously, in this study, a novel experimental design was required. Whereas conventionally all replicates (usually ± 6) of all formulations would be tested simultaneously and the results statistically compared using hypothesis testing such as analysis of variance (ANOVA) (Bauer *et al.*, 2016a; Li *et al.*, 2016; Ederth *et al.*, 2019), in the present study four settlement experiments were run including two replicates of each formulation over the course of a month. The settlement data were then analysed using meta-analysis with subgroup analysis, which is a statistical procedure that integrates results from independent studies. The integrated settlement results were then further analysed using ANOVA and Tukey post-hoc analysis to reveal specific significant differences between formulations. Meta-analysis of barnacle settlement assays was performed in RStudio v.1.1.442 using metafor package v.1.9-9. To validate the meta-analysis approach for future studies, the single settlement experiment was also conducted and the settlement trends were found to be equivalent. These data are presented in Appendix E.

2.2.9 Attachment strength of juvenile barnacles

To achieve synchronous settlement of cyprids on the coatings, ASW (22 ppt) was modified by adding a settlement-inducing chemical, 1-isobutylmethylxanthine (IBMX, Sigma-Aldrich) to a concentration of 10^{-5} M (Clare *et al.*, 1995). Slides were put into quadriPERM[®] dishes, and a 2.5 mL droplet of 10^{-5} M IBMX in ASW was added on each surface, followed by addition of 50-100 fresh cyprids. Dishes were covered with wet towel and an aluminium foil and placed in an incubator for 72 h at 28 °C to allow cyprid settlement. After three days, slides were gently rinsed under tap water to remove any unsettled larvae and remaining juveniles enumerated. To each slide containing settled juveniles, ASW with a small amount of *T. suecica* was added and barnacles were allowed to grow for another three days. Removal of attached juveniles was performed using a calibrated flow cell at a wall shear stress of 81 Pa (Atlar, 2011). After the removal experiment, surfaces were carefully inspected using a dissection microscope and the number of remaining barnacles was enumerated.

2.2.10 Removal of diatom cells

Six replicate slides of each polymer set along with PDMS (Dow Corning 3-0213) standard were transferred to quadriPERM[®] dishes and 10 mL of *N. incerta* suspension was added to each well. Diatom cells were allowed to sink by gravity and settle on the surfaces. After approximately 2 h,

slides were gently rinsed in ASW, without exposing to the air, to remove any weakly attached cells. Three polymer replicate slides were fixed with 2.5% glutaraldehyde in filtered ASW for 15 min and subsequently washed in deionized water. This procedure was repeated three times, and the slides were then dried and stored. The remaining three slides were exposed to flow in a calibrated, fully turbulent, water channel (Schultz *et al.*, 2000) with a wall shear stress of 31 Pa for 5 min. After the removal experiment, slides were fixed in 2.5% glutaraldehyde, washed with deionized water, and air-dried. To determine the number of cells attached to the surface, 30 fields of view (0.17 mm^2) within the slide center were captured using an epifluorescence microscope (Leica DMI8 with Texas Red filter set) and the stored images were later used for cell enumeration. The percent removal, which is a proxy of diatom adhesion strength, was calculated by comparing the number of cells from unexposed control slides and the slides used in the removal experiment in the water channel.

2.2.11 Biofilm growth and release testing

In order to test the polymers against the multispecies biofilm, all polymers except polymer P-L10 were tested in a multispecies culturing reactor, or ‘slime farm’ (Longyear, 2014). In this system, coatings are challenged against marine biofilms developed under controlled, warm temperate conditions, with temperature set to $20 \pm 2 \text{ }^\circ\text{C}$, salinity $33 \pm 1 \text{ psu}$ and pH 8.2 ± 0.2 . Additionally, to compare the performance of prepared hydrophilic coatings to a silicone standard, PDMS (Dow Corning 3-0213) was also included in the testing. Three replicates of each polymer were used for testing and biofilm was allowed to grow on the surfaces for two weeks. Slides were then removed from the reactor, and the amount of biofilm growth was determined using a fluorescence plate reader (Tecan GENios Plus) with excitation and emission parameters set to 430 nm and 670 nm respectively (Finlay *et al.*, 2008a). Subsequently, the coatings were exposed to turbulent flow (8.2 Pa) in the calibrated water channel for 5 min, and the amount of remaining biomass was remeasured with the fluorescence plate reader directly after the removal experiment. The percent removal was calculated from the amount of biomass before and after exposure to flow.

2.3 Results

2.3.1 Sample preparation and characterization

^1H NMR experiments were carried out to determine the chemical compositions of polymer solutions, and in general there was a good agreement between the monomer feeds and the actual copolymer compositions (Table 2.3). The number average molecular weight (M_n) determined by SEC was between 13 kDa and 29 kDa. The PDI of polymers in the majority of cases ranged between 2.5 and

3.7; with the exception of polymer Z-L20, which presented bimodal distribution and had the PDI of 11.7. Glass-transition temperatures (T_g) of copolymers were in the range of 21 to 27 °C, with the exception of polymer M-L which had T_g of 42 °C, possibly attributable to the presence of the MAA monomer, which homopolymer has a T_g as high as 228 °C.

Sample	Monomer feed ratio		Amount of monomers in polymer (mol %)	M_n (kDa)	PDI (M_w/M_n)	$T_g \pm SD$ (°C)
	Hydrophobic monomer (mol %)	Hydrophilic monomer (mol %)				
H-0	100 n-BMA	0	100 n-BMA	14	2.7	20.9 \pm 0.3
E-L	57 n-BMA 33 IBoMA	10 mPEG350MA	54 n-BMA 34 IBoMA 12 mPEG350MA	29.2	1.8	26.9 \pm 1.3
H-L	90 n-BMA	10 HEMA	91 n-BMA 9 HEMA	15.8	2.6	21.3 \pm 1.3
G-L	90 n-BMA	10 DHPMA	90 n-BMA 10 DHPMA	17.4	2.5	23.9 \pm 0.1
M-L	90 n-BMA	10 MAA	91 n-BMA 9 MAA	13.7	2.8	41.5 \pm 0.8
Z-L	90 n-BMA	10 SBMA	93 n-BMA 7 SBMA	15.5	3.6	25.5 \pm 0.3
Z-L20	80 n-BMA	20 SBMA	93 n-BMA 7 SBMA	15.3	11.7	26 \pm 0.5
A-L	90 n-BMA	10 SPMA	92 n-BMA 8 SPMA	18.7	2.5	25.3 \pm 0.3
C-L	90 n-BMA	10 METAC	90 n-BMA 10 METAC	17.4	2.7	24.7 \pm 0.6
P-L10	90 n-BMA	5 SPMA 5 METAC	91 n-BMA 4 SPMA 5 METAC	22	1.8	22.5 \pm 0.8
P-L20	80 n-BMA	10 SPMA 10 METAC	82 n-BMA 9 SPMA 9 METAC	12.6	3.7	25 \pm 0.3

Table 2.3 Copolymer compositions and characteristic data for prepared polymers.

2.3.2 Wettability of polymers

The initial wettability of polymers and after six-week immersion in deionized water was determined using underwater contact angles of two water immiscible fluids, namely, air and silicone oil. On the basis of the contact angle measurements, SFE calculations of the fully hydrated and water-equilibrated polymers are presented in Table 2.4.

Sample	Angle inside air bubble (θ_m°)		Angle inside silicone oil (ϕ_m°)		Dispersive component γ_{pa}^d (mN·m ⁻¹)		Polar component γ_{pa}^p (mN·m ⁻¹)		Total surface energy (SFE) γ_{pa}^{TOT} (mN·m ⁻¹)		Interfacial energy (IFE) γ_{pw} (mN·m ⁻¹)	
	initial	6 wk	initial	6 wk	initial	6 wk	initial	6 wk	initial	6 wk	initial	6 wk
H-0	100 ±0.9	110.3 ±1.4	58.7 ±0.5	74.3 ±1.9	38.3 ±2.0	46.9 ±8.6	6.6 ±0.1	9.3 ±0.9	44.8 ±1.9	56.2 ±7.7	32.2 ±0.8	30.9 ±6
E-L	114.7 ±0.5	179.7 ±0.5	102 ±0.9	178 ±0.9	22.8 ±1	44.8 ±0.1	19.2 ±0.4	34.5 ±0	42 ±0.7	79.3 ±0	11.6 ±0.3	6.5 ±0
H-L	112.7 ±2.3	136 ±0.9	94 ±0.9	178.7 ±0.5	26.6 ±3.4	15.2 ±0.6	16.2 ±0.5	40.6 ±0.2	42.8 ±3	55.8 ±0.5	14.7 ±0.4	3.4 ±0.4
G-L	119.7 ±1.4	155.3 ±1.9	106.7 ±0.5	169.7 ±2.1	26.1 ±1.7	31.8 ±1.3	20.2 ±0.1	36.1 ±0.1	46.3 ±1.6	67.9 ±1.3	10.3 ±0.1	1.8 ±0.2
M-L	116.3 ±0.5	159.7 ±1.9	94.3 ±1.9	179 ±0.9	32.7 ±2.2	34.5 ±1.6	15.6 ±0.8	36.1 ±0.3	48.3 ±1.5	70.6 ±1.3	16 ±1.4	2.4 ±0.5
Z-L	149.7 ±1.1	179 ±0.9	148.3 ±0.5	179.7 ±0.5	34.9 ±1	44.7 ±0.1	31.8 ±0	34.5 ±0	66.7 ±0.9	79.2 ±0.1	3.9 ±0.3	6.4 ±0
Z-L20	157 ±0.9	178.7 ±0.5	167 ±0.9	178.7 ±0.5	34 ±0.6	44.7 ±0	35.4 ±0	34.5 ±0	69.4 ±0.6	79.2 ±0	2.4 ±0.1	6.4 ±0
A-L	151.3 ±1.1	179.7 ±0.5	149 ±0.9	179.7 ±0.5	36.5 ±1.9	44.7 ±0	31.7 ±0.5	34.5 ±0	68.3 ±1.4	79.2 ±0	4.4 ±0.7	6.5 ±0
C-L	149 ±1.6	179 ±0.9	133 ±1.8	178.7 ±0.5	49.7 ±5.6	44.7 ±0	25.8 ±1.1	34.5 ±0	75.5 ±4.5	79.2 ±0	13.2 ±3.5	6.4 ±0
P-L10	131.3 ±0.5	179.3 ±0.5	119.7 ±0.5	179.7 ±0.5	32.5 ±1.5	44.7 ±0	23.6 ±0.4	34.5 ±0	56.2 ±1.1	79.2 ±0	8.1 ±0.6	6.4 ±0
P-L20	138.3 ±1.1	177.7 ±1.4	138 ±0.9	157 ±1.8	27.6 ±1.4	53.7 ±1.4	30.2 ±0.4	31.3 ±0.5	57.9 ±1.1	85 ±1	3.5 ±0.3	12.3 ±1
PVC (substrate)	102.7 ±0.5	-	67 ±1.6	-	33.1 ±0.6	-	8.9 ±0.1	-	42.1 ±0.7	-	26.1 ±0	-

Table 2.4 Initial underwater measured angles within the air bubble (θ_m) and silicone oil (ϕ_m) and calculated surface energies of hydrated polymers together with results after six weeks of leaching in deionized water. Errors are 95% CIs.

2.3.3 Determination of swelling and water states in experimental polymers

DSC was applied to study water states inside the polymer matrix after six weeks of immersion in deionized water. DSC heating thermograms of swollen polymers are presented in Figure 2.1.

The swelling behaviour of polymers was directly measured using TGA and expressed as the equilibrium water content (EWC) (Figure 2.2A). Based on the DSC measurements and EWC values it was possible to calculate the mass of freezable and nonfreezable water relative to the mass of polymer (Figure 2.2B and 2.2C). The number of nonfreezable water molecules per repeating polymeric unit is given in Figure 2.2D.

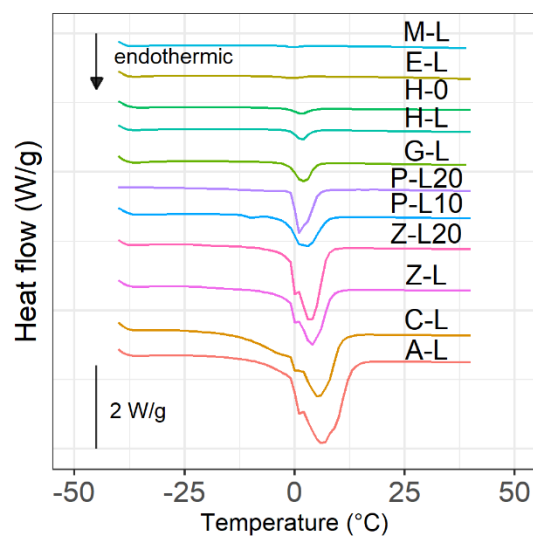


Figure 2.1 DSC thermograms at the heating rate of $10\text{ }^{\circ}\text{C}\cdot\text{min}^{-1}$ for copolymers of n-BMA with different hydrophilic functionalities.

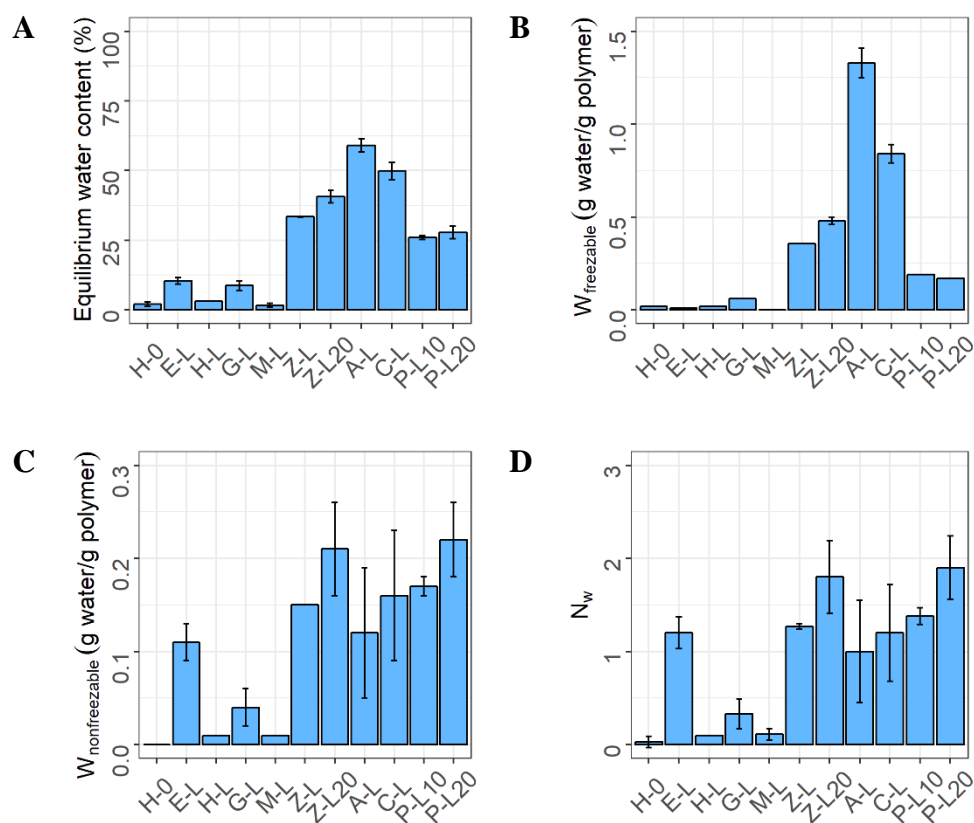


Figure 2.2 (A) EWC (%) in swollen polymers after six-week immersion in deionized water. (B) Mass ratio of freezable water to the mass of polymer ($W_{\text{freezable}}$). (C) Mass ratio of nonfreezable to the mass of polymer ($W_{\text{nonfreezable}}$). (D) Number of nonfreezable water molecules (N_w) per repeating copolymer unit. Error bars are 95% CIs.

2.3.4 Settlement and removal of barnacle cyprids

The results from four independent settlement experiments were synthesized using meta-analysis. A typical graphical representation of meta-analysis is a Forest plot. Figure 2.3 shows such a plot with calculated statistics: summary settlement effect size (ES) across relevant studies together with corresponding confidence intervals (CIs). The majority of the ionic polymers (Z-L, Z-L20, A-L, P-L10, P-L20) and nonionic polymer E-L presented negative values of ES, meaning that they received lower settlement than the polymer H-0, which was selected as the control. In the case of nonionic hydrophilic copolymers (H-L, G-L, M-L) and cationic polymer C-L, the ES was similar or only slightly higher than H-0, indicating no improvement in antifouling performance. The relatively wide confidence intervals suggest large heterogeneity (variability) in estimates of ESs. On the basis of the p-values associated with calculated Q-statistics, it was determined that in the majority of tested formulations the heterogeneity within the settlement results of a polymer set was statistically significant (in all relevant cases $p < 0.0001$ at $\alpha = 0.05$), with the exception of polymer H-0 (summary effect size was zero), C-L and polymers P-L10 and E-L (single settlement experiments, thus no between study variation). The computed I^2 index for the polymers with detected heterogeneity ranged from 84 to 97% suggesting that the main source of this variability was true heterogeneity between the settlement assays rather than sampling error. As each polymer set was fabricated in a similar manner, using the same polymer solution, the true variation among the ES of the polymers could be attributed to different populations of larvae used in settlement experiments. It is well known that different batches of larvae can vary in terms of their settlement responses (Holm, 1990). A mixed-effects model was fitted to the entire settlement data set with polymer and study as categorical moderators. With polymer as the only moderator in the model the amount of heterogeneity accounted for (R^2) was 57%, whereas with the inclusion of the study moderator the R^2 increased to 82%. Additionally, a Wald-type test with Knapp and Hartung adjustment (for better control of type I error) showed that the study moderator was indeed significant ($F_{3,22} = 9.779$, $p < 0.001$) clearly indicating that part of the variability in settlement results could be attributed to different batches of larvae used in experiments. A design incorporating multiple batches could therefore be considered advantageous (Guerin and Clare, 2019).

To assess the overall effect of charge on settlement of cyprids, a subgroup analysis based on the ionic/nonionic character of the polymer was performed. The results are presented at the bottom of Figure 2.3 as diamond symbols. Ionic polymers received lower settlement (ES = -23.05, 95% CI = -38.19, -7.9) than the nonionic ones (ES = 6.05, 95% CI = -8.19, 20.29), and the difference was highly significant (Wald-type test, $z = 2.743$, $p = 0.006$).

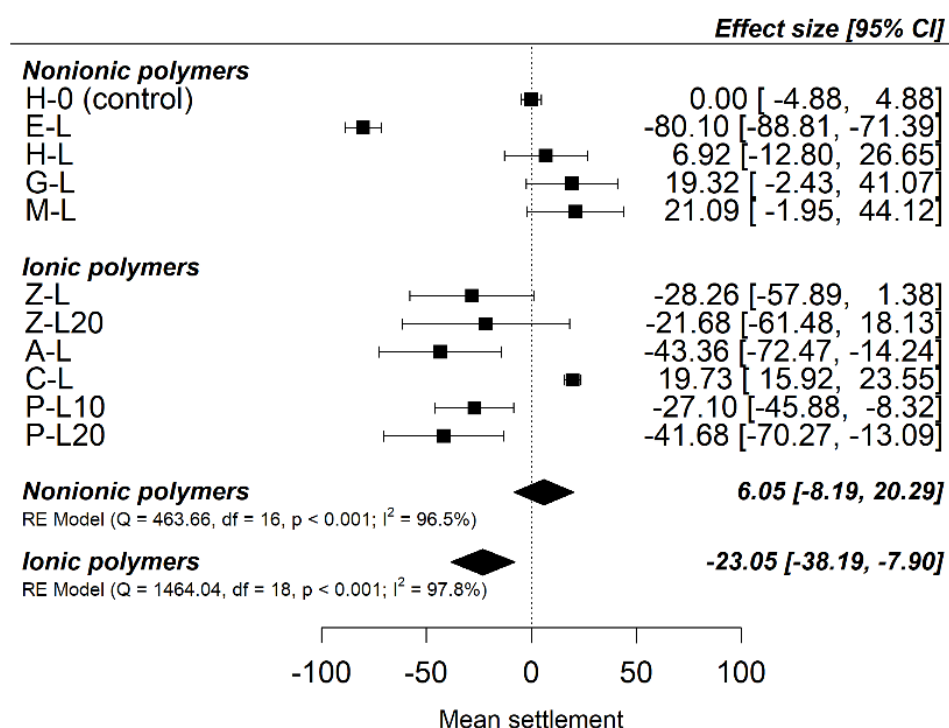


Figure 2.3 Forest plot of barnacle *B. improvisus* combined settlement with polymer H-0 selected as a control treatment. Individual points show summary effect sizes (raw mean differences) and 95% CIs. Vertical dotted line indicates effect size of zero and similar performance to polymer H-0. The effect sizes for the nonionic/ionic polymers together with corresponding statistics were generated using separate subgroup analysis.

In a barnacle removal experiment, differences in removal between polymers (Figure 2.4) were significant (one-way ANOVA $F_{10,33} = 28.73$, $p \leq 0.001$). The highest removal of barnacles was observed from polymers Z-L ($79.19 \pm 13.13\%$), A-L ($73.9 \pm 6.04\%$) and P-L20 ($69.18 \pm 6.03\%$) and this removal was found to be significantly higher than removal from other polymers that were tested (Tukey tests, $p \leq 0.001$).

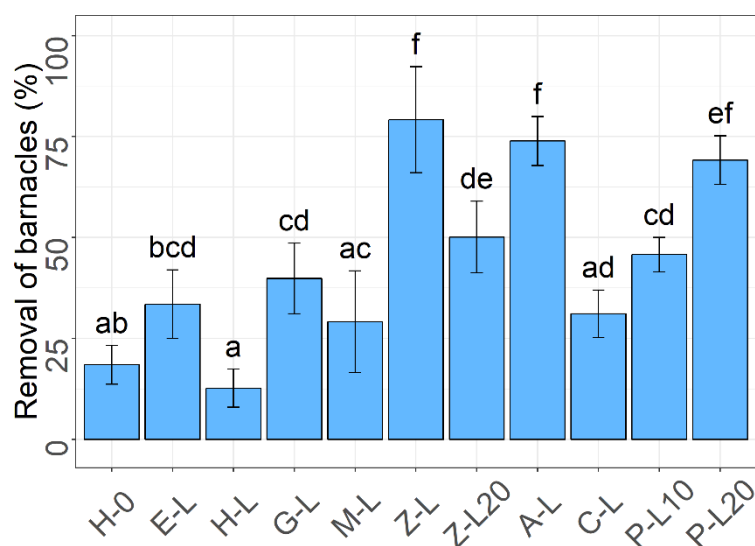


Figure 2.4 Mean removal of four-day-old juvenile barnacles, *B. improvisus*, together with corresponding 95% CIs. Each point represents the mean from four replicate slides. Letters indicate Tukey's pairwise comparisons and bars that do not share a letter are significantly different.

2.3.5 Attachment strength of the diatom, *N. incerta*, and a multispecies biofilm

Diatoms are slime-forming algae that, in an evaluation setting, reach the coating surface by gravity. Thus, the initial settlement density should be similar on all tested coatings. The number of cells removed from the surface can be used as a proxy of their adhesion strength. The coatings with attached cells were exposed to 31 Pa wall shear stress in a calibrated water channel, and the removal results are presented in Figure 2.5A. Removal varied significantly between surfaces (one-way ANOVA $F_{11,1140} = 74.19$, $p \leq 0.001$). Highest removal of diatoms was observed for anionic polymer A-L ($75.59 \pm 8.65\%$), and from zwitterionic polymers Z-L ($65.62 \pm 3.37\%$) and Z-L20 ($81.22 \pm 2.72\%$), with the removal from polymers A-L and Z-L20 being significantly different from other surfaces (Tukey tests, $p \leq 0.01$). In addition to the single cell assay, all polymers except polymer P-L10 were exposed in the slime farm to microbial colonisation and acquired multispecies biofilms. In order to determine the fouling-release properties of surfaces with attached multispecies biofilms, coatings were exposed to a wall shear stress of 8.2 Pa in the calibrated water channel. Percentage removal was calculated from the amount of biomass before and after exposure to flow (Figure 2.5B). The variation in removal was statistically significant (one-way ANOVA using square-root transformed data $F_{10,22} = 13.48$, $p \leq 0.001$). The highest removal was observed on polymer Z-L ($86.76 \pm 5.32\%$), followed by polymers A-L ($84.07 \pm 2.85\%$), C-L ($81.59 \pm 2.2\%$) and P-L20 ($83.27 \pm 3.39\%$). The removal of biofilm from nonionic polymers H-L, G-L and M-L did not differ significantly from PDMS standard

(Tukey tests, $p > 0.05$). Appendix F contains additional biofilm growth data and the amount of biomass left after the removal experiment.

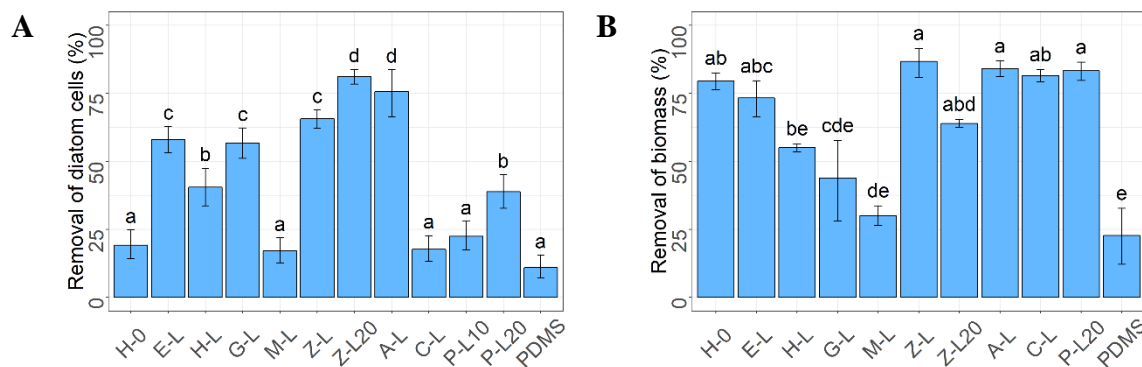


Figure 2.5 (A) Percent removal of *N. incerta* cells. Each point represents the mean from 90 counts on three replicate slides. Error bars are 95% CIs from arcsine transformed data. (B) Percentage removal of biomass. Each point represents the mean from three replicate slides. Error bars represent SEs of the mean. Letters indicate Tukey's pairwise comparisons and points that do not share a letter are significantly different.

2.4 Discussion

A range of commercially relevant, mechanically robust bulk copolymers were prepared by copolymerizing n-BMA with different hydrophilic comonomers with ionic and nonionic character. The molar amounts of hydrophilic comonomers in the feeds ranged between 0 and 20 mol% and in general there was a good agreement between the feeds and actual copolymer compositions as determined by ¹H NMR experiments (Table 2.3). The only exceptions were zwitterionic polymers Z-L and Z-L20 where a discrepancy between the initial composition of the reaction mixture and final copolymer composition was observed. This behaviour is not unusual for the n-BMA/SBMA pair of monomers and was reported in the past by Strehmel *et al.* (2006). Authors speculated that the difference in monomer polarities could affect the solvation of the growing macroradical with preferential incorporation of one of the monomers into the copolymer which could ultimately result in the compositional drift.

The wettability of polymers was determined using underwater contact angles (Table 2.4), as this technique gives better estimates of polar contributions than the advancing contact angle measurements in air because the functional groups are fully interacting with water (King *et al.*, 1982). Initially, ionic polymers presented significantly higher measured angles inside air/oil probing liquids θ_m/ϕ_m (which correspond to increased surface hydrophilicity) and total SFE (γ_{pa}^{TOT}) than the nonionic polymers. The higher wettability of ionic polymers could be explained by formation of strong ion-

dipole interactions between charged functional groups present at the polymer surface and surrounding water molecules. In the case of nonionic polymers, addition of neutral hydrophilic functionality did not show a marked effect on polymer wettability, presumably due to weaker hydrogen-bonding interactions with water which could not outcompete the significant dispersive component deriving from the hydrophobic n-BMA monomer. IFE (γ_{pw}) is said to play an important role in determining a polymer's effectiveness against adsorption of biomolecules (Andrade, 1973). Reduced IFE at the polymer/water interface should facilitate reversible adsorption processes and ultimately minimize fouling of the surface. Ionic polymers that presented high surface energy also had low interfacial energy with water, meaning that the polar regions of the polymer were fully interacting with water due to strong solvation of hydrophilic functionalities by water molecules.

Surface wettability of polymers was also evaluated after six weeks of immersion in deionized water (Table 2.4). The reason for testing the wettability after this time was to match the leaching time of the panels that were used in biological testing. Clearly, most of the polymers, including the nonionic ones, increased their SFE and lowered their IFE during immersion in water. Increased wettability of ionic polymers Z-L, Z-L20, A-L, C-L, P-L10, P-L20 and nonionic polymers E-L (having PEG functionality) and G-L (having two hydroxy groups) could be explained by increased chain mobility in the swelled polymer matrix that facilitates rearrangement of the functional groups toward the surface and interacts more effectively with water molecules. With regard to nonionic polymers such as H-0 and H-L, the changes in surface wettability can be explained by the plasticizing effect of a small amount of water absorbed in the polymer matrix. In the case of polymer H-0, the plasticizing effect of water was expressed by the reduction of IFE and reduction of its glass transition temperature from 21 °C to 15 °C (no such effect was observed with other tested polymers). Such a drop in T_g implies a change in mechanical state of polymer chains from plastic to rubbery, which facilitate backbone chain reorientations and side-chain relaxations that would help reduce IFE polymer/water (Hogt *et al.*, 1985; Grohens *et al.*, 2003). In the case of polymer M-L, the increase in wettability cannot be exclusively explained by swelling as the EWC in this polymer is low (EWC 1.7%), and it is necessary to relate this drastic change in wettability to the pK_a value of MAA comonomer. The pK_a value of MAA is 4.83, indicating that in deionized water ($pH \approx 7$) the majority of acid groups are deprotonated and the leached copolymer should have an anionic character capable of attracting more water molecules through electrostatic interactions, leading to higher underwater contact angles.

In order to further study the hydration characteristics of polymers after prolonged immersion in water, contact angle measurements were accompanied by swelling experiments and determination of different forms of water present in the swollen polymer. On the basis of structure and interaction of

water molecules with polymer chains, the water in the polymer matrix can be classified as nonfreezable, freezable bound water and free water. A commonly used tool to conduct water state studies is the DSC as it can reveal phase transitions such as melting of the freezable water inside the polymer. In the case of ionic polymers, the endothermic peaks seen on the thermograms are relatively broad and start below 0 °C (Figure 2.1), indicating high water content and existence of both free and freezable type of water (Ping *et al.*, 2001). This was further confirmed by calculating the mass of freezable water relative to that of the polymer $W_{\text{freezable}}$ (Figure 2.2B), which was much higher for ionic polymers, suggesting that these polymers are much more effective in accommodating water than the non-ionic polymers. In the case of polymer E-L, containing mPEG350MA monomer, the endothermic peak was negligible and corresponded to a weight percent of freezable water of around 0.5%. This observation corresponds with that of Yamauchi and Tamai (2003) who failed to find freezable water in PEG500 homopolymer.

Nonfreezable water is strongly bound to the polymer matrix and does not show thermal transitions in DSC experiments, even when cooled down to -100 °C (Tanaka and Mochizuki, 2004). Figure 2.2C, D presents the calculated ratios of the mass of nonfreezable water relative to that of the polymer and number of nonfreezable molecules around each polymeric unit. As in the case of $W_{\text{freezable}}$, ionic polymers show significantly higher $W_{\text{nonfreezable}}$ and N_w values than the non-ionic polymers, with the exception of polymer E-L. The $W_{\text{nonfreezable}}$ values for ionic polymers range between 0.12 g H₂O/g polymer for anionic polymer A-L and 0.22 g H₂O/g polymer for amphiphilic polymer P-L20. With regard to zwitterionic polymers Z-L and Z-L20, bearing the SB group, the $W_{\text{nonfreezable}}$ values were 0.15 g H₂O/g polymer and 0.21 g H₂O/g polymer respectively. These values correspond to calculated N_w values of 1.24 for polymer Z-L and 1.8 for polymer Z-L20. Wu *et al.* (2017) prepared various HEMA-SBMA hydrogels and a hydrogel with 10 mol% SBMA loading had $W_{\text{nonfreezable}}$ value of around 0.25 g H₂O/g polymer and N_w of around 2.5, which is higher than results obtained for our polymer Z-L. Furthermore, when comparing the EWC, $W_{\text{freezable}}$ and $W_{\text{nonfreezable}}$ results for our zwitterionic polymer with the hydrogel HEMA-SBMA system from Wu *et al.* (2017) it seems likely that (1) it is mainly the zwitterionic SBMA that is responsible for the presence of nonfreezable water in these polymers, and (2) the differences in EWC and $W_{\text{freezable}}$ in both systems are due to usage of different comonomers, with HEMA being capable of accommodating more freezable water than the n-BMA monomer. The N_w values obtained here and by Wu *et al.* (2017) for copolymers containing zwitterionic SBMA are significantly lower than for SBMA homopolymer where the number of nonfreezable molecules calculated from enthalpy changes of freezable water was between 5.85 – 6.79 (Wu *et al.*, 2012). The lower saturation of SB units with water molecules in Z-L copolymer could be

potentially explained by the hydrophobic effect deriving from the n-BMA monomer. The hydrophobic n-BMA prevents the copolymer from swelling to a similar degree as free SBMA homopolymer, and with the additional high chain entanglement/crowding the infiltration of copolymer by water molecules is reduced ultimately limiting the SB-water interactions.

While the majority of nonionic, hydrophilic copolymers tested did not show indications of nonfreezable water, the polymer E-L with PEG functionality presented high $W_{\text{nonfreezable}}$ and N_w values, 0.11 g H₂O/g polymer and 1.24 respectively, comparable to the polymers bearing ionic functionalities. The majority of bound water molecules in this polymer were in the form of nonfreezable water, which could be attributed to the presence of hydrogen bonding. The number of nonfreezable water molecules around one polymeric unit in polymer E-L was significantly lower ($N_w = 1.24$) than in PEG500 homopolymer with $N_w \approx 9$ (Yamauchi and Tamai, 2003). As in the case of zwitterionic polymers, the reduction in the number of water molecules per repeating unit of PEG in the copolymer in comparison to its homopolymer could be attributed to presence of n-BMA and IBoMA units, which limit swelling, increase chain entanglement/crowding, and reduce the availability of PEG groups to water.

The polymers were tested in the laboratory for their antifouling resistance against cyprids of *B. improvisus* (Figure 2.3). In general, ionic polymers attracted a smaller number of cyprids than the nonionic ones. Settlement was lowest on ionic polymers Z-L, Z-L20, A-L, P-L10, P-L20 and the nonionic polymer E-L containing PEG functionality. The low cyprid settlement recorded for copolymers containing zwitterions and PEG accords with earlier observations by (Yandi *et al.*, 2016) who prepared various polymer brushes including a homopolymer of SBMA and a copolymer of pHEMA-*co*-PEG₁₀MA and found that the barnacle settlement on these surfaces after 48 h was lowest of all surfaces tested. However, in contrast to the studies by Yandi *et al.* (2016), where the SPMA homopolymer attracted the highest settlement of *B. improvisus* cyprids, in our study polymer A-L presented very high resistance. The reason for this could be that the limited amount of SPMA in the copolymer induces surface hydration through sulfonate groups without increasing the overall magnitude of the surface charge. As for the positively charged polymer C-L (containing METAC functionality), contradictory results obtained with a single settlement experiment (Appendix E, Figure E.2A) and four experiments combined with meta-analysis (Figure E.2B) are likely a result of interbatch variability of larvae used in the experiments and, if so, vindicate the batch-averaging effect of the meta-analysis design. The settlement experiments were also accompanied by the removal of settled, four-day-old juveniles (Figure 2.4). The highest release of barnacles was recorded on zwitterionic (Z-L), anionic (A-L) and amphiphilic (P-L20) polymers.

Polymers were also tested for their fouling-release properties with the diatom *N. incerta* (Figure 2.5A). The highest release rate, which exceeded 65%, was on the zwitterionic polymers Z-L, Z-L20 and anionic polymer A-L. This performance was comparable to that of the highly effective Intersleek® 1100SR FRC (Benschop *et al.*, 2018; Guerin and Clare, 2019). The high removal of *N. incerta* cells from the polymers containing a zwitterionic moiety is in line with work by Bauer *et al.* (2016b) who also found low attachment strength to a sulfobetaine SAM, and hypothesized that not only the presence of charge but also additional contribution of hydrogen bonding affects surface hydration and hinders potential surface/bioadhesive interactions. Diatoms are known for their high tenacity to hydrophobic surfaces such as PDMS (Holland *et al.*, 2004), thus it was interesting to see no significant difference in removal between PDMS and hydrophilic polymers such as polymer C-L and P-L10 (Tukey tests, $p > 0.05$). As these surfaces composed of the cationic METAC moiety, it can be hypothesized that the positive charge or potentially unbalanced positive charge on polyampholyte surfaces can increase the adhesion strength of diatoms. Additionally, surfaces were exposed to colonisation by multispecies biofilms. In general, the majority of prepared polymers presented significantly lower amounts of biomass when compared to hydrophobic PDMS (Appendix F, Figure F.1), which could be attributed to the weaker initial attachment strength of biofilm to the hydrophilic surfaces. The removal experiment of the attached biofilm further confirmed the slime-release properties of polymers containing zwitterionic or anionic moieties.

In general, the lower settlement of barnacles on ionic polymers could be related to the presence of nonfreezable water molecules at the hydrated polymer surface. Aldred *et al.* (2010a) speculated that inhibition of settlement on zwitterionic materials could result from such a tightly bound water layer. The presence of this layer could weaken the intramolecular forces between the cyprid's adhesive disk and the surface, limiting exploratory behaviour of cyprids and ultimately preventing permanent cyprid settlement. On the basis of our settlement results and earlier calculations of number of nonfreezable water molecules in the polymer, it can be hypothesized that just a single water molecule around each polymeric unit is sufficient to achieve high fouling resistance against barnacles. Moreover, the fouling-release properties of zwitterionic and anionic polymers could be potentially attributed to the high degree of swelling that affects the conformational freedom and viscoelastic properties of the polymer chains. With regard to nonionic polymers only polymer E-L presented very good AF performance (comparable to best performing ionic polymers Z-L, Z-L20 and A-L), which again could be attributed to presence of nonfreezable water in the polymer structure. The high effectiveness of polymer E-L in comparison to that of other nonionic polymers can be also potentially attributed to

the lack of hydrogen bond donors fulfilling thus one of the postulates formulated by Ostuni *et al.* (2001a) concerning the development of low fouling surfaces.

To summarise, the presented data suggest that different hydrophilic chemistries can be incorporated into bulk coatings in relatively low amounts (10-20 mol%) and that the putative mechanism of fouling prevention, based on the existence of a tightly bound water layer, remains the same as in the laboratory model systems tested to date. The laboratory assays with barnacles of *B. improvisus*, cells of *N. incerta* and multispecies biofilm revealed that the best performing polymers were those based on the zwitterionic SBMA and anionic SPMA. The fact that these polymers are resistant towards both barnacles and diatoms/slime is very unusual and shows potential route to translation of these hydrophilic chemistries into practical, industrially relevant coating formulations.

Chapter 3. Analysis of the settlement behaviour of barnacle cyprids, *Balanus improvisus*, on different hydrophilic polymer brushes

3.1 Introduction

For informed development of next-generation, eco-friendly, fouling-resistant coatings that discourage marine invertebrates from colonising surfaces, it is important to first understand settlement behaviour and larval adhesion (Callow and Callow, 2011). Unfortunately, our understanding of natural adhesion phenomena is rather limited and includes investigations mainly on large, adult organisms such as spiders (Sahni *et al.*, 2011), geckos (Zhou *et al.*, 2013), and some marine invertebrates like mussels (Waite, 2017), tubeworms (Stewart *et al.*, 2004) and barnacles (Kamino, 2013). Smaller organisms like barnacle larvae or diatoms are more challenging to investigate due to their scale, small quantities of secreted adhesives, and considerable speed of behaviours (Aldred and Clare, 2008).

The cyprid is a highly selective larva that uses a pair of specialized organs called antennules to explore potential settlement locations. Surfaces must fulfil various criteria, which vary with species, but include physicochemical properties of the surface, presence of a biofilm, proximity to potential mates and hydrodynamic conditions. Once cyprids encounter a suitable settlement site they engage in three phases of exploratory behaviour (Crisp, 1976), which can be described as (1) wide search, (2) close search and (3) inspection. During wide and close search cyprids attach reversibly and ‘walk’ across surfaces using a temporary adhesion mechanism, leaving behind the proteinaceous adhesive (footprint) secreted onto the attachment disc of the antennule (Aldred *et al.*, 2013). Using scanning electron microscopy, Nott (1969) revealed that the surface of each attachment disc is covered with cuticular villi (“hairs”) and it was speculated by Phang *et al.* (2008) that their role may be to increase adhesion by contact splitting, although no evidence to support this hypothesis has been provided. In addition, Aldred *et al.* (2013) observed that during stress-induced peeling the villi acted as a mechanical buffer between the surface and 3rd segment of the antennular disc, absorbing the applied stress and reducing the lateral slip, which could be advantageous in the turbulent marine environment (Koehl, 2007).

The exact role of the cyprid’s temporary adhesive is not completely understood and remains a subject of investigation. The first evidence of the existence of cyprid temporary adhesive was provided by Walker and Yule (1984), who visualized the deposited footprints on silanized glass surfaces after cyprid exploration. Phang *et al.* (2008) used atomic force microscopy (AFM) measurements to study cyprid footprints and found that the deposits were indeed sticky. Aldred and Clare (2008) suggested

that the temporary adhesive could also displace water from the surface further enhancing the adhesive interactions. It was also demonstrated that footprints act as pheromone and induce cyprids to settle gregariously, thus promoting cross-fertilization (Yule and Walker, 1987; Clare *et al.*, 1994). Cyprid temporary adhesive is a proteinaceous material, however its composition is relatively poorly characterized. It has been shown by Dreanno *et al.* (2006) that the cyprid footprint contains a significant quantity of a cuticular α_2 -macroglobulin-like protein called the settlement-inducing protein complex (SIPC). This glycoprotein was found to induce gregarious settlement (Matsumura *et al.*, 1998; Clare and Matsumura, 2000), while Petrone *et al.* (2015) revealed that SIPC molecule is 'sticky' in nature, and suggested that it could be involved in the process of temporary adhesion.

The investigation of adhesion processes for microscopic marine organisms 'in-situ', in real time, is a difficult task and requires a combination of techniques. One of the methods commonly employed to understand larval behaviour is video tracking (Aldred *et al.*, 2010a; Maleschlijski *et al.*, 2012; Maleschlijski *et al.*, 2015). Until recently its usefulness was limited mainly to recording the location of larvae and it provided little information on broader behavioural patterns. The development of a novel, automated, tracking and classification system by Alsaab *et al.* (2017) enabled detailed analysis of pre-settlement behaviour of cyprids, i.e., wide search, close search and inspection, which are believed to be important in decision making of settling cyprids. While tracking provides valuable information on cyprid behaviour in "macroscale", it does not provide any information on the "microscale" events taking place during cyprid surface exploration. Imaging surface plasmon resonance (iSPR) is a surface sensitive technique which combines the conventional and imaging SPR methods (Andersson *et al.*, 2009) offering a unique ability to visualize bioadhesion events in-situ and to quantify the amount of deposited footprint, which could in turn help to make broad assumptions about the stickiness of the adhesive to different surfaces (Aldred *et al.*, 2011).

In this chapter the settlement behaviour of barnacle cyprids, *B. improvisus*, was studied on various hydrophilic polymer brushes. Hydrophilic chemistries were selected on the basis of the antifouling (AF) performance of bulk polymers presented in the previous chapter. The surfaces were prepared on glass slides using a 'grafting-from' approach, and polymers on gold were prepared with a 'grafting-to' method. The reason for manufacturing the surfaces on gold and glass using two different techniques was the difficulty in obtaining stable polymer films on gold with the grafting-from method. Still, several attempts were made to synthesize polymers from gold surfaces using the grafting-from approach. In order to confirm successful grafting of polymers to surfaces, various sensitive techniques for surface characterisation were used, such as X-ray photoelectron spectroscopy (XPS), X-ray reflectivity (XRR), infrared reflection-absorption spectroscopy (IRAS) and ellipsometry.

To determine the response of cyprids towards the polymer brushes, settlement assays were conducted supported by video tracking and iSPR experiments. It was anticipated that the results obtained would increase our understanding of the settlement behaviour of cyprids and guide the development of novel surfaces that will resist fouling, not only by barnacles, but also by other marine fouling organisms.

3.2 Materials and methods

3.2.1 Materials

N-(2-methacryloyloxyethyl)-N,N-dimethyl-N-(3-sulfopropyl)ammoniumbetaine (SBMA) was supplied by Raschig GmbH under trade name Ralumer SPE. 3-Sulfopropyl methacrylate potassium salt (SPMA, 98%), 2-(methacryloyloxy)ethyltrimethylammonium chloride (METAC) (80% in H₂O), isobornyl methacrylate (IBoMA), (3-aminopropyl)-triethoxysilane (APTES), 4-cyano-4-(phenylcarbonothioylthio)pentanoic acid N-succinimidyl ester (CPSE), 4-cyano-4-(phenylcarbonothioylthio)pentanoic acid (CPAD), azobisisobutyronitrile (AIBN), 1-butanol (BuOH), triethylamine (TEA), aluminium oxide (Al₂O₃), potassium carbonate (K₂CO₃), anhydrous tetrahydrofuran (THF) and (3-aminopropyl)trimethoxysilane (APTMS) were purchased from Sigma-Aldrich. Methoxy PEG methacrylate (mPEG350MA) was supplied by GEO Speciality Chemicals. n-Butyl methacrylate (n-BMA, 99%) was obtained from Acros Organics. (3-Mercaptopropyl)trimethoxysilane (MPS), methanol (MeOH), anhydrous MeOH, dichloromethane (DCM), tetrahydrofuran (THF), isopropanol (IPA), toluene and ethylene glycol (EG) were purchased from Fisher Scientific. Dimethylformamide (DMF) was supplied by Rathburn Chemicals. DCM was dried over 3 Å molecular sieves and stored under an Argon (Ar) atmosphere. Hexafluoroisopropanol (HFIP) was purchased from Fluorochem. TEA was refluxed over CaH₂, distilled and kept over 3 Å sieves under Ar protection. Prior to running polymerizations, inhibitor was removed from n-BMA, IBoMA, mPEG350MA and METAC by passing the monomers through a Büchner funnel containing Al₂O₃ and K₂CO₃. All other materials were used as supplied. Glass slides were obtained from Fisher Scientific and tracking tubes were purchased from Cambridge Glassblowing, UK.

3.2.2 Preparation of polymer brushes on glass substrates using grafting-from approach (SI-RAFT)

Polymer brushes on glass were prepared using a grafting-from technique (SI-RAFT), according to the method of Gurbuz *et al.* (2011). A schematic illustration of the polymerization procedure, together with lists of monomers used for specific polymer preparation, is presented in Figure 3.1. Typically, glass slides were first sonicated in IPA three times for 15 min, then subjected to oxygen plasma for

15 min. Immediately afterwards, slides were transferred to 1% v/v solution of APTES in toluene and kept there under stirring for 1 h. Slides were then washed and sonicated in toluene for 15 min, dried under stream of N₂ and eventually annealed in the oven for 20 min at 110 °C. Once cooled, the silanized glass slides were transferred to a staining dish with magnetic stirrer, and then CPSE was added (0.255 g, 0.677 mmol), which readily dissolved in anhydrous DCM (120 mL). Finally, anhydrous TEA (113 µL) was added under N₂ protection. After 18 h, slides were removed from the solution, cleaned with DCM and dried under a stream of N₂.

The glass substrates functionalized with CPSE were used for subsequent RAFT polymerization using the following reagent ratio [M]:[CPAD]:[I] = 1500:5:1. The following procedure concerns the preparation of polymer brush Z-L (pBMA-*co*-SBMA_{10mol%}). To a glass reactor holding slides with immobilized CPSE and equipped with magnetic stirrer, SBMA (14.58 g, 52.2 mmol) was added and dissolved in EG (50 mL) after sonication. Next, BuOH (250 mL) was added, followed by addition of inhibitor-free n-BMA (66.8 g, 470 mmol), 1 mL solution of AIBN in DMF (57 mg/mL, 0.347 mmol) and CPAD (0.483 g, 1.73 mmol). After mixing the reagents, the reactor was kept in an ice bath and degassed by bubbling with Ar for 5 h. Subsequently, the reactor was placed in a preheated oil bath fitted with a mechanical stirrer and polymerization was run for 18 h at 70 °C under constant Ar flow. The next day, the reaction was quenched and immediately subjected to atmospheric air to terminate polymerization. Slides were then cleaned in DCM and dried under a flow of N₂. The remaining polymer solutions were dialysed once in a mixture of MeOH and DCM (1:1) and twice in MeOH and DCM (1:2).

For tracking experiments, open quartz glass tubes 30 mm long x 12.6 mm inner diameter were cleaned for 30 min in piranha solution (caution: piranha solution reacts violently with organic materials and should be handled carefully!) and after washing several times with DIW (Milli-Q water, ≥ 18.2 M Ω ·cm, Merck Millipore), and once in IPA, tubes were blow-dried with N₂. Subsequently, the tubes were put in vials containing a 1% v/v solution of APTES in toluene for 1 h. Next, tubes were rinsed with toluene several times and annealed in the oven at 110 °C for 20 min. After cooling, the tubes were transferred to vials containing a solution of CPSE (0.043 g, 0.113 mmol) in DCM (20 mL) and then immediately 19 µL of anhydrous TEA was added. After 18 h, the functionalized tubes were rinsed with DCM and dried with N₂.

The tracking tube grafted with polymer brush was prepared in the following manner. To the Schlenk reaction flask equipped with a PTFE O-ring holder and magnetic stirrer, SBMA (0.243 g, 0.87 mmol) was added and dissolved in EG (1.5 mL) after sonication, followed by addition of BuOH (7.5 mL), inhibitor-free n-BMA (1.245 g \approx 1.11 g, 7.83 mmol), 805 µL solution of CPAD in DMF (10

mg/mL, 0.029 mmol) and 95 μ L solution of AIBN in DMF (10 mg/mL, 0.0067 mmol). Subsequently, the tube with immobilized CPSE was carefully deposited within the Schlenk flask with the reaction mixture. The flask was sealed and rapidly degassed five times using vacuum/backfill cycles (Ar backfill) before immersing the flask in the preheated oil bath at 70 °C. The reaction was allowed to proceed for 18 h, and the next day the flask was quickly quenched and opened to air to terminate the reaction. The tracking tube was cleaned in DCM and blow-dried with N₂. The remaining polymer solution was dialysed once using a mixture of MeOH and DCM (1:1) and twice with MeOH and DCM (1:2).

Detailed descriptions of polymerization procedures for other polymers are available in Appendix G.

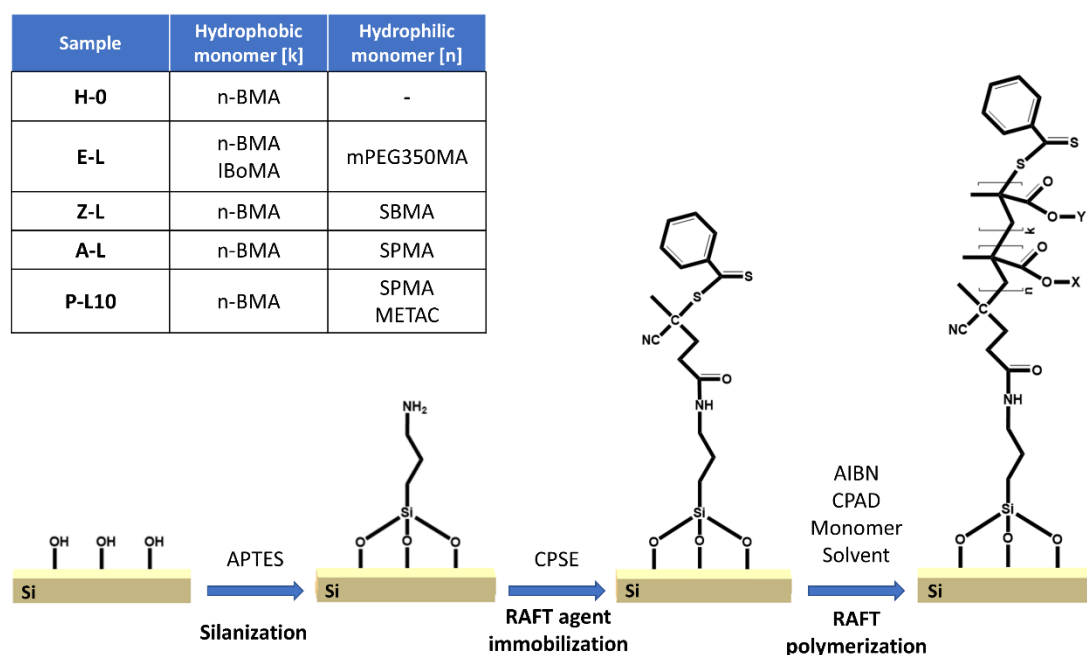


Figure 3.1 Schematic illustration of preparation of polymer brushes on glass using grafting-from approach. The inset table presents the monomers used in the synthesis of specific polymers.

3.2.3 Direct grafting of polymers to gold using a grafting-to approach

In order to attach polymers to gold, a grafting-to procedure was conducted (Figure 3.2) as described by Duwez *et al.* (2006). These surfaces were used in the iSPR experiments.

Briefly, polymer solutions remaining after the grafting-from procedure were dried and then dissolved in DCM (H-0, E-L) or HFIP (Z-L, A-L, P-L10) to a concentration of 3 mM. Subsequently, the gold substrates were cleaned in oxygen plasma for 10 min and then immediately immersed for 24 h in the

polymer solutions under magnetic stirring. Finally, the functionalized gold slides were thoroughly rinsed with DCM and blow-dried with N₂.

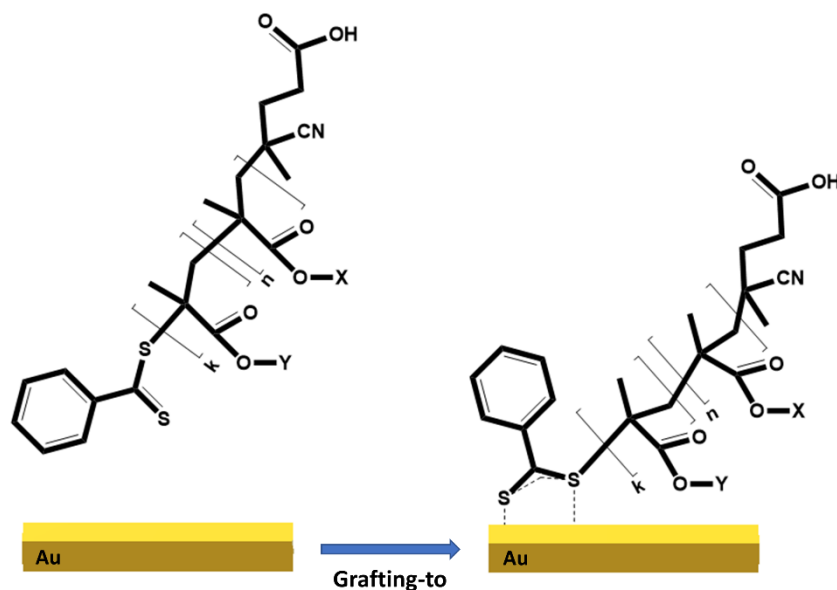


Figure 3.2 Schematic illustration of preparation of polymer brushes on gold using a grafting-to approach.

3.2.4 Preparation of polymer brushes on gold substrates using SI-RAFT from a chemisorbed CPAD SAM

This approach was presented by Catli (2016) who immobilized various RAFT reagents on gold through self-assembly and subsequently, successfully grafted various methacrylate polymers. The schematic illustration of preparation of polymer brushes on gold using grafting-from approach using chemisorbed CPAD is presented on Figure 3.3.

First, the gold slide was sonicated in DIW and EtOH for 15 min, dried under stream of N₂, treated with oxygen plasma for 10 min and then immediately transferred to a flask containing a 1 mM solution of CPAD in anhydrous THF, under N₂ atmosphere for 24 h, to form the CPAD initiator SAM. After immobilization, the gold slide was washed thoroughly with THF and EtOH and dried under a stream of N₂.

The CPAD functionalized gold slide was transferred to the main Schlenk reaction flask, which was equipped with PTFE O-ring holder, and a magnetic stirrer, and the flask was sealed with a rubber septum and exposed to five evacuation-N₂ cycles before being left under constant flow of N₂. In the second flask the SBMA (0.608 g, 2.18 mmol) was dissolved with EG (3.75 mL) after sonication, followed by addition of BuOH (18.75 mL), n-BMA (3.11 mL \approx 2.78 g, 19.55 mmol), CPAD (0.02 g,

0.072 mmol) and 1 mL solution of AIBN in DMF (2.38 mg/mL, 0.014 mmol). The reaction mixture was subjected to five freeze-pump-thaw cycles and then transferred via cannula to the main reaction flask, which was then put into a 70 °C oil bath for 18 h. The next morning, the flask was rapidly quenched and opened to air to terminate the reaction. Other experimental designs with varying reagent ratio $[M]:[CPAD]:[I]$ in the feed, polymerization time and temperature were also tested and a summary of these trials is presented in Table 3.4.

The gold slide was cleaned with DCM and EtOH and blow-dried with N₂. The remaining polymer solution was dialysed three times using a mixture of MeOH and DCM (1:2), and subsequently submitted for NMR and SEC analysis.

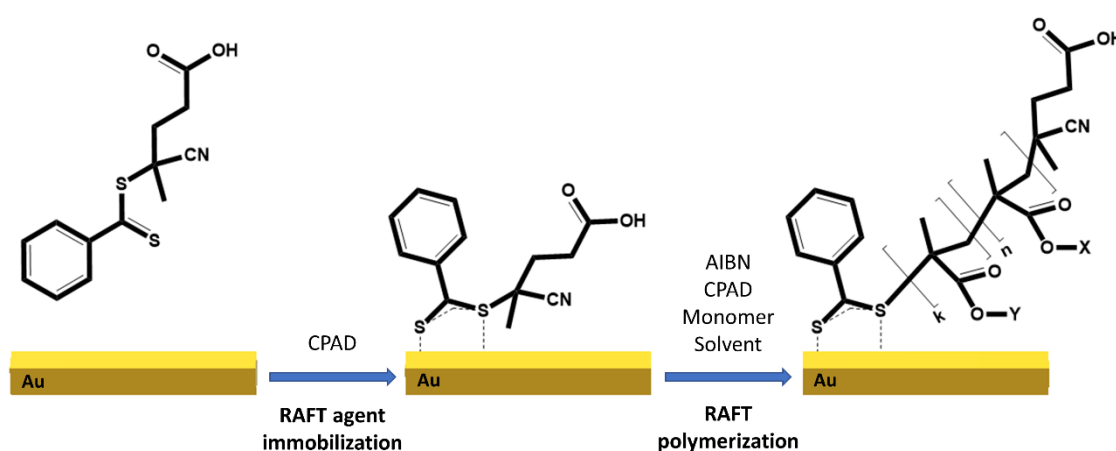


Figure 3.3 Schematic illustration of preparation of polymer brushes on gold using grafting-from approach using chemisorbed CPAD.

3.2.5 Preparation of polymer brushes on gold substrates using SI-RAFT from a stabilized gold surface

This procedure was first proposed by Huang *et al.* (2001) who prepared thick polystyrene films on gold at elevated temperatures using cross-linked initiators. Based on this approach, Saha *et al.* (2011) successfully grafted polymer brushes of poly(methyl methacrylate), poly(styrene), and poly(vinyl pyridine) using surface-initiated atom transfer radical polymerization (SI-ATRP). In a similar way, Liu *et al.* (2012) grafted N-vinylpyrrolidone using SI-ATRP, and showed that the polymer brush remained thermally stable for several hours at 130 °C. Based on the above reports, two attempts were made to prepare the hydrophilic copolymer brushes from stabilized gold substrates using SI-RAFT (Figure 3.4).

The gold substrates were first sonicated in DIW and EtOH for 15 min, blow dried with N₂ and then exposed to oxygen plasma for 20 min. Subsequently, surfaces were transferred to 2 mM or 5 mM anhydrous methanolic solutions of MPS for 24 h at room temperature to form a silane-terminated SAM. Such modified gold surfaces were then subjected to different silanization treatments.

In a first attempt, the gold substrate with 5 mM MPS SAM was immersed for 24 h in a 5% v/v solution of APTMS in a mixture of DIW and EtOH (5:95 v/v %). Next, the surface was cleaned extensively and sonicated in EtOH, toluene and acetone for 5 min, and then kept in the oven at 52°C for 5 h. The APTMS-functionalized surface was then transferred to a vial containing a solution of CPSE (0.043 g, 0.113 mmol) in anhydrous THF (20 mL) and then 19 µL of anhydrous TEA was added immediately. Vials were purged with N₂, sealed tightly and kept in the dark for 17 h. The next day, the colour of the solution containing CPSE changed from deep pink to pale yellow, implying the loss of the dithioester functionality, which could be attributed to the aminolysis reaction triggered by the remaining, loosely attached APTMS. This undesired process of end-group removal of RAFT moiety yielded thiols and disulfides that prevented successful RAFT polymerization (data not presented).

In the second attempt, the gold substrate with 2 mM MPS SAM was exposed to 0.1 M HCl for 24 h to form a cross-linked hydroxylated surface. After cleaning the surface with deionized water and drying under stream of N₂, it was immersed in a 1% v/v solution of APTES in toluene for 1 h to form an amino-terminated surface. Next, the gold substrate was rinsed with toluene several times and annealed in the oven at 110 °C for 20 min. After cooling, the slide was transferred to a vial containing solution of CPSE (0.043 g, 0.113 mmol) in anhydrous THF (20 mL) and then immediately 19 µL of anhydrous TEA was added. Vials were then purged with N₂, tightly sealed and kept in the dark for 17 h. The next day, the colour of the RAFT solution remained deep pink suggesting that this time aminolysis did not take place. After this step the gold substrate was washed with DCM and dried with N₂.

Grafting of the polymer brush from the gold substrate was conducted using a reagent ratio of [M]:[CPAD]:[I] = 2200:5:1 in the following manner. Firstly, the gold coverslip with immobilized CPSE was carefully deposited within a Schlenk reaction flask equipped with PTFE O-ring holder, magnetic stirrer and the flask was vacuum/backfilled with N₂ five times. In a second Schlenk flask, SBMA (0.796 g, 2.85 mmol) was dissolved in 3.4 mL of EG after sonication and then the first volume of BuOH (11 mL) was added. Next the inhibitor-free n-BMA (4.082 mL \approx 3.65 g, 26 mmol) was added, followed by addition of CPAD (0.018 g, 0.065 mmol), BuOH (6 mL) and 213 µL solution of AIBN in DMF (10 mg/mL, 0.013 mmol). This mixture was then degassed using five freeze-pump-thaw cycles and the flask was refilled with N₂. The solution was then transferred using a N₂ filled

syringe to the main reaction flask, which was rapidly vacuum/backfilled with N₂. The reaction flask was immersed in oil bath at 70 °C for 14 h. The next morning, the flask was rapidly quenched and opened to air to terminate the reaction. The gold slide was cleaned in DCM and blow-dried with N₂. The remaining polymer solution was dialysed three times using a mixture of MeOH and DCM (1:2).

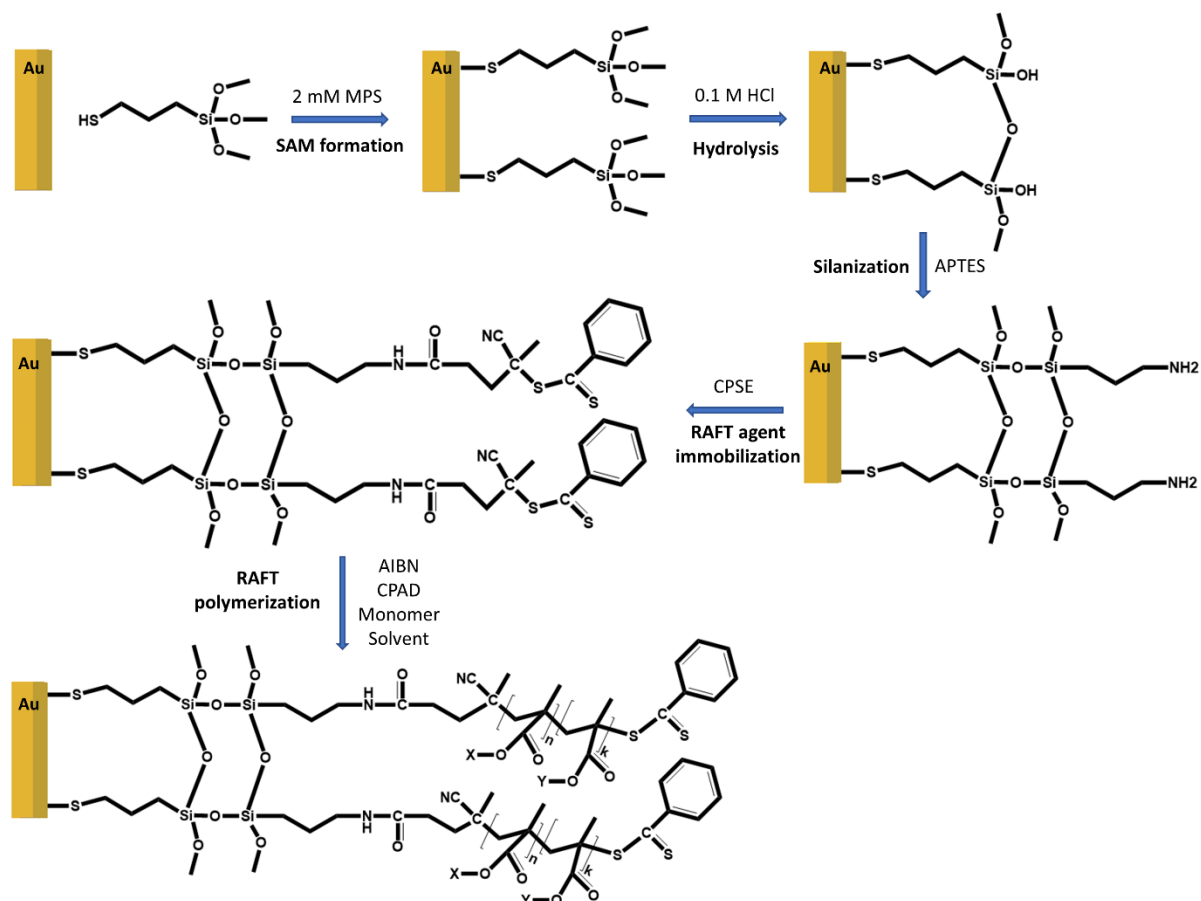


Figure 3.4 Schematic illustration of preparation of polymer brushes on gold using grafting-from approach from stabilized gold surface.

3.2.6 Characterization of polymer brush solutions

The polymer compositions of solutions remaining after the grafting-from procedure were determined with ¹H NMR experiments using a Bruker AVANCE III 300 MHz NMR spectrometer and CDCl₃ as a solvent. Copolymer compositions were calculated according to protocol described in Appendix B. The molecular weights and polydispersity indices (PDIs) were analysed by SEC as described in section 2.2.3. Detailed characterization data including NMR spectra with peak assignments, and SEC traces are available in Appendix H and I.

3.2.7 Characterization of polymer brushes attached to glass and gold

To determine the chemical composition of polymer brushes grafted from glass, X-ray photoelectron spectroscopy (XPS) was performed using an Axis UltraDLD instrument (Kratos Analytical, Manchester, UK) with monochromatic Al(K α) as the X-ray source (150 W). The XPS measurements included both survey scans as well as core level spectra of the C 1s, O 1s, S 2p and N 1s regions. The survey spectra were acquired with a pass energy of 160 eV, whereas core level spectra used 20 eV pass energy. Additionally, charge compensation was applied in order to neutralise potential charge build-up during measurements. The XPS data were analysed using CasaXPS 2.3.16 Pre-rel 1.4 and all binding energies were referenced to the C 1s hydrocarbon signal at binding energy (BE) 285 eV. Thickness and roughness of polymer films were estimated by fitting a multilayer model in GenX 2.4.10 to measured X-Ray diffraction data, which was obtained with a PANalytical X'pert Pro Diffractometer instrument with Cu(K α) as the X-ray source.

To confirm the successful grafting of polymers to gold, Infrared Reflection-Absorption Spectroscopy (IRAS) was conducted using a Bruker IFS66 spectrometer with a liquid nitrogen cooled MCT detector. The IRAS spectra were obtained at fixed 85° grazing angle. The background spectrum was recorded using a deuterated SAM of hexadecanethiol on gold. All polymer spectra were corrected for water vapour absorption. Thickness of the polymers on gold was determined using an AutoEL ellipsometer from Rudolph Research at 70° incident angle and $\lambda = 6328$ Å wavelength (He-Ne laser). An optical model based on ambient/polymer film/gold layer was used and the refractive index of the polymer film layer was set to 1.5. The refractive indices of the non-coated gold substrates were assumed to be similar among the batch and averaged from three measurements of clean gold substrates. The average polymer thickness was determined from five measurements within the sample.

3.2.8 Underwater contact angle measurements and surface energy calculations of polymer brushes on glass

Captive bubble contact angles were measured based on the method presented in section 2.2.4. The SFE of hydrated polymers and IFE at the polymer/water interface were calculated using equations presented in Appendix D.

3.2.9 Culturing of barnacles

Barnacle cyprids used in experiments were cultured according to the method presented in section 2.2.7.

3.2.10 Settlement assay using cypris larvae of *B. improvisus*

Before performing settlement experiments the slides with polymer brushes were leached in deionized water for six weeks to remove any untethered chains, unreacted monomers and other toxic residues. The single settlement experiment was performed in a similar manner as described in section 2.2.8 but this time seven replicates of each polymer brush set were tested and three-day-old cyprids were used. Settlement was evaluated after 24 h, and the results were statistically compared using one-way ANOVA.

3.2.11 Tracking experiments

Tracking experiments were conducted using an in-house built system, which has been described in detail elsewhere (Alsaab *et al.*, 2017). Briefly, two 10-L volume tanks were filled with 22 ppt ASW, where a polymer brush-functionalized microscope slide and a tube were deposited. To each tube a specific number of cyprids was added and the tube was closed with a second functionalized slide. In order to simultaneously record cyprid activity in both tanks, two monochrome cameras (Basler sc1300-32gm) were located above them. The experiments were conducted at 22 °C in complete darkness with illumination of tracking tubes from IR-LED light source located beneath the tanks. Once the recording was finished, images were imported to the tracking system, which determined coordinates of the moving cyprids. Subsequently, the tracking data were fed into the classification system which identified cyprid inspection and walking behaviours based on body movements of the larvae. Finally, the classification data were post-processed, where small body movements were discarded and treated as noise. The processed data were then used for statistical analysis, or in the plotting of exploratory behaviours of cyprids against time. In this study two types of tracking experiments were performed which provided complementary information on the cyprid behaviour.

In the short-term experiments around 20 ± 3 , three-day-old cyprids were repeatedly recorded for 1 h. For each recording the average inspection and walking metrics were calculated by summing the number of events and dividing them by the number of cyprids in each experiment. The simultaneous tracking of a large number of cyprids, during three independent experiments, with larvae obtained at different time points, provided enough statistical power for comparing the surfaces in terms of the average behavioural response of larvae. The combined data from three independent experiments were presented as means \pm standard error of the mean. The statistical analysis was conducted in R-Studio v.1.2.1335. The inspection related behaviours were normally distributed as determined by the normal probability plot and Shapiro-Wilk's test and the data were compared statistically using one-way analysis of variance (ANOVA) at 95% alpha. Walking related activities were not normally distributed

and as such they were statistically analysed using Kruskal-Wallis at 95% alpha and post-hoc Dunn's test if statistically significant.

Contrary to the short-term assays, the long-term experiments aimed to provide maximum information for cyprid behaviour prior to settlement. In this experimental design, around 10 ± 2 , three-day-old cyprids were recorded up to 24 h, but only one cyprid was tracked through its entire pelagic and benthic periods leading up to permanent attachment. Due to overlapping of cyprids, a manual larval re-assignment was sometimes necessary to maintain the identity of the cyprid. Two long-term tracking experiments were performed for each surface using cyprids from two independent larval cultures and the data were presented as cyprid trajectory tracks and cumulative plots of body movements. The data are available in Appendix K.

3.2.12 Imaging surface plasmon resonance (iSPR)

iSPR experiments were performed using an in-house built instrument schematically presented in Figure 3.5. The white light from a 250 W tungsten lamp was directed to a grating monochromator, collimated, and passed through a polarizer to a prism to reach the surface of an optically-coupled, gold-coated, coverslip at a 70° angle of incidence (AOI) (Kretschmann configuration). The reflected light was detected by a CCD camera without an IR filter (Retiga EXi, Qimaging Corp, 12 bit 1.4 MPixel) with attached 10x telecentric lens (Sill Correctal T). The resolution of the images in the direction parallel to the propagation wave was dependent on the angle of incidence (AOI), while in the perpendicular direction resolution depended solely on the lens. With the above setup and selected AOI, the total area covered by the image was determined to be $900 \times 2200 \mu\text{m}^2$ and each pixel on the image depicted an area of $0.66 \times 2.12 \mu\text{m}^2$. Before beginning the experiment, a cuvette was placed on the polymer-grafted coverslip and filled with 22 ppt natural seawater. A 600-700 nm wavelength scan was performed at 1 nm^{-1} steps to determine the SPR conditions for each pixel. After the initial SPR wavelength scan, around 30 ± 3 , four-day-old cyprids were added to the cuvette and the larvae were left to freely explore the surface for approximately 10 min. During this period the images were grabbed from the camera at the rate of 1 Hz. The cyprids were then removed from the compartment and a wavelength scan was once again performed. By fitting the reflectivity data from each pixel of the image stack into special numeric algorithm in Matlab (MathWorks, Inc.) it was possible to generate a SPR wavelength map of the selected region of interest (ROI), revealing spots with increased SPR wavelength after the experiment, which were caused by deposited footprints. In some cases, the footprints were not very well defined on SPR maps and it was necessary to manually review the SPR images, comparing the image scans before and after the experiment. Additionally, single

footprints were also analyzed by selecting a 20 x 20 pixel area from their center and calculating the SPR wavelength shift, which corresponds to the amount of deposited adhesive. The touchdowns made by barnacle cyprids during experiments were manually enumerated by going through the image sequences recorded during 10 min experiments.

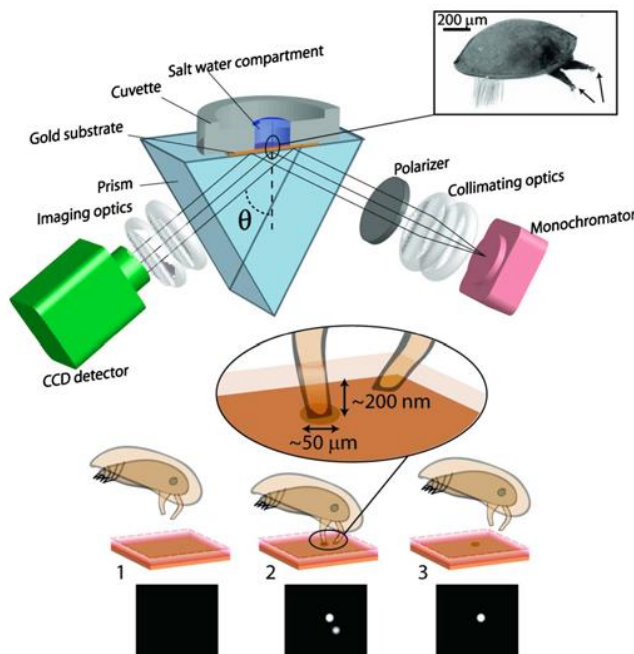


Figure 3.5 Cartoon image showing the iSPR experimental setup. Cyprids are showed touching the surface with their antennules and leaving the footprints behind (Andersson *et al.*, 2009).

3.3 Results

3.3.1 Sample preparation and characterization

The polymer solutions remaining after RAFT polymerization were analysed using ^1H NMR. In the majority of cases there was good agreement between the monomer feeds and the copolymer compositions, with the exception of polymers Z-L and A-L (Table 3.1). As in the case of bulk polymers, the small compositional drift observed for these two copolymers can be attributed to differences in monomer polarities affecting solvation of the growing macroradical, with preferential incorporation of one of the monomers into the copolymer ultimately resulting in compositional drift.

The SEC results confirmed that the polymerizations ran in a controlled manner ($PDI < 1.2$), with number average molecular weights (M_n) ranging between and 30 and 41 kDa.

Sample	Monomer feed ratio		Amount of monomers in polymer (mol %)	M_n (kDa)	PDI (M_w/M_n)
	Hydrophobic monomer (mol %)	Hydrophilic monomer (mol %)			
H-0	100 n-BMA	0	100 n-BMA	31	1.16
E-L	57 n-BMA 33 IBoMA	10 mPEG350MA	58 n-BMA 32 IBoMA 10 mPEG350MA	41	1.13
Z-L	90 n-BMA	10 SBMA	93 n-BMA 7 SBMA	37	1.13
A-L	90 n-BMA	10 SPMA	93 n-BMA 7 SPMA	30	1.19
P-L10	90 n-BMA	5 SPMA 5 METAC	92 n-BMA 4 SPMA 4 METAC	38	1.17

Table 3.1 Characteristic data of polymer brush solutions remaining after grafting-from reactions on glass.

The successful grafting of polymers on glass was confirmed by XPS analysis. Figure 3.6 shows the survey spectra of all surfaces, with highly dominant C 1s and O 1s signals with binding energies (BEs) around 285 eV and 534 eV respectively, confirming the presence of an acrylic-based film. Furthermore, in the case of ionic polymers (Z-L, A-L, P-L10), additional N 1s, S 2s, S 2p peaks were present with BEs at 400 eV, 229 eV and 164 eV respectively, confirming the existence of hydrophilic moieties (SBMA, METAC, SPMA) in these films. The XPS ratios of N/S elements for polymers Z-L and P-L10 were 0.98 and 1.05, respectively (Table 3.2), which deviates slightly from the stoichiometric ratios of SBMA and SPMA / METAC and could be attributed to deviations in copolymer compositions and/or additional contributions of the dithioester end-group of the CPAD described earlier. In the case of polymers A-L and P-L10, strong Si 2s (BE = 149 eV) and Si 2p (BE = 99 eV) peaks most probably originated from the underlying glass substrate and/or siloxane APTES layer.

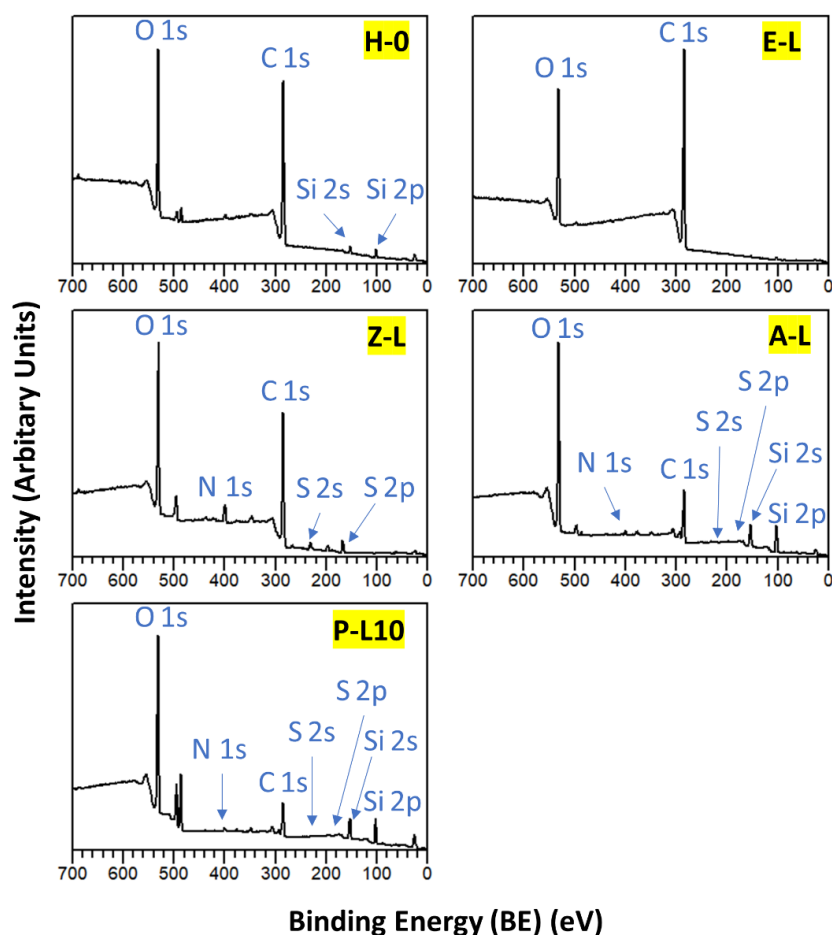


Figure 3.6 XPS survey spectra of polymer brushes attached to glass using grafting-from method.

Sample	Thickness (nm)	Roughness (nm)	N/S ratio theoretical	N/S ratio by XPS
H-0	26	1	-	-
E-L	20	3	-	-
Z-L	-	-	1	0.98
A-L	15	2	-	-
P-L10	14	3	1	1.05

Table 3.2 Characteristic data of polymer brushes attached to glass using grafting-from method.

The XPS C 1s core level spectra were curve-fitted with various peak components and are presented in Figure 3.7. In all cases, spectra consist of three main peaks at about 284.7, 286.2 and 288.6 eV, which can be attributed to C-C/C-H, C-O and O-C=O species that are typical of methacrylates. In addition, polymer Z-L, A-L and P-L10 contain C-S and C-SO₃⁻ contributions at about 285.6 eV, which is mainly attributable to SBMA and SPMA moieties in the copolymer. Furthermore, polymers Z-L and P-LI have an overlapping C-O, C-N, C-N⁺ peak at 286.4 eV with contribution of C-N⁺ that can be ascribed to the presence of tertiary ammonium moiety in the SBMA and METAC comonomers.

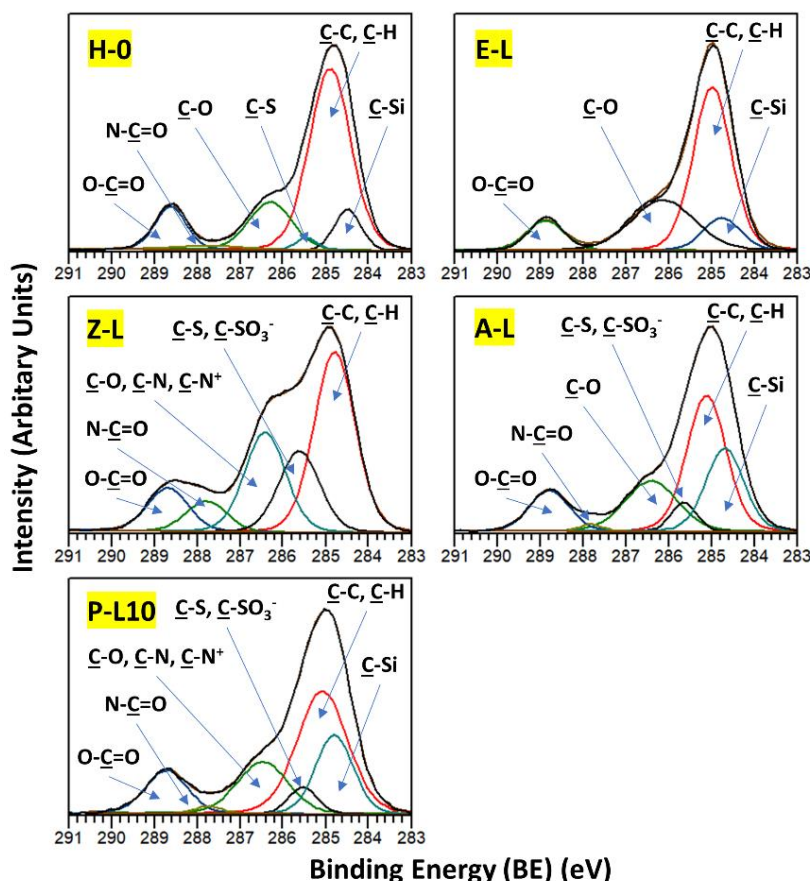


Figure 3.7 XPS C 1S core level spectra of polymer brushes attached to glass using grafting-from method.

The thickness of polymer brushes on glass was determined by fitting a multilayer model to measured X-ray diffraction data. Based on the model's best fit, estimates of the thickness ranged between 26 nm for polymer H-0 and 15 nm for amphiphilic polymer P-L10, whereas roughness was between 1 and 3 nm (Table 3.2). In the case of polymer Z-L, the surface was too rough for the model to be able to predict the thickness.

The grafting of polymers to gold was employed through the dithioester functionality of the RAFT end-group as described by Duwez *et al.* (2006). To confirm the successful attachment, IRAS measurements were conducted and the resulting spectra are presented in Figure 3.8. The two bands at $1715\text{--}1730\text{ cm}^{-1}$ and $1150\text{--}1250\text{ cm}^{-1}$ are characteristic for methacrylates and can be assigned to stretching of C=O and C-O respectively. Additionally, C-H scissoring can be observed at around $1450\text{--}1500\text{ cm}^{-1}$ and C-H twisting near $1250\text{--}1300\text{ cm}^{-1}$. In the case of polymer E-L, the broad band at around $1100\text{--}1250\text{ cm}^{-1}$ is a result of overlapping of C-O ester stretching with C-O-C stretching of PEG chains (expected at around $1100\text{--}1150\text{ cm}^{-1}$ (Lee *et al.*, 2009)). For polymers Z-L, A-L and P-L10, the identification of SO_3^- group deriving from SBMA and SPMA is difficult due to overlapping

of asymmetric S=O stretching peaks with a C-O peak at 1140-1200 cm^{-1} and relatively small and poorly resolved symmetric S=O stretching peak at around 1040 cm^{-1} . The presence of METAC in polymer P-L10 can be confirmed by presence of a small peak near 950 cm^{-1} , which can be attributed to quaternary ammonium (Peng *et al.*, 2013).

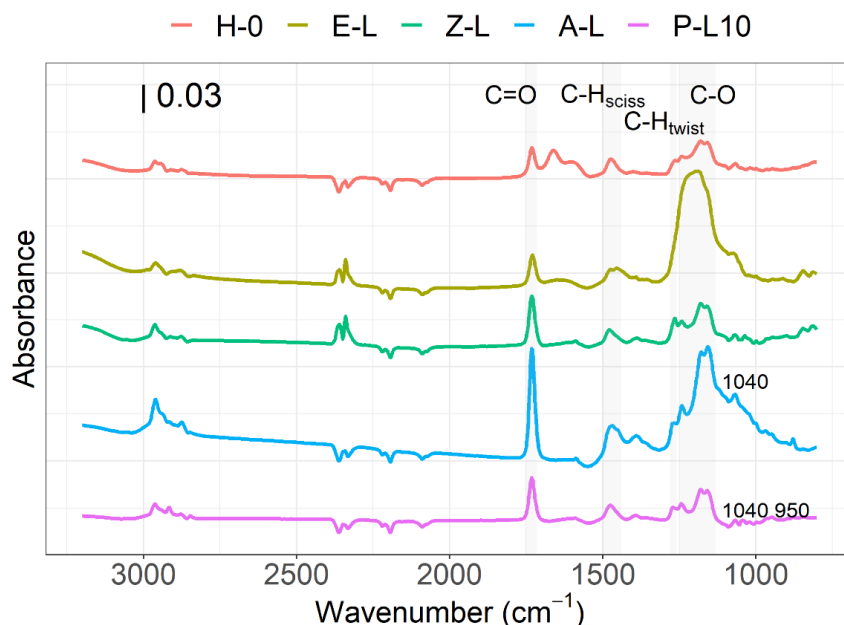


Figure 3.8 Infrared reflection-absorption spectra of polymers attached to gold using grafting-to approach.

The thicknesses of polymers attached to gold were determined by ellipsometry and the results are presented in Table 3.3. In all cases the film thickness was low and ranged between 3 and 5 nm.

Sample	Thickness \pm SD (nm)
H-0	2.99 ± 0.16
E-L	3.84 ± 0.11
Z-L	3.69 ± 0.49
A-L	5.06 ± 0.38
P-L10	3.23 ± 0.11

Table 3.3 Thicknesses of polymers grafted-to gold as measured by ellipsometry.

3.3.2 Grafting of polymer Z-L to gold using two experimental SI-RAFT methods

Due to the low thickness of polymers attached to gold using the grafting-to approach, several attempts were made to improve the thickness of polymer films. In the first method, the CPAD RAFT agent was immobilized on the gold surface and then polymerization was conducted using earlier established conditions for polymer brush Z-L. The successful grafting of polymer was confirmed by IRAS where

all major methacrylate ester bands ($\text{C}=\text{O}$ and $\text{C}-\text{O}$) were present as well as the characteristic sulfonate peak of SBMA at 1040 cm^{-1} . The measured thickness was $4.95 \pm 0.16\text{ nm}$, which is higher than the $3.69 \pm 0.49\text{ nm}$ obtained using the grafting-to method. Based on this promising first result, attempts were made to further increase the thickness by changing the polymerization conditions. The summary of these trials is presented in Table 3.4. Unfortunately, the ellipsometry measurements did not reveal a major improvement in thickness regardless of the polymerization conditions. As expected, increasing the $[\text{M}]:[\text{CPAD}]$ ratio also increased the number average molecular weight (M_n) of the polymer in the solution, but this did not have an impact on the film thickness. In the case of 3000:5 ratio, the thickness even decreased.

In order to improve the stability of the gold substrate a cross-linked initiator monolayer was formed and then the grafting reaction was performed in a similar manner as for the glass substrate (section 3.2.2). IRAS measurements confirmed the successful grafting of polymer and ellipsometry revealed a final film thickness of $8.69 \pm 0.3\text{ nm}$, which is much higher than was achieved using other grafting methods.

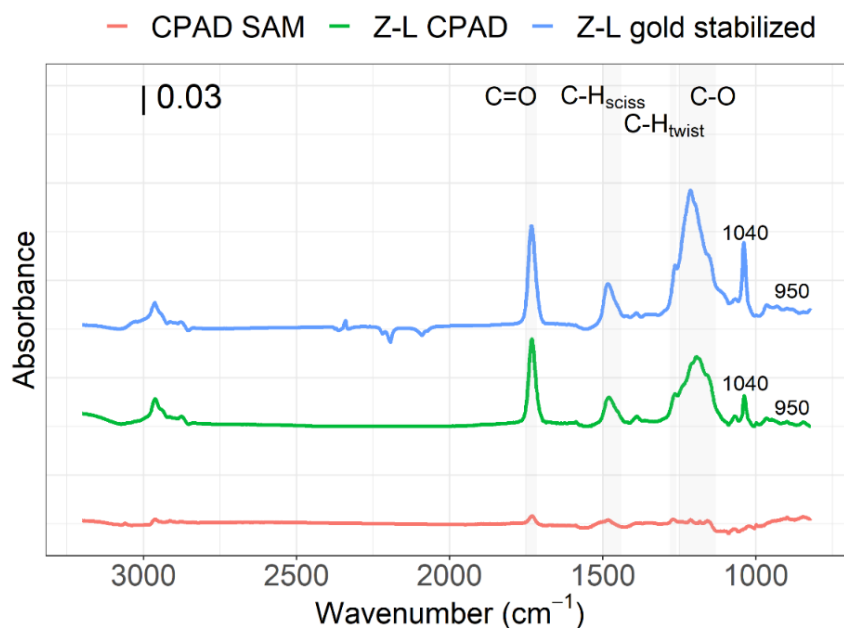


Figure 3.9 Infrared reflection-absorption spectra of polymers attached to gold using two different grafting-from methods.

Method	Polymerization time (h)	T (°C)	Conversion BMA (%)	Conversion SBMA (%)	Mn (kDa)	PDI	%SBMA (mol %)	Thickness ^a ± SD (nm)
CPAD chemisorption 1500:5:1	18	70	71	66	30.2	1.19	10	4.95 ± 0.16
CPAD chemisorption 1500:4:1	24	70	66	82	34.0	1.24	9.2	3.32 ± 0.14
CPAD chemisorption 1500:4:1	24	60	33 ^b	50 ^b	34.8	1.23	8.9	2.32 ± 0.09
CPAD chemisorption 2200:5:1	13	70	61	45	42.3	1.31	9.3	4.34 ± 0.49
CPAD chemisorption 3000:5:1	24	70	82	73	143.4 ^c	-	6.7	2.51 ± 0.7
Stabilized gold surface 2200:5:1	14	70	65	61	21.2 ^c	-	8.3	8.69 ± 0.3

Table 3.4 Characteristic data of polymer Z-L prepared on gold using various grafting-from methods with different [M]:[CPAD]:[I] ratios; ^a Thickness determined by ellipsometry; ^b Conversion determined after 18 h; ^c Number average molecular weight (M_n) determined by end-group analysis with ¹H NMR.

3.3.3 Wettability of polymer brushes

Underwater contact angles of air bubbles and silicone oil droplets were measured to determine the wettability of polymer brushes attached to glass. Based on the contact angle measurements, surface energy calculations were performed for the fully hydrated and water-equilibrated surfaces (Table 3.5). The highest wettability, as expressed by the high measured angles inside the air/oil probing liquids θ_m/ϕ_m and large SFE values, was observed on polymers Z-L and A-L. These polymers had also low IFE values.

Surface wettability of polymer brushes was also evaluated after six weeks of immersion in DIW (Table 3.5). There was no sign of major wettability change and the observed changes in contact angles and surface energies could be attributed to the measurement uncertainty rather than to significant water-induced surface reorganizations.

Sample	Angle inside air bubble (θ_m°)		Angle inside silicone oil (ϕ_m°)		Dispersive component γ_{pa}^d (mN·m ⁻¹)		Polar component γ_{pa}^p (mN·m ⁻¹)		Total surface energy (SFE) γ_{pa}^{TOT} (mN·m ⁻¹)		Interfacial energy (IFE) γ_{pw} (mN·m ⁻¹)	
	initial	6 wk	initial	6 wk	initial	6 wk	initial	6 wk	initial	6 wk	initial	6 wk
H-0	126 ± 0.9	125.3 ± 0.5	111.7 ± 0.5	111.3 ± 0.5	31.6 ± 1.7	30.8 ± 1.3	21.1 ± 0.3	21.1 ± 0.3	52.8 ± 1.4	51.9 ± 1	10 ± 0.5	9.8 ± 0.5
E-L	118.7 ± 2.1	115 ± 0	101.3 ± 0.5	98 ± 0.9	29.6 ± 3.4	26.5 ± 0.8	18.1 ± 0.4	17.4 ± 0.4	47.7 ± 3	43.9 ± 0.4	12.8 ± 0.7	15.2 ± 0.4
Z-L	158 ± 1.6	158.3 ± 0.5	157.3 ± 1.9	158.3 ± 1.1	38.9 ± 1.2	38.7 ± 1.1	33.2 ± 0.4	33.4 ± 0.4	72.1 ± 1.1	72.1 ± 0.8	4.6 ± 0.5	4.5 ± 0.5
A-L	150 ± 0.9	148.3 ± 2.1	146.7 ± 1.1	145 ± 1.6	36.5 ± 1.4	35.7 ± 3.6	31.2 ± 0.4	30.9 ± 0.9	67.7 ± 1.1	66.6 ± 2.8	4.6 ± 0.6	4.6 ± 1.4
P-L10	122.7 ± 1.4	123.3 ± 2.1	103.3 ± 0.5	105.3 ± 1.1	34.8 ± 2.9	33.8 ± 3.8	18.1 ± 0.4	18.8 ± 0.5	52.9 ± 2.5	52.7 ± 3.5	13.6 ± 1.1	12.7 ± 1.3

Table 3.5 Initial underwater contact angles measured inside the air bubble (θ_m) and silicone oil (ϕ_m) and calculated surface energies of hydrated polymer brushes together with results after six weeks of leaching in deionized water. Errors are 95% CIs.

3.3.4 Settlement of barnacles

The mean percentage settlement of barnacles is presented in Figure 3.10. Settlement was lowest on zwitterionic polymer Z-L ($4.93 \pm 3.09\%$) and, based on one-way ANOVA ($F_{4,30} = 17.8$, $p \leq 0.001$) with post-hoc Tukey test ($p < 0.05$), it was significantly different from other tested polymers. Highest settlement was recorded on polymers H-0 ($39.15 \pm 7.46\%$) and P-L10 ($45.15 \pm 8.16\%$), but not significantly different from polymers A-L ($32.15 \pm 9.51\%$) and E-L ($24.52 \pm 6.35\%$).

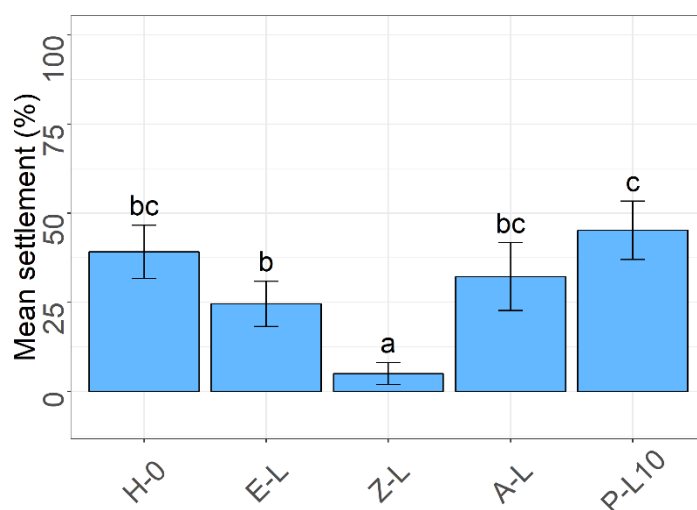
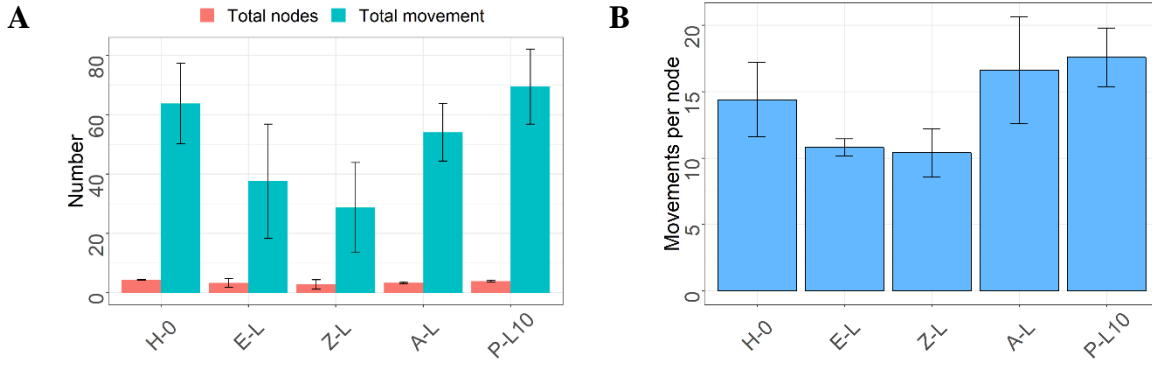


Figure 3.10 Mean percent settlement of three-day old cyprids of *B. improvisus* on polymer brushes after 24 h, together with corresponding 95% CIs. Letters represent Tukey's pairwise comparisons and bars that do not share a letter are significantly different.

3.3.5 Tracking experiments: analysis of cyprid behaviour on various surfaces

In order to statistically compare the surfaces in terms of the behavioural response of cyprids, short-term experiments were employed (Aldred *et al.*, 2018). The behavioural measures recorded for all tested surfaces from three independent short-term experiments are presented in Figure 3.11 (A-F). The only statistically significant behavioural metric was ‘steps per minute’ walking measure (Kruskal-Wallis $H = 10.82$, $df = 4$, $p = 0.029$) with polymers H-0 and Z-L being statistically different (Dunn’s test $p < 0.05$). Although the ‘total walking period’ metric was not statistically different (Kruskal-Wallis $H = 5.58$, $df = 4$, $p = 0.233$), cyprids spent the least amount of time walking on polymers E-L, Z-L, P-L10, whereas on polymers H-0 and A-L, they were much more engaged in walking activities; a larger number of experiments would probably resolve this. Interestingly, in case of polymer Z-L, when comparing the magnitude of ‘steps per minute’ / ‘total steps’ / ‘total number of periods of walking’ metrics with ‘total walking period’ it can be concluded that cyprids often engaged in walking behaviour but these interactions were very brief. While all inspection-related movements were not significantly different between polymers (one-way ANOVA tests, $p > 0.05$), smallest values were recorded for polymer Z-L, whereas highest for polymers H-0, A-L and P-L10. It is noteworthy, however, that there was a positive correlation between the ‘total number of movements’ and settlement (Pearson $r = 0.9610$, $p = 0.009$).

Inspection behaviour



Walking behaviour

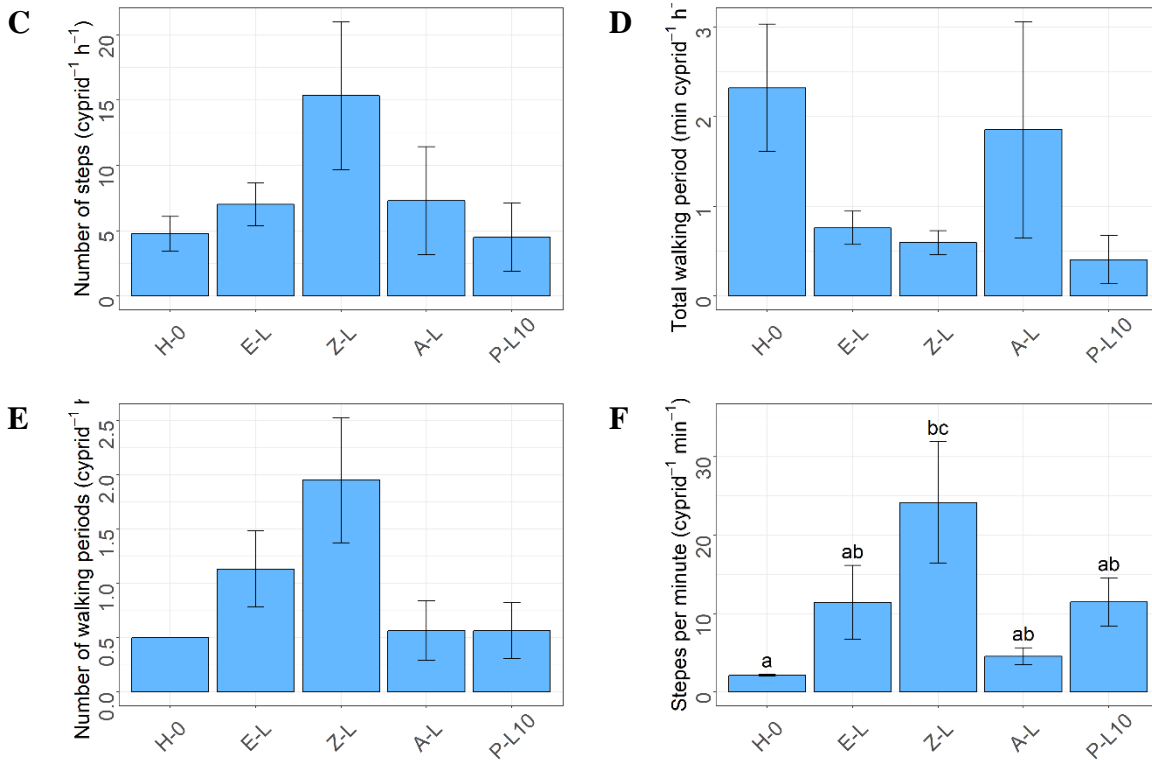


Figure 3.11 Data collected from short-term tracking experiments. Bars represent means from three replicate experiments and error bars are standard error of the mean. (A) Total nodes (one-way ANOVA $F_{4,10} = 0.37$, $p = 0.822$), Total movement (one-way ANOVA $F_{4,10} = 1.433$, $p = 0.293$); (B) Movements per node (one-way ANOVA $F_{4,10} = 1.642$, $p = 0.239$); (C) Number of steps (Kruskal-Wallis $H = 3.5$, $df = 4$, $p = 0.477$); (D) Total walking period (Kruskal-Wallis $H = 5.58$, $df = 4$, $p = 0.233$); (E) Number of walking periods (Kruskal-Wallis $H = 6.51$, $df = 4$, $p = 0.164$); (F) Steps per minute (Kruskal-Wallis $H = 10.82$, $df = 4$, $p = 0.029$). Letters represent Dunn's pairwise comparisons and bars that do not share a letter are significantly different.

To gain insight into the full cyprid behaviour leading up to settlement, a long-term tracking experiment was employed. Figures K.1-K.5 (Appendix K) present the actual tracks and number of body movements for walking and inspection behaviours of two individual cyprids tracked on each surface in two separate experiments. Looking at the tracks it can be observed that all polymers except the anionic A-L show classical exploratory behaviours, e.g., wide search, close search and inspection. The fact that no exploration was observed on polymer A-L is in stark contrast with the short-term assays where the inspection and walking behaviours were frequent. Quite remarkably, however, considering different trajectories of polymers A-L and H-0, the first cyprids settled on these surfaces at a similar time; 370 min (± 40) on the former and 357 min (± 28) on the latter. The surfaces that resisted cyprid settlement for the longest time were the zwitterionic polymer Z-L (970 min ± 42) and mixed-charged P-L10 (960 min ± 68).

3.3.6 Visualization of deposition of barnacle footprints in-situ using iSPR

The total number of surface contacts (touchdowns) and number of deposited footprints are presented in Figure 3.12A. The number of touchdowns was significantly different between surfaces (one-way ANOVA $F_{4,10} = 5.78$, $p = 0.011$), with the lowest number of touchdowns recorded on homopolymer H-0 (17 ± 0.58) and the highest on polymer P-L10 (36.33 ± 1.45). The number of deposited footprints did not vary significantly across surfaces (Kruskal-Wallis $H = 6.12$, $df = 4$, $p = 0.191$). In addition, the footprint data were expressed as a likelihood of successful footprint deposition, which was the ratio of number of footprints to the number of touchdowns (Figure 3.12B). Although this metric was not statistically significant between surfaces (Kruskal-Wallis $H = 7.35$, $df = 4$, $p = 0.119$), the data revealed that the potential success of footprint deposition was highest on the polymer H-0 ($21.73 \pm 2.57\%$) and lowest on zwitterionic polymer Z-L ($2.29 \pm 2.29\%$).

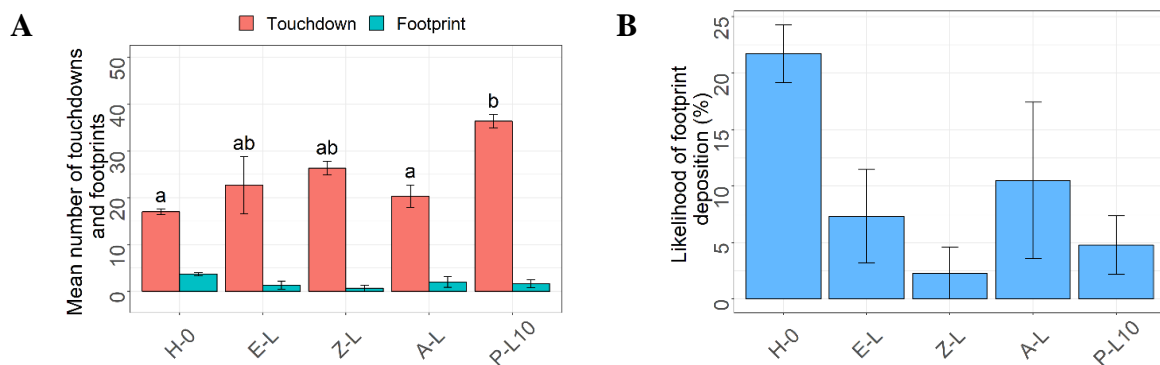


Figure 3.12 (A) Mean number of touchdowns and deposited footprints on each tested surface. Bars that do not share a letter are significantly different. (B) Likelihood of footprint deposition calculated as a ratio of touchdowns events and persistent footprints. Error bars represent standard error of the mean.

In addition, to quantify the temporary adhesive deposited on surfaces, SPR wavelength maps were generated after each experiment. Figure 3.13 shows a representative SPR wavelength map for ROI area for polymer H-0 after cyprid exploration.

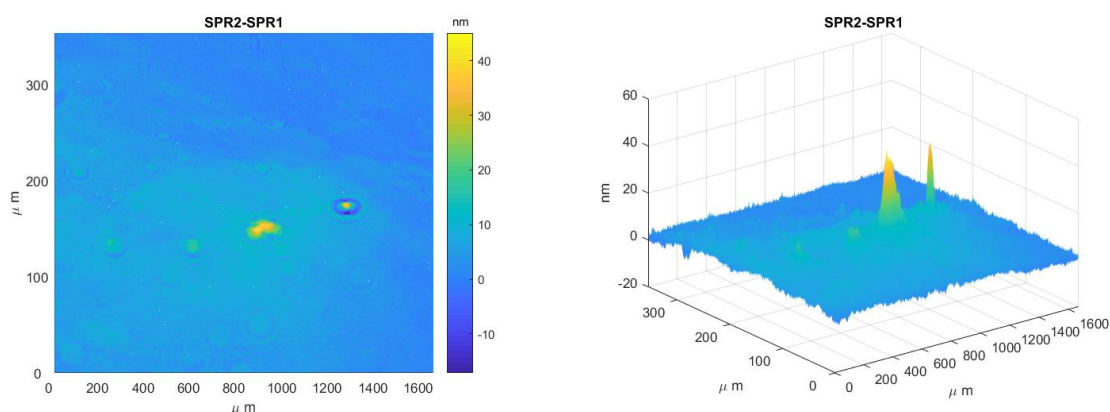


Figure 3.13 The illustrative SPR wavelength maps (2D and 3D) generated for polymer H-0. Yellow colored areas depict shifts in SPR wavelength due to deposition of footprints.

The bright yellow areas depict changes in SPR wavelength due to the deposition of barnacle temporary adhesive and these were further analyzed to determine the SPR wavelength shift. Figure 3.14B shows reflectivity curves for the selected area before and after footprint deposition, and the differences between curves determine the SPR wavelength shift. For the footprint presented (Figure 3.14A), the SPR wavelength shift $\Delta\lambda_{\text{SPR}}$ was 19.5 nm. According to Andersson et al. (2009), a SPR shift of 20 nm would correspond to a 10 nm footprint thickness (when assuming a refractive index of

1.45 for adsorbed footprints). To determine the relative thickness of deposited adhesives three random footprints (in case of polymer Z-L, two) were selected from each surface and average SPR wavelength shift $\Delta\lambda_{\text{SPR}}$ was calculated (Figure 3.15). The differences in SPR wavelength shifts were determined to be significant (one-way ANOVA $F_{4,9} = 24.4$, $p \leq 0.001$). The smallest SPR shift was recorded on polymer Z-L, followed by polymer E-L and P-L10. The highest SPR shift was found on polymer H-0 and it was significantly higher than on other tested surfaces (Tukey tests, $p < 0.05$).

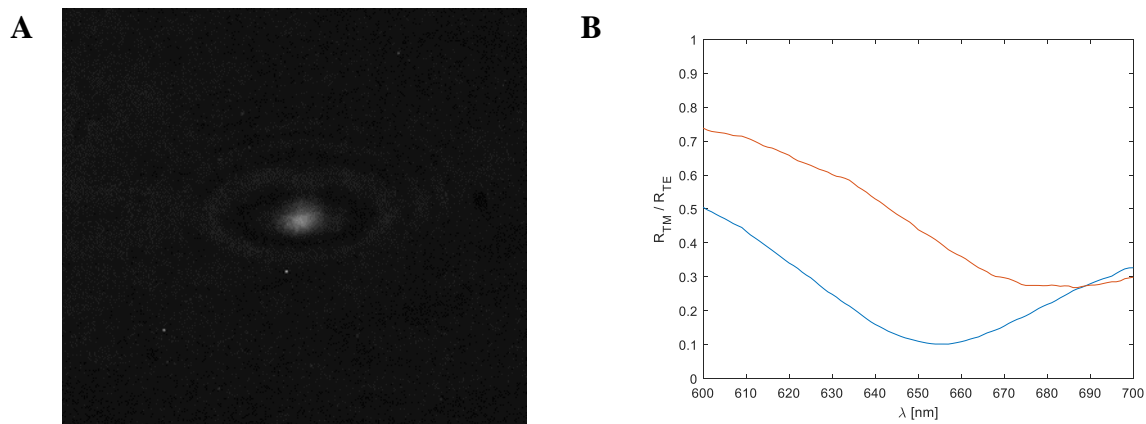


Figure 3.14 (A) Image of actual deposited footprint. (B) the reflectivity curves showing shift in SPR wavelength. The curves were acquired before (blue line) and after (red line) the experiment.

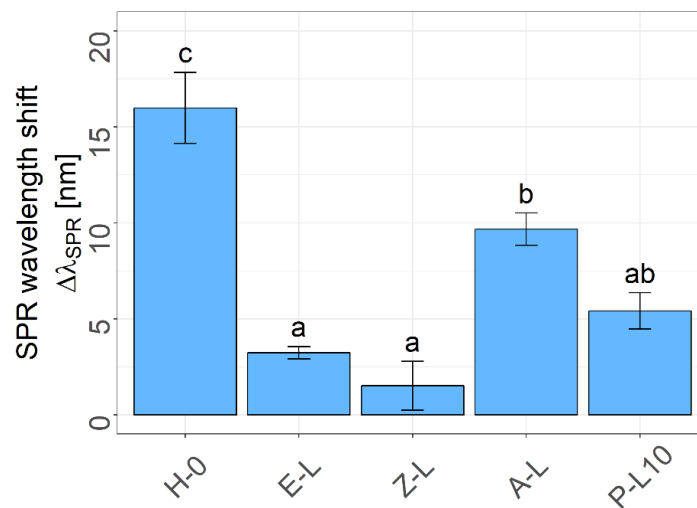


Figure 3.15 SPR wavelength shifts generated by the deposited footprints together with their corresponding standard errors of the mean. Bars that do not share a letter are significantly different.

3.4 Discussion

The polymer brushes used in the settlement and tracking experiments were prepared using SI-RAFT technique. The polymers were prepared in a controlled manner ($PDI < 1.2$) and the successful grafting from glass was confirmed with XPS and XRR methods. The thickness varied somewhat among surfaces, and nonionic polymers presented slightly higher values than the ionic ones. In the case of surfaces containing SBMA functionality, it was not possible to determine their thickness due to high surface roughness. Obviously, the roughness estimates obtained here are in the dry state, which means that in seawater, the roughness parameters for all tested samples could be different. Nevertheless, the high roughness of the SBMA surface is in line with results obtained by Ventura *et al.* (2017) who found that with increasing SBMA content the roughness of lauryl methacrylate-SBMA copolymers increased, and it was speculated that phase separation could be responsible for this effect.

The polymers used in iSPR experiments were attached to gold substrates using the ‘grafting-to’ approach. The prepared surfaces were relatively thin (between 3 and 5 nm), which could be attributed to excluded volume interactions, that act as a diffusion barrier and limit the availability of the gold surface to polymer chains (Zdyrko and Luzinov, 2011). In order to increase the thickness of polymer brushes on gold, various ‘grafting-from’ approaches were attempted. In the first attempt polymers were grown from a chemisorbed CPAD SAM layer on gold. Different reaction conditions were tested but the obtained thicknesses did not increase considerably and did not exceed 5 nm. The potential reason for the low thickness could be the instability/lability of the Au-S bond above 60 °C, which was previously reported in the literature (Kim *et al.*, 2000; Shah *et al.*, 2000). With elevated temperature the dithioester functionality and grafted polymer desorb, reducing the polymer thickness. The polymerization was also run at a lower temperature (60 °C), but this did not improve the final film thickness.

Huang *et al.* (2001) showed that free radicals can increase the desorption of thiols, so it can be hypothesized that the same mechanism also applies to immobilized dithioesters. In order to improve the stability of the gold surface a cross-linked initiator monolayer was formed. The polymer grafted using this method had a final film thickness of around 9 nm. Clearly, this method gave best results and confirmed the importance of stabilizing the gold surface before running polymerizations at elevated temperatures (> 60 °C). Further optimization of polymerization conditions such as time, or $[M]:[CPAD]$ ratio would nevertheless be beneficial.

The wettability of polymer brushes attached to glass was determined using underwater contact angles (Table 3.5). The highest wettability was observed on polymers Z-L and A-L and could be explained

by the strong ion-dipole interactions forming between charged SBMA and SPMA functionalities and water molecules. In addition, the strong polymer-water interactions in these polymers were manifested in low IFE values. The relatively low wettability of polymer P-L10 can potentially be explained by the ion pairing of the SPMA and METAC monomers, which could limit the number of electrostatic interactions with water, and/or possibly lead to collapsed conformation of the polymer brush with limited surface hydration. Finally, in the case of polymer E-L, the low wettability was a result of weaker hydrogen-bonding interactions of mPEG350MA with water and the presence of two hydrophobic monomers n-BMA and IBoMA. The wettability results obtained for polymer brushes P-L10 and E-L are in stark contrast with the results obtained for bulk polymers (Table 2.4), where the changes in wettability after immersion for six weeks were considerable. It can be hypothesized that bulk polymers have much higher conformational freedom than the single point attached polymer brushes and can more easily arrange their hydrophilic functional groups towards water, resulting in higher surface wettability.

From the barnacle settlement results (Figure 3.10) it was clear that among all prepared surfaces only polymer brush Z-L was resistant towards cyprids. Very low settlement of cyprids on this polymer was attributed to its high surface hydration, maintained through strong ion-dipole interactions between the zwitterionic SBMA and water molecules. On the other hand, high cyprid settlement recorded for the hydrophilic polymers E-L and A-L is in stark contrast with the results obtained for similar chemistries presented as bulk polymers (Appendix J, Figure J.1). The reason for this inconsistency can be potentially explained by the additional swelling effect of the thick bulk polymers, which results in higher conformational freedom of polymer chains and enables hydrophilic functional groups to more easily rearrange, increasing the effective surface hydration. The polymer brushes prepared in this work are relatively thin, and with the single point attached chains they are less flexible than bulk equivalents, which severely limits their hydration capacity. The limited hydration capacity of the polymer brushes is also expressed by minimal changes in wettability after six weeks immersion in deionized water (Table 3.5).

The importance of swelling, hydration capacity and conformational freedom on the antifouling efficacy is well documented in the literature. For instance, Yandi *et al.* (2014) prepared poly(HEMA-*co*-PEG₁₀MA) polymer brushes with increasing thicknesses and found that 20-40 nm was optimal for resisting zoospores of *Ulva linza* and marine bacteria *Cobetia marina*. The authors hypothesized that in this thickness range the highly hydrated polymer chains of poly(HEMA-*co*-PEG₁₀MA) create dense networks of water molecules with moderate elasticity that provide high fouling resistance, whereas polymers with lower thicknesses present reduced surface hydration that negatively affects

their performance. In a similar report by Yang *et al.* (2018), neutral HEMA polymer brushes with various grafting densities and chain lengths were synthesized and the adhesion of green algae *Dunaliella tertiolecta* and diatoms of *Navicula* sp. was investigated. It was speculated that the interplay between film thickness, elasticity and polymer/water intermolecular associations governed the antifouling properties of these coatings. Although the aforementioned fouling organisms clearly show different attachment strategies from barnacles, it seems reasonable to assume that a similar mechanism of action based on high hydration capacity is necessary to obtain barnacle-resistant surfaces.

As for the anionic polymer brush A-L, the relatively high barnacle settlement is in good agreement with previously published reports of high settlement of *B. improvisus* on negatively charged SAMs and polymer brushes (Di Fino *et al.*, 2014; Yandi *et al.*, 2016). In the case of amphiphilic polymer brush P-L10, containing both anionic SPMA and cationic METAC, the XPS experiment suggests that the prepared polymer brush was somewhat enriched with METAC. The observed trend could be potentially explained by preferential solvation of the grafted polymer brush with METAC comonomer, which could lead to phase separation and possible polymer ‘blockiness’. This surface heterogeneity and cationic character could induce the barnacle settlement.

In order to determine the behavioural response of cyprids exposed to different surfaces, video tracking experiments were conducted. From the short-term experiments (Figure 3.11A-F) it was clear that cyprids actively explored all surfaces once introduced to the experimental tube, however the analysis of the tracking data revealed that among various walking and inspection metrics only the ‘steps per minute’ walking measure was statistically significant (Figure 3.11F). More interestingly, however, we found a strong correlation between the ‘total movement’ inspection metrics and settlement response of cyprids; i.e., with increasing number of inspection behaviours an increase in settlement was also observed. This finding supports previous observations (Aldred *et al.*, 2018; 2019) that also reported that cyprids tend to inspect more on surfaces that also attract high barnacle settlement.

While the short-term assays did not show significant differences in cyprid behaviours, the long-term tracking experiments revealed more pronounced differences. The most prominent observation was the limited wide- and close-search behaviours on anionic polymer A-L. Aldred *et al.* (2019) speculated that such reduction of exploratory measures could indicate a ‘desperate’ larva, or high affinity towards the surface. Interestingly, the settlement time recorded on polymers A-L and H-0 was similar, which considering different exploratory behaviour of cyprids on those surfaces, was quite unexpected. The surfaces that resisted cyprid settlement for the longest period of time were polymers Z-L and P-L10. The fact that cyprids settled at a similar rate on both polymers is surprising

considering significant differences in number of settled cyprid on glass slides. One possible explanation for the trends observed here is gregarious settlement of cyprids on polymer P-L10. As the tracking experiment proceeded and cyprids actively explored the surface, more temporary adhesive could have been deposited which builds-up over time and acts as a settlement signal (Walker and Yule, 1984; Yule and Walker, 1985).

To gain additional insight into behaviour of cyprids exposed to different polymers, and to quantify cyprid-surface interactions, iSPR experiments were performed. iSPR revealed that cyprids actively explored all surfaces immediately after being introduced to the experimental chamber, confirming earlier findings from tracking experiments. The highest number of touchdowns (surface contacts) was recorded on mixed-charged polymer P-L10, followed by zwitterionic polymer Z-L and PEG containing polymer E-L (Figure 3.12A). Due to the fact that not all touchdowns resulted in the deposition of footprints, to account for this variability, a likelihood of footprint deposition was calculated (Figure 3.12B). Based on this metric it was determined that the polymer H-0 retained the highest number of footprints, whereas the lowest affinity of adhesive to surface was on polymer Z-L. Interestingly, the number of touchdowns and the ‘steps per minute’ walking measure were very consistent among all tested surfaces. This finding is significant, not least, because it implies that the surface controls the biomechanics of movement of a cyprid and ultimately affects its exploration behaviour at the point of temporary adhesion. In the context of the zwitterionic polymer Z-L it can be hypothesized that the attachment discs of the cyprid are weakly attached to the polymer surface (low likelihood deposition value), providing rapid walking (large ‘steps per minute’ value) with very short walking durations (low ‘total walking period’ value). On the contrary, in the case of polymers H-0 and A-L it seems that the attachment discs bind more strongly to these surfaces (large deposition likelihood value), which affects the walking characteristics of the cyprid (low ‘steps per minute’ and high ‘total walking period’ values) and results in a higher number of close search/wide search inspection events. The above findings are in line with the work by Aldred *et al.* (2013) who observed that cyprids engaged in close search or inspection are more strongly attached to the surface.

In addition to footprint deposition observations, thickness of the deposited material was also estimated. The thickest footprints were on hydrophobic polymer H-0 and anionic polymer A-L, while the footprints on polymer Z-L and polymer E-L were very thin (Figure 3.15). Notably, the iSPR results obtained here are in good agreement with similar work by Aldred *et al.* (2011) who used a different species of barnacle (*Semibalanus balanoides*) and found that negatively charged -COOH and hydrophobic -CH₃ SAMs adsorbed the thickest footprints, while the mPEG and hydrogel chemistry tested in that study accumulated the least amount of adhesive. Clearly, when comparing

our results and results obtained by Aldred *et al.* (2011) it seems likely that the stickiness of footprints, as expressed by the deposition likelihood and footprint thickness, is a surface related property with both wettability and surface charge governing the binding of the cyprid temporary adhesive. The effect of surface wettability on the binding of the cyprid adhesive was also studied using AFM. Phang *et al.* (2009) studied the interactions of footprints with hydrophobic and hydrophilic AFM tips and found that adhesion strength, as expressed by larger pull-off force, was higher with a hydrophobic tip than with a hydrophilic tip. Similar results were obtained in a study by Guo *et al.* (2015), who modified a colloidal AFM probe with cyprid temporary adhesive protein and conducted adhesion studies on a range of monolayers with varying wettability. The study showed that the strongest adhesion of footprint proteins was on hydrophobic surfaces and that adhesion was lowest on hydrophilic surfaces, further confirming both the present findings and those of Aldred *et al.* (2011).

Finally, assuming that the footprint serves a double function, not only as a glue but also as a settlement signal, it can be hypothesized that surfaces with the least amount of deposited adhesive should present lowest settlement (Yule and Walker, 1985; Clare *et al.*, 1994). Indeed, with the exception of polymer P-L10, there was an indirect correlation between the stickiness of footprint and settlement, with the polymer Z-L having the least amount of deposited footprints and showing lowest settlement, and polymer H-0 presenting the opposite trend. The reason for the inconsistency between footprint deposition and settlement observed on polymer P-L10 can be potentially explained by the fact that during extensive surface exploration (as expressed by high number of touchdowns) only a limited amount of adhesive is actually deposited, with the majority of the material being retained on the attachment disc. This, in turn, could accumulate over time increasing the attractiveness of the surface and result in gregarious settlement of cyprids (Walker and Yule, 1984; Yule and Walker, 1985).

To summarize the findings from this chapter and put them in the context of antifouling testing and potential development of hydrophilic resistant coatings, the following points have to be considered: (1) The cyprid exploratory behaviour, stickiness of the adhesive and settlement are related. (2) The stickiness of the adhesive on the surface affects the biomechanics of movement and ultimately controls the walking/inspection behaviour of cyprids. (3) Cyprids are more strongly attached to surfaces which they tend to inspect more. (4) Inspection behaviour appears to be the best predictor of cyprid settlement. (5) Surfaces that are both highly hydrated and neutral minimize the exploratory behaviour of cyprids and ultimately reduce settlement. (6) Surfaces should minimise the deposition of footprints to prevent their action as a conspecific signal.

Chapter 4. Development of hybrid coating incorporating both fouling-resistant and fouling-release properties

4.1 Introduction

One of the main materials used in the development of commercial fouling-release coatings (FRCs) is polydimethylsiloxane elastomer (PDMS). PDMS is a low surface energy, and low elastic modulus material that has fouling-release properties but suffers from slime build-up which tends to attach strongly to hydrophobic surfaces (Anderson *et al.*, 2003; Molino *et al.*, 2009). For this reason, in recent years a lot of research was undertaken in order to improve the antifouling properties of PDMS.

PEG and poly(ethylene oxide) are examples of functionalities that are hydrophilic and non-toxic, and are regularly introduced into PDMS to improve its FR and antifouling performance (Zhang and Chiao, 2015). Sundaram *et al.* (2011) synthesized a surface active block copolymer (SABC) containing PDMS and PEG blocks and reported very good FR properties against both *Ulva linza* sporelings and diatoms of *Navicula*. Based on contact angle measurements it was hypothesized that upon immersion in water the hydrophilic PEG side chains reorient towards the surface and the PDMS chains move away from the surface. Martinelli *et al.* (2012) synthesized amphiphilic copolymers containing PEG-fluoroalkyl acrylate and polysiloxane methacrylates and introduced them into a PDMS matrix. It was demonstrated using XPS that the fluoroalkyl chains in copolymers were capable of surface segregation in PDMS blends. This was further confirmed by AFM measurements, which showed that the coatings underwent micro- and nanophase segregation, resulting in morphological and topographical ambiguity of the surface. The biological performance of the coatings was evaluated both in the laboratory and in the field. The laboratory assays using sporelings of *U. linza* revealed excellent FR properties of the experimental coatings when compared to PDMS, while the 4-month-long static field immersion tests revealed good antifouling performance against hard fouling species comparable to the commercial product Intersleek® 700.

A different approach to improve the AF properties of PDMS is to render its surface hydrophilic through various surface modification methods such as UV-irradiation (Oláh *et al.*, 2005), oxygen plasma (Bodas and Khan-Malek, 2007), or by grafting polymers directly onto PDMS. Plasma and UV activation are the simplest methods to render PDMS surface hydrophilic. Unfortunately, due to the flexibility of the siloxane backbone, hydrophilicity is sustained only for a short period of time (Plegue *et al.*, 2018). In order to prevent this phenomenon, known as hydrophobic recovery, polymers with hydrophilic character are often directly grafted to PDMS. For instance, Kovach *et al.* (2014)

grafted a PEG-functional silane to a PDMS substrate and reported low adsorption of fibrinogen and low platelet adhesion in a silicone microfluidic device for periods of up to four months. Makamba *et al.* (2005) reported synthesis of highly stable, protein-resistant hydrophilic PDMS surfaces with coupled, cross-linked polyelectrolyte multilayers as anchoring points for subsequent attachment of PEG chains. PEG is not the only hydrophilic chemistry that is used to modify the surface of PDMS and render it less hydrophobic, however. Wu *et al.* (2006) copolymerized glycidyl methacrylate (GMA) with dimethylacrylamide, polyvinylalcohol and polyvinylpyrrolidone and subsequently grafted these polymers to APTES-modified PDMS. Significant reduction of protein adsorption was recorded on all tested surfaces, with only 10% of the value of the non-modified PDMS. In a more recent report by De Vera *et al.* (2018), pH-responsive zwitterionic copolymers composed of GMA, SBMA and (dimethylamino)ethyl methacrylate were synthesized and grafted-to UV activated PDMS through a ring-opening reaction of GMA. Those surfaces displayed pH-dependent wettability, meaning that they could switch their character from hydrophilic to hydrophobic based on the pH of the environment, thereby modulating the attachment and release of bacteria. A different approach to grafting a zwitterionic polymer to a silicone elastomer was presented by Keefe *et al.* (2012). They grafted a pCBMA on PDMS using ATRP and reported low adsorption of fibrinogen and reduced serum binding for more than a month. In a similar report, Shivapooja *et al.* (2015) attached pSBMA to a poly(vinylmethylsiloxane) (PVMS) elastomer using activator regenerated by electron transfer ATRP. The surfaces were reported to have good release properties for bacterial biofilm.

In this chapter a novel hybrid coating based on a silicone elastomer and zwitterionic copolymer was prepared by grafting a pBMA-*co*-SBMA-*co*-GMA copolymer onto PDMS. The GMA segment was used to covalently attach the polymer to the PDMS surface using a ring-opening reaction of the epoxide group. In order to confirm the grafting of the copolymer to silicone, ATR-IR spectra were acquired. Changes in the wettability of the silicone substrate after copolymer grafting were determined by sessile drop contact angle measurements and surface energy calculations using the Owens-Wendt method. Finally, the functionalized PDMS was subjected to laboratory assays to determine its potential to resist the settlement and reduce the adhesion of the cells of the diatom, *Navicula incerta* and zoospores of the green alga, *U. linza*.

4.2 Materials and methods

4.2.1 Materials

N-(2-methacryloyloxyethyl)-N,N-dimethyl-N-(3-sulfopropyl)ammoniumbetaine (SBMA) was purchased from Raschig GmbH under the trade name Ralumer SPE. n-Butyl methacrylate (n-BMA,

99%), glycidyl methacrylate (GMA) was obtained from Acros Organics. Ethylene glycol (EG), butanol, xylene, tetrahydrofuran (THF), dichloromethane (DCM), dioxane and methanol (MeOH) were purchased from Fisher Scientific. The 2,2'-azobis(2-methylbutyronitrile) (AMBN) initiator was supplied by AkzoNobel Chemicals B.V. as Perkadox AMBN-gr. Silicone (PDMS) used as the substrate for grafting was Dow Corning 3-0213 obtained from Dow Corning Corporation. The cross-linker used in PDMS preparation was Wacker TES 40 purchased from Brenntag and the catalyst was bis(2-ethylhexyl)hydrogen phosphate obtained from Sigma-Aldrich. All materials were used as supplied except for triethylamine (TEA) which was refluxed over CaH_2 , distilled and kept over 3 Å sieves under Argon (Ar) protection.

4.2.2 Synthesis of copolymer Z-GL (pBMA-co-SBMA-co-GMA)

The pBMA-co-SBMA-co-GMA copolymer was prepared as follows. Briefly, SBMA (14.09 g, 50 mmol) was added to a 250 mL flask and dissolved in EG (51.68 g) followed by addition of butanol (165.38 g). This mixture made up the first feed. The second feed consisted of first lot of AMBN initiator (2.42 g, 13 mmol) dissolved in n-BMA (50.18 g, 353 mmol) and GMA (14.33 g, 101 mmol). The main reactor contained butanol (31 g), was equipped with a mechanical stirrer and was heated to 75 °C. Both feeds were simultaneously added to the reactor using two Watson Marlow 101/U peristaltic pumps for 4 h. One hour after completion of feeding, the remaining AMBN (0.582 g, 3 mmol) was dissolved in butanol (10.34 g) and added to the main reactor to convert residual monomers. The vessel was stirred for another hour, then stopped and left overnight. The next day, the polymer solution was transferred to dialysis tubing and dialysed twice using mixture of MeOH and DCM (1:1) and then twice using a mixture of dioxane and DCM (1:1). The resulting polymer was cloudy in appearance. Subsequently, the dialysed polymer was transferred to an evaporating flask and the solvent was removed under reduced pressure using a Büchi rotary evaporator. Finally, the dried polymer was dissolved in a mixture of dioxane and MeOH (1:1) to a concentration of 10 mg/mL.

4.2.3 Grafting of copolymer Z-GL to PDMS substrate

Before grafting copolymer Z-GL to PDMS, silicone (Dow Corning 3-0123) was bonded to glass slides in the following manner. First glass microscope slides (VWR) were sonicated twice in isopropanol (IPA) for 15 min, then blow-dried with N_2 and subjected to oxygen plasma for 15 min. In the meantime, the PDMS mixture was prepared by mixing the silicone resin Dow Corning 3-0123 (94.9 g) with Wacker TES 40 curing agent (4.2 g), bis(2-ethylhexyl)hydrogen phosphate catalyst (0.86 g) and 20 g of xylene. The mixture was gently stirred with a spatula to avoid the incorporation of air bubbles. After completion of the plasma-oxidation process the slides were immediately

transferred to Petri dishes and the PDMS mixture (110 g) was poured onto the clean glass slides. The PDMS was left overnight to cure and bond to glass at room temperature. The next morning, slides were cut from the PDMS mould and sonicated for 2 min in IPA to clean and degrease the silicone surface before grafting the copolymer. Next, the slides with bonded PDMS were transferred to a plasma cleaner, where the surface was activated in oxygen plasma for 1 min. The successful activation of the PDMS substrate was confirmed by very low contact angle $< 5^\circ$ (Figure 4.1). Subsequently, the plasma-treated slides were transferred to slide staining dishes containing a solution of polymer Z-GL. Dishes were then sonicated for 15 min and stirred for another hour with a magnetic stir bar. TEA (55 μL) was then added using a micropipette and the stirring continued for another 30 min. Finally, wet slides were immediately transferred to Petri dishes and fully covered with 80 mL of remaining polymer solution and dishes were put in the oven at 60 $^\circ\text{C}$ for 18 h. A schematic illustration of the grafting procedure is presented in Figure 4.1. The next day, the slides with grafted copolymer were sonicated in IPA for 1 min and blow dried with N_2 .

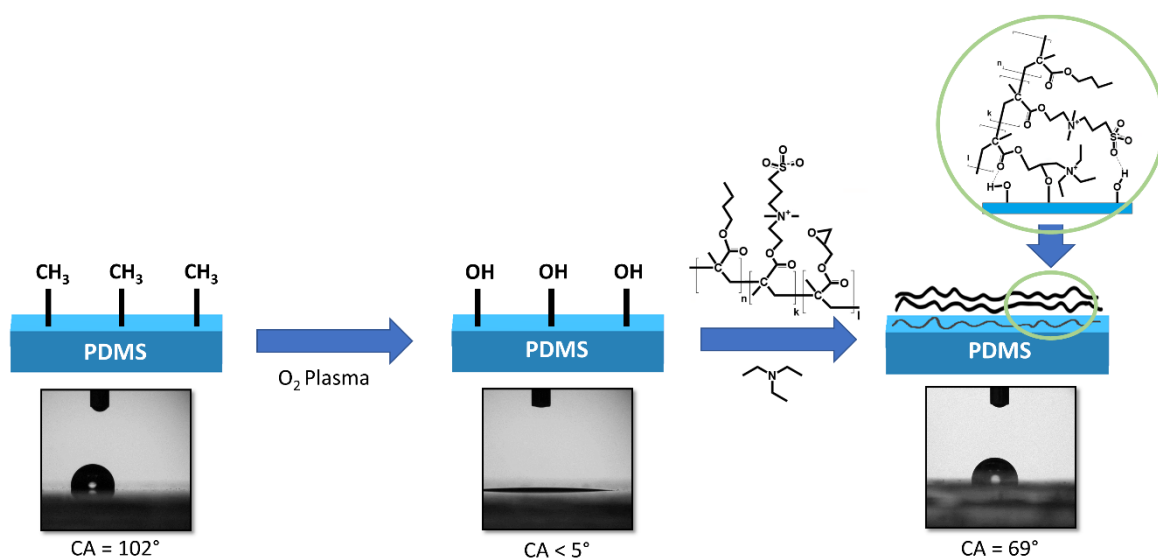


Figure 4.1 Schematic illustration of the grafting procedure of the Z-GL copolymer to PDMS substrate.

4.2.4 Characterization of Z-GL copolymer in the solution and grafted to PDMS.

The composition of the copolymer was determined with ^1H NMR experiment using Bruker Avance III 300 MHz NMR spectrometer and CDCl_3 as a solvent. Copolymer composition was calculated according to protocol described in Appendix B. The molecular weights and polydispersity index (PDI) were analysed by SEC as described earlier in section 2.2.3.

In order to confirm successful grafting of copolymer to silicone, ATR-IR measurements were performed using Shimadzu IRAffinity-1S FT-IR spectrometer equipped with a Quest attenuated total reflection (ATR) diamond accessory. The IR spectra were acquired by averaging 52 scans at a resolution of 4 cm⁻¹.

4.2.5 Wettability measurements

The wettabilities of the virgin PDMS and PDMS grafted with zwitterionic copolymer Z-GL were determined by sessile drop contact angle measurements of two probe liquids: DIW (Milli-Q water, ≥ 18.2 M Ω ·cm, Merck Millipore) and diiodomethane (CH₂I₂; Sigma-Aldrich) using DataPhysics OCA 35 goniometer. Additionally, for comparison, two bulk polymers were included in the analysis; a hydrophobic polymer H-0 and a zwitterionic polymer Z-L. The surface energy of the samples was determined using Owens-Wendt method (Owens and Wendt, 1969).

4.2.6 Attachment and removal of *N. incerta* diatom cells

The diatom removal assay was carried out using the method described in section 2.2.10. Before running the experiments, slides were leached in a tank with deionized water for six weeks to remove any unreacted monomers and solvent residues that could be leaching out from coatings. In the removal experiment, the wall shear stress used was 31 Pa.

4.2.7 Settlement and removal of *U. linza* zoospores

The methodology followed an earlier published report by Finlay *et al.* (2002). Mature, fertile plants of green algae *U. linza* were collected from Northumbrian coast, UK. The plants were allowed to release zoospores according to the protocol described by Callow *et al.* (1997). Next, 10 mL of zoospore suspension (typically 1.5·10⁶ spores ml⁻¹) was pipetted into the individual wells of a quadriPERM[®] dish, each well containing a slide. Six replicate slides were incubated in the dark for 60 min before washing in ASW to remove any motile and thus non-attached zoospores. Subsequently, three slides were fixed in 2.5% glutaraldehyde solution in filtered ASW for 45 min, washed several times in deionized water, dried and then stored. The three remaining slides were subjected to a 52 Pa wall shear stress for 5 min in the calibrated water channel (Schultz *et al.*, 2000). After the removal experiment, slides were fixed in 2.5% glutaraldehyde, washed with deionized water and air-dried. The density of the attached cells was determined by capturing 30 fields of view (0.17 mm²) on each replicate slide using an epifluorescence microscope (Leica DMI8 with Texas Red filter set) and the stored images were later used for spore enumeration. The percent removal was determined by

comparing the number of spores from unexposed control slides and the slides used in the removal experiment in the water channel.

4.3 Results and discussion

4.3.1 Synthesis and chemical characterization of copolymer Z-GL and grafting it to the PDMS

^1H NMR experiments were carried out to determine the chemical composition of the polymer before conducting the grafting procedure. Figure 4.2 presents the spectrum of the pBMA-*co*-SBMA-*co*-GMA copolymer. There was an excellent agreement between monomer feed and actual copolymer composition (Table 4.1). The number average molecular weight (M_n) determined by SEC was 11 kDa and PDI was 2.5.

Sample	Monomer feed ratio		Amount of monomers in polymer (mol %)	M_n (kDa)	PDI (M_w/M_n)
	Hydrophobic monomer (mol %)	Hydrophilic monomer (mol %)			
Z-GL	70 n-BMA 20 GMA	10 SBMA	70 n-BMA 20 GMA 10 SBMA	11	2.5

Table 4.1 Copolymer composition and characteristic data for polymer Z-GL.

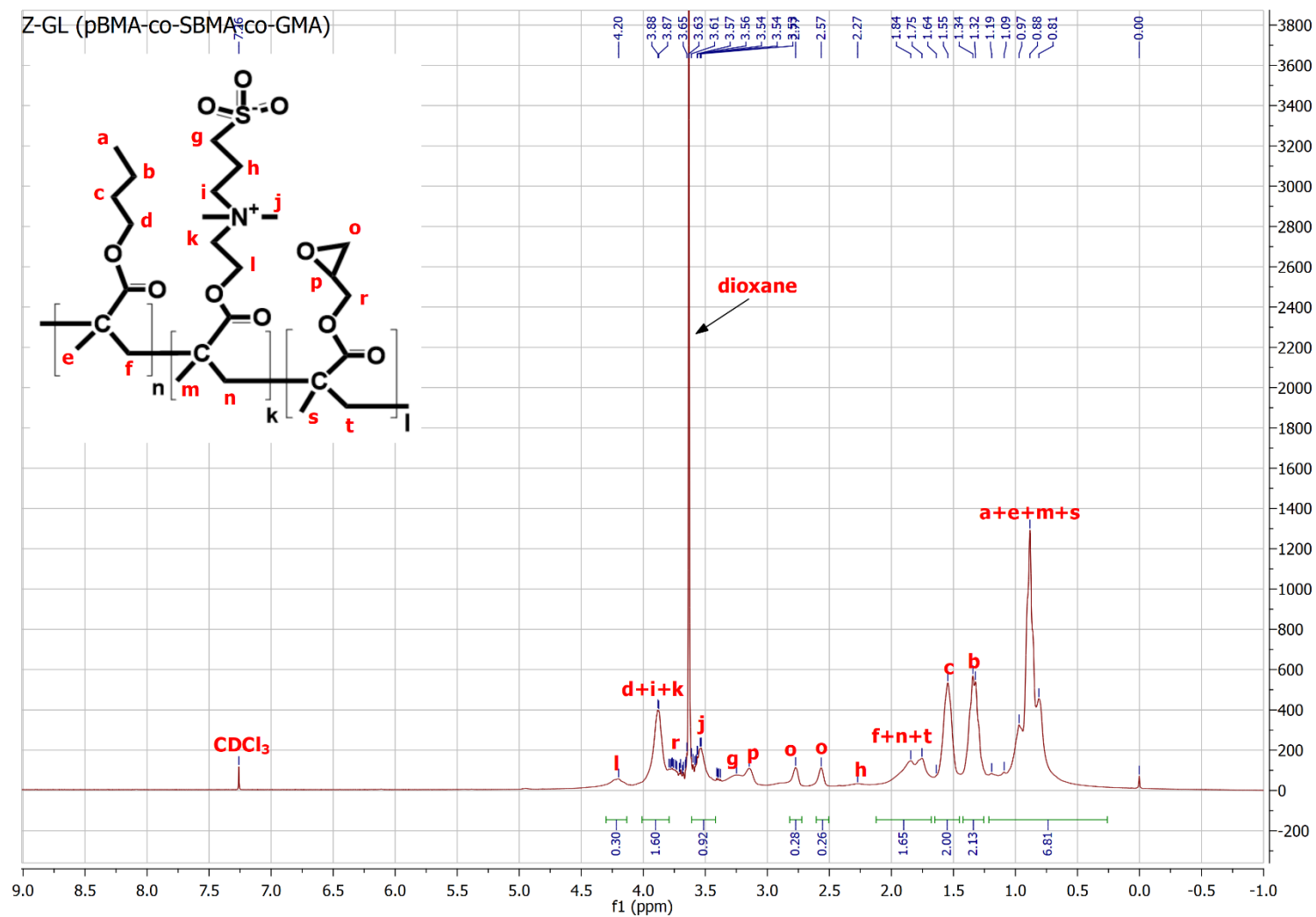


Figure 4.2 ¹H NMR spectrum of Z-GL copolymer (pBMA-co-SBMA-co-GMA) in CDCl₃.

ATR-IR was used to confirm the successful grafting of the copolymer to the PDMS substrate. As can be seen from Figure 4.3, the most noticeable difference between the virgin and grafted PDMS is the presence of the small band at around 1715-1730 cm^{-1} on the latter, which can be attributed to the C=O ester stretching of methacrylate comonomers. As for the SBMA unit, two peaks deriving from sulfonate SO_3^- are expected at around 1040 cm^{-1} (symmetric stretching of S=O) and 1200 cm^{-1} (asymmetric stretching of S=O). Unfortunately, due to large siloxane peaks at around 1020-1200 cm^{-1} which overlap with the two SO_3^- peaks, the presence of zwitterionic SBMA could not be directly confirmed using the ATR-IR. Still, based on the NMR spectra (Figure 4.2) and presence of the C=O ester stretching peak in the PDMS – Z-GL spectrum, it can be concluded with a high degree of confidence that the SBMA units are present in the modified PDMS sample.

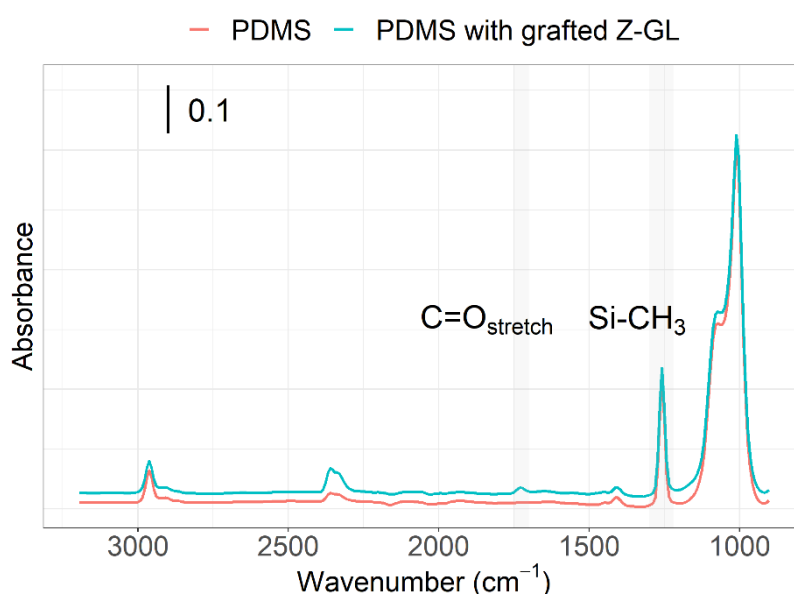


Figure 4.3 ATR-IR spectrum of virgin PDMS (red line) and PDMS with grafted polymer Z-GL (green line).

4.3.2 Wettability

The wettability of pure PDMS and one modified with Z-GL polymer was determined using sessile contact angles of two probing liquids (DIW and CH_2I_2) in air and the corresponding surface energies were calculated using Owens-Wendt method (Owens and Wendt, 1969). The reason for performing sessile measurements of contact angles instead of captive bubble was adsorption of silicone oil on the PDMS surface.

Clearly, when looking at the surface wettability results of the virgin and modified PDMS (Table 4.2), grafting of Z-GL copolymer has increased the wettability of PDMS as expressed by reduced contact

angles of DIW (θ_m°) and CH_2I_2 (ϕ_m°), and increased value of SFE (γ^{TOT}). The SFE of the modified PDMS is very similar to that of the bulk polymer Z-L, which is not surprising considering their relatively similar copolymer composition.

Sample	DIW in air (θ_m°)	CH_2I_2 in air (ϕ_m°)	Dispersive component (γ_s^d) ($\text{mN}\cdot\text{m}^{-1}$)	Polar component (γ_s^p) ($\text{mN}\cdot\text{m}^{-1}$)	Total surface energy (γ^{TOT}) ($\text{mN}\cdot\text{m}^{-1}$)
H-0	96.7 ± 0.5	43.7 ± 0.5	37.7 ± 0.3	0	37.7 ± 0.3
Z-L	77.3 ± 1.1	41.7 ± 1.1	38.8 ± 0.6	3.3 ± 0.3	42.1 ± 0.7
PDMS	97.7 ± 0.5	62.3 ± 0.5	27.2 ± 0.3	0.5 ± 0.1	27.7 ± 0.3
PDMS – Z-GL	68.7 ± 0.5	52.3 ± 1.1	33 ± 0.6	8.7 ± 0.4	41.7 ± 0.3

Table 4.2 Measured contact angles of sessile droplets of DIW and CH_2I_2 in air and corresponding surface energies determined using the Owens-Wendt method.

4.3.3 Attachment and removal of diatom cells and zoospores

Diatoms reach surfaces passively, under gravity in laboratory experiments, so after the incubation period a similar number of cells should be present on all surfaces tested. Differences in the number of cells before exposure to flow can be attributed to gentle washing or dish movement, and these differences reflect the cells ability to adhere to surfaces (Weinman *et al.*, 2009). Figure 4.4A shows the number of cells per mm^2 attached to modified PDMS – Z-GL, polymer Z-L and virgin PDMS before and after exposure to flow. Differences in the number of cells initially attached to surfaces were significant (one-way ANOVA $F_{2,265} = 495.5$, $p \leq 0.001$). The lowest number of attached cells before the removal experiment was recorded on bulk polymer Z-L and it was significantly different from other tested surfaces (Tukey tests, $p \leq 0.05$).

The removal experiment using a calibrated water channel revealed significant differences in attachment strength of cells (one-way ANOVA $F_{2,264} = 166.7$, $p \leq 0.001$). As expected, diatom cells were strongly attached to hydrophobic PDMS and the removal of cells from this surface was very low (below 5%). Perhaps more interestingly, in spite of similar number of initially adhered cells on PDMS – Z-GL sample and virgin PDMS, significantly more cells were removed from the modified PDMS (Tukey tests, $p \leq 0.05$).

To further investigate the FR properties of the modified silicone elastomer, experiments with zoospores of *U. linza* were performed. In contrast to diatom cells, spores are motile and negatively phototactic and respond to several cues such as wettability, topography and charge, and can recognize a surface that is not suitable for settlement (Callow *et al.*, 2014). Figure 4.5A shows the number of

spores before and after the removal experiment using the calibrated water channel. The number of settled spores differed significantly between surfaces (one-way ANOVA $F_{2,265} = 29.17$, $p \leq 0.001$), and the lowest number of spores was recorded on bulk polymer Z-L, followed by PDMS – Z-GL and PDMS. In general, spores tend to settle in high numbers on hydrophobic surfaces such as PDMS (Weinman *et al.*, 2009; Sundaram *et al.*, 2011; Bauer *et al.*, 2016b), and tend to avoid settlement on hydrophilic surfaces (Callow *et al.*, 2000). The low settlement of spores on zwitterionic polymer Z-L is in good agreement with work by Bauer *et al.* (2016b) who prepared sulfobetaine SB-SAM and also recorded low initial settlement of spores.

The difference in spore removal was significant (one-way ANOVA $F_{2,264} = 3.774$, $p = 0.0242$), with the highest removal recorded on modified silicone PDMS – Z-GL sample, and lowest on zwitterionic polymer Z-L (Figure 4.5B). Although the removal from modified PDMS was not significantly different from virgin PDMS (Tukey tests, $p > 0.05$), clearly, grafting of zwitterionic copolymer improved the FR properties of the silicone. As for the polymer Z-L, despite having the lowest number of initially attached spores (Figure 4.5A), the spores that adhered to the surface were strongly attached as evidenced by the low removal rate. This result is somewhat in contrast with the work by Bauer *et al.* (2016b) and Zhang *et al.* (2009), where excellent release of spores from zwitterionic surfaces was reported. The reason for this discrepancy can be explained by differences in wettability of surfaces. Bauer *et al.* (2016b) showed that with increasing contact angle the removal of spores decreases. Indeed, the SB-SAM prepared by Bauer *et al.* (2016b) had a water contact angle of around 15° , whereas the contact angle recorded for polymer Z-L was 77° .

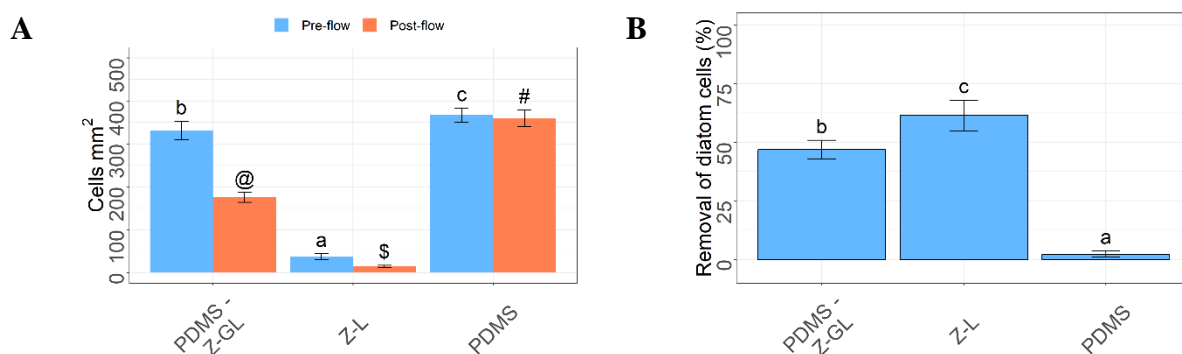


Figure 4.4 (A) Density of *N. incerta* cells. Pre-flow counts are the number of cells before exposure to 31 Pa wall shear stress in the calibrated water channel. Post-flow counts are the number of diatom cells remaining after exposure to flow. Each point represents the mean from 90 counts on three replicate slides. Error bars are 95% CIs. Letters/symbols indicate Tukey's corresponding pairwise comparisons between surfaces before and after flow, and points that do not share a letter/symbol are significantly different. (B) Same data presented as percentage removal. Error bars are 95% CIs from arc-sine transformed data. Letters/symbols indicate Tukey's corresponding pairwise comparisons, and points that do not share a letter/symbol are significantly different.

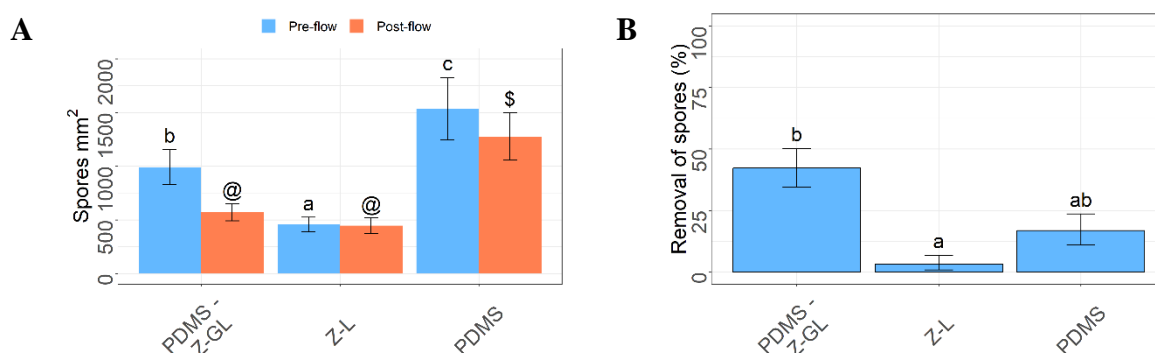


Figure 4.5 (A) Density of *U. linza* spores. Pre-flow counts are the number of spores before exposure to 52 Pa wall shear stress in the calibrated water channel. Post-flow counts are the number of spores remaining after exposure to flow. Each point represents the mean from 90 counts on three replicate slides. Error bars are 95% CIs. Letters/symbols indicate Tukey's corresponding pairwise comparisons between surfaces before and after flow, and points that do not share a letter/symbol are significantly different. (B) Same data presented as percentage removal of spores. Error bars are 95% CIs from arc-sine transformed data. Letters/symbols indicate Tukey's corresponding pairwise comparisons, and points that do not share a letter/symbol are significantly different.

To summarize, in this chapter a hybrid coating consisting of PDMS and zwitterionic copolymer (pBMA-*co*-SBMA-*co*-GMA) was prepared, characterized and tested for its AF and FR properties using diatom cells of *N. incerta* and spores of *U. linza*. In general, the PDMS with grafted zwitterionic copolymer presented improved FR properties over the non-modified silicone, with considerably higher removal of diatom cells and algal spores. Furthermore, the low spore settlement observed for the modified PDMS, as well as the zwitterionic bulk copolymer, confirm high AF potential of zwitterionic SBMA against a range of fouling organisms. Although the results obtained for the PDMS-zwitterionic hybrid are quite promising, the fabrication process of these surfaces is not practical and cannot be directly applied in an industrial environment. Future work could include synthesis of true random PDMS-SBMA copolymers, as well as development of more sophisticated hybrid coatings with zwitterionic SBMA embedded into the silicone-hydrogel system.

Chapter 5. Long-term stability of selected bulk polymer coatings

5.1 Introduction

The typical service life for antifouling (AF) paint is from three to five years. The development of a commercially successful coating is therefore a difficult task, requiring long-term performance testing in variety of conditions ranging from cold waters of the North Sea to tropical waters of Southeast Asia and India. The majority of published work on new AF technologies is devoted to model/experimental systems, which in most cases have limited long-term effectiveness and are not suitable for real-life applications. The cost of potential failure of AF coatings is very high, thus the introduction of a new AF system is a lengthy process involving several years of formulation development, optimisation and testing (Kiil *et al.*, 2006).

In general, AF paint contains binders, pigments, solvents and additives, all playing specific roles in the formulation. The most important part of any paint is the binder (polymer/resin), which creates a continuous film adhering to and protecting the surface it is applied to. Obviously, the stability of the binder is of utmost importance, as it affects the functionality and long-term performance of the coating. This is especially true for marine AF paints where the seawater is particularly aggressive and can induce polymer hydrolysis, which depending on the case, can be desirable thing (e.g. self-polishing coatings) or detrimental as in case of fouling-resistant coatings, where loss of pendant group functionality can lead to compromised AF performance.

Hydrolysis is a complex process that is dependent on various factors including steric effects, branching, degree of crystallinity, molecular weight, porosity, pH and water uptake in the polymer matrix (Laycock *et al.*, 2017). Hydrolysis can take place within the polymer backbone (e.g. polylactides, polyamides), or through the ester bond (e.g. acrylics) (Vallee-Rehel *et al.*, 1998). The immediate result of hydrolysis is polymer degradation, which can be described as the process of chain cleavage, resulting in loss of oligomers and monomers from the polymeric matrix. This is termed erosion (Göpferich, 1997). Overall, the erosion processes can be divided into processes occurring in the bulk and those happening at the surface (Figure 5.1). In the bulk erosion the degradation occurs throughout the material by hydrolytic chain scissions, and the rate of water diffusion is greater than the rate of hydrolysis. The different phenomena involved in bulk erosion are presented schematically in Figure 5.2. As for surface erosion, the polymer starts to degrade from the surface with noticeable decrease in thickness over time. Contrary to bulk erosion, in surface erosion the rate of hydrolysis is higher than the rate of water diffusion. Additionally, in surface erosion, the bulk of the polymer retains

Polyacrylates and polymethacrylates are two groups of binders that are commonly used in AF paints. In general, polyacrylates are considered less hydrolytically stable than polymethacrylate analogues (van de Wetering *et al.*, 1998; Zhao *et al.*, 2013; Zhu *et al.*, 2015) and for this reason they are commonly used as binders in SPCs. As noted earlier, the hydrolysis is highly dependent on environmental conditions, with pH and water uptake playing a significant role in the process. Thus, the highly hydrated copolymers such as those containing SBMA could be particularly susceptible to hydrolysis. In a recent report by Schönemann *et al.* (2018), hydrolytic behaviour of zwitterionic polymethacrylates and polymethacrylamides was explored and it was found that polysulfobetaines were very stable at ambient temperature over a range of pH from 0 to 14 for at least one year. In addition, the pOEGMA polymer was evaluated and similarly high hydrolytic stability was reported. It was speculated that the reason for the high resistance of these polymers towards hydrolysis is high steric crowding which protects the carboxyl ester groups against water attack (Schönemann *et al.*, 2018).

Testing of the chemical stability of polymers by analytical methods such as NMR, SEC and gas chromatography mass spectrometry (GC-MS) is an important part of the testing regime as it can predict changes at the macromolecular level, however these experiments provide no information regarding real-life performance of coatings when exposed to marine environment. In order to determine the antifouling effectiveness of coatings, different test methods can be employed, and these can generally be divided into laboratory-based assays and field tests. Laboratory assays allow rapid evaluation of coatings in a controlled, reproducible manner and are not limited to specific testing sites or seasons of the year. Furthermore, with laboratory testing, the settlement and adhesion processes can be studied in detail, providing information about the behaviour of fouling organisms and helping to develop mechanisms that could be involved in their deterrence (Callow *et al.*, 2014). Another advantage of laboratory assays is that they can reveal potential instability and/or toxicity of the coating which could save time and resources before running full sea trials. Contrary to laboratory assays, static field tests are run in the natural marine environment and more closely resemble conditions encountered during typical paint service. The immersed panels are visually inspected at regular time intervals to determine the degree and category of fouling. These tests can take up-to five years depending on the type of AF system and the commercialization stage of the product.

The work presented in this chapter is aimed at determining the chemical stability and AF performance of selected bulk polymer coatings after prolonged immersion in seawater. The coatings selected for testing included polymers H-0, E-L, Z-L20 and A-L. In the first part of this chapter chemical stability, water states and wettability of aged polymers are presented. The second part of this chapter is devoted

to AF testing with results presented both from laboratory assays and field tests. The data and discussion presented in this chapter are aimed at answering such questions as: Why and when do the coatings fail? And which polymer properties change during service life, therefore having potential as indicators of failure?

5.2 Materials and methods

5.2.1 Preparation and storage of panels used in the laboratory-based assays

Selected polymer solutions were applied to PVC panels according to the method described in section 2.2.2. Fully dried panels were then put in custom slide holders and kept for six months at 5-6 °C in plastic, closed containers filled with deionised water (DIW) and equipped with a carbon filter pump. To minimize potential bacterial contamination of coatings, water was changed every four-five weeks.

5.2.2 Polymer characterization after long-term storage in water

In order to investigate the long-term chemical stability of polymers, different analytical techniques were used, i.e., ^1H NMR, attenuated total reflectance infrared spectroscopy (ATR-IR) and gas chromatography-mass spectrometry (GC-MS). Dried polymer samples (10 mg) were put in glass vials and 20 mL of DIW (Milli-Q water, $\geq 18.2 \text{ M}\Omega\cdot\text{cm}$, Merck Millipore) or ASW (Tropic Marin; 22 ppt) was added to each vial. The vials were then closed and left at ambient temperature (22 ± 1 °C) for six months.

After this time the polymer samples were removed from water, dried and subsequently analysed using ^1H NMR as described in section 2.2.3. The polymer leachates were analysed by GC-MS to monitor potential products of degradation. Approximately 1 g of the polymer leachate sample was transferred to a 20 mL glass vial and diluted with around 15 mL of a 30% v/v solution of bis-Trimethylsilyl Trifluoroacetamide (BSTFA) in THF and allowed to incubate at 45 °C overnight. A small volume of this solution was transferred to a 2 mL auto-sampler vial. Prior to injecting each sample, the 30% solution of BSTFA in THF was injected. The equipment used was Agilent 6890-5973 GC-MS with capillary column (Agilent DB-5MS; 30 m long x 0.25 mm inner diameter x 0.5 μm film thickness). The operating conditions were following: initial temperature 80 °C (4 min hold), final temperature 300 °C at 10 °C/min (12 min hold). Helium was used as a carrier gas and the injection temperature was 280 °C. Ionization mode was Electron Impact (EI). The mass spectra scan range was 50-650 m/z.

To complement the ^1H NMR spectra, ATR-IR measurements of panels aged in DIW were also conducted. The equipment used was the Shimadzu IRAffinity-1S FT-IR spectrometer equipped with

a Quest attenuated total reflection (ATR) diamond accessory. The IR spectra were acquired by averaging 52 scans at a resolution of 4 cm^{-1} .

5.2.3 Wettability measurements

The wettability of panels coated with polymers was evaluated after six months of storage in deionized water based on the method described in section 2.2.4.

5.2.4 Determination of swelling and water states

Swelling of polymers, as expressed by the equilibrium water content (EWC), and different types of water present in the hydrated samples were determined after six months of storage in DIW and ASW according to the methods described in sections 2.2.5 and 2.2.6.

5.2.5 Settlement assays using cypris larvae

Barnacle settlement experiments were performed according to the method described in section 2.2.8.

5.2.6 Attachment strength of juvenile barnacles

The ease of removal of juvenile barnacles was determined as described in section 2.2.9, except for the use of an automated water jet instead of a water channel. The impact pressure used in the removal experiments was 62 kPa, which is approximately equivalent to a ship speed of 13 knots.

5.2.7 Removal of diatom cells

The diatom removal assay was carried out using the method described in section 2.2.10.

5.2.8 Field testing

Field testing was conducted using 11 different bulk coatings (including Intersleek® 1100SR as a standard) in the summer of 2017 at two different locations: Hartlepool Marina, UK ($54^{\circ}41'31.1''\text{N}$ $1^{\circ}12'00.2''\text{W}$) and Changi Sailing Club, Singapore ($1^{\circ}23'35.4''\text{N}$ $103^{\circ}58'43.5''\text{E}$). The immersion boards were prepared in the following manner. For each coating, three PVC panels (8 x 8 cm) were sanded, wiped with xylene and polymer solutions were applied using a paint brush. In order to ensure sufficient coating thickness, panels were recoated three times and left to dry for few days. Next, PVC panels were attached to 61 x 61 cm plywood using epoxy glue and the position of each panel was varied using a 'Latin square' design. The board edges and the reverse side of the board were painted using a fouling-release system (Intersleek® 1100SR) for increased durability of the substrate. The boards were fully immersed vertically so that the top was 0.5 meter below the water surface. Every

couple of weeks, the immersed boards were taken out of the sea and high-resolution images were taken. The fouling levels were assessed by eye and percentage coverage of each fouling category was established. The biofouling community was divided into following categories: hard-shelled animals, soft-bodied animals, weeds, microfouling. The fouling results from each replicate panel were averaged and the mean percentage coverage of total biofouling for each surface was compared using non-parametric testing i.e. Kruskal-Wallis with Bonferroni correction.

5.3 Results and Discussion

5.3.1 Chemical stability of polymers after immersion in DIW and ASW

The ^1H NMR spectra of the polymer samples before and after long storage in DIW and ASW are presented in Figure 5.3-5.6. It can be observed that the polymer spectra before and after immersion look similar, with no significant changes in peak intensities. This implies that the free polymer films were stable under both conditions for a period of at least six months. This observation was also confirmed by the compositional data where the calculated amounts of comonomers in the polymers remained unchanged (Table 5.1). Account must be taken, however, of the fact that in this method of monitoring, changes in small degradation products, such as alcohols or amines, could be missing in the NMR spectrum and they could remain in the aged water medium. In order to analyse the leachates for potential products of polymer degradation, GC-MS measurements were employed (Figure 5.7). No sign of polymer degradation was observed in all tested samples, and the only major peak observed was the diethyldimethyl succinonitrile (DDSN), which is the breakdown product of the AMBN initiator.

Another approach to studying hydrolytic stability of polymers is by performing the experiments directly in the NMR tube (Schönemann *et al.*, 2018; Xie *et al.*, 2018a). In this method, polymers are dissolved in deuterated solvent, a small amount of water (Milli-Q water or ASW) is added to the mixture and NMR experiments are conducted at set time intervals. This method could be theoretically applied with deuterated hexafluoroisopropanol (HFIP- d_2) as the NMR solvent. The only potential problem with this approach is the formation of water clusters in the HFIP-water mixture (Yoshida *et al.*, 2003), which could affect the sorption and diffusion of water in the polymer matrix (Davis and Elabd, 2013) and ultimately reduce the effectiveness of hydrolytic attack.

Sample	Initial amounts of monomers in polymer (mol %)	Amounts of monomers in polymer after six months in DIW (mol %)	Amounts of monomers in polymer after six months in ASW (mol %)
H-0	100 n-BMA	100 n-BMA	100 n-BMA
E-L	54 n-BMA 34 IBoMA 12 mPEG350MA	53 n-BMA 35 IBoMA 12 mPEG350MA	53 n-BMA 35 IBoMA 12 mPEG350MA
Z-L20	93 n-BMA 7 SBMA	93 n-BMA 7 SBMA	93 n-BMA 7 SBMA
A-L	92 n-BMA 8 SPMA	92 n-BMA 8 SPMA	92 n-BMA 8 SPMA

Table 5.1 Initial copolymer compositions and after six months of storage in DIW and ASW as determined by ^1H NMR experiments.

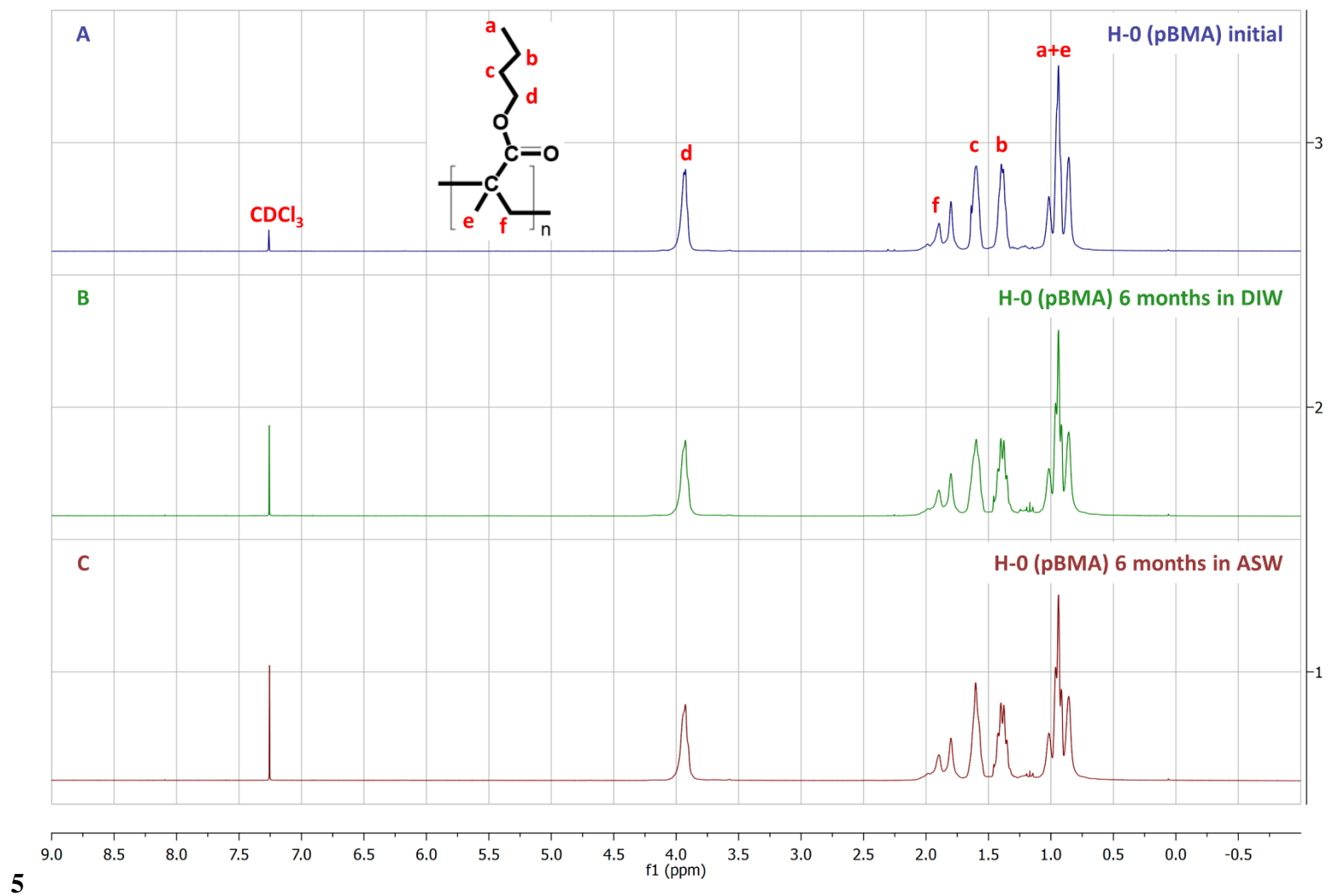


Figure 5.3 ^1H NMR spectrum of H-0 homopolymer (pBMA) in CDCl_3 . (A) initial (B) after six months in DIW (C) after six months in ASW.

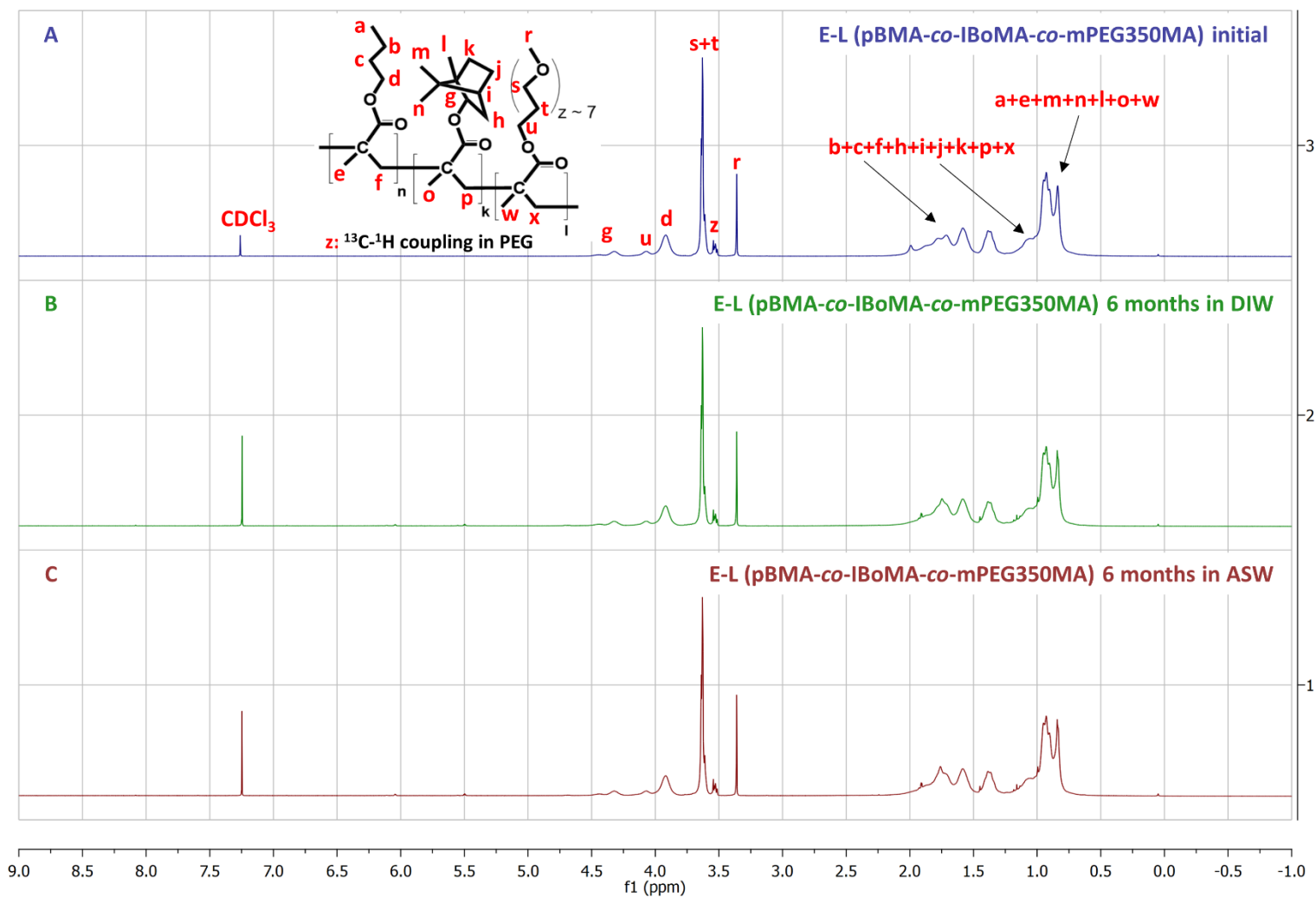


Figure 5.4 ^1H NMR spectrum of E-L copolymer (pBMA-co-IBoMA-co-mPEG350MA) in CDCl_3 . (A) initial (B) after six months in DIW (C) after six months in ASW.

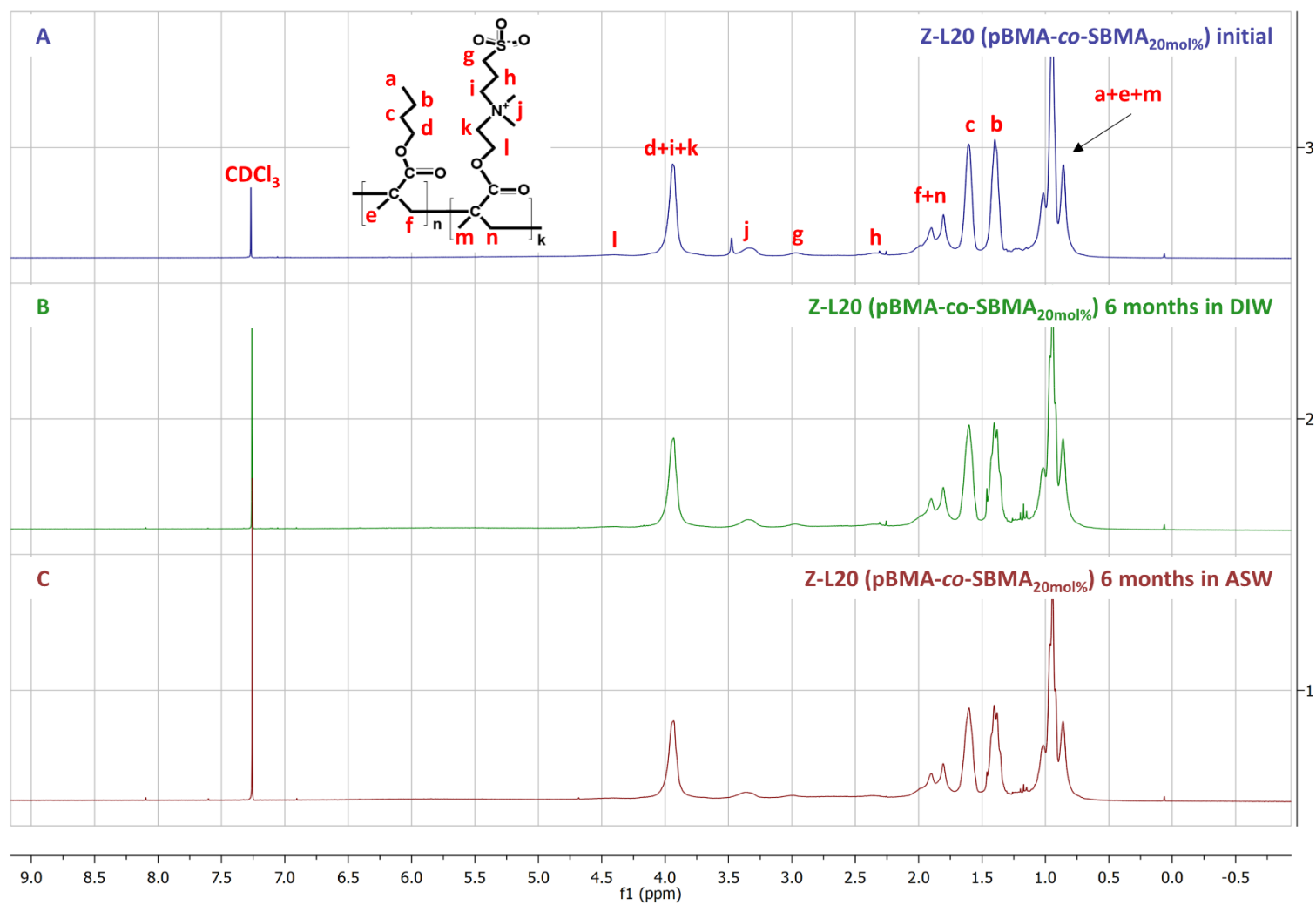


Figure 5.5 ^1H NMR spectrum of Z-L20 copolymer (pBMA-co-SBMA_{20mol%}) in CDCl_3 . (A) initial (B) after six months in DIW (C) after six months in ASW.

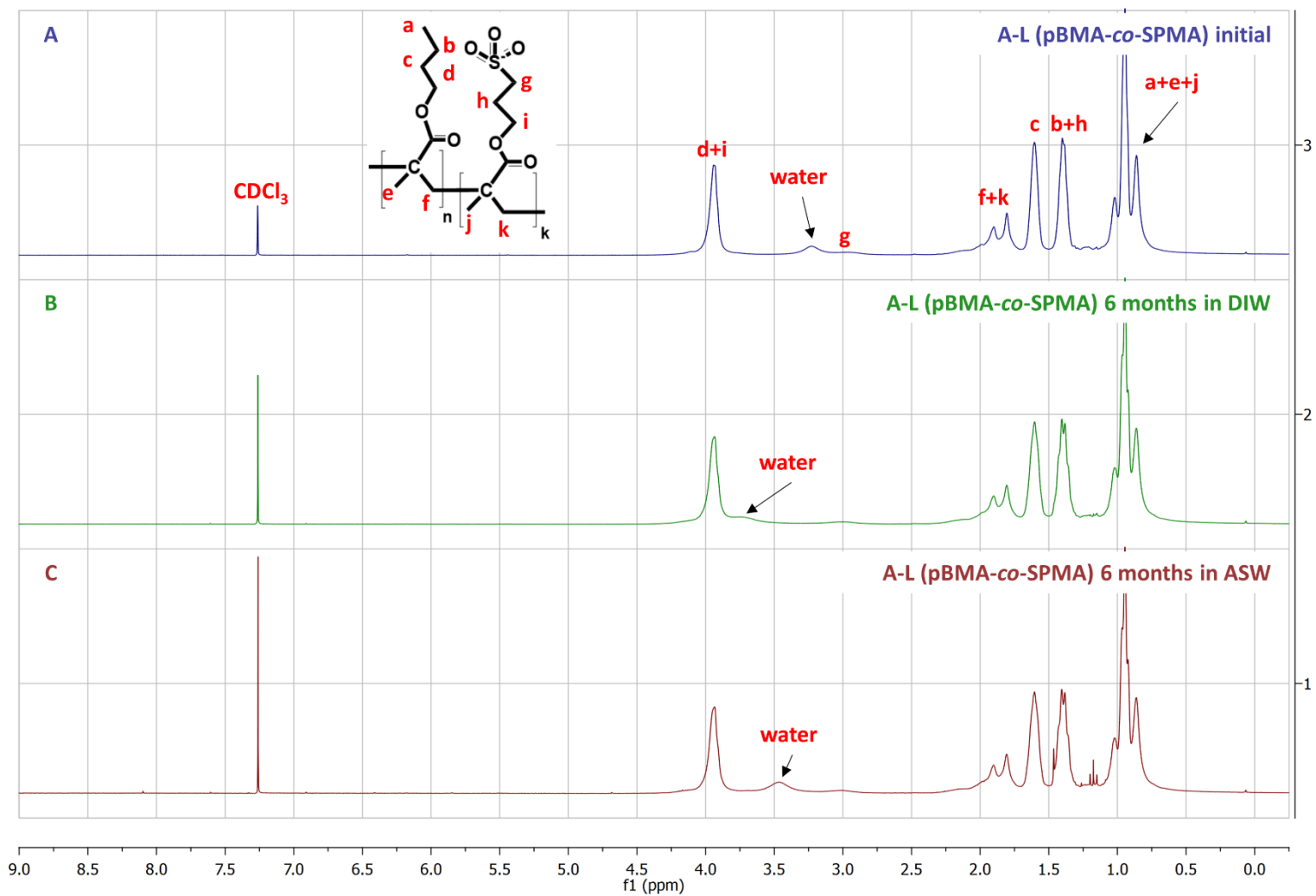


Figure 5.6 ^1H NMR spectrum of A-L copolymer (pBMA-co-SPMA) in CDCl_3 . (A) initial (B) after six months in DIW (C) after six months in ASW.

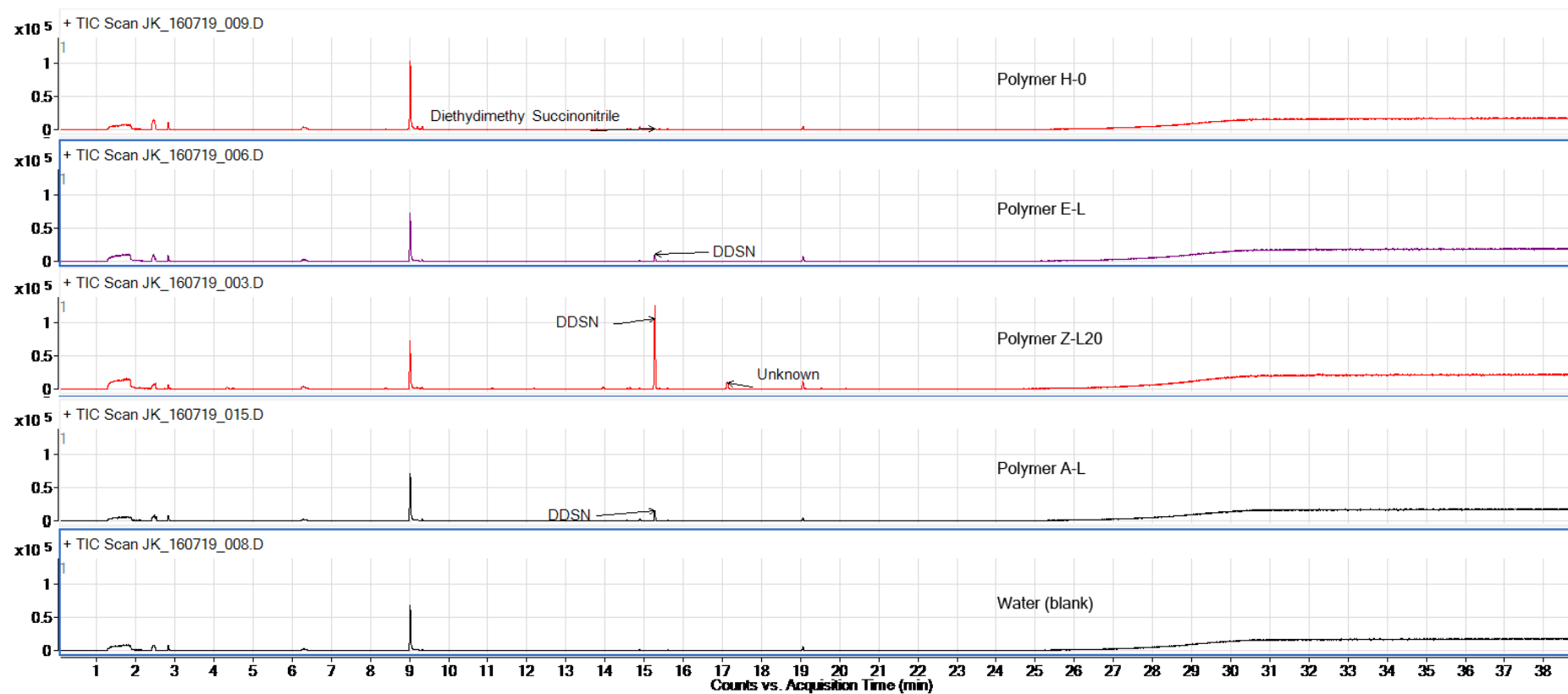


Figure 5.7 The GC-MS spectra of polymer leachates after six months of storage in DIW.

To further analyse the chemical stability of coatings exposed to DIW, ATR-IR measurements were performed and the spectra before and after six months of testing are presented in Figures 5.8-5.11. In all cases two bands characteristic for methacrylates are observed, i.e., C=O stretching band at around 1715-1730 cm^{-1} and C-O stretching at around 1150-1250 cm^{-1} . In the case of polymer E-L, the broad band at around 1100-1250 cm^{-1} is a result of overlapping of C-O ester stretching with C-O-C stretching of PEG chains (expected at around 1100-1150 cm^{-1} (Lee *et al.*, 2009)). With regard to polymers Z-L20 and A-L, the SO_3^- group was identified at around 1040 cm^{-1} , assigned to S=O stretching. There are no visible changes in the characteristic IR bands before and after long-term storage in DIW, implying that no major chemical changes occurred in the tested samples.

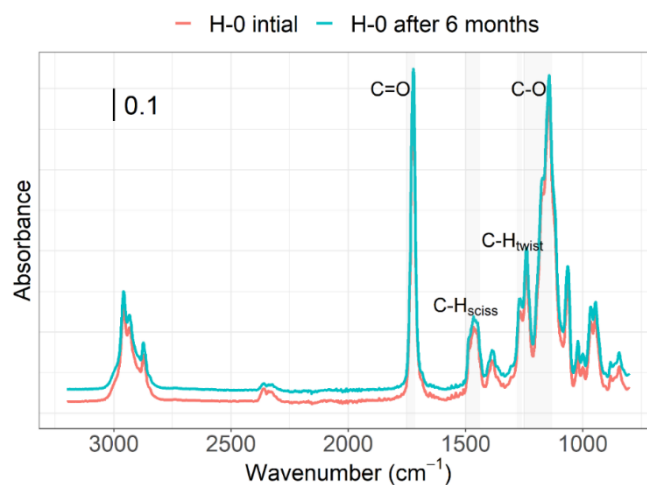


Figure 5.8 ATR-IR spectrum of polymer H-0 (pBMA) before (red line) and after (green line) immersion in DIW for six months.

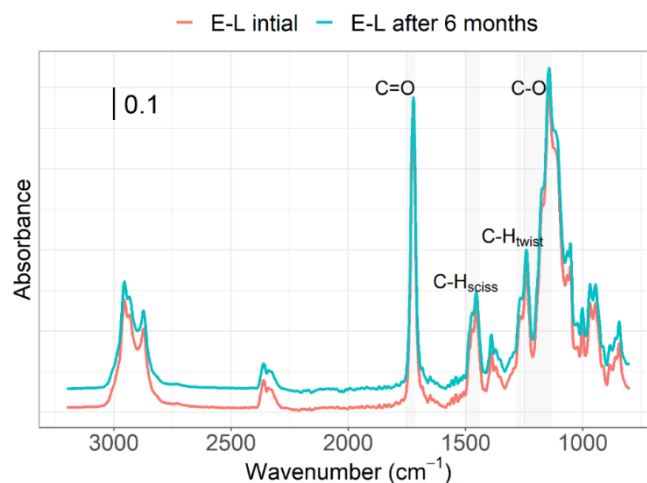


Figure 5.9 ATR-IR spectrum of polymer E-L (pBMA-co-IBoMA-co-mPEG350MA) before (red line) and after (green line) immersion in DIW for six months.

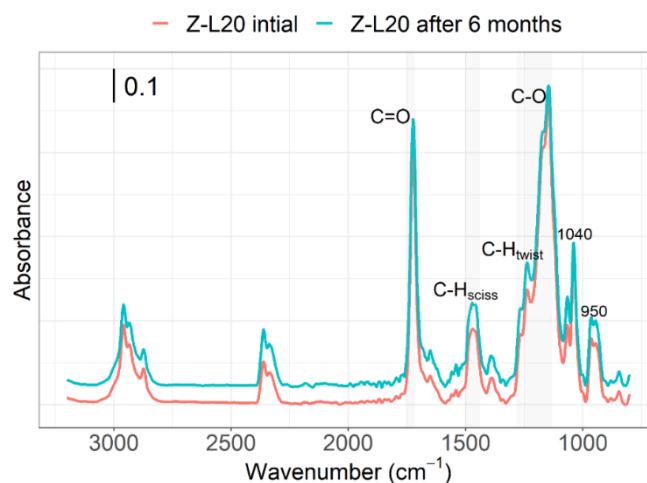


Figure 5.10 ATR-IR spectrum of polymer Z-L20 (pBMA-*co*-SBMA_{20mol%}) before (red line) and after (green line) immersion in DIW for six months.

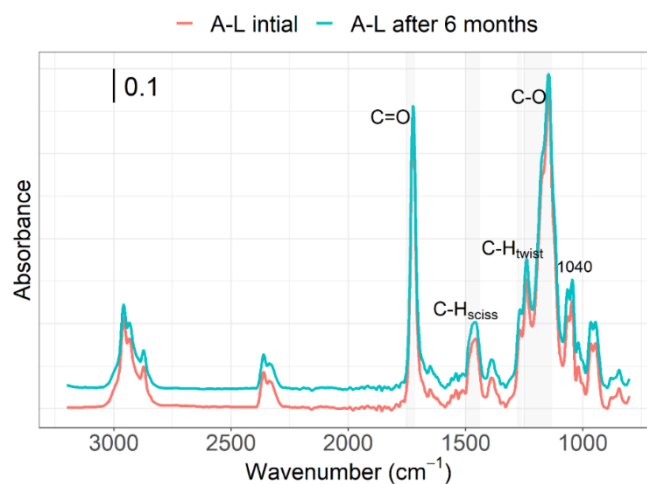


Figure 5.11 ATR-IR spectrum of polymer A-L (pBMA-*co*-SPMA) before (red line) and after (green line) immersion in DIW for six months.

The NMR, GC-MS and ATR-IR data suggest that the bulk polymers are hydrolytically stable both in DIW and ASW for at least six months, which is quite remarkable considering their high degree of swelling. The high resistance towards hydrolysis could be ascribed to high steric crowding of the methacrylate moiety, which protects the carboxyl group from water attack (Schönemann *et al.*, 2018).

5.3.2 Wettability

The wettability of polymers after long immersion in DIW was determined using underwater contact angles and was accompanied by surface energy calculations (Table 5.2). To graphically visualize changes in surface energies, the results were also plotted as bar plots (Figure 5.12 and 5.13).

The zwitterionic polymer Z-L20 and anionic A-L maintained their high surface wettability even after six months of storage in DIW. After an initial increase in wettability, which could be explained by water-induced surface reorganization, these surfaces became stable and the hydrophilic functional groups fully interacted with water. As for the hydrophobic polymer H-0, the contact angles within the air bubble and silicone oil also increased, meaning that the surface had become more hydrophilic. The calculated value of dispersive energy γ_{pa}^d (197.2 mN·m⁻¹), and the resulting SFE and IFE values are unreasonably high for a polymeric system and should be discarded. A different set of probing liquids would probably solve this problem. Still, the observed wettability increase for polymer H-0 is rather unusual considering that it is a homopolymer of n-butyl methacrylate and could be possibly explained on the basis of the plasticizing effect of water, which could facilitate backbone and side chain reorientation (Grohens *et al.*, 2003). Wang *et al.* (2001) studied the behaviour of pBMA in water using sum frequency generation (SFG) vibrational spectroscopy and reported that the side-chain methyl groups of pBMA are indeed capable of reorientation in water. Unfortunately, the changes in structure of pBMA were monitored only for 12 h, which is probably not long enough to observe more pronounced surface reorganizations which could trigger major changes in wettability. Regarding the polymer E-L, the reduced underwater contact angles of both probing liquids after six months suggest that the polymer lost some of its hydrophilic character and became more hydrophobic. This behaviour could be explained by the limited chemical stability of PEG and/or interaction of probe liquids with the surface. As the ¹H NMR and ATR-IR spectra remained practically unchanged after aging in water, it seems likely that the reducing contact angles could be attributed to penetration of the air bubble and silicone oil into the coating. Indeed, after close inspection of the surface it was porous and the reason for this degradation could be the phase separation of crystalline PEG in the polymer matrix (Murthy *et al.*, 2010).

Sample	Angle inside air bubble (θ_m°)			Angle inside silicone oil (ϕ_m°)			Dispersive component γ_{pa}^d (mN · m ⁻¹)			Polar component γ_{pa}^p (mN · m ⁻¹)			Total surface energy (SFE) γ_{pa}^{TOT} (mN · m ⁻¹)			Interfacial energy (IFE) γ_{pw} (mN · m ⁻¹)		
	Initial	6 wk	6 mth	Initial	6 wk	6 mth	Initial	6 wk	6 mth	Initial	6 wk	6 mth	Initial	6 wk	6 mth	Initial	6 wk	6 mth
H-0	100 ±0.9	110.3 ±1.4	142.3 ±1.9	58.7 ±0.5	74.3 ±1.9	99.3 ±1.4	38.3 ±2.0	46.9 ±8.6	197.2 ±55.8	6.6 ±0.1	9.3 ±0.9	12.00 ±1.0	44.8 ±1.9	56.2 ±7.7	209.4 ±54.8	32.2 ±0.8	30.9 ±6	151.5 ±53.3
E-L	114.7 ±0.5	179.7 ±0.5	159.7 ±0.5	102 ±0.9	178 ±0.9	113.7 ±0.5	22.8 ±1	44.8 ±0.1	238.6 ±3.7	19.2 ±0.4	34.5 ±0	15.3 ±0.2	42 ±0.7	79.3 ±0	253.8 ±3.5	11.6 ±0.3	6.5 ±0	185.6 ±3.8
Z-L20	157 ±0.9	178.7 ±0.5	179 ±0	167 ±0.9	178.7 ±0.5	177.7 ±2.1	34 ±0.6	44.7 ±0	44.8 ±0.2	35.4 ±0	34.5 ±0	34.5 ±0.1	69.4 ±0.6	79.2 ±0	79.3 ±0.1	2.4 ±0.1	6.4 ±0	6.5 ±0.1
A-L	151.3 ±1.1	179.7 ±0.5	178.7 ±0.5	149 ±0.9	179.7 ±0.5	178.7 ±0.5	36.5 ±1.9	44.7 ±0	44.7 ±0.1	31.7 ±0.5	34.5 ±0	34.5 ±0	68.3 ±1.4	79.2 ±0	79.2 ±0	4.4 ±0.7	6.5 ±0	6.4 ±0

Table 5.2 Underwater contact angles within the air bubble (θ_m) and silicone oil droplet (ϕ_m) and calculated surface energies of coatings before and after storage in DIW for six weeks and six months. Crossed out values do not have a physical meaning and should be ignored. Errors are 95% CIs.

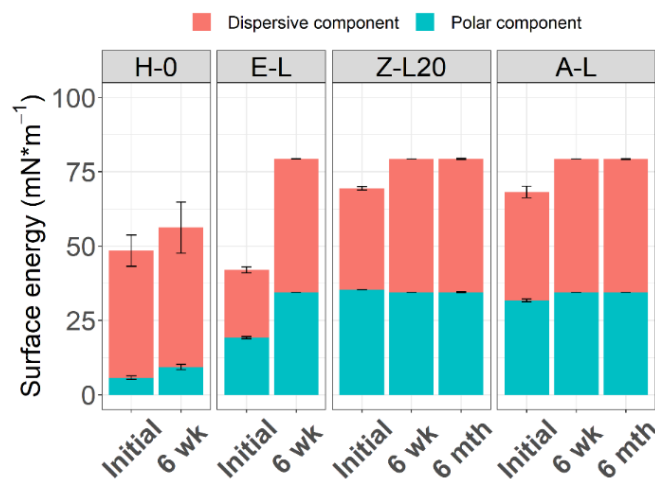


Figure 5.12 Changes in total surface energy (SFE) of polymers together with corresponding polar and dispersive contributions after storage in DIW. Errors bars are 95% CIs.

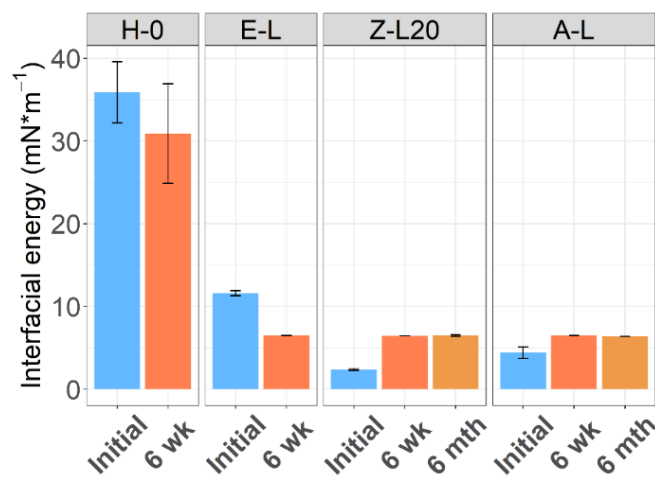


Figure 5.13 Changes in interfacial energy polymer/water (IFE) after storage in DIW. Errors bars are 95% CIs.

5.3.3 Determination of swelling and water states in aged polymer samples

TGA measurements were conducted on polymers immersed in DIW and ASW to determine the degree of swelling after six months of storage in the two aqueous media. It can be seen from Figure 5.14 that the swelling of polymers in DIW, as expressed by EWC, did not change considerably over the period of six months, which implies that after initial high water uptake polymers were fully saturated with water and the hydration shells around hydrophilic functionalities were stable. In the case of samples stored in ASW, all polymers presented reduced water uptake, which could be attributed to the effect of osmotic

deswelling of the polymer chains causing polymers to shrink (Geise *et al.*, 2014). For the single charged polymer A-L, where a considerable reduction in swelling was observed, there is also an additional effect of screening of charges on the pendant anionic groups by the counterions present in ASW. This charge screening effect minimizes the electrostatic repulsion forces between polymeric chains and induces a collapsed conformation of the polymer (Azzaroni *et al.*, 2007).

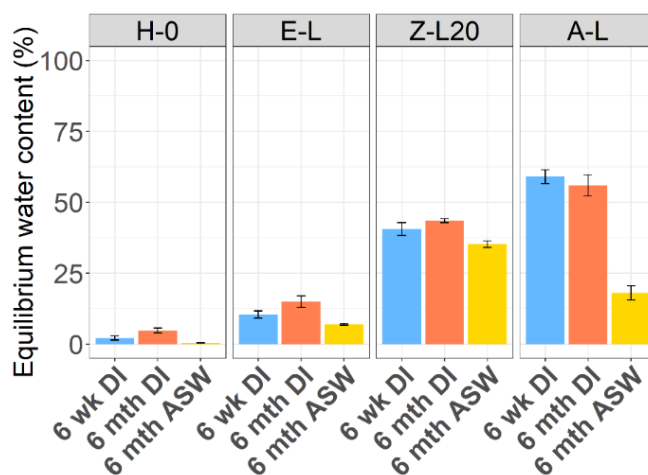


Figure 5.14 Equilibrium water content (EWC) of polymers stored for six weeks in DIW and six months in DIW and ASW. Error bars are 95% CIs.

In order to determine potential changes in water states in aged polymers, DSC experiments were performed and the heating thermograms of the samples hydrated with DIW and ASW are presented in Figure 5.15. Clearly the heating curves of polymers swollen in the two aqueous media show different behaviours. The most prominent difference is the smaller freezable water peak for samples hydrated in ASW, which can be attributed to reduced swelling in ASW. Furthermore, for polymers hydrated in ASW, a downward shift of the freezable water peak can be observed, which can be assigned to the freezing-point depression phenomena. In addition, in the case of polymer A-L, two melting peaks are present on the ASW heating curve, which correspond to two phase transitions. The weaker peak at around -23°C is the so-called eutectic melting peak (P_{eu}), which can be attributed to the presence of eutectic ion-bound water and implies that there is an excess of salt ions in the hydrated polymer (Jhan and Tsay, 2014). The second, bigger peak observed in all tested samples can be assigned to the melting of freezable water.

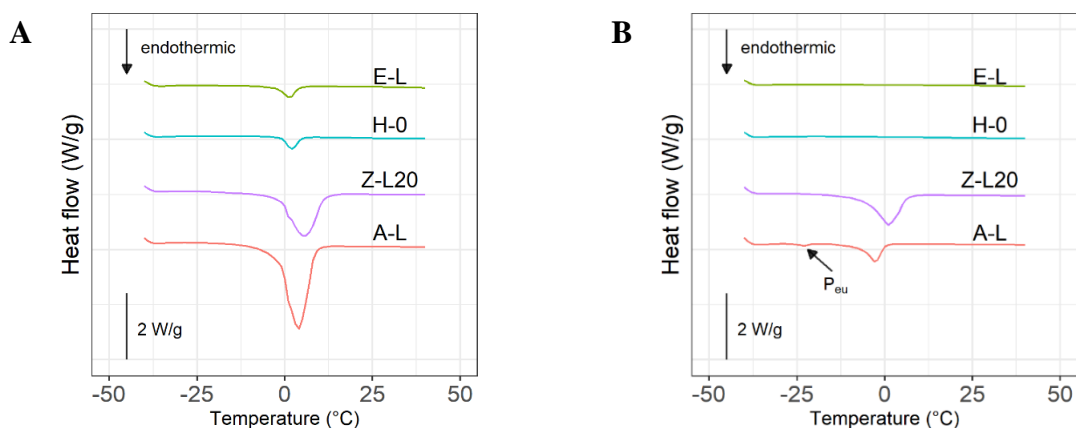


Figure 5.15 DSC heating thermograms of samples stored for six months in DIW (A) and ASW (B) at the heating rate of $10\text{ }^{\circ}\text{C}\cdot\text{min}^{-1}$.

According to Figure 5.16, the mass of freezable water relative to the mass of polymer ($W_{\text{freezable}}$) remained practically unchanged after six months of immersion in DIW, with the exception of polymer A-L where the $W_{\text{freezable}}$ decreased. In the case of polymers hydrated in ASW, the calculated $W_{\text{freezable}}$ values were smaller than those in DIW and the reason for this behaviour is reduced polymer swelling in ASW.

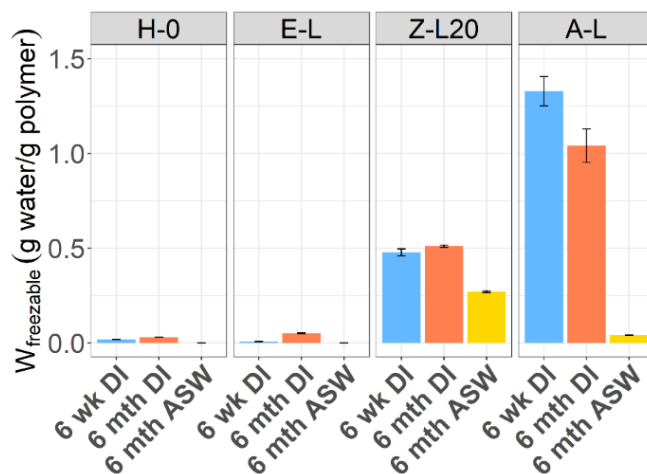


Figure 5.16 Mass ratio of freezable water to the mass of polymer ($W_{\text{freezable}}$) after six weeks and six months of storage in DIW and ASW. Error bars are 95% CIs.

Regarding the nonfreezable water, all polymers showed increased values of $W_{\text{nonfreezable}}$ and N_w after six months in DIW (Figure 5.17 and 5.18). For polymers H-0, E-L and Z-L, this increase is a result of increased EWC. However, for polymer A-L the same explanation does not apply as the EWC had decreased. This unusual behaviour observed for polymer A-L is possibly attributable to the mobility of

freezable water molecules in the polymer matrix (expressed by reduced $W_{\text{freezable}}$) which, over time, can interact more strongly with polymer chains and essentially become nonfreezable. The mobility of water molecules between various water states was also observed in highly hydrated pSBMA-water systems by Jhan and Tsay (2014). As for the $W_{\text{nonfreezable}}$ and N_w in ASW, the obtained values for ionic polymers Z-L20 and A-L are not considerably different from the values recorded in DIW, suggesting that the presence of ions in the seawater does not really affect the binding of water molecules in these copolymers, and that the tightly bound water layer is still present.

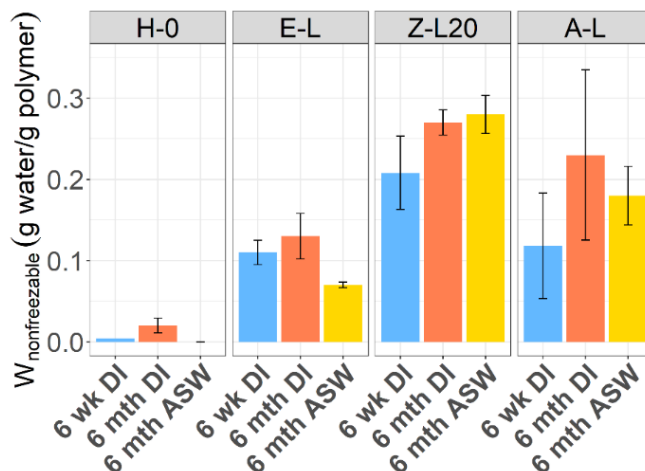


Figure 5.17 Mass ratio of nonfreezable water to the mass of polymer ($W_{\text{nonfreezable}}$) after six weeks and six months of storage in DIW and ASW. Error bars are 95% CIs.

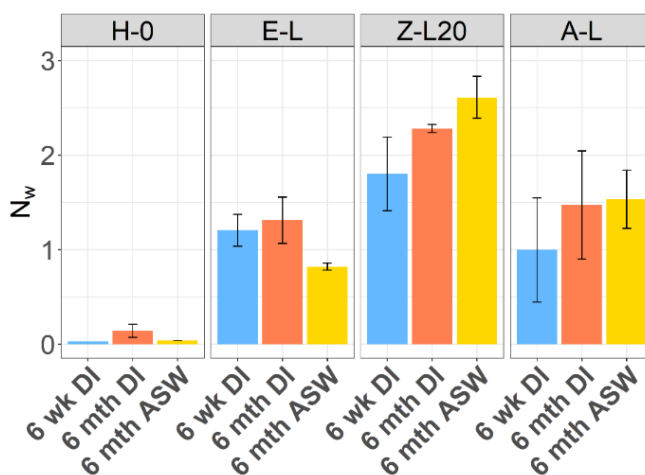


Figure 5.18 Number of nonfreezable water molecules (N_w) per repeating copolymer unit after six weeks and six months of storage in DIW and ASW. Error bars are 95% CIs.

4.1.1. Barnacle settlement and removal assay

To determine the effect of coating age on the settlement of barnacles, laboratory assays were conducted after six months of storage in DIW (Figure 5.19B). The differences in settlement were significant (one-way ANOVA, $F_{3,12} = 6.06$, $p = 0.009$). The lowest settlement was recorded on polymer Z-L20 and it was significantly lower than on the control polymer H-0 (Tukey tests, $p \leq 0.05$). In order to visually compare results with initial settlement data, the data available in Appendix E were replotted on Figure 5.19A. Barnacle settlement increased on all coatings tested after aging in DIW. In the case of polymer E-L, the high settlement could be attributed to surface degradation and increased surface roughness. As for coatings Z-L20 and A-L, the ~20% settlement increase can be potentially explained by the formation of bacterial films on the aged coatings. Indeed, according to O'Connor and Richardson (1996), bacterial films grown on coatings under more natural conditions acted as settlement cues for cyprids of *B. improvisus* and increased the attractiveness of surfaces that were initially perceived by cyprids as unattractive (e.g. glass).

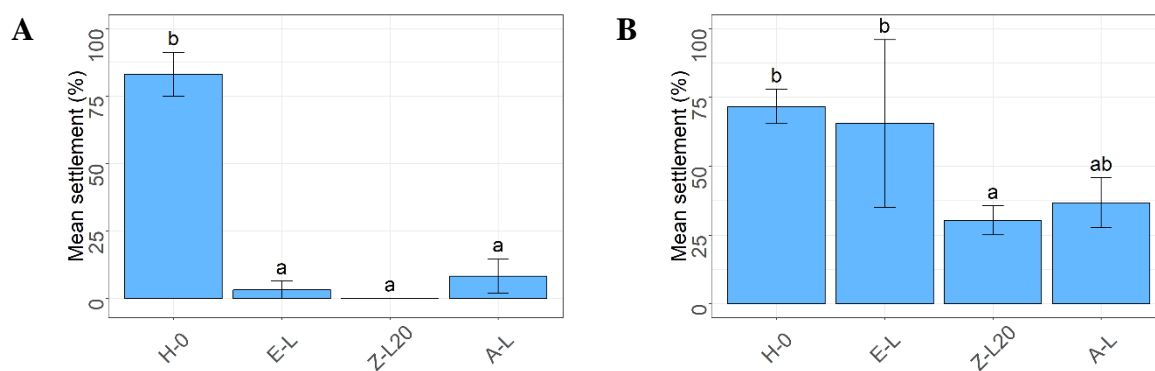


Figure 5.19 Mean percent settlement of cyprids of *B. improvisus* (A) initial (B) after six months of storage in DIW. Error bars are 95% CIs. Letters represent Tukey's pairwise comparisons and bars that do not share a letter are significantly different.

In barnacle removal experiments, a water jet was used instead of the water channel (section 2.2.9) due to incompatibility of the batch of PVC slides with the water channel. In the water jet, the hydrodynamic force is applied perpendicular rather than parallel to the surface (i.e. impact pressure vs wall shear stress). The detailed description of the water jet apparatus is available in research articles by Swain and Schultz (1996) and in Aldred *et al.* (2010b). The barnacle removal results from aged coatings are presented in Figure 5.20B. The removal of juvenile barnacles differed among surfaces (one-way ANOVA with Tukey post-hoc tests, $F_{3,12} = 6.69$, $p \leq 0.007$), with the highest removal of juvenile barnacles recorded on

polymer E-L ($72.86 \pm 12.61\%$) and polymer Z-L20 ($57.67 \pm 19.64\%$). The unusually high removal of barnacles from polymer E-L can be possibly explained by the reduced mechanical properties of the aged coating.

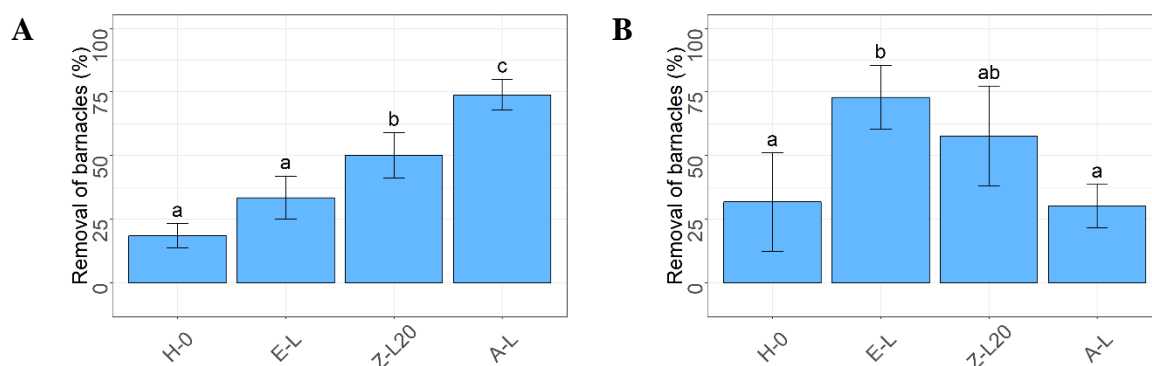


Figure 5.20 Removal results of four-day-old juveniles barnacles, *B. improvisus*. (A) Initial using the water channel; (B) After six months of storage in DIW using the water jet. Error bars are 95% CIs. Letters represent Tukey's pairwise comparisons and bars that do not share a letter are significantly different.

4.1.2. Diatom removal assay

In order to further assess the FR properties of aged coatings, a diatom removal assay was conducted (Figure 5.21B). Removal varied significantly between polymers (one-way ANOVA $F_{4,445} = 288.8$, $p \leq 0.001$). The highest removal of diatom cells was recorded from polymers A-L ($85.52 \pm 2.11\%$) and Z-L20 ($60.49 \pm 6.74\%$) and, in both cases, the removal was significantly higher than on other surfaces tested (Tukey tests, $p \leq 0.001$). As explained in Chapter 2, the high FR properties of these two ionic copolymers could be attributed to their high degree of swelling, which was retained after long-term storage in DIW (Figure 5.14).

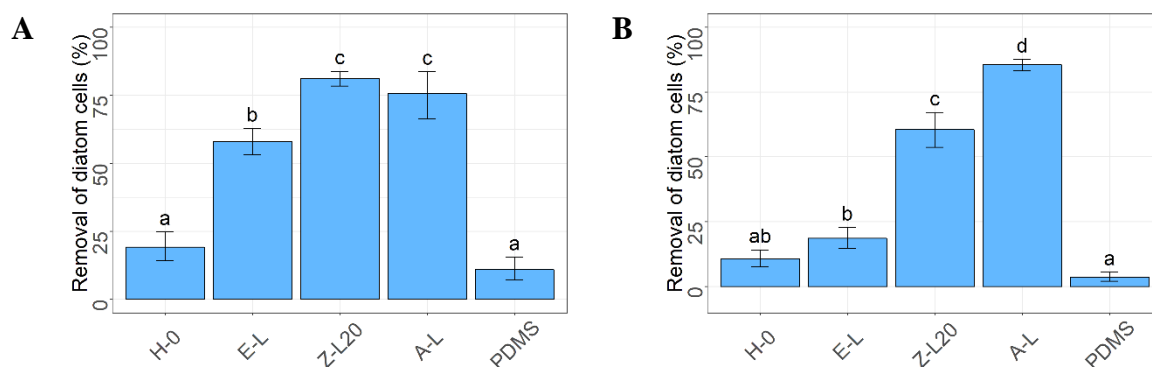


Figure 5.21 Percent removal of *N. incerta* cells (A) initially, and (B) after six months of storage in DIW. Each point represents the mean from 90 counts on three replicate slides. Error bars are 95% CIs from arc-sine transformed data. Letters represent Tukey's pairwise comparisons and bars that do not share a letter are significantly different.

4.1.3. Field immersion tests

In order to determine resistance of coatings to fouling in the marine environment raft boards with panels coated with polymers H-0, E-L, H-L, G-L, M-L, Z-L10, Z-L20, A-L, C-L and P-L20 were deployed at two testing sites; Hartlepool Marina, UK and at Changi Sailing Club, Singapore. The layout of the boards is presented in Figure 5.22.

Z-L10	Z-L20	A-L	C-L	P-L20	E-L
H-L	M-L	G-L	V-L	IS1100	H-0
P-L20	E-L	Z-L10	Z-L20	A-L	C-L
IS1100	H-0	H-L	M-L	G-L	V-L
A-L	C-L	P-L20	E-L	Z-L10	Z-L20
G-L	V-L	IS1100	H-0	H-L	M-L

Figure 5.22 Layout of the panels deployed in Hartlepool and Changi.

The first panel was deployed in the temperate waters of Hartlepool Marina, which is a medium-sized harbour located on the North East coast of England. Figure 5.23 is a photograph of the board after immersion in the sea for two months. All samples were mainly covered with microfouling (slime), weeds and soft-bodied animals. In order to quantify the levels of fouling, visual assessment of the board was conducted and the antifouling performance of each coating was reported as percentage cover of each fouling category (Figure 5.24). Significant variation in the fouling coverage was observed among surfaces (Kruskal-Wallis $H = 19.74$, $df = 10$, $p = 0.032$), with IS1100 (standard coating) showing exceptionally low fouling levels. No hard-shelled animal fouling was observed on any surface tested.

The image of the board after immersion for four months at Hartlepool is presented in Figure 5.25. Clearly, after additional two months in the sea, the board was more fouled and larger number of soft-bodied animals was observed. These soft-bodied animals were mainly ascidians of *Ascidella aspersa* and *Ciona intestinalis* (Aldred and Clare, 2014). These fouling organisms are common in Hartlepool Marina on vessels which have been moored for prolonged periods. The difference in fouling coverage was not significant among coatings (Kruskal-Wallis $H = 10.86$, $df = 10$, $p = 0.37$), however, on IS1100 the degree of fouling was minimal.

To summarise, it is evident that none of these experimental hydrophilic coatings could match the performance of the IS1100 standard. It is nevertheless interesting that among all of the hydrophilic coatings it was the anionic polymer, A-L, that performed best in the temperate waters of the North Sea.



Figure 5.23 Image of the panel deployed at Hartlepool Marina after immersion for two months.

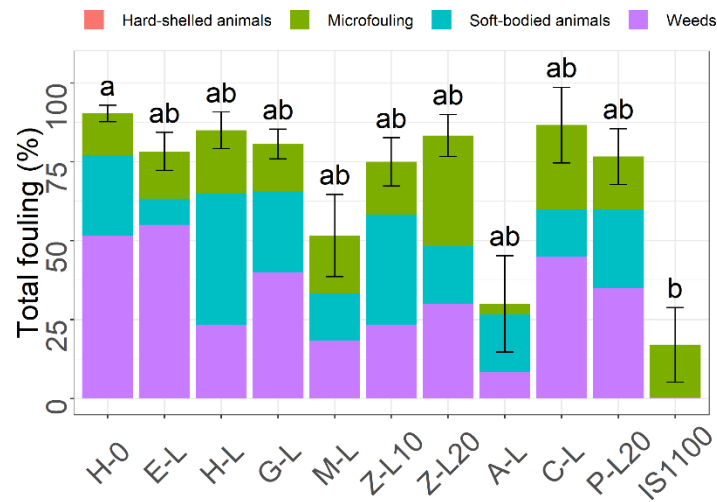


Figure 5.24 Percentage coverage of total biofouling divided into four categories after immersion for two months in Hartlepool Marina. Error bars represent SEs of the total sample biofouling from three replicates. Bars that do not share a letter are significantly different.



Figure 5.25 Image of the panel deployed at Hartlepool Marina after immersion for four months.

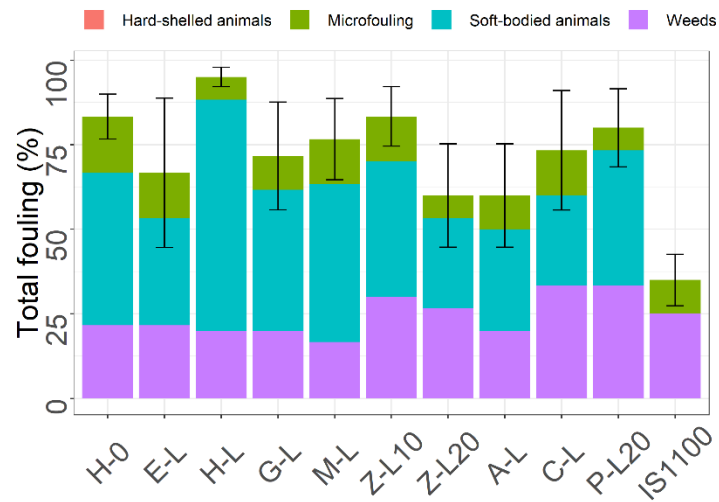


Figure 5.26 Percentage coverage of total biofouling divided into four categories after immersion for four months in Hartlepool Marina. Error bars represent SEs of the total sample biofouling from three replicates.

In order to test polymers in more challenging fouling conditions, one of the prepared boards was sent to Changi in Singapore. In the tropical waters of Singapore, the animal fouling is particularly aggressive. Figure 5.27 shows a picture of the deployed board after immersion in the sea for two weeks. All experimental coatings were heavily fouled with tunicates and tubeworms, and only panels coated with IS1100 presented good AF performance. This observation was further confirmed by estimating the percentage coverage of fouling (Figure 5.28), where the differences between coatings were found to be significant (Kruskal-Wallis $H = 28.62$, $df = 10$, $p = 0.0014$). The lowest fouling was recorded on IS1100.

After two months of immersion in Changi, all coatings were almost completely covered with hard-shelled animals like mussels and tubeworms (Figure 5.29), the microfouling was presumably 'hidden' under the layer of hard-shelled animals. The total fouling coverage was not significantly different between coatings (Kruskal-Wallis $H = 13.48$, $df = 10$, $p = 0.2$). Clearly, the immersion testing in Singapore showed rapid failure of all hydrophilic coatings. It should be noted, however, that this was a static raft test with limited shear stress effects on fouling development, resulting in even the commercial standard IS1100 becoming heavily fouled.

The differences in fouling communities and fouling levels observed at the two testing sites were considerable and reiterated the importance of running field tests at different geographical locations. For instance, the fouling challenge at the Hartlepool site was relatively low and polymers Z-L20 and A-L showed relatively good AF performance even after four months of testing. However, the same coatings immersed in Changi failed rapidly just after two weeks. In addition, the field tests performed at the two locations revealed high fouling levels on all tested coatings from two organisms: tunicates (Hartlepool) and tubeworms (Changi).



Figure 5.27 Image of the panel deployed at Changi after immersion for two weeks.

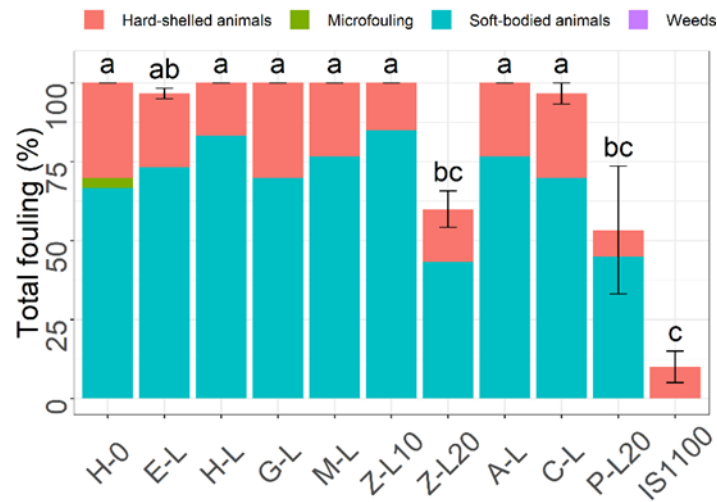


Figure 5.28 Percentage coverage of total biofouling divided into four categories after immersion for two weeks in Changi. Error bars represent SEs of the total sample biofouling from three replicates. Points that do not share a letter are significantly different.



Figure 5.29 Image of the panel deployed at Changi after immersion for two months.

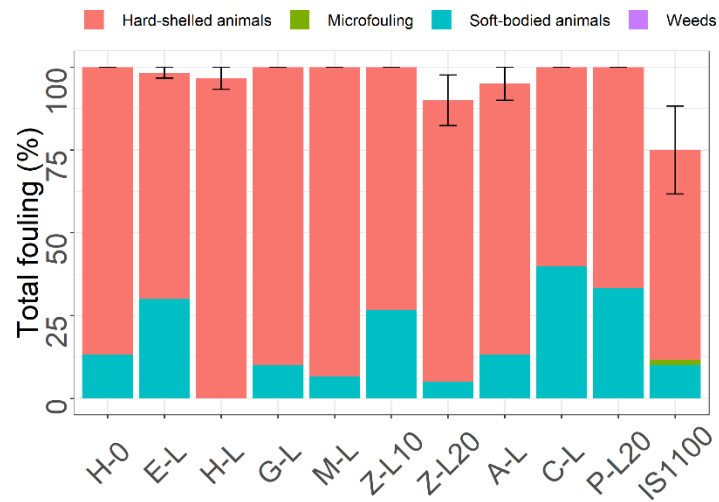


Figure 5.30 Percentage coverage of total biofouling divided into four categories after immersion for two months in Changi. Error bars represent SEs of the total sample biofouling from three replicates.

In summary, the poor antifouling performance of hydrophilic coatings deployed in the field could be attributed to high salinity and temperature fluctuations, which could dramatically alter surface charge and wettability. These changes in surface characteristics could lead to adsorption of biogenic macromolecules and promote settlement and adhesion of higher fouling organisms and eventually lead to wider coating failure.

In this chapter the long-term chemical stability and antifouling performance of selected coatings (H-0, E-L, Z-L20, A-L) was evaluated after exposure to DIW and ASW in the laboratory. The ^1H NMR, GC-MS and ATR-IR data indicated that all tested polymers were chemically stable with no sign of hydrolytic degradation, which is quite surprising considering their high swelling. Underwater contact angle measurements showed that after an initial increase in wettability for ionic polymers, the hydration became stable. For nonionic polymers it did change. This was particularly noticeable for polymers bearing the PEG moiety where reduced hydrophilicity was observed, and which was attributed to surface degradation and increased roughness. The water state experiments did not reveal major changes in nonfreezable water in polymers E-L, Z-L20, A-L after six months of immersion in DIW and ASW. The laboratory assays using barnacles and diatom cells showed that good AF performance was only retained in anionic A-L and zwitterionic Z-L20 polymers. Despite promising results from laboratory assays, field tests revealed limited long-term antifouling performance of the majority of hydrophilic surfaces. Only polymers A-L and Z-L20 tested in Hartlepool showed satisfactory performance, which is in agreement with the laboratory assays. The obtained results confirm the necessity of running both types of complementary tests. While the laboratory tests are useful for mechanistic understanding of the biofouling processes, and can help to quickly down-select best performing coatings, they must be accompanied by field tests where the coatings are subjected to more challenging environmental and fouling conditions. The field tests revealed high fouling levels from tubeworms and tunicates, which suggests that these two fouling species should be included in future laboratory assays.

Chapter 6. Discussion

6.1 General discussion and conclusions

The central aim of this thesis was to investigate the potential of (super)hydrophilic coatings as novel, eco-friendly, fouling-resistant marine coatings and to answer the following research questions: What hydrophilic chemical moieties are both effective AF agents and possible to incorporate into bulk coatings? What are the physicochemical properties of (super)hydrophilic surfaces that make them effective against marine biofouling, and what is the mechanism of rejection of those surfaces by selective fouling species? Finally, are there any physico-chemical parameters of polymers that could be used to predict coating failure?

6.1.1 Production of industrially relevant bulk hydrophilic coatings for marine antifouling applications

The majority of previous work published on hydrophilic chemistries in the context of antifouling has been devoted to small-scale, well-defined laboratory systems such as polymer brushes, hydrogels or self-assembled monolayers (SAMs) that function via retention of a tightly-bound water layer. The novel contribution of the present work, compared to previous reports, was the investigation of these well-established concepts in more industrially relevant bulk copolymers. The bulk polymers were synthesized using non-controlled free-radical polymerization by copolymerizing n-BMA with hydrophilic comonomers such as methoxy PEG methacrylate (mPEG350MA), hydroxyethyl methacrylate (HEMA), 2,3-dihydroxypropyl methacrylate (DHPMA), methacrylic acid (MAA), sulfobetaine methacrylate (SBMA), 3-sulfopropyl methacrylate potassium salt (SPMA) and 2-(methacryloyloxy)ethyltrimethylammonium chloride (METAC). The antifouling efficacy of polymers containing PEG and SBMA is often ascribed to surface hydration that is maintained through hydrogen-bonding and/or electrostatic interactions. In the case of model polymer systems, hydration is regularly investigated using sum frequency generation (SFG) vibrational spectroscopy or by conducting modelling studies. In this work, however, a different approach was employed. By combining both TGA & DSC measurements it was possible to determine both swelling and presence of different water states (nonfreezable, freezable and bulk water) within the hydrated bulk polymer matrix. Ionic polymers showed a high degree of swelling and a considerable amount of nonfreezable water at the interface, whereas the PEG-containing coating was alone among the nonionic polymers in showing the presence

of nonfreezable water. Antifouling testing in the laboratory revealed that, in general, the ionic polymers resisted the settlement of cyprids well compared to the nonionic polymers, and this behaviour was ascribed to the presence of nonfreezable water at the hydrated polymer surface. Removal experiments using juvenile barnacles, diatom slime and multispecies biofilm showed that polymers containing zwitterionic SBMA and anionic SPMA also presented good FR properties. This was attributed to high swelling of those surfaces affecting the conformational freedom and viscoelastic properties of the polymer chains.

6.1.2 Determination of the mechanism of action of hydrophilic coatings against barnacle larvae

In order to better understand the antifouling mechanism of the highly hydrated surfaces against barnacle settlement, polymer brushes with well-defined chemistry and thickness were used. This area of AF research has, surprisingly, been largely ignored to date despite the well-documented potential of hydrophilic materials and theoretical understanding of the mechanism of action. One potential mechanism is voluntary rejection of the surfaces by fouling organisms. A second is physical interference, by the surface, with the process of adhesion - i.e. the organisms try to attach but cannot. A combination of these is also possible. The selection of chemistries for these experiments was made based on the results of bulk polymers and included the following functionalities: mPEG350MA, SBMA, SPMA, METAC, as well as a mixed-charged polyampholyte. Of the five polymer brushes tested, only zwitterionic SBMA surfaces were truly resistant to barnacle settlement and this was attributed to the unique surface hydration state and neutral charge of the material. Two experimental methods, iSPR and behavioural analysis via remote video tracking, were used to analyse the behaviour of larvae on surfaces. The experiments revealed that cyprids explored all surfaces, however different behavioural responses were observed. For instance, a large number of walking/inspection events were recorded on hydrophobic and anionic surfaces and this was interpreted to suggest high affinity of the secreted adhesive for those surfaces. Among various behavioural metrics, the nature of the inspection events was shown to accurately predict cyprid settlement.

6.1.3 Incorporation of zwitterionic moiety into silicone elastomer for improved fouling resistance

According to Clare *et al.* (1992), a universal antifouling solution will most probably require a combination of approaches, rather than a single prevention strategy. In this work, a silicone elastomer (PDMS) was modified with a highly hydrophilic SBMA copolymer to provide the mechanical advantages

of a low-modulus coating with the fouling-resistance properties of a more hydrophilic material. An experiment performed with motile spores of the green alga *Ulva linza* revealed that the modified silicone was more resistant to settlement of spores than virgin PDMS. In addition, the modified PDMS showed improved FR properties against both diatom cells and settled spores when compared to regular PDMS. The results obtained also suggest that zwitterionic moieties could be incorporated into other materials to provide additional functionality, opening new possibilities for the development of AF surfaces. Clearly, however, the presented grafting method is not applicable in an industrial environment and a different manufacturing approach would be required for this material.

6.1.4 Long-term stability of selected bulk polymer coatings

Marine antifouling coatings are subjected to harsh and variable seawater environments and the evaluation of long-term performance is an important part of the testing regime. Significant time was devoted in this project to determining the physicochemical stability of selected bulk coatings in combination with laboratory assays and field tests. Experiments revealed that the surfaces, even the highly hydrated SBMA- and SPMA-containing moieties, were hydrolytically stable for a period of at least six months. The only exception was the polymer bearing PEG, where visible surface degradation was observed. Water state experiments confirmed the presence of nonfreezable water in the aged polymers, suggesting that the antifouling mechanism based on tightly bound water should still be valid. Furthermore, experiments in seawater revealed that despite lower swelling, the nonfreezable water was still present in the polymers. Assays in the laboratory revealed slightly reduced AF performance of polymers containing SBMA and SPMA, and considerable degradation in the polymer containing PEG. Static immersion tests at two locations revealed relatively poor performance of all coatings, when compared to a commercially available standard (IS1100SR FRC) and reiterated the importance of testing coatings in real-world conditions as well as in the laboratory. Field tests revealed that the hydrophilic coatings prepared here are prone to tunicate and tubeworm fouling, and inclusion of these two fouling species in future laboratory testing would be beneficial.

6.2 Future research and recommendations

Despite significant efforts towards development of non-biocidal coatings, it seems that the current usage of biocidal coatings for ships' hulls will likely continue for the foreseeable future. Among the various 'green' antifouling technologies that have been proposed in recent years, the (super)hydrophilic surfaces seem to be serious contenders for translation into practical antifouling coatings. However, further

research is required to develop new hydrophilic chemistries and for a better understanding of how these surfaces prevent the accumulation of fouling at a macromolecular level.

With regard to SBMA, the present work confirmed its potential as an antifouling agent, and future studies should be extended by inclusion of other zwitterionic chemistries such as carboxybetaine methacrylate (CBMA). The AF properties of CBMA are well documented in the literature (Aldred *et al.*, 2010a; Finlay *et al.*, 2013; Ventura *et al.*, 2017), and are often presented alongside SBMA. The addition of CBMA to the tested chemistries would be a huge benefit to the ongoing discussion regarding the difference in hydration capacity and AF performance of the two betaines. Other examples of zwitterionic chemistries that should be considered were recently presented in a work by Koc *et al.* (2019a). Authors synthesized a range of zwitterionic sulfo- and sulfobetaine methacrylates and methacrylamides in order to determine the effect of chemical structure of the zwitterionic moiety on the AF properties of surface. As the presented copolymers consisted almost exclusively of zwitterionic monomers, incorporation of these chemistries into a bulk polymer system with more hydrophobic character should further confirm the usefulness of these novel monomers as AF agents. Obviously, zwitterionic chemistries are not the only sources of hydrophilicity that should be tested in the future studies. Polysaccharides are an interesting group of natural polymers that are hydrophilic and have shown promising results in the biomedical applications (Morra and Cassinelli, 1999; Dai *et al.*, 2000; Ombelli *et al.*, 2011), and recently in the marine AF field (Bauer *et al.*, 2013; Bauer *et al.*, 2016b; Jakobi *et al.*, 2018). Finally, the next stage of development of (super)hydrophilic surfaces would benefit from underwater AFM experiments where surface topography and roughness could be determined. It is well-known that surface roughness affects not only the surface wettability, but also the AF performance of coatings (Schumacher *et al.*, 2007; Scardino *et al.*, 2009), and it cannot be excluded that the obtained results are also partially affected by the roughness parameter.

The investigation of bulk polymers and polymer brushes also highlighted the importance of caution when extrapolating conclusions drawn from fundamental studies of polymer brushes to practical bulk polymers. This was borne out in cyprid settlement experiments, where low cyprid settlement was observed on bulk polymers containing ionic and PEG functionalities, and in the case of model surfaces only the SBMA brush showed performance comparable to the bulk counterpart. It was speculated that the reason for this inconsistency was higher conformational freedom of the swollen bulk copolymers which could have a marked effect on their hydration capacity. Due to the nature of polymer brushes,

investigation of their hydration requires surface sensitive techniques such as quartz crystal microbalance with dissipation (Yandi *et al.*, 2014) or neutron reflectivity (Ederth and Ekblad, 2018), and future studies could benefit from these experiments. The present study revealed also significant difficulties in producing thick polymer brushes on gold surfaces at elevated temperatures using SI-RAFT technique. Thickness is an important polymer brush parameter which affects the hydration and ultimately AF properties of the surface (Yang *et al.*, 2008; Yandi *et al.*, 2014; Yang *et al.*, 2018). For future studies, the protocol developed here for obtaining stable polymer films on gold substrates should aid the synthesis of polymer brushes with varying thicknesses, to be used to study surface-fouling organism interactions, spreading dynamics and composition of secreted adhesive with regard to changing surface hydration.

The lack of understanding of the mechanisms involved in the surface selection and adhesion by fouling organisms is the main bottleneck in the development of universal antifouling strategies that are not based on toxic biocides. At present, it appears that the best route to broad-spectrum fouling resistance is through development of multifunctional materials like hydrogel-silicone paints with dual fouling resistance and fouling release properties. These coatings could additionally incorporate a self-replenishing mechanism for surface recovery after mechanical damage. According to Koc *et al.* (2019b), the limited AF performance of zwitterionic hydrogels in the marine environment can be attributed to the deposition of sediment and solid particles, which could mechanically weaken the highly swollen film, and replenishment would be clearly of benefit for long-term coating performance.

Another interesting concept that should be explored in the next generation marine AF coatings is the development of hydrophilic coatings with both antifouling and antimicrobial properties (Mi and Jiang, 2012). The incorporation of an antimicrobial agent should help keep the coating free from bacteria and potentially reduce the formation of marine biofilms on the surface. This concept was recently expanded by Xie *et al.* (2018b) who created a biodegradable, SPC-like copolymer with hydrolysis-induced zwitterionic moieties that resisted nonspecific protein adsorption and inhibited marine bacteria growth.

To summarise, the present study has identified different hydrophilic chemistries that could be used in the development of the next generation of AF coatings. It produced a framework for future research and highlighted the importance of testing coatings not only in the controlled environment of the laboratory, but also in the field. Fundamental research on the behaviour of larvae and their attachment mechanisms should continue, and the information obtained from these experiments may inform the design of novel polymeric chemistries in a hypothesis-driven manner. It seems unlikely that a single fouling prevention

strategy will be universally effective, and a combination of strategies seems to be the most likely antifouling solution. It is hoped that the findings of this work will encourage greater industrial participation in the development of fouling-control technologies that function via non-biocidal means.

Appendix A. Preparation of bulk polymers

Polymer H-0 (pBMA): The n-butyl methacrylate homopolymer was prepared in a following manner. To the main polymerization vessel equipped with mechanical stirrer, 22.5 g of methylated spirit was added and heated to 75 °C. Next two polymerization feeds were prepared. The first feed consisted only of methylated spirit (120 g), whereas the second feed consisted of first lot of AMBN initiator (4.87 g, 25 mmol) and n-BMA (143.96 g, 1012 mmol). Both feeds were gradually added to the vessel during 4 h feeding period using two Watson Marlow 101 U/R peristaltic pumps. One hour after feeding completion the remaining amount of AMBN (1.17 g, 6 mmol) was dissolved in methylated spirit (7.5 g) and added directly to the reaction mixture to convert the residual monomer. The vessel was then stirred for another hour, cooled down and left overnight for subsequent postprocessing. The next day the polymerization flask was fitted with a condenser, heated to 85 °C and methylated spirit (100 g) was distilled with simultaneous feed of xylene (131 g). After the distillation, polymer solution was allowed to cool down to room temperature.

Polymer E-L (pBMA-co-IBoMA-co-mPEG350MA): Due to high softness of pBMA-co-mPEG350MA copolymer (glass-transition temperature $T_g = -36.5$ °C), the polymer composition was modified by adding a third comonomer isobornyl methacrylate (IBoMA) which increased polymer's T_g . The new copolymer pBMA-co-IBoMA-co-mPEG350MA was polymerized as follows. The mPEG350MA monomer (31.71 g, 74 mmol) was added to methylated spirit (120 g) and this made up the first feed. The first lot of AMBN (3.55 g, 18 mmol) was dissolved in n-BMA (59.78 g, 421 mmol) and IBoMA (54.11 g, 243 mmol) and this mixture made up the second feed. Both feeds were simultaneously added for 4 h to the main reaction vessel containing 22.5 g of methylated spirit and the reaction was conducted at 75 °C. After feeding completion and mixing for another hour, the remaining AMBN (0.85 g, 4.4 mmol) in 7.5 g of methylated spirit was added to the vessel and the mixing continued for another hour before stopping the reaction. The next day the postprocessing step included distillation of methylated spirit (100 g) at 85 °C with simultaneous addition of xylene (131 g).

Polymer H-L (pBMA-co-HEMA): To the main polymerization vessel, 22.5 g of methylated spirit was added and heated to 75 °C. Next two polymerization feeds were prepared with first feed consisting of HEMA (13.28 g, 102 mmol) and methylated spirit (120 g) and second feed made up of first lot of AMBN (4.91 g, 26 mmol) and n-BMA (130.63 g, 919 mmol). Both feeds were simultaneously added to the vessel

for 4 h. One hour after feeding completion remaining AMBN (1.18 g, 6 mmol) was dissolved in small amount of methylated spirit (7.5 g) and added directly to the reaction mixture. The vessel was then mixed for another hour and then the reaction was stopped. The next day methylated spirit (100 g) was distilled at 85 °C with simultaneous feed of xylene (131 g).

Polymer G-L (pBMA-co-DHPMA): The main vessel that contained small amount of methylated spirit (22.5 g) was heated to 75 °C. Two monomer feeds were prepared. The first feed contained DHPMA (16.03 g, 100 mmol) and methylated spirit (120 g), and the second feed comprised of AMBN (4.81 g, 25 mmol) and n-BMA (128.01 g, 900 mmol). Both feeds were simultaneously added to the reaction vessel for 4 h. One hour after feeding completion remaining AMBN (1.15 g, 6 mmol) was dissolved in 7.5 g of methylated spirit and added directly to reaction mixture. After additional 1 h of mixing the reaction was stopped and left overnight. The next day methylated spirit (100 g) was distilled at 85 °C with simultaneous feed of xylene (131 g).

Polymer M-L (pBMA-co-MAA): To the main polymerization vessel small amount of methylated spirit was added (22.5 g) and the vessel was heated to 75 °C. Next, MAA (9.06 g, 105 mmol) was added to methylated spirit (120 g) and this made up the first feed. The second feed was made of AMBN (5.06 g, 26 mmol) and n-BMA (134.67 g, 947 mmol). Both feeds were simultaneously added to the vessel for 4 h. One hour after feeding completion remaining AMBN (1.21 g, 6 mmol) was dissolved in 7.5 g of methylated spirit and added to the vessel and the mixing proceeded for another hour before stopping the reaction. The next day 100 g of methylated spirit was distilled at 85 °C with simultaneous feed of 131 g of xylene.

Polymer Z-L (pBMA-co-SBMA_{10mol%}): The main polymerization vessel contained methylated spirit (22.5 g) and was heated to 75 °C. Two monomer feeds were prepared prior to running reaction. The first feed consisted of zwitterionic SBMA (25.89 g, 93 mmol) and methylated spirit (120 g), and the second feed comprised of first lot of AMBN initiator (4.46 g, 23 mmol) and n-BMA (118.59 g, 834 mmol). To improve the solubility of SBMA the flask was preheated to 70 °C under magnetic stirrer. Both feeds were gradually added to the main reactor for 4 h. When necessary, the first feed line was gently heated with a heat gun to remove blocking deriving from SBMA crystallization. One hour after feeding completion second lot of AMBN (1.06 g, 6 mmol) was dissolved in methylated spirit (7.5 g), added to the main vessel and the mixing continued for another hour before turning it off. The next day methylated spirit (100 g) was distilled at 85 °C with simultaneous feed of xylene (131 g). The obtained polymer was

viscous and difficult to apply and in order to ease its application additional 60 g of xylene was added to the ready polymer.

Polymer Z-L20 (pBMA-co-SBMA_{20mol%}): The polymerization procedure was similar to that of polymer Z-L, however different amounts of reagents were used: n-BMA (97.18 g, 683 mmol), AMBN (5.09 g, 26 mmol), SBMA (47.73 g, 170 mmol). As in case of polymer Z-L the final polymer solution was diluted with additional amount of xylene (60 g).

Polymer A-L (pBMA-co-SPMA): The polymerization vessel that contained small amount of methylated spirit (22.5 g) was heated to 75 °C. Next, two monomer feeds were prepared. The first feed contained the anionic SPMA salt (23.3 g, 95 mmol) and methylated spirit (120 g) and was preheated to 70 °C under magnetic stirrer. The second feed consisted of first lot of AMBN (4.55 g, 24 mmol) and n-BMA (121.06 g, 851 mmol). Both feeds were added to the main vessel for 4 h. As in the case of SBMA, the SPMA salt also was prone to crystallization and heat gun was used when necessary to remove feed line blocking. One hour after feeding completion remaining AMBN (1.09 g, 6 mmol) was dissolved in methylated spirit (7.5 g) and added to the vessel and the mixing continued for another hour. After that time the reaction was stopped and left overnight. The next day methylated spirit (100 g) was distilled at 85 °C with simultaneous feed of xylene (131 g). The obtained polymer was viscous and difficult to apply and in order to ease its application additional 60 g of xylene was added to the ready polymer.

Polymer C-L (pBMA-co-METAC): Before preparing the actual polymer, residual water was removed from METAC (25.18 g) by precipitating the monomer in THF and discarding the supernatant. The polymerization vessel that contained small amount of methylated spirit (22.5 g) was heated to 75 °C. Two polymerization feeds were prepared as follows. First feed consisted of earlier dried METAC (20.14 g, 97 mmol) and was added to methylated spirit (120 g) and this made up first feed, whereas feed two consisted of AMBN (4.66 g, 24 mmol) and n-BMA (124.08 g, 872 mmol). When needed the first feed line was heated with heat gun to remove line blocking deriving from crystalizing METAC. The feeds were added simultaneously to the vessel for 4 h and one hour after feeding completion the remaining AMBN (1.12 g, 6 mmol) was dissolved in methylated spirit (7.5 g) and added to the reaction mixture. After additional hour the stirring and heating was turned off. The next day 100 g of methylated spirit was distilled at 85 °C with simultaneous feed of 131 g of xylene. The obtained polymer was viscous and difficult to apply and in order to ease its application additional 60 g of xylene was added to the ready polymer.

Polymer P-L10 (pBMA-co-SPMA_{5mol%}-co-METAC_{5mol%}): Prior to running polymerization specific amount of METAC (12.45 g) was precipitated in THF and the resulting supernatant discarded. Dried METAC (9.96 g, 48 mmol) together with SPMA (11.81 g, 48 mmol) were dissolved in methylated spirit (120 g) and this solution constituted as feed one. The second feed consisted of first lot of AMBN (4.61 g, 24 mmol) and n-BMA (122.7 g, 863 mmol). The main reaction vessel that contained 22.5 g of methylated spirit was heated to 75 °C and two monomer feeds were simultaneously added for 4 h. When necessary the first feed line was heated with heat gun to remove blocking from salt crystallisation. One hour after feed completion second lot of AMBN (0.92 g, 5 mmol) in methylated spirit (7.5 g) was added to the vessel and the mixing continued for another hour, before turning it off and leaving overnight. The next day 100 g of methylated spirit was distilled at 85 °C with simultaneous feed of 131 g of xylene.

Polymer P-L20 (pBMA-co-SPMA_{10mol%}-co-METAC_{10mol%}): First METAC (23.61 g) was precipitated in THF and the supernatant was removed. Dried METAC (18.89 g, 91 mmol) and SPMA (22.4 g, 91 mmol) were dissolved in methylated spirit (120 g) and this solution constituted as feed one. The second feed consisted of first lot of AMBN (4.37 g, 23 mmol) and n-BMA (103.46 g, 728 mmol). The main reaction vessel that contained 22.5 g of methylated spirit was heated to 75 °C and two monomer feeds were simultaneously added for 4 h. When necessary the feed line one was heated with heat gun to remove blocking from salt crystallisation. One hour after feed completion second lot of AMBN (0.88 g, 5 mmol) was dissolved in methylated spirit (7.5 g) and added to the vessel. After additional hour of mixing the reaction was turned off and left overnight. The next day 100 g of methylated spirit was distilled at 85 °C with simultaneous feed of 131 g of xylene. The obtained polymer was viscous and difficult to apply and in order to ease its application additional 90 g of xylene was added to the ready polymer.

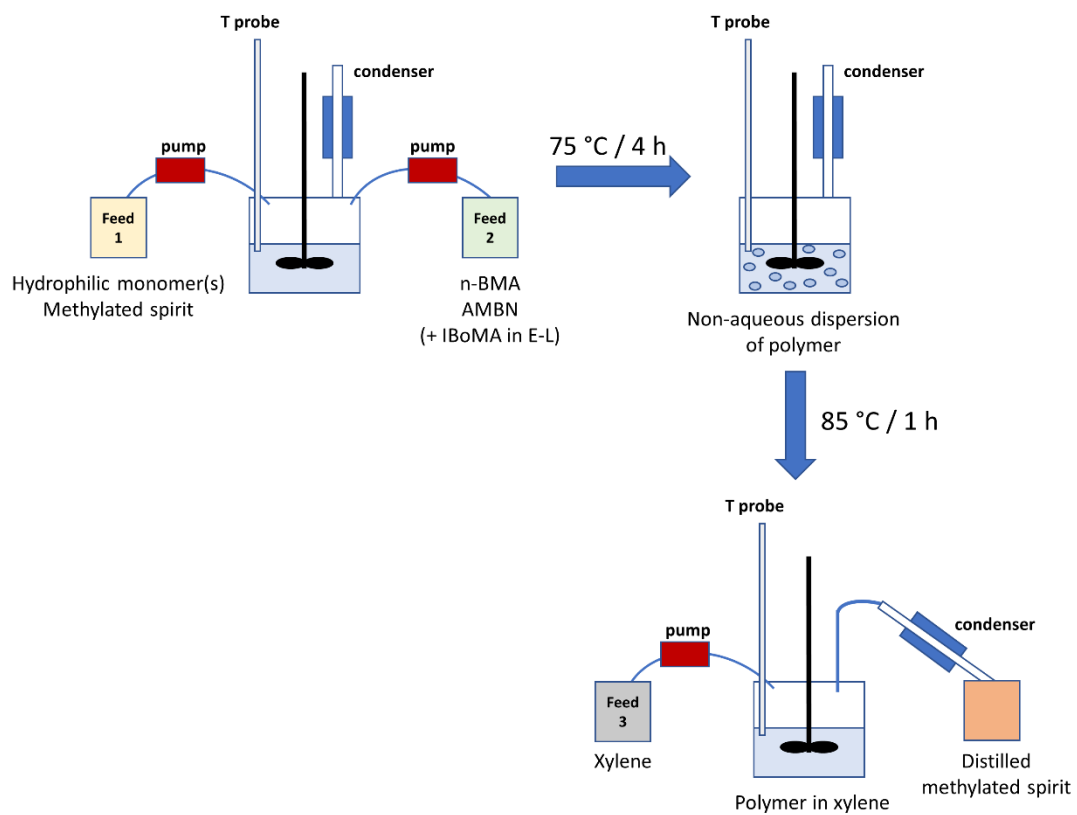


Figure A.1 Schematic representation of preparation of hydrophilic bulk copolymers using the dual-feed technique.

Appendix B. Bulk polymer composition determination by ^1H NMR

Polymer E-L (pBMA-co-IBoMA-co-mPEG350MA): In case of the IBoMA monomer the single proton at around 4.5 ppm (-OCH) was assigned based on the published data for the pMMA-co-IBoMA copolymer (Khandelwal *et al.*, 2011). The peaks deriving from mPEG350MA were assigned according to Harrell and Bergbreiter (2017). The copolymer composition was established by integrating and comparing the areas of the -CH₂ group of the n-BMA (**d**; $\delta = 3.99 - 3.83$ ppm), -OCH proton of the IBoMA (**g**; $\delta = 4.5 - 4.25$ ppm) and -CH₃ terminal group of the mPEG350MA (**r**; $\delta = 3.44 - 3.31$ ppm). Based on the integral data, the mole basis of n-BMA = $2.00 / 2\text{H} = 1$ mole, IBoMA = $0.63 / 1\text{H} = 0.63$ mole and mPEG350MA = $0.66 / 3\text{H} = 0.22$ mole. Final molar composition: n-BMA = $1 / 1.85 = 54$ mol %, IBoMA = $0.63 / 1.85 = 34$ mol %, mPEG350MA = $0.22 / 1.85 = 12$ mol %.

Polymer H-L (pBMA-co-HEMA): In order to estimate the copolymer composition a following procedure was undertaken. Knowing that the signal at $\delta = 1.69 - 1.5$ ppm belonged to -CH₂ group of n-BMA (**c**) and the signal at $\delta = 4.28 - 3.51$ ppm could be assigned to -CH₂ groups of n-BMA and HEMA (**d + g + h**), thus the integral value $I = 2.39$ was assigned to 2 protons of n-BMA and 0.39 protons of HEMA. Ultimately, the mole basis of n-BMA = $2.00 / 2\text{H} = 1$ mole and mole basis of HEMA = $0.39 / 4\text{H} = 0.098$ mole. Final molar composition: n-BMA = $1 / 1.098 = 91$ mol % and HEMA = $0.098 / 1.098 = 9$ mol %.

Polymer G-L (pBMA-co-DHPMA): Copolymer composition was determined in a following manner. Knowing that the signal at $\delta = 1.69 - 1.52$ ppm belonged only to -CH₂ group of the n-BMA (**c**) and the signal at $\delta = 4.25 - 3.50$ ppm belonged to both n-BMA and DHPMA (**d + g + h + i**), thus the integral value $I = 2.53$ was assigned to 2 protons from n-BMA and 0.53 protons of DHPMA. Based on the above information the mole basis of n-BMA = $2.00 / 2\text{H} = 1$ mole and mole basis of DHPMA = $0.53 / 5\text{H} = 0.106$ mole. Final molar composition: n-BMA = $1 / 1.106 = 90$ mol % and DHPMA = $0.106 / 1.106 = 10$ mol %.

Polymer M-L (pBMA-co-MAA): The composition of this copolymer was established in a following manner. Knowing that the signal at $\delta = 1.71 - 1.5$ ppm belonged only to -CH₂ group of n-BMA (**c**), the large -CH₃ signal at $\delta = 1.28 - 0.31$ ppm was assigned to -CH₃ groups (**a + e + g**) of both n-BMA and MAA. Consequently, the integral value $I = 6.29$ was attributed to 6 protons from -CH₃ of n-BMA (**a + e**)

and 0.29 protons from -CH₃ of MAA (**g**). Taking into consideration only -CH₃ groups in polymer backbone (**e** + **g**) the copolymer composition was determined as follows: n-BMA = 3 / 3.29 = 91 mol % and MAA = 0.29 / 3.29 = 9 mol %.

Polymer Z-L (pBMA-co-SBMA_{10mol%}): The composition of zwitterionic copolymer was determined by comparing integrated areas of the -CH₂ group of n-BMA (**c**; $\delta = 1.69 - 1.5$ ppm) with -CH₃ groups of the SBMA (**j**; $\delta = 3.56 - 3.15$ ppm). Based on the integral data the mole basis of n-BMA = 2.00 / 2H = 1 mole and SBMA = 0.45 / 6H = 0.075 mole. Final molar composition: n-BMA = 1 / 1.075 = 93 mol % and SBMA = 0.075 / 1.075 = 7 mol %.

Polymer Z-L20 (pBMA-co-SBMA_{20mol%}): The composition of zwitterionic copolymer with higher SBMA loading was determined by comparing integrated areas of the -CH₂ group of n-BMA (**c**; $\delta = 1.69 - 1.5$ ppm) with -CH₃ groups of the SBMA (**j**; $\delta = 3.46 - 3.19$ ppm). Based on the integral data the mole basis of n-BMA = 2.00 / 2H = 1 mole and SBMA = 0.47 / 6H = 0.078 mole. Final molar composition: n-BMA = 1 / 1.078 = 93 mol % and SBMA = 0.078 / 1.078 = 7 mol %.

Polymer A-L (pBMA-co-SPMA): Copolymer composition was established by comparing integrated area of the -CH₂ group of n-BMA (**c**; $\delta = 1.67 - 1.52$ ppm) with -CH₂ group of SPMA (**g**; $\delta = 3.45 - 3.04$ ppm). Based on the integral data, the mole basis of n-BMA = 2.00 / 2H = 1 mole and SPMA = 0.17 / 2H = 0.085 mole. Final molar composition: n-BMA = 1 / 1.085 = 92 mol % and SPMA = 0.085 / 1.085 = 8 mol %.

Polymer C-L (pBMA-co-METAC): The chemical composition of the copolymer was determined by comparing integrated area of the -CH₂ group of n-BMA (**c**; $\delta = 1.68 - 1.47$ ppm) with -CH₃ groups of METAC (**g**; $\delta = 3.7 - 3.32$ ppm). Based on the integral data the mole basis of n-BMA = 2.00 / 2H = 1 mole, METAC = 0.96 / 9H = 0.107 mole. Final molar composition: n-BMA = 1 / 1.107 = 90 mol % and METAC = 0.107 / 1.107 = 10 mol %.

Polymer P-L10 (pBMA-co-SPMA_{5mol%}-co-METAC_{5mol%}): The composition of this mixed-charged copolymer was determined by comparing integrated areas of the -CH₂ group of n-BMA (**c**; $\delta = 1.66 - 1.51$ ppm) with -CH₂ group of SPMA (**g**; $\delta = 3.09 - 2.83$ ppm) and -CH₃ groups of METAC (**i**; $\delta = 3.62 - 3.34$ ppm). Based on the integral data the mole basis of n-BMA = 2.00 / 2H = 1 mole, SPMA = 0.09 /

$2H = 0.045$ mole, $METAC = 0.5 / 9H = 0.056$ mole. Final molar composition: $n\text{-BMA} = 1 / 1.101 = 91$ mol %, $SPMA = 0.045 / 1.101 = 4$ mol %, $METAC = 0.056 / 1.101 = 5$ mol %.

Polymer P-L20 (pBMA-co-SPMA_{10mol%}-co-METAC_{10mol%}): The composition of this copolymer was determined by comparing integrated areas of the $-\text{CH}_2$ group of n-BMA (**c**; $\delta = 1.67 - 1.5$ ppm) with $-\text{CH}_2$ group of SPMA (**g**; $\delta = 2.99 - 2.77$ ppm) and $-\text{CH}_3$ groups of METAC (**l**; $\delta = 3.58 - 3.3$ ppm). Based on the integral data the mole basis of $n\text{-BMA} = 2.00 / 2H = 1$ mole, $SPMA = 0.21 / 2H = 0.105$ mole, $METAC = 1.00 / 9H = 0.111$ mole. Final molar composition: $n\text{-BMA} = 1 / 1.216 = 82$ mol %, $SPMA = 0.105 / 1.216 = 9$ mol %, $METAC = 0.111 / 1.216 = 9$ mol %.

Polymer Z-GL (pBMA-co-SBMA-co-GMA): The composition of the copolymer was determined by comparing integrated areas of the $-\text{CH}_2$ group of n-BMA (**c**; $\delta = 1.65 - 1.45$ ppm) with $-\text{CH}_2$ group of the SBMA (**l**; $\delta = 4.3 - 4.13$ ppm) and $-\text{CH}_2$ proton of the GMA (**o**; $\delta = 2.82 - 2.72$ ppm). Based on the integral data the mole basis of $n\text{-BMA} = 2.00 / 2H = 1$ mole, $SBMA = 0.3 / 2H = 0.15$ mole, $GMA = 0.28 / 1H = 0.28$ mole. Final molar composition: $n\text{-BMA} = 1 / 1.43 = 70$ mol %, $SBMA = 0.15 / 1.43 = 10$ mol % and $GMA = 0.28 / 1.43 = 20$ mol %.

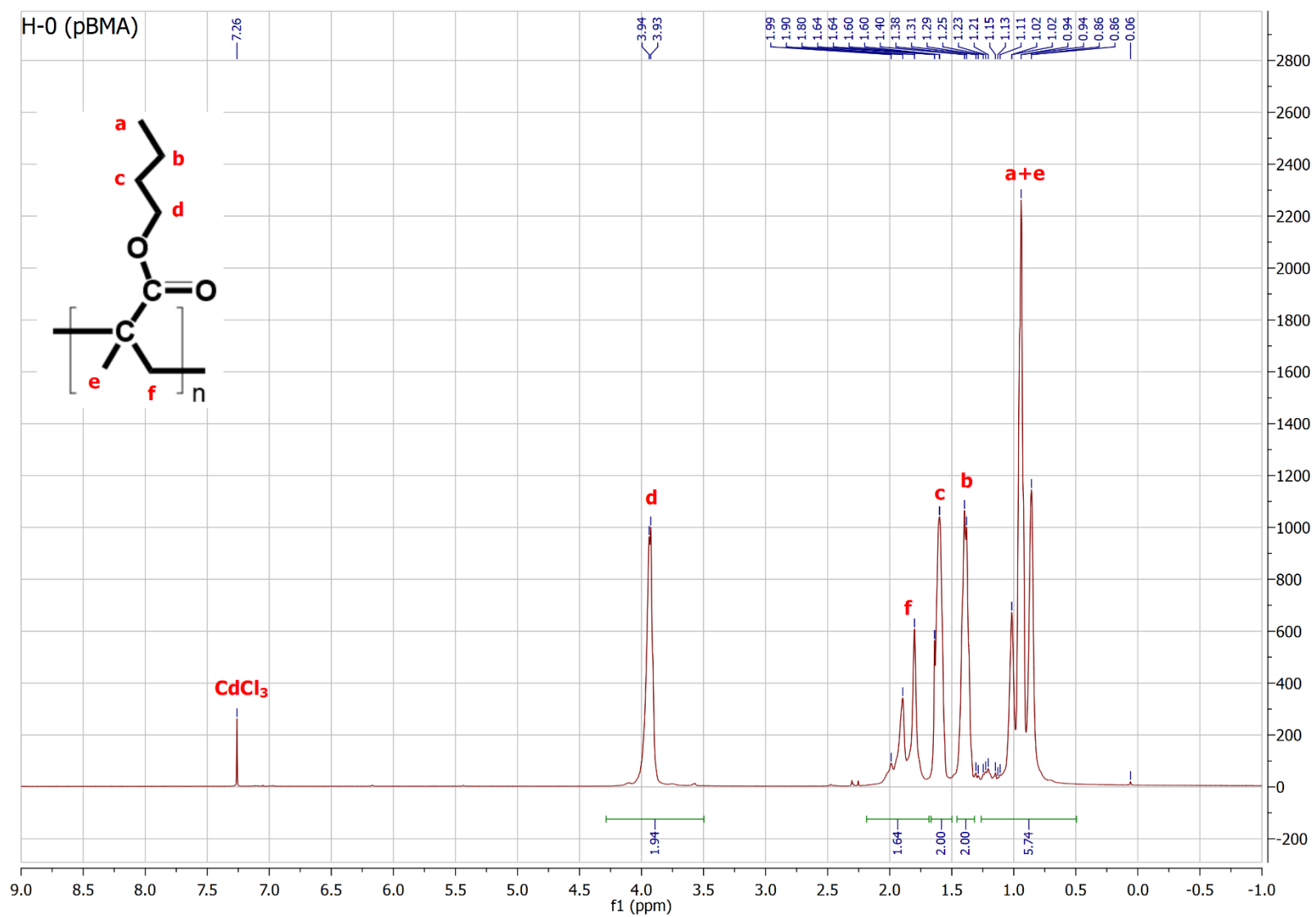


Figure B.1 ^1H NMR spectrum of bulk H-0 homopolymer (pBMA) in CdCl_3 .

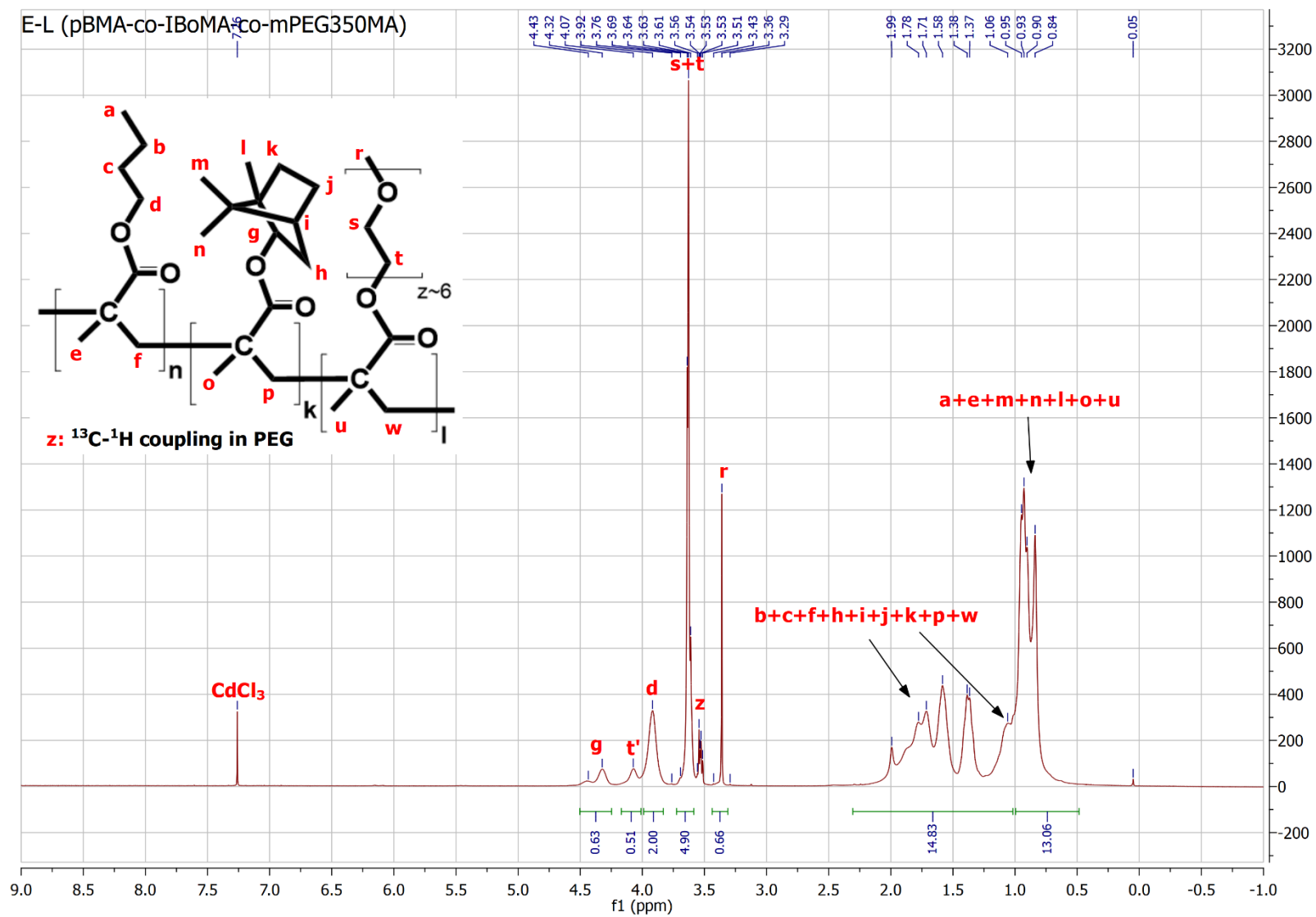


Figure B.2 ^1H NMR spectrum of bulk E-L copolymer (pBMA-co-IBoMA-co-mPEG350MA) in CdCl_3 .

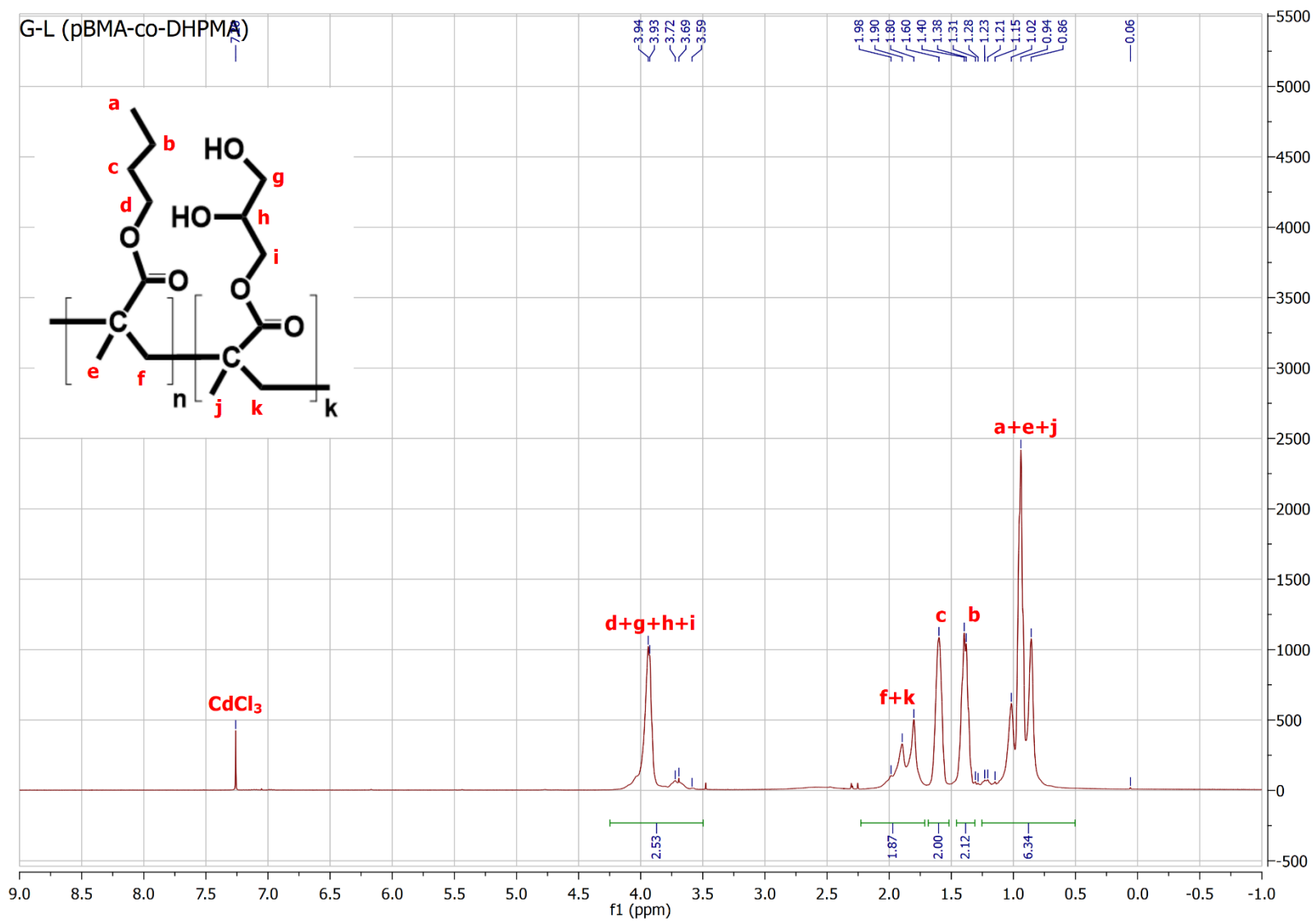


Figure B.4 ^1H NMR spectrum of bulk G-L copolymer (pBMA-co-DHPMA) in CdCl_3 .

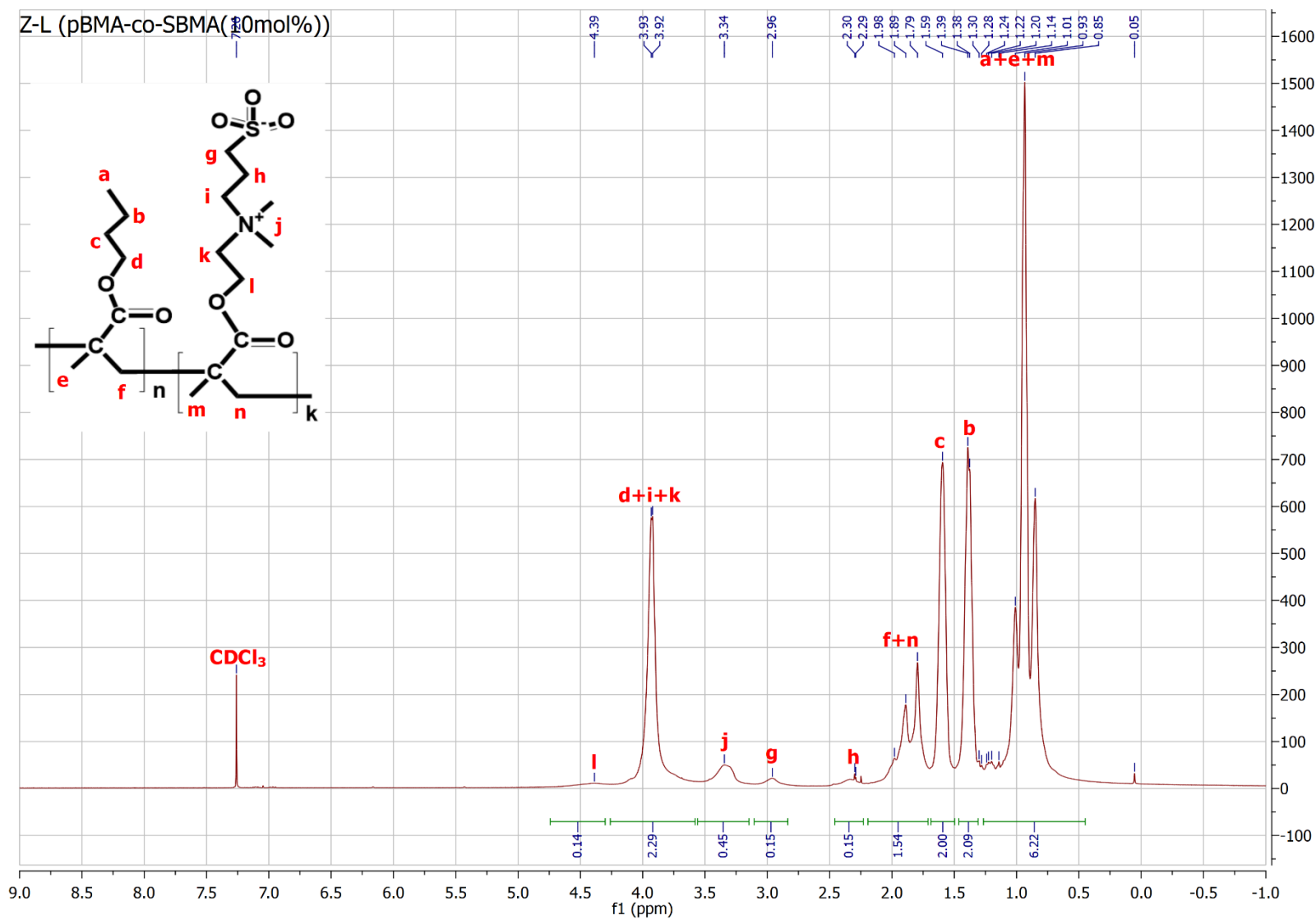


Figure B.6 ¹H NMR spectrum of bulk Z-L copolymer (pBMA-co-SBMA_{10mol%}) in CDCl₃.

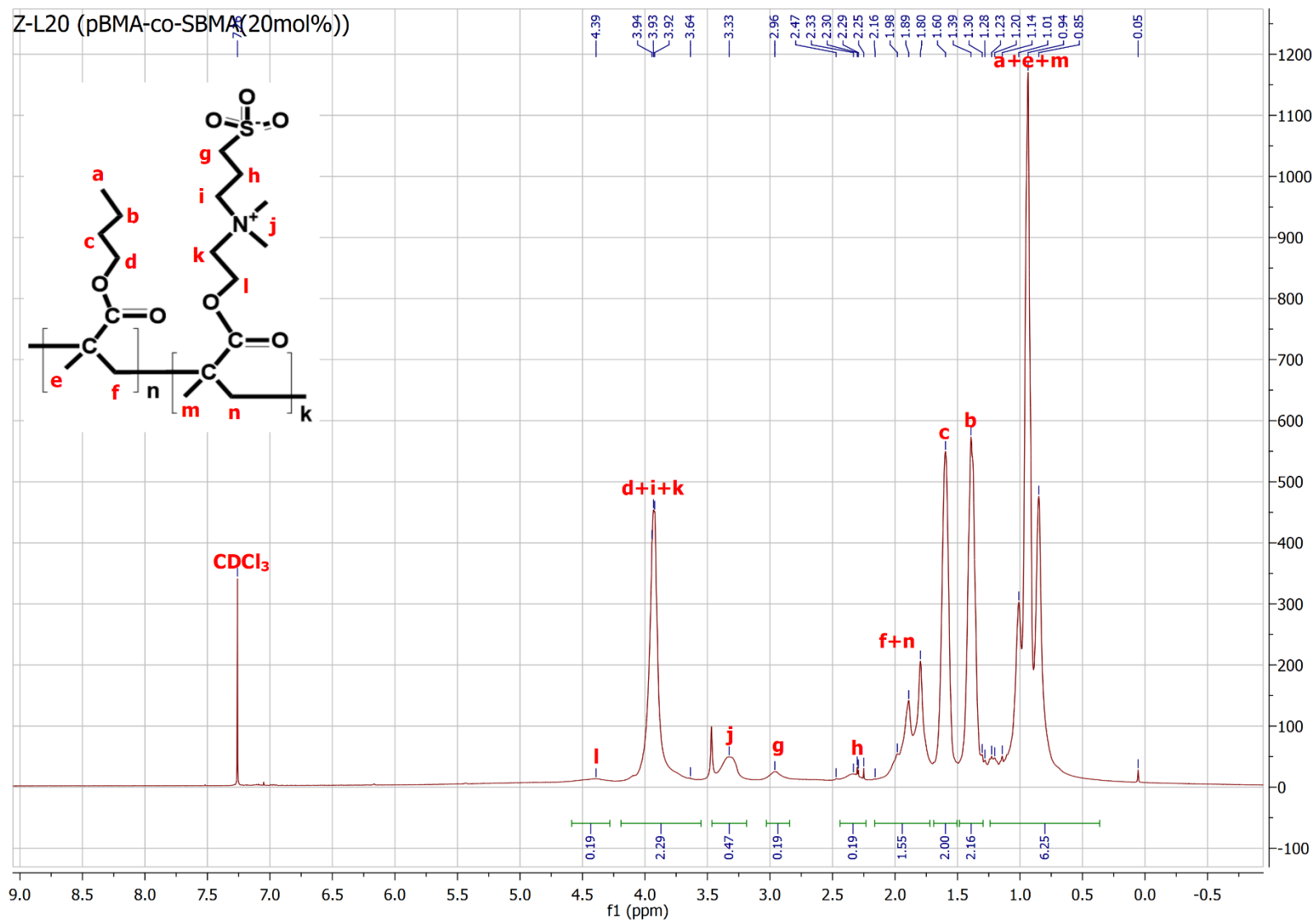


Figure B.7 ¹H NMR spectrum of bulk Z-L20 copolymer (pBMA-co-SBMA_{20mol%}) in CdCl₃.

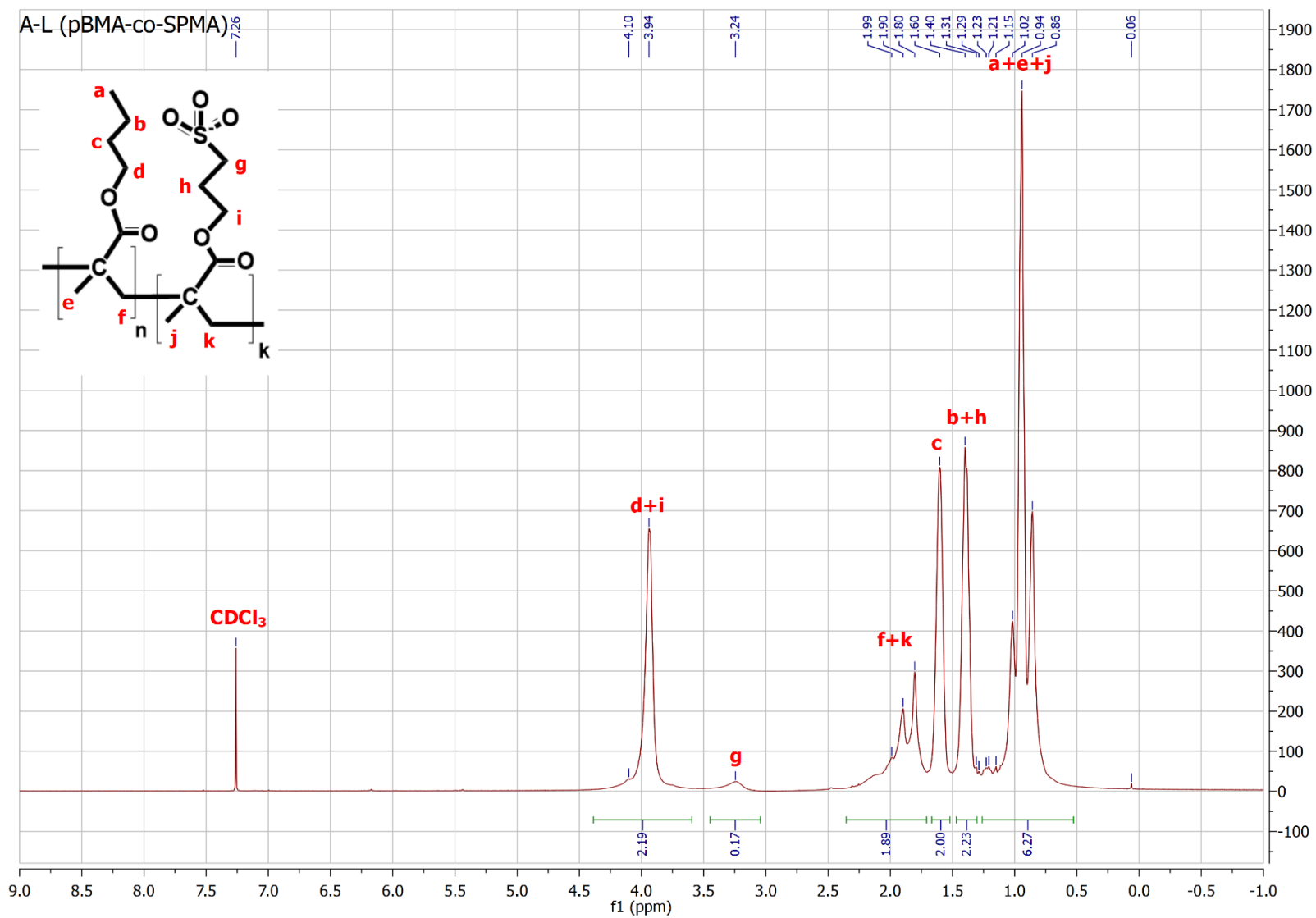


Figure B.8 1H NMR spectrum of bulk A-L copolymer (pBMA-co-SPMA) in $CDCl_3$.

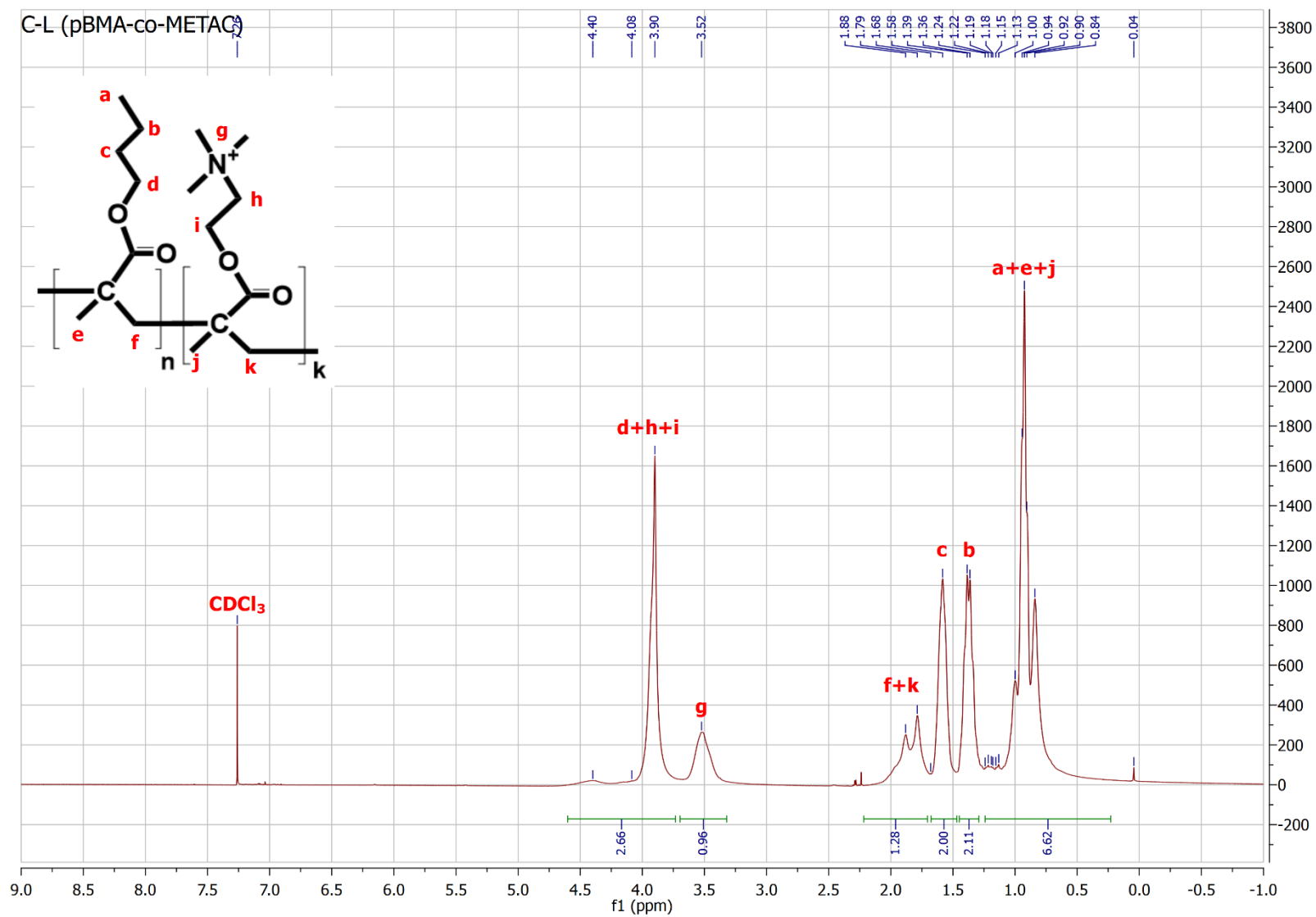


Figure B.9 ^1H NMR spectrum of bulk C-L copolymer (pBMA-co-METAC) in CDCl_3 .

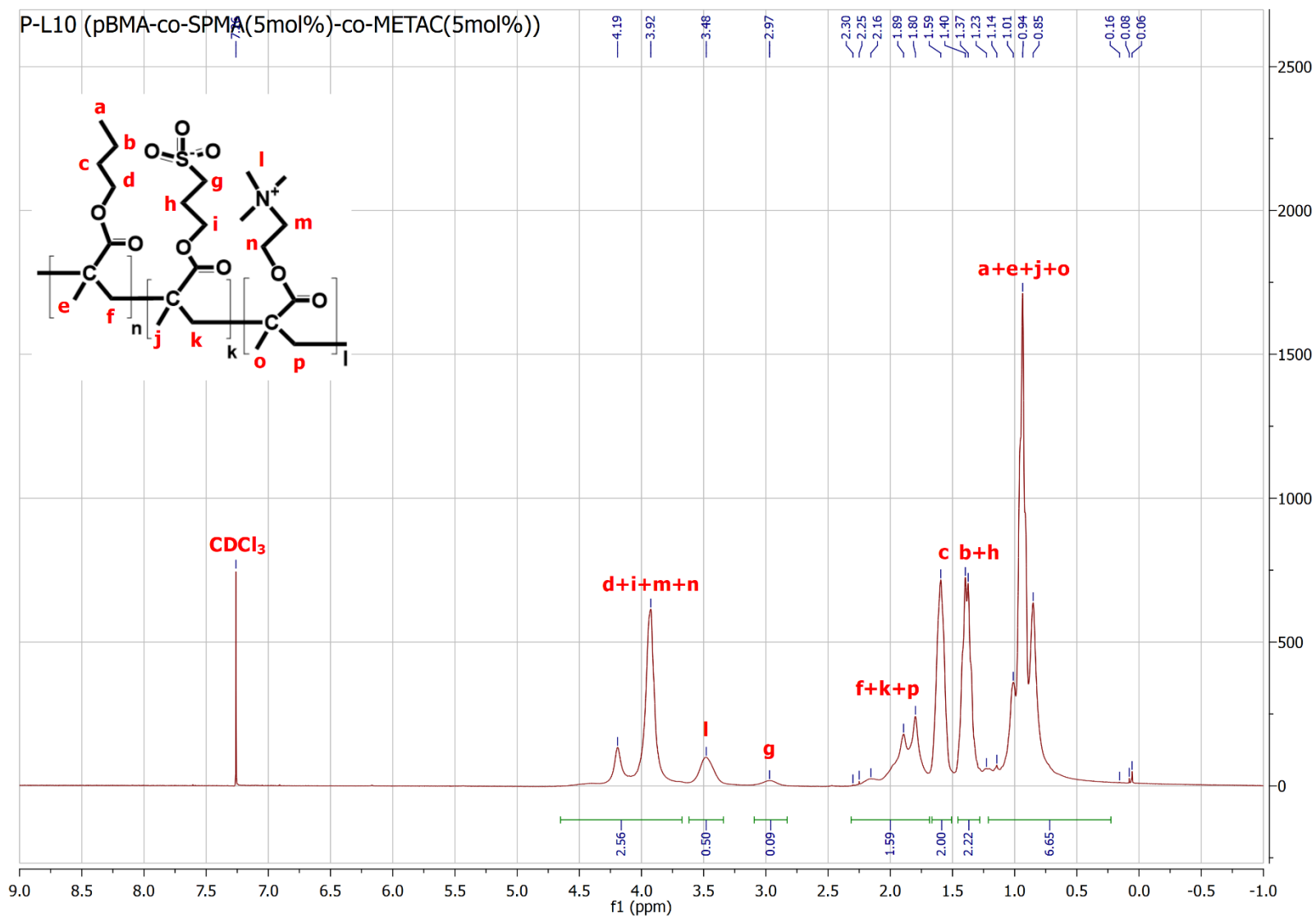


Figure B.10 ^1H NMR spectrum of bulk P-L10 copolymer (pBMA-co-SPMA_{5mol%}-co-METAC_{5mol%}) in CDCl_3 .

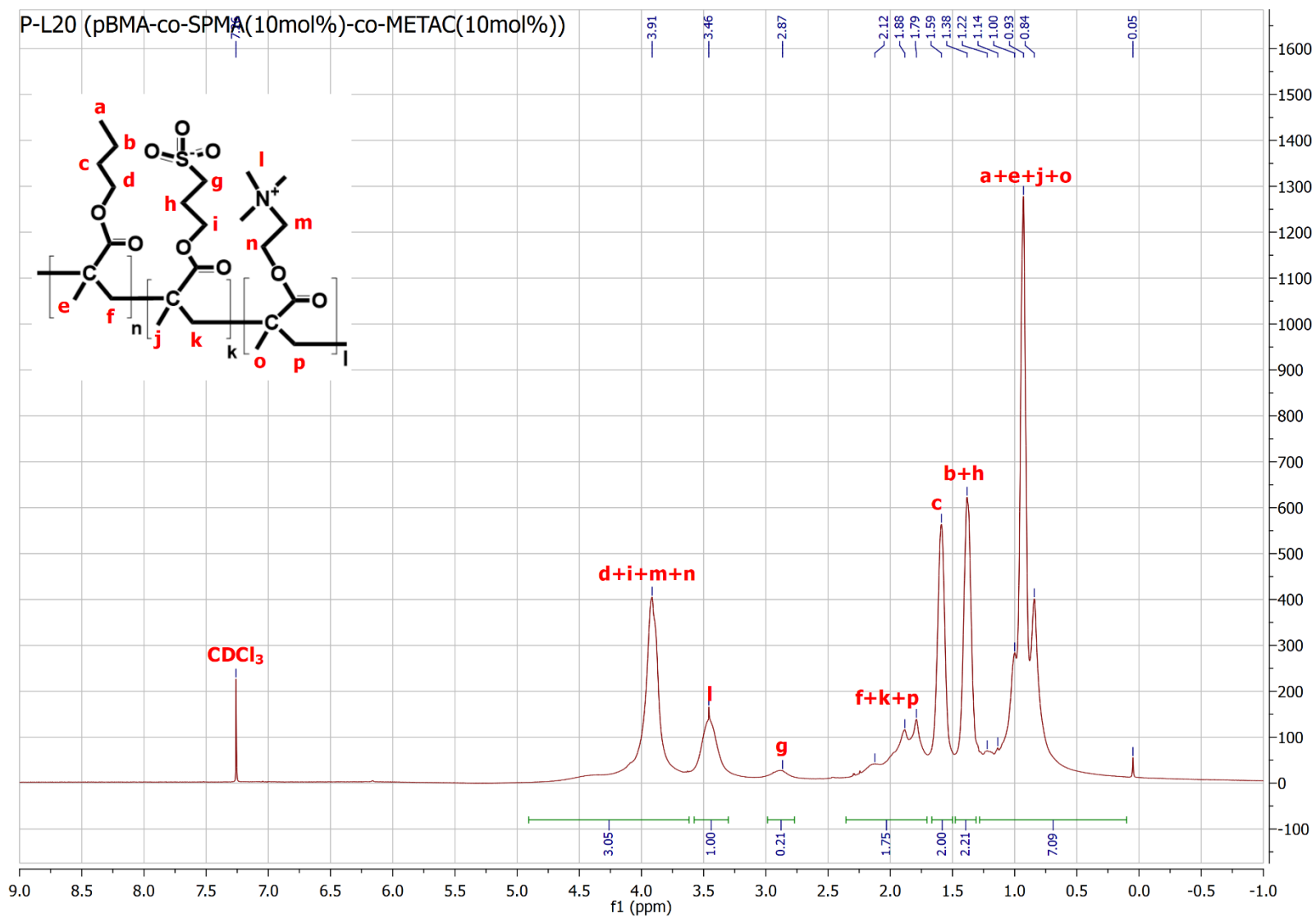


Figure B.11 ¹H NMR spectrum of bulk P-L20 copolymer (pBMA-co-SPMA_{10mol%}-co-METAC_{10mol%}) in CdCl₃.

Appendix C. SEC traces of bulk polymers

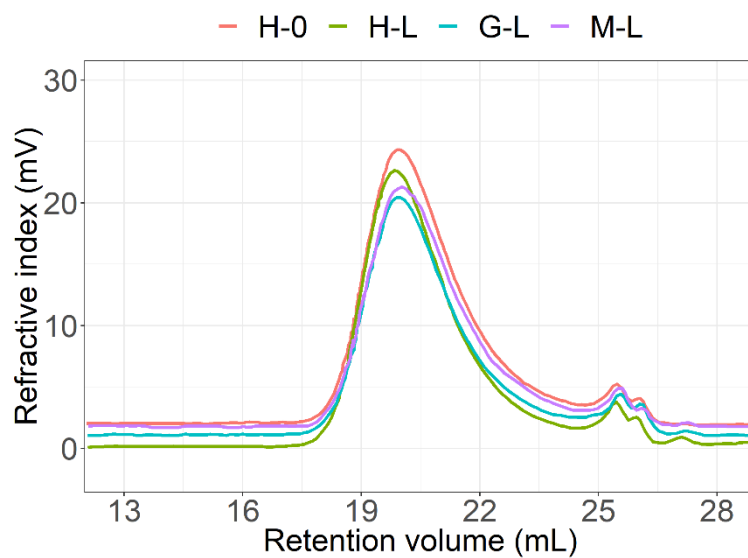


Figure C.1 SEC traces of bulk polymers H-0, H-L, G-L, M-L. Refractive index (mV) vs Retention volume (mL).

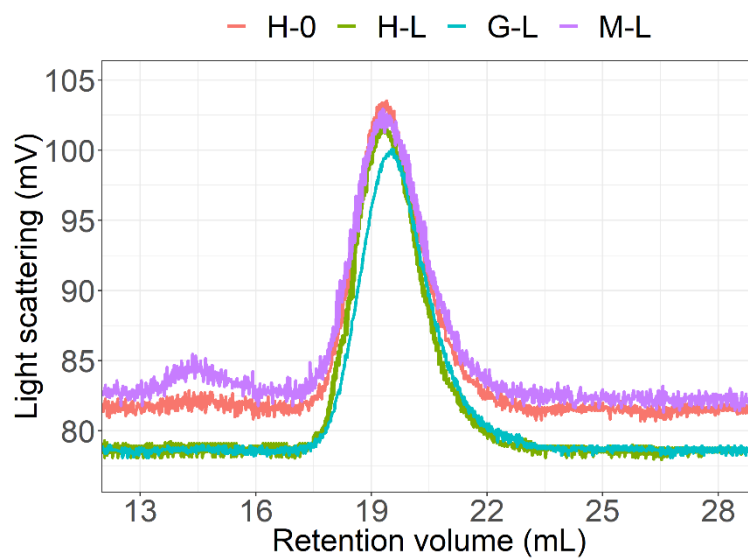


Figure C.2 SEC traces of bulk polymers G-L, H-0, H-L, M-L. Light scattering (mV) vs Retention volume (mL).

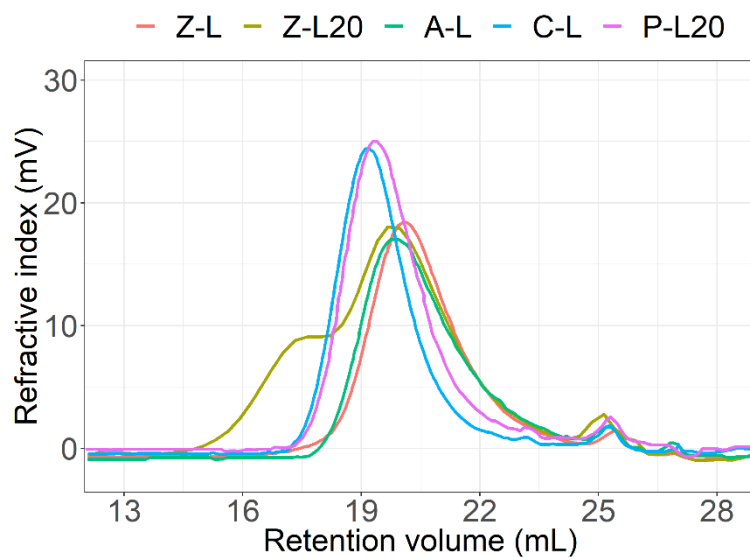


Figure C.3 SEC traces of bulk polymers Z-L, Z-L20, A-L, C-L, P-L20. Refractive index (mV) vs Retention volume (mL).

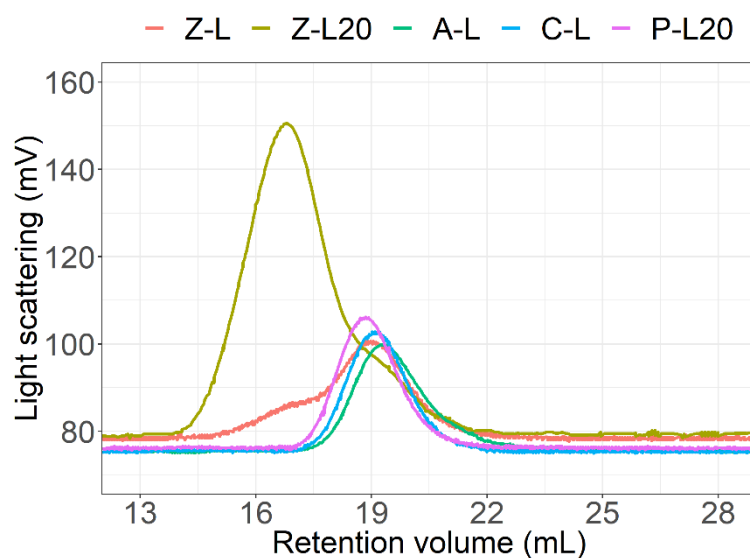


Figure C.4 SEC traces of bulk polymers Z-L, Z-L20, A-L, C-L, P-L20. Light scattering (mV) vs Retention volume (mL).

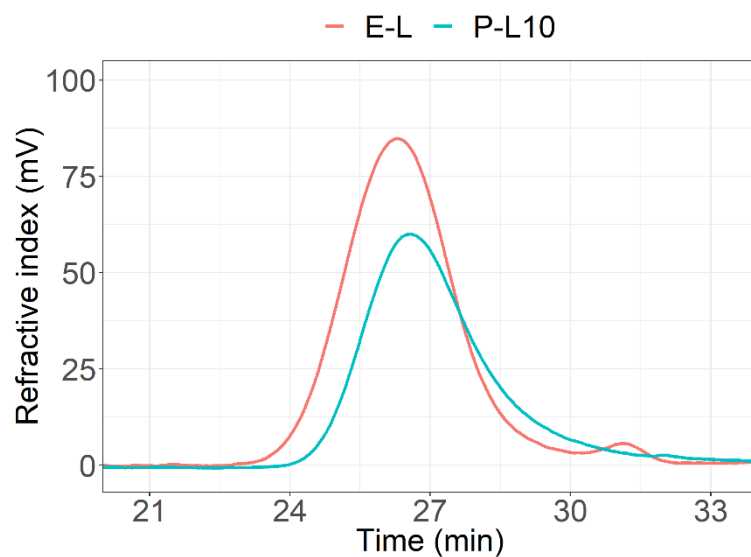


Figure C.5 SEC traces of bulk polymers E-L, P-L10. Refractive index (mV) vs Time (min).

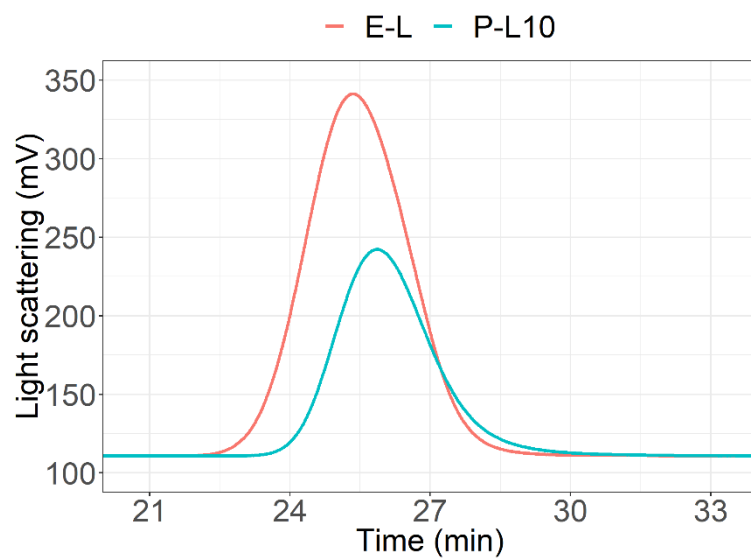


Figure C.6 SEC traces of bulk polymers E-L, P-L10. Light scattering (mV) vs Time (min).

Appendix D. Surface energy derivations for underwater contact angle measurements

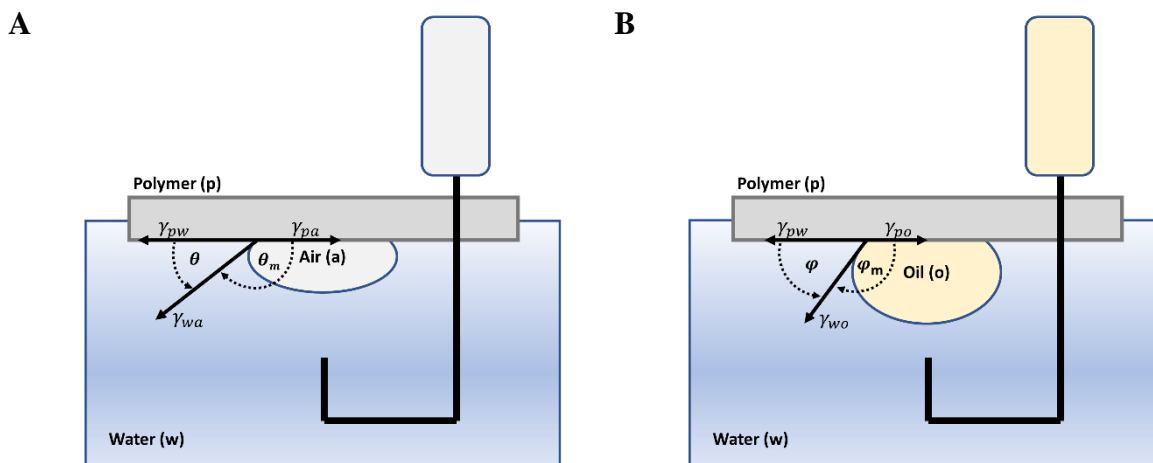


Figure D.1 Schematic representation of underwater contact angles measurements using air bubble (A) and silicone oil droplet (B). θ_m , ϕ_m in degrees is the measured angle between the polymer surface and the air bubble/oil droplet inside the probing liquid. Larger measured angle inside the bubble/droplet corresponds to higher surface wettability. The actual contact angles used in surface energy calculations are expressed as $\theta = 180^\circ - \theta_m$ for air bubble and $\phi = 180^\circ - \phi_m$ for oil droplet.

ESTIMATION OF DISPERSIVE COMPONENT OF SFE OF HYDRATED POLYMER γ_{pa}^d :

Young's equation of air bubble:	Young's equation of oil droplet:
$\theta = 180^\circ - \theta_m$ $\gamma_{pa} - \gamma_{pw} - \gamma_{wa} \cos \theta = 0$ $\gamma_{pa} - \gamma_{pw} = \gamma_{wa} \cos \theta$ $\gamma_{pa} - \gamma_{po} + \gamma_{wo} \cos \varphi = \gamma_{wa} \cos \theta$ $-\gamma_{oa} + 4 \frac{\gamma_{pa}^d \gamma_{oa}^d}{\gamma_{pa}^d + \gamma_{oa}^d} + \gamma_{wo} \cos \varphi = \gamma_{wa} \cos \theta$ $4 \frac{\gamma_{pa}^d \gamma_{oa}^d}{\gamma_{pa}^d + \gamma_{oa}^d} = \gamma_{wa} \cos \theta - \gamma_{wo} \cos \varphi + \gamma_{oa}$ <p>(...)</p> $\gamma_{pa}^d = \frac{\gamma_{oa}(\gamma_{wa} \cos \theta - \gamma_{wo} \cos \varphi) + \gamma_{oa}^2}{\gamma_{wo} \cos \varphi - \gamma_{wa} \cos \theta + 3\gamma_{oa}}$ <p>Where:</p> $\gamma_{oa} = \gamma_{oa}^d = 19.7 \frac{mN}{m}$ $\gamma_{wa} = 72.8 \frac{mN}{m}$ $\gamma_{wo} = 37.8 \frac{mN}{m}$	$\varphi = 180^\circ - \varphi_m$ $\gamma_{po} - \gamma_{pw} - \gamma_{wo} \cos \varphi = 0$ $\gamma_{pw} = \gamma_{po} - \gamma_{wo} \cos \varphi$
	<p>Wu's harmonic mean estimation of interfacial energy at polymer-oil interface:</p>
	$\gamma_{po} = \gamma_{pa} + \gamma_{oa} - 4 \frac{\gamma_{pa}^d \gamma_{oa}^d}{\gamma_{pa}^d + \gamma_{oa}^d}$ $- 4 \frac{\gamma_{pa}^p \gamma_{oa}^p}{\gamma_{pa}^p + \gamma_{oa}^p} (\sim 0)^*$ $\gamma_{po} = \gamma_{pa} + \gamma_{oa} - 4 \frac{\gamma_{pa}^d \gamma_{oa}^d}{\gamma_{pa}^d + \gamma_{oa}^d}$ <p>(*) Silicone oil does not have polar contributions of energy, thus $\gamma_{oa}^p = 0$.</p>

ESTIMATION OF POLAR COMPONENT OF SFE OF HYDRATED POLYMER γ_{pa}^p :

Young's equation of air bubble:	Wu's harmonic mean estimation of interfacial energy at polymer-water interface:
$\theta = 180^\circ - \theta_m$ $\gamma_{pa} - \gamma_{pw} - \gamma_{wa} \cos \theta = 0$ $\gamma_{pa} - \gamma_{pw} \leftarrow \gamma_{wa} \cos \theta$ $-\gamma_{wa} + 4 \frac{\gamma_{pa}^d \gamma_{wa}^d}{\gamma_{pa}^d + \gamma_{wa}^d} + 4 \frac{\gamma_{pa}^p \gamma_{wa}^p}{\gamma_{pa}^p + \gamma_{wa}^p} = \gamma_{wa} \cos \theta$ <p>(...)</p> $\gamma_{pa}^p = \frac{\gamma_{wa}^p (\gamma_{wa} (1 + \cos \theta) - 4 \frac{\gamma_{pa}^d \gamma_{wa}^d}{\gamma_{pa}^d + \gamma_{wa}^d})}{4 \gamma_{wa}^p + 4 \frac{\gamma_{pa}^d \gamma_{wa}^d}{\gamma_{pa}^d + \gamma_{wa}^d} - \gamma_{wa} (1 + \cos \theta)}$ <p><u>Where:</u></p> $\gamma_{wa}^p = 46.4 \frac{mN}{m}$ $\gamma_{wa}^d = 26.4 \frac{mN}{m}$ $\gamma_{wa} = 72.8 \frac{mN}{m}$ $\gamma_{pa}^d = \frac{\gamma_{oa} (\gamma_{wa} \cos \theta - \gamma_{wo} \cos \varphi) + \gamma_{oa}^2}{\gamma_{wo} \cos \varphi - \gamma_{wa} \cos \theta + 3 \gamma_{oa}}$	$\gamma_{pw} = \gamma_{pa} + \gamma_{wa} - 4 \frac{\gamma_{pa}^d \gamma_{wa}^d}{\gamma_{pa}^d + \gamma_{wa}^d} - 4 \frac{\gamma_{pa}^p \gamma_{wa}^p}{\gamma_{pa}^p + \gamma_{wa}^p}$

ESTIMATION OF TOTAL SFE OF HYDRATED POLYMER γ_{pa}^{TOT} :

$$\gamma_{pa}^{TOT} = \gamma_{pa}^d + \gamma_{pa}^p$$

ESTIMATION OF IFE POLYMER / WATER γ_{pw} :

$$\gamma_{pw} = \gamma_{pa}^{TOT} + \gamma_{wa} - 4 \frac{\gamma_{pa}^d \gamma_{wa}^d}{\gamma_{pa}^d + \gamma_{wa}^d} - 4 \frac{\gamma_{pa}^p \gamma_{wa}^p}{\gamma_{pa}^p + \gamma_{wa}^p}$$

Appendix E. Single settlement experiment using barnacle cypris larvae and comparison with meta-analysis approach

In a single settlement experiment eight slides per polymer set were used. Leached slides were transferred to quadriPERM® dishes and on each slide 0.5 mL of ASW (22 ppt) was added, followed by addition of 20 ± 2 freshly filtered larvae (zero-day) in a minimal volume of ASW. The dishes were then wrapped with paper towel, covered with aluminium foil and placed in the incubator at 28 °C in the dark. After 72 h dishes were carefully removed from incubator and number of settled cyprids was enumerated using a dissection microscope.

Figure E.1 presents settlement data as percent of settled cyprids of *B. improvisus*. Settlement differed across all surfaces (Welch ANOVA $F_{10,77} = 45.16$, $p \leq 0.001$) and in general surfaces could be divided based on their antifouling performance into two distinct groups following their ionic/non-ionic character (Games-Howell tests, $p \leq 0.001$). Smallest settlement was observed on ionic polymers i.e. Z-L20 ($0 \pm 0\%$), Z-L ($9.98 \pm 6.07\%$), A-L ($8.27 \pm 6.39\%$), C-L ($1.32\% \pm 2.58\%$), P-L20 ($0.63 \pm 1.23\%$) and the non-ionic polymer E-L with PEG functionality ($3.19 \pm 3.25\%$).

In order to compare settlement results obtained with both statistical approaches and graphically visualize any potential trends, the mean settlement from single experiment and summary effect sizes derived from meta-analysis were plotted on box plots (Figure E.2).

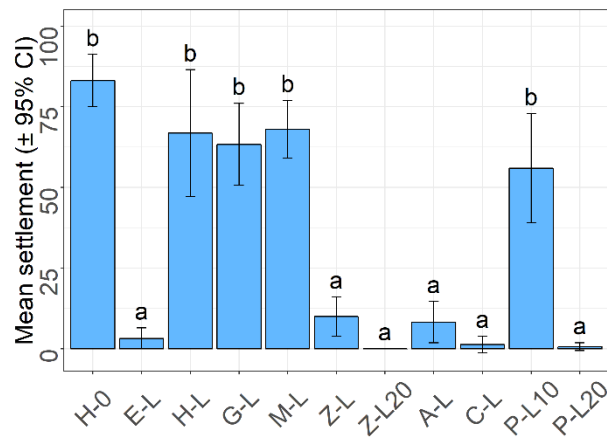
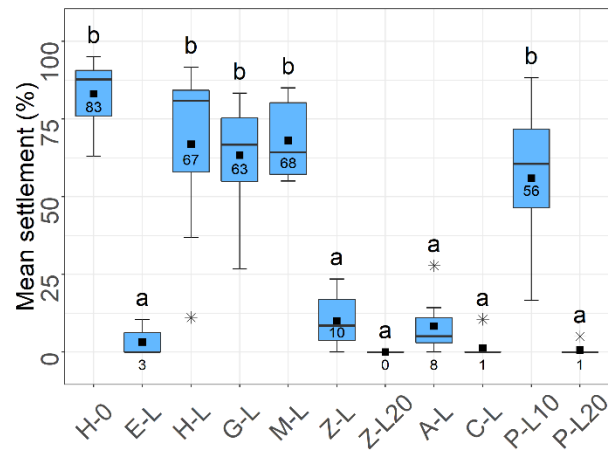


Figure E.1 Mean percent settlement with 95% CIs of *B. improvisus* after 72 h. Letters represent pairwise comparisons and bars that do not share a letter are significantly different.

(A)



(B)

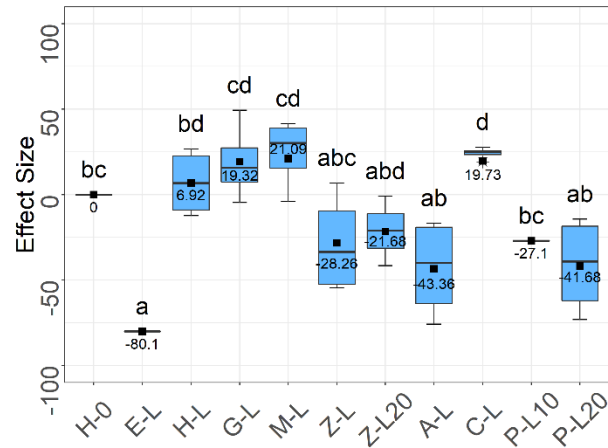


Figure E.2 (A) Box plot presenting single settlement experiment results of cyprids larvae of *B. improvisus*. (B) Box plot presenting settlement results from four independent studies combined using meta-analysis. Black squares inside the boxes together with attached labels represent the mean settlement or summary effect sizes. Outliers are presented with asterisks. Letters indicate pairwise comparisons and boxes that do not share a letter are significantly different.

Appendix F. Biofilm growth and removal data

Figure F.1 presents the results of biofilm (biomass) growth after 14 days of immersion in slime farm as determined by fluorescence plate reader and expressed using relative fluorescence units (RFUs). The amount of biomass varied significantly among surfaces (one-way ANOVA using square-root transformed data $F_{10,22} = 15.16$, $p \leq 0.001$). The smallest amount of biomass was recorded on polymers Z-L20, Z-L, A-L and P-L20, whilst the highest biomass growth was on PDMS (Dow Corning 3-0213).

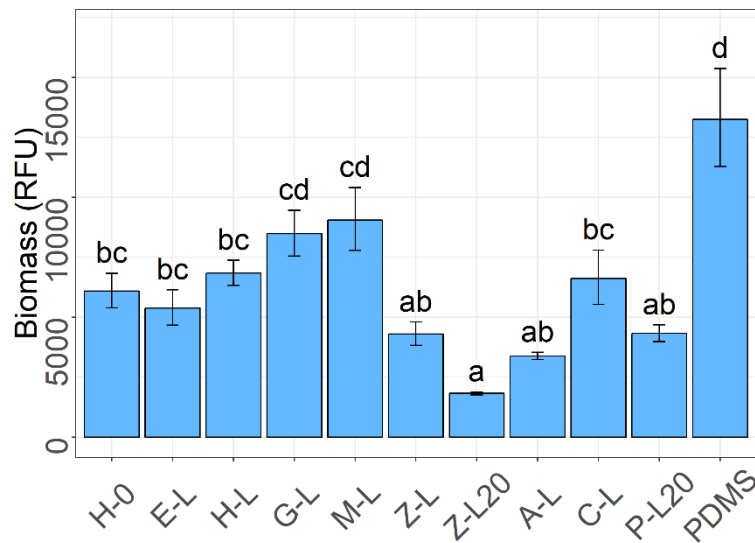


Figure F.1 Biomass generated by multispecies biofilm after 14 days of immersion in the slime farm quantified as relative fluorescence units (RFUs) using fluorescence plate reader. Mean RFUs were calculated from three slides using square root transformed data. Error bars represent SEs of the mean. Letters indicate Tukey's pairwise comparisons and points that do not share a letter are significantly different.

Coatings with attached biofilm were exposed to 8.2 Pa wall shear stress and the amount of retained biomass was measured directly after testing (Figure F.2). There was a significant variation in the amount of biomass retained among the polymers after exposure to flow (one-way ANOVA using square-root transformed data $F_{10,22} = 20.14$, $p \leq 0.001$). Furthermore, all polymers except polymer M-L retained significantly lower biomass after flow than the PDMS (Tukey tests, $p > 0.05$).

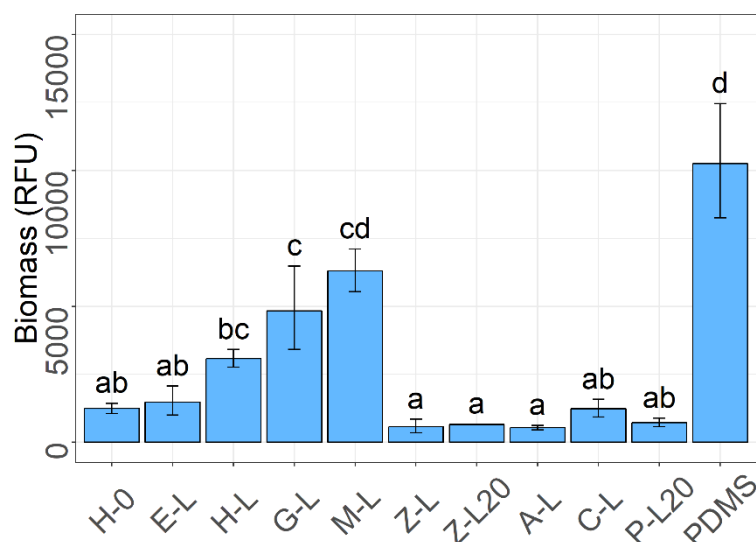


Figure F.2 Amount of remaining biomass after removal in the water channel quantified as relative fluorescence units (RFUs) using fluorescence plate reader. Mean RFUs were determined from three replicates after exposure to flow (8.2 Pa) and were calculated using square root transformed data. Letters indicate Tukey's pairwise comparisons and points that do not share a letter are significantly different.

Appendix G. Preparation and characterization of polymer brushes

Polymer brush H-0 (pBMA): To a glass reactor holding slides with immobilized CPSE CTA agent, CPAD (0.483 g, 1.73 mmol) was added followed by addition of first lot of DMF (217 mL), 1 mL solution of AIBN in DMF (57 mg/mL, 0.347 mmol) and n-BMA (74.23 g, 522 mmol). To fully cover the slides with reaction mixture a second lot of DMF (83 mL) was added. After mixing reagents the reactor was kept in an ice bath and degassed by bubbling with argon (Ar) for 5 h. Subsequently the reactor was placed in an oil bath fitted with mechanical stirrer and polymerization was run for 18 h at 70 °C under constant Ar flow. The next day reactor was quenched and immediately subjected to atmospheric air to terminate polymerization reaction. Slides were then cleaned in DCM and dried under flow of N₂ and remaining polymer solutions were dialysed three times against MeOH and DCM (1:2) mixture. SEC results: $M_n = 31$ kDa, PDI = 1.16. The tracking tube with pBMA polymer brush was prepared in a following manner. Firstly, the tube with immobilized CPSE CTA agent was carefully deposited within a Schlenk reaction flask equipped with PTFE O-ring holder and magnetic stirrer and then following reagents were added: DMF (9 mL), n-BMA (1.23 g, 8.68 mmol), 805 μ L solution of CPAD in DMF (10 mg/mL, 0.029 mmol) and finally 95 μ L solution of AIBN in DMF (10

mg/mL, 0.0058 mmol). The reaction mixture was degassed five times using vacuum/backfill cycles (Ar backfill) and then the reaction flask was immersed in oil bath at 70 °C for 16 h. The next morning, the flask was rapidly quenched and opened to air to terminate the reaction. The tracking tube was cleaned in DCM and blow-dried with N₂. The remaining polymer solution was dialysed three times using a mixture of MeOH and DCM (1:2). SEC results: M_n = 23 kDa, PDI = 1.25.

Polymer brush E-L (pBMA-co-IBoMA-co-mPEG350MA): The grafting of polymer brush containing PEG moiety on slides was performed in a similar manner as described above but the following reagents were used: DMF (two lots: 217 + 83 mL), CPAD (0.483 g, 1.73 mmol), 1 mL solution of AIBN in DMF (57 mg/mL, 0.347 mmol), n-BMA (42.31 g, 298 mmol), IBoMA (38.3 g, 172 mmol) and mPEG350MA (22.45 g, 52.2 mmol). The polymerization was run for 8 h at 70 °C. SEC results: M_n = 41 kDa, PDI = 1.13. The amounts of reagents used for preparation of tracking tube were as follows: DMF (9 mL), n-BMA (0.7 g, 5 mmol), IBoMA (0.64 g, 2.87 mmol), mPEG350MA (0.39 g, 0.91 mmol), 805 μ L solution of CPAD in DMF (10 mg/mL, 0.029 mmol) and 95 μ L solution of AIBN in DMF (10 mg/mL, 0.0058 mmol). Polymer solutions were dialysed three times in MeOH and DCM (1:2) mixture. SEC results: M_n = 43 kDa, PDI = 1.14.

Polymer brush Z-L (pBMA-co-SBMA_{10mol%}): The polymer brushes with SBMA functionality were synthesized in a similar manner as earlier described polymers, but the order of addition of reagents was different. Firstly, SBMA (14.58 g, 52.2 mmol) was dissolved in EG (50 mL) after sonication, followed by addition of BuOH (250 mL), n-BMA (66.8 g, 470 mmol), CPAD (0.483 g, 1.73 mmol) and 1 mL solution of AIBN in DMF (57 mg/mL, 3.47 mmol). After mixing the reagents the reactor was kept in an ice bath with constant flow of Ar for 5 h, which was then put for 18 h to an oil bath heated to 70 °C. After cooling the reaction using an ice bath to a room temperature a small amount of polymer precipitated from the solution. SEC results: M_n = 37 kDa, PDI = 1.13. The tracking tube was prepared using the same protocol as above but with following amounts of reagents: SBMA (0.243 g, 0.87 mmol), EG (1.5 mL), BuOH (7.5 mL), n-BMA (1.245 mL \approx 1.11 g, 7.83 mmol), 805 μ L solution of CPAD in DMF (10 mg/mL, 0.029 mmol) and 95 μ L solution of AIBN in DMF (10 mg/mL, 0.0058 mmol). Polymer solutions were dialysed once in mixture of MeOH and DCM (1:1) and twice in MeOH and DCM (1:2). SEC results: M_n = 29 kDa, PDI = 1.19.

Polymer brush A-L (pBMA-co-SPMA): The polymer brushes with anionic SPMA monomer were prepared in a similar manner as described above. First, SPMA was added (12.86 g, 52.2 mmol) which was dissolved after sonication in EG (50 mL), followed by addition of DMF (250 mL), n-BMA (66.8 g, 470 mmol), 1 mL solution of AIBN in DMF (57 mg/mL, 3.47 mmol) and CPAD (0.483 g, 1.73 mmol). The reaction solution was purged with Ar for 5 h and then polymerization was left in the oil

bath for 18 h at 70 °C. After cooling the reaction using an ice bath to a room temperature a small amount of polymer precipitated from the solution. SEC results: $M_n = 30$ kDa, PDI = 1.19. The tracking tube was prepared with following amounts of reagents: SPMA (0.214 g, 0.87 mmol), EG (1.5 mL), DMF (7.5 mL), n-BMA (1.245 mL \approx 1.11 g, 7.83 mmol), 805 μ L solution of CPAD in DMF (10 mg/mL, 0.029 mmol) and 95 μ L solution of AIBN in DMF (10 mg/mL, 0.0058 mmol). Polymer solutions were dialysed three times in mixture of MeOH and DCM (1:2). SEC results: $M_n = 27$ kDa, PDI = 1.27.

Polymer brush P-L10 (pBMA-*co*-SPMA_{5mol%}-*co*-METAC_{5mol%}): The polyampholyte brushes comprising of anionic SPMA and cationic METAC were produced in a following manner. Briefly, to a reactor holding CPSE functionalized slides, SPMA was added (6.43 g, 26.1 mmol) which was dissolved after sonication in EG (100 mL), followed by addition of METAC (6.78 g, 26.1 mmol), DMF (200 mL), n-BMA (66.8 g, 470 mmol), CPAD (0.483 g, 1.73 mmol) and 1 mL solution of AIBN in DMF (57 mg/mL, 3.47 mmol). Before running the polymerization, the reaction solution was purged with Ar for 5 h and after this time the reactor was put in the oil bath for 18 h at 70 °C. After cooling the reaction to room temperature, a small amount of polymer precipitated from the solution. SEC results: $M_n = 38$ kDa, PDI = 1.17. The tracking tube was prepared using with the same order of addition as for slides but with following amounts of reagents: SPMA (0.107 g, 0.434 mmol), EG (3 mL), METAC (0.09 g, 0.435 mmol), DMF (6 mL), n-BMA (1.245 mL \approx 1.11 g, 7.83 mmol), 805 μ L solution of CPAD in DMF (10 mg/mL, 0.029 mmol) and 95 μ L solution of AIBN in DMF (10 mg/mL, 0.0058 mmol). Polymer solutions were dialysed once in mixture of MeOH and THF (1:1) and then twice in MeOH and DCM (1:1). SEC results: $M_n = 36$ kDa, PDI = 1.18.

Appendix H. Polymer brush solution composition determination by ^1H NMR

Figures H.1-H.5 present the ^1H NMR spectra of polymer solutions remaining after polymer brush synthesis. The copolymer compositions were determined in a similar manner as presented in Appendix B. The calculated amounts are given in Table 3.1.

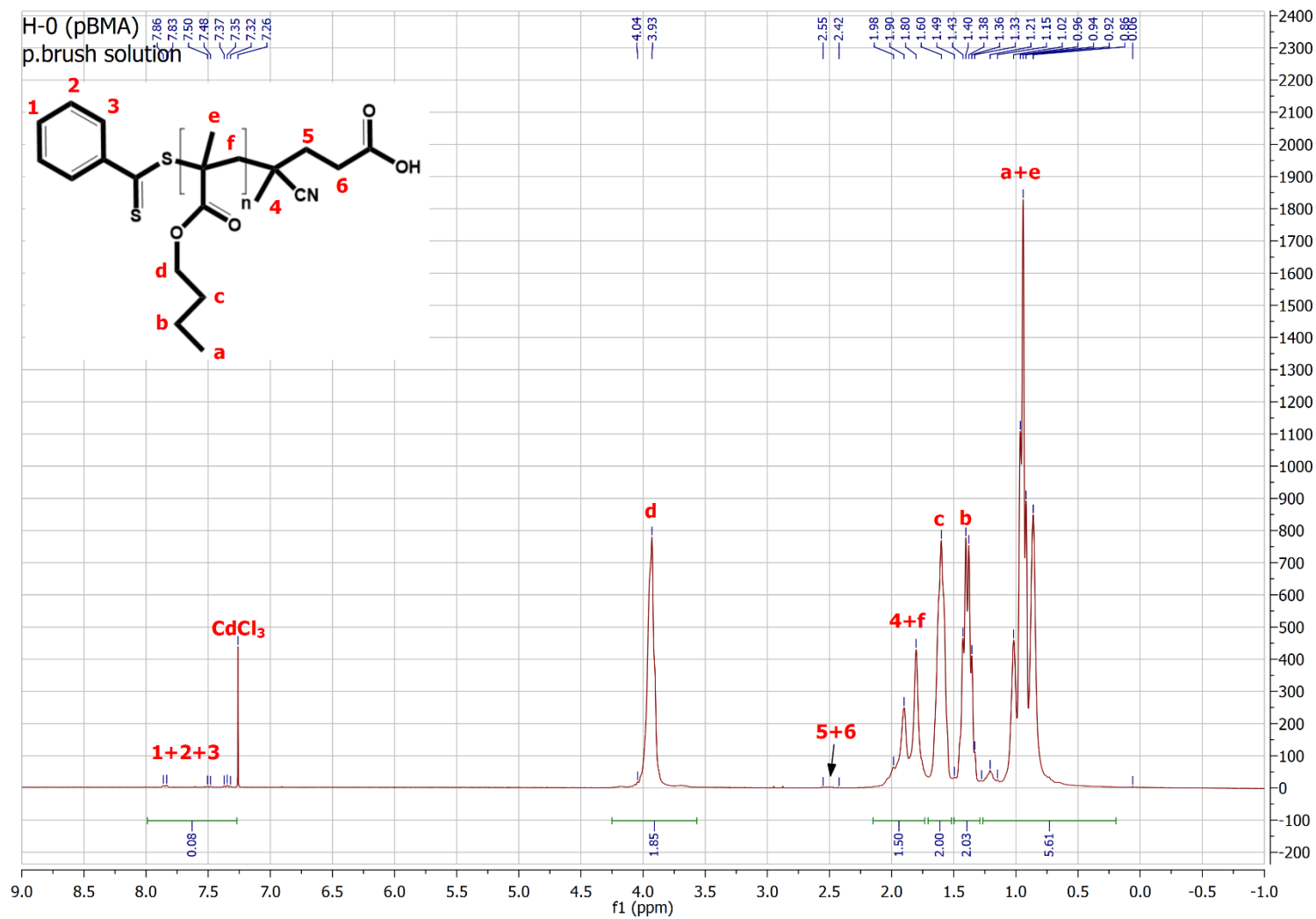


Figure H.1 ¹H NMR spectrum of H-0 polymer brush solution (pBMA) in CdCl₃.

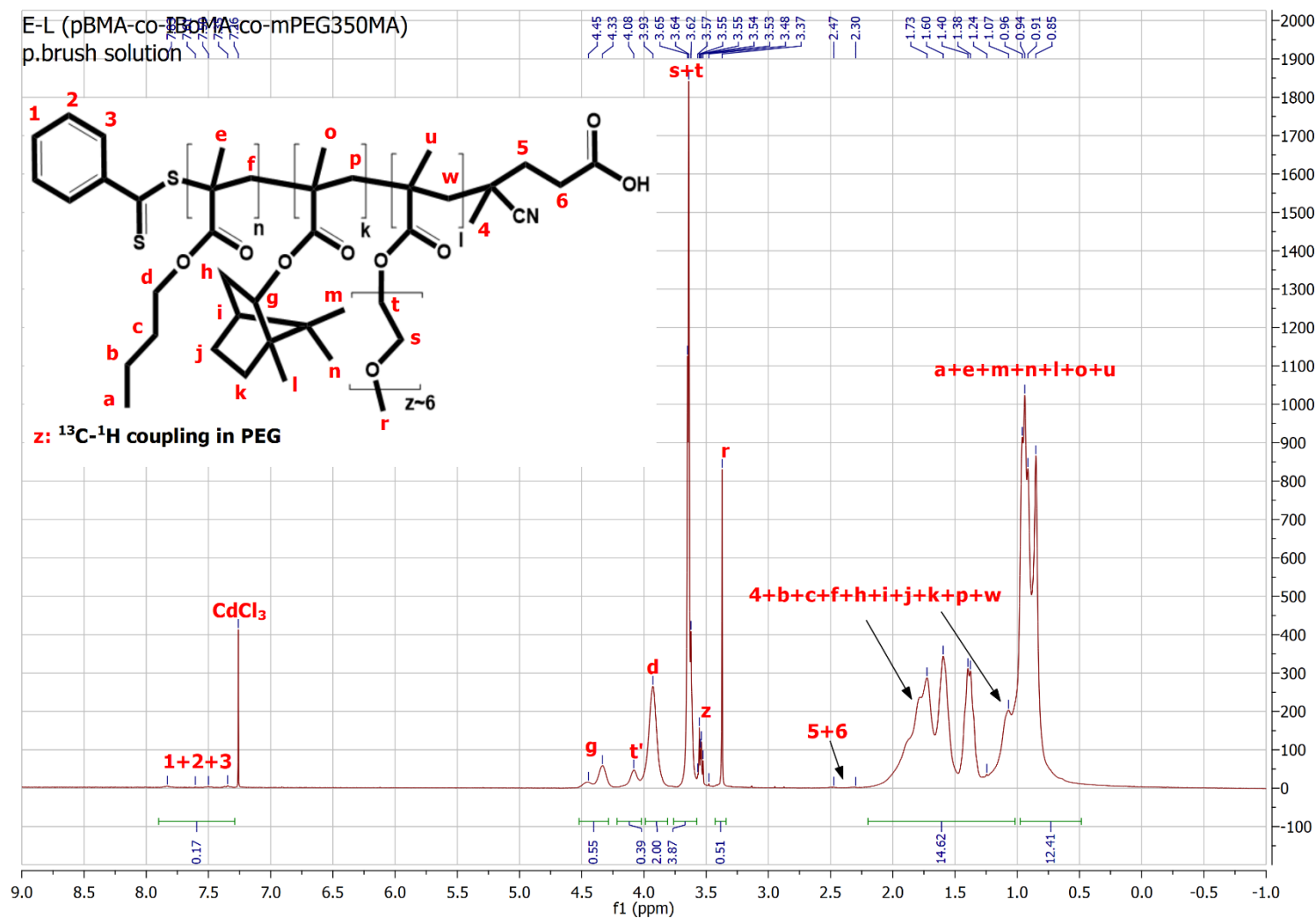


Figure H.2 ^1H NMR spectrum of E-L polymer brush solution (pBMA-co-IBoMA-co-mPEG350MA) in CdCl_3 .

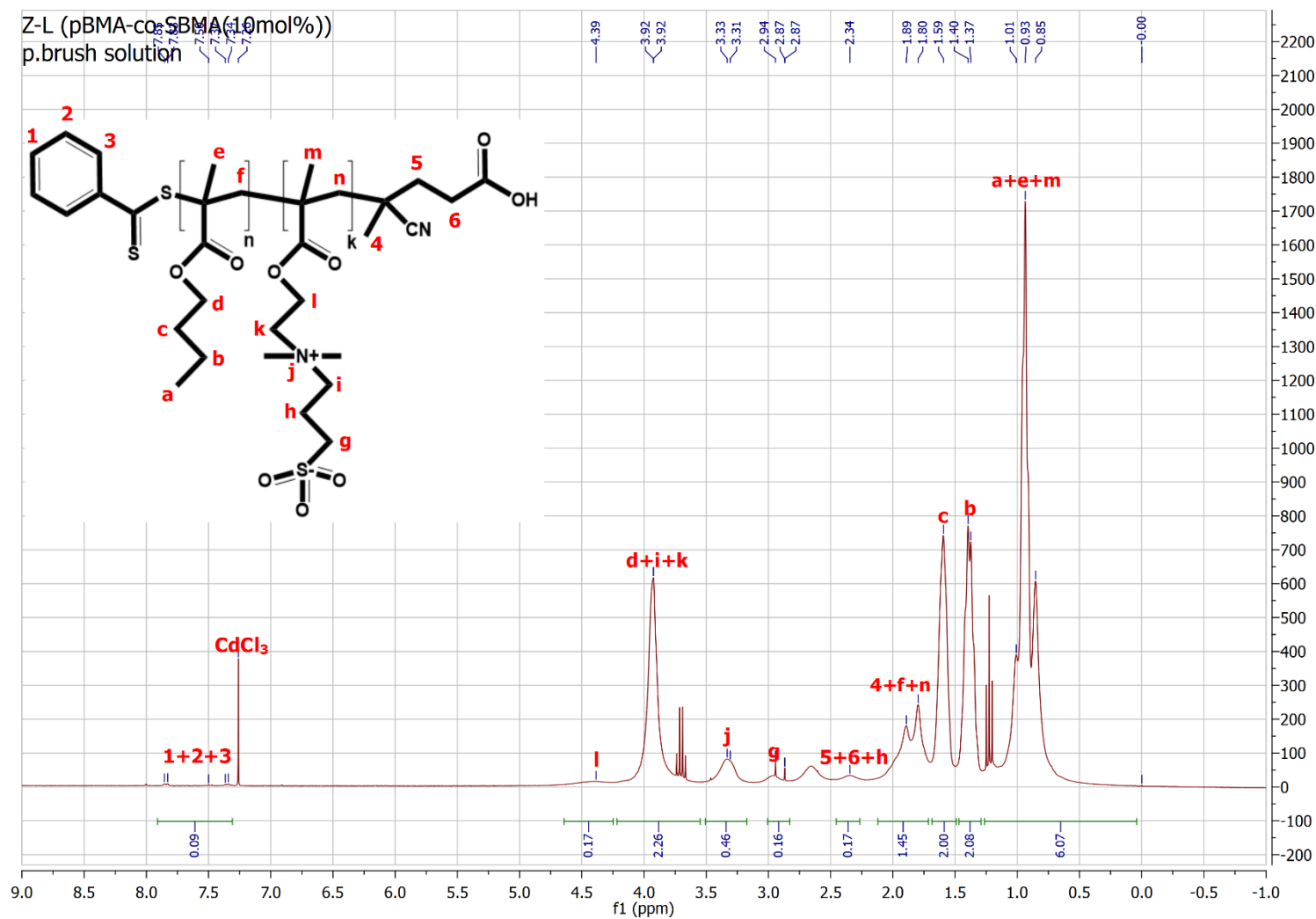


Figure H.3 ^1H NMR spectrum of Z-L polymer brush solution (pBMA-co-SBMA_{10\text{mol}\%}) in CdCl_3 .

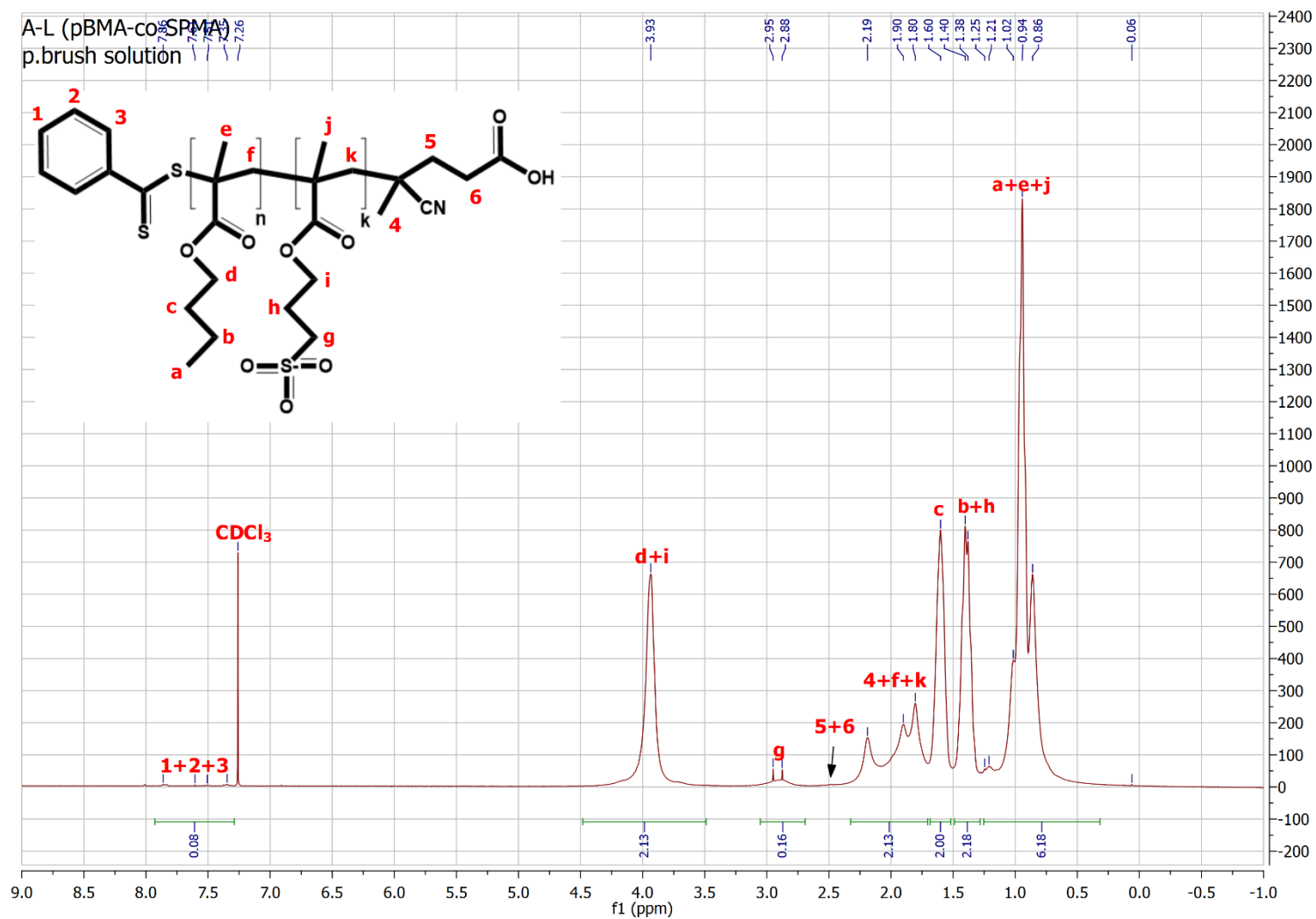


Figure H.4 ^1H NMR spectrum of A-L polymer brush solution (pBMA-co-SPMA) in CDCl_3 .

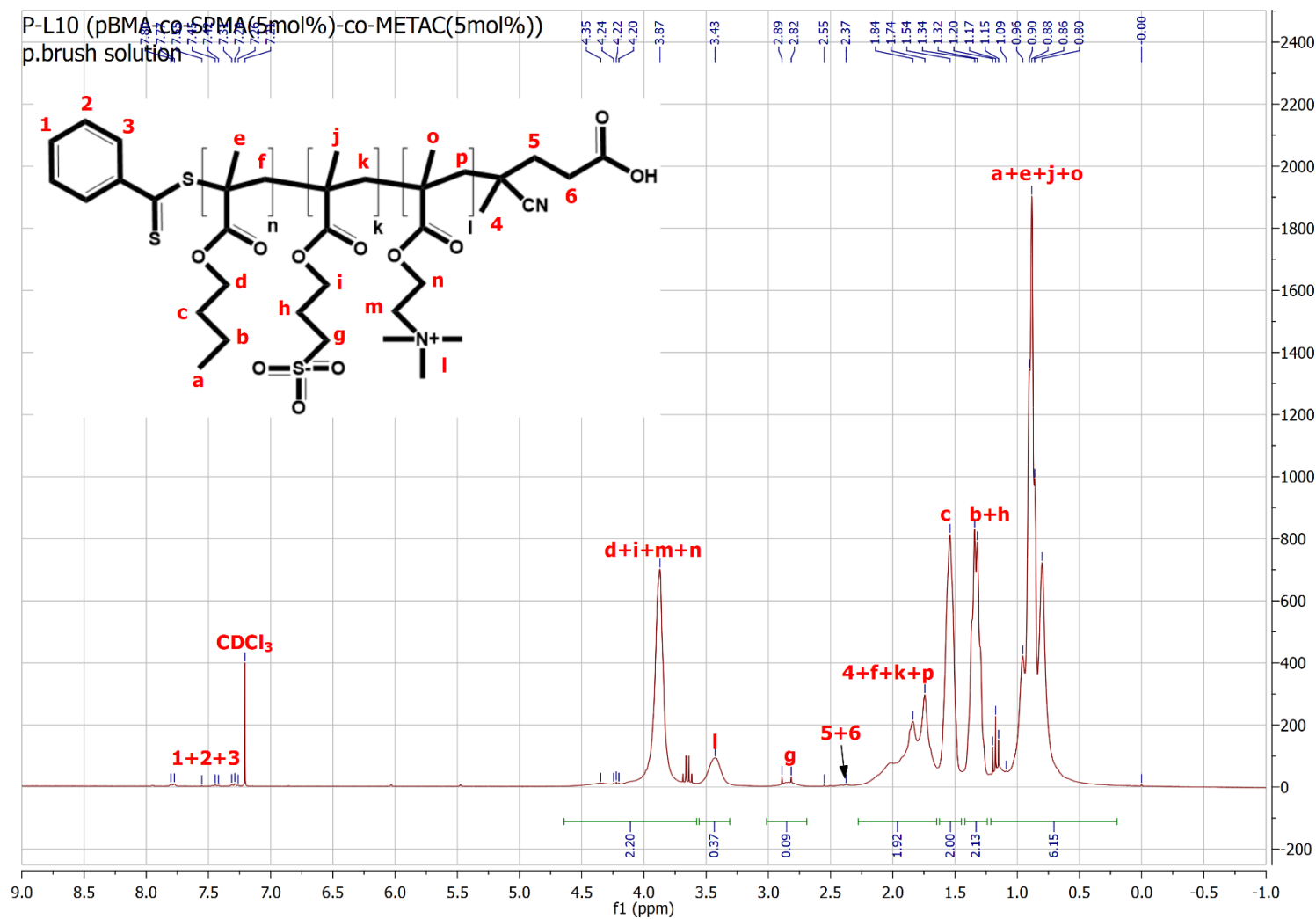


Figure H.5 ^1H NMR spectrum of P-L10 polymer brush solution (pBMA-co-SPMA_{5mol%}-co-METAC_{5mol%}) in CDCl_3 .

Appendix I. SEC traces of polymer brush solutions

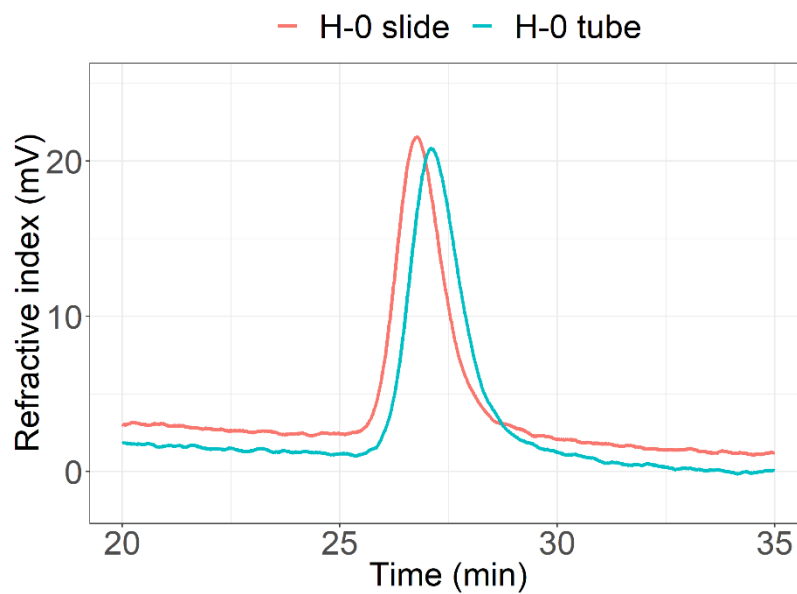


Figure I.1 SEC traces of H-0 polymer brush solutions. Refractive index (mV) vs Time (min).

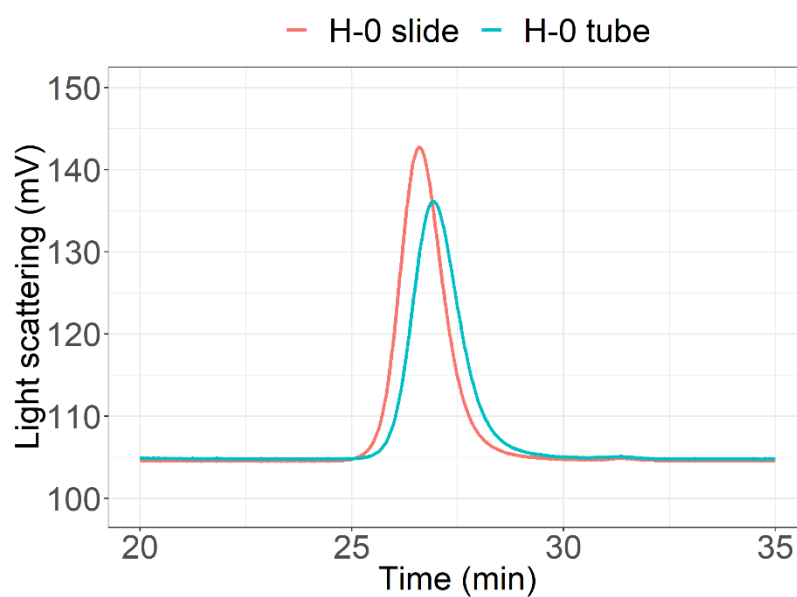


Figure I.2 SEC traces of H-0 polymer brush solutions. Light scattering (mV) vs Time (min).

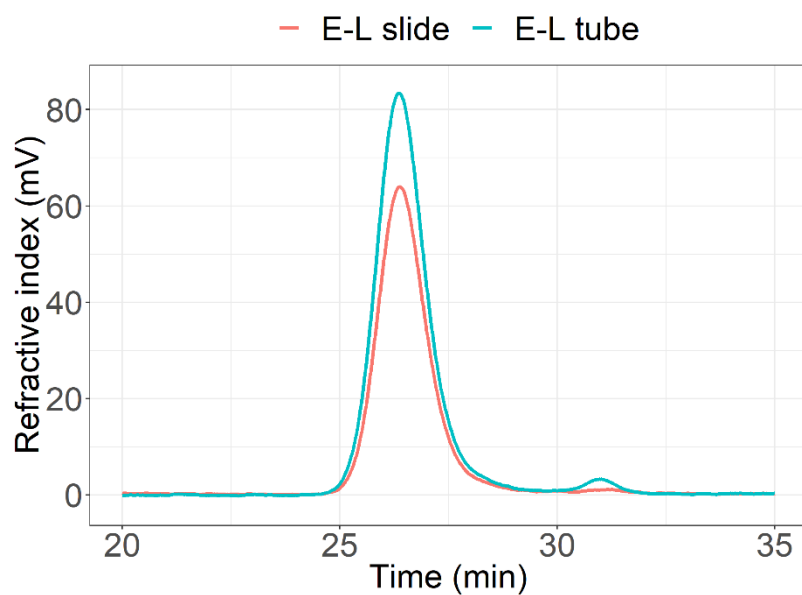


Figure I.3 SEC traces of E-L polymer brush solutions. Refractive index (mV) vs Time (min).

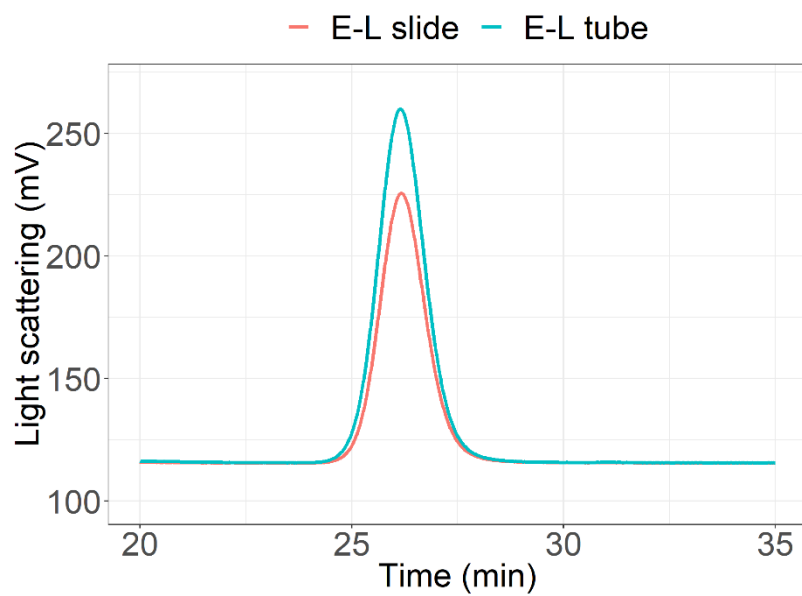


Figure I.4 SEC traces of E-L polymer brush solutions. Light scattering (mV) vs Time (min).

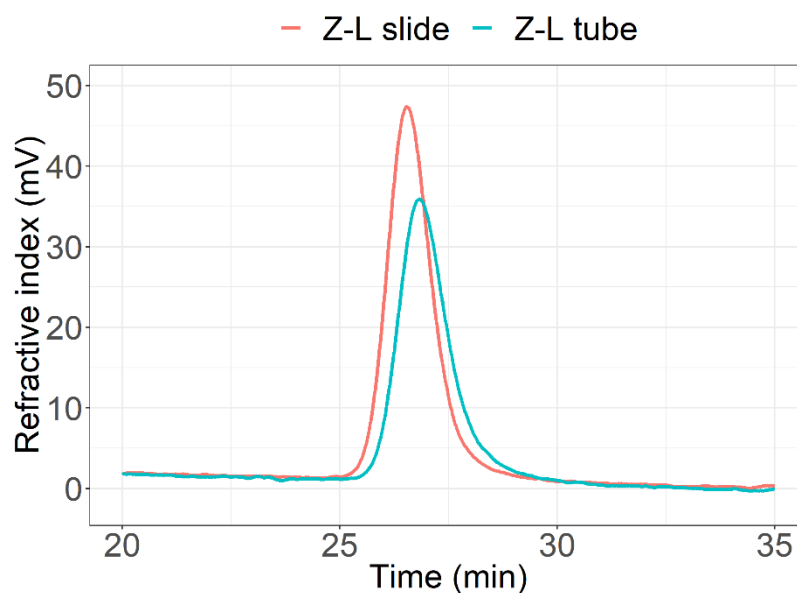


Figure I.5 SEC traces of Z-L polymer brush solutions. Refractive index (mV) vs Time (min).

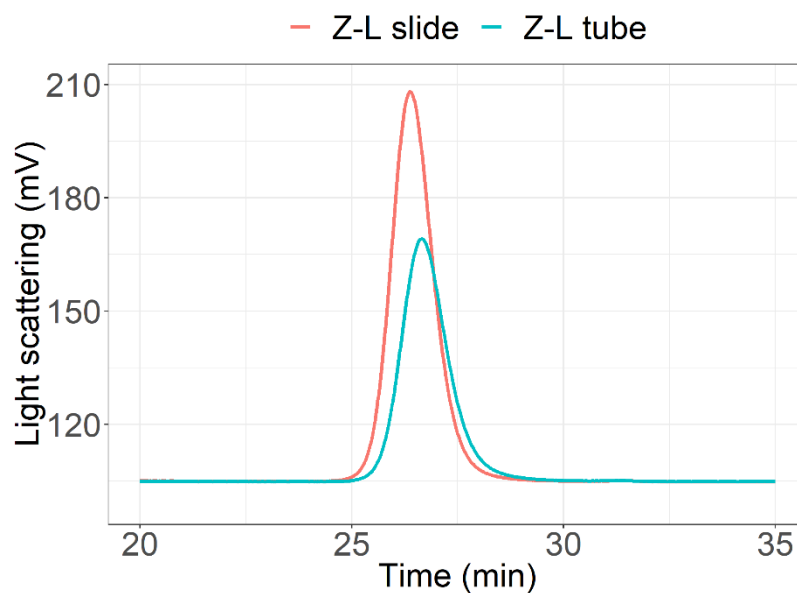


Figure I.6 SEC traces of Z-L polymer brush solutions. Light scattering (mV) vs Time (min).

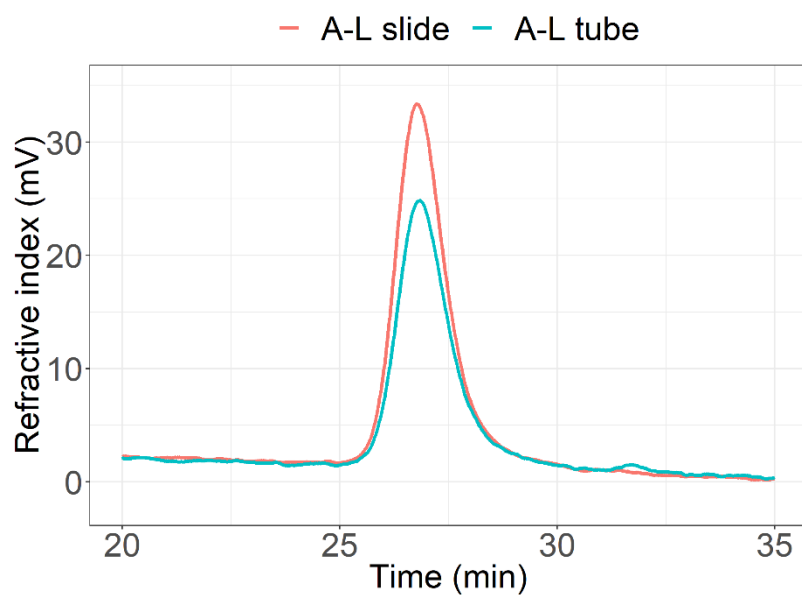


Figure I.7 SEC traces of A-L polymer brush solutions. Refractive index (mV) vs Time (min).

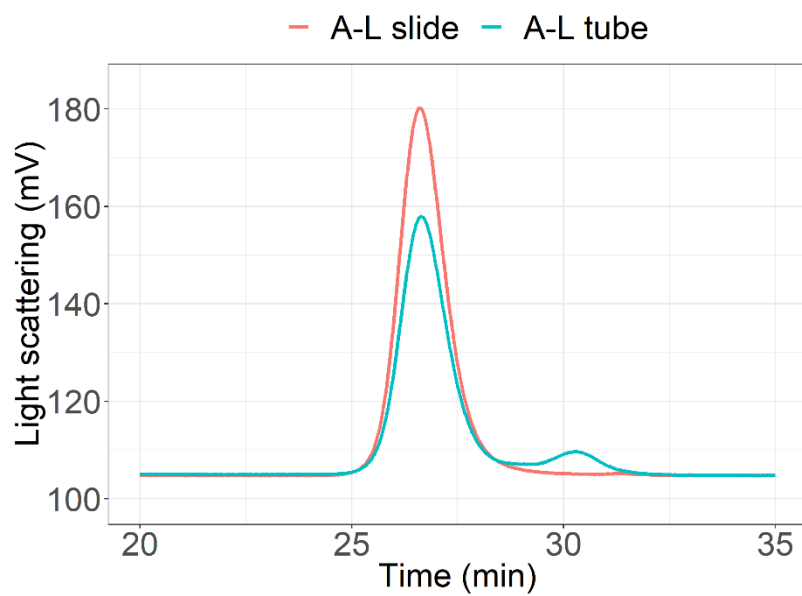


Figure I.8 SEC traces of A-L polymer brush solutions. Light scattering (mV) vs Time (min).

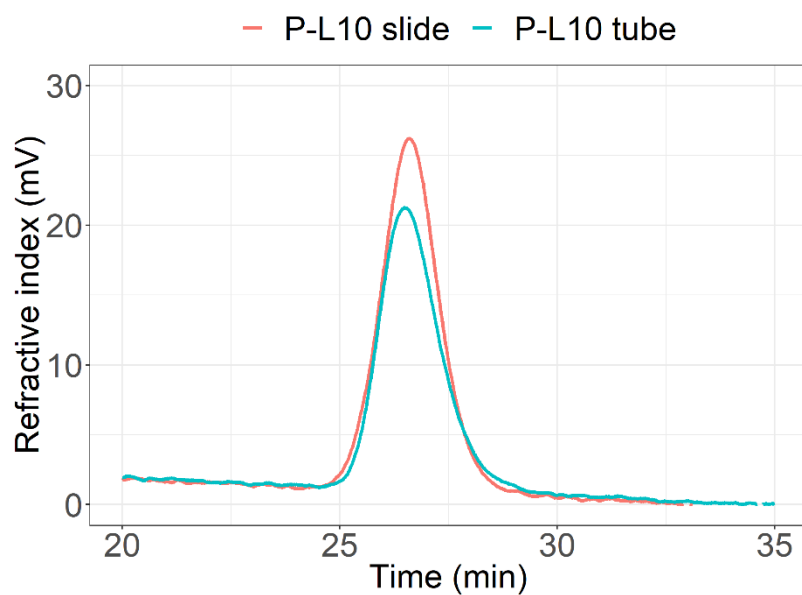


Figure I.9 SEC traces of P-L10 polymer brush solutions. Refractive index (mV) vs Time (min).

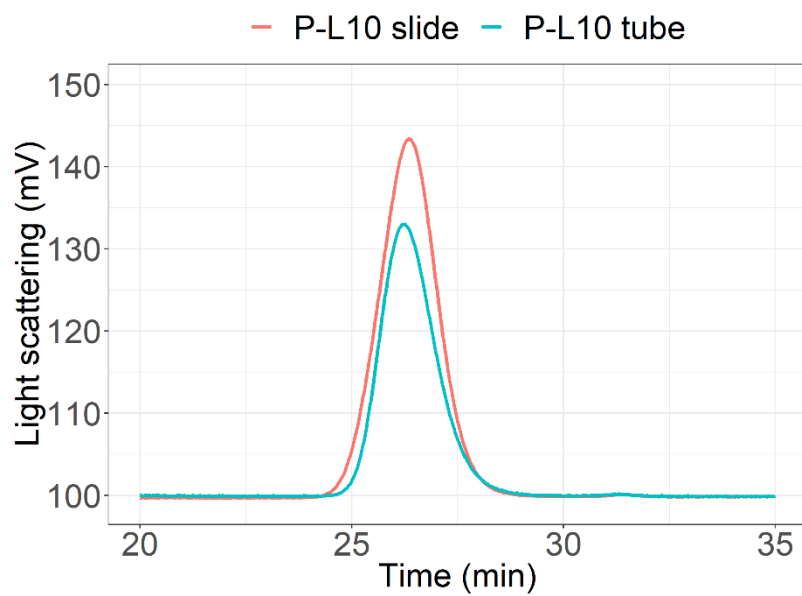


Figure I.10 SEC traces of P-L10 polymer brush solutions. Light scattering (mV) vs Time (min).

Appendix J. Comparison of settlement of barnacle cypris larvae on bulk polymers and polymer brushes

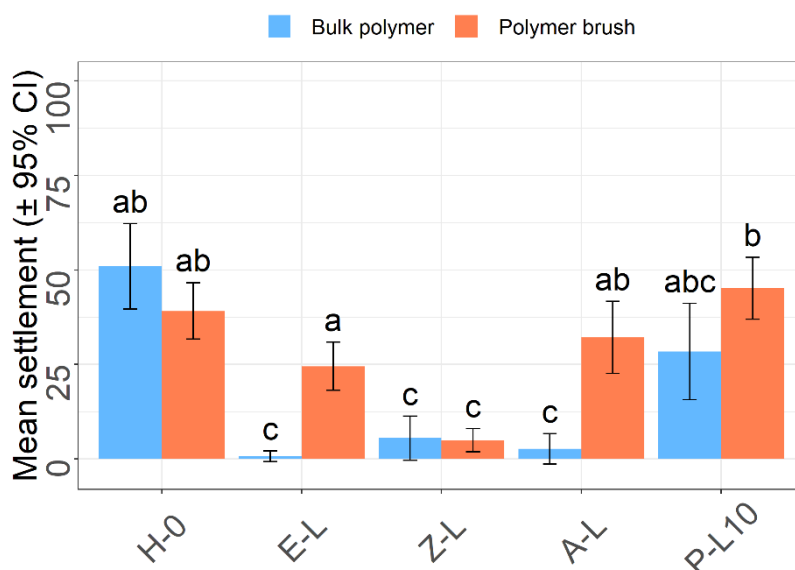


Figure J.1 Mean percent settlement of three-day-old *B. improvisus* cyprids on bulk polymers and polymer brushes after 24 h. Error bars are 95% CIs. The difference in settlement was statistically significant (Welch ANOVA $F_{9,60} = 22.54$, $p \leq 0.001$ with Games-Howell tests). Letters represent pairwise comparisons and bars that do not share a letter are significantly different.

Appendix K. Long-term tracking experiments

Figures K.1-K.5 present the actual tracks and number of body movements for walking and inspection behaviours of two individual cyprids tracked on each surface in two separate experiments. The track trajectories depict cyprid position in the tube only during surface exploration, with other behaviours such as swimming and resting ignored by the classification system. The tracking movement plots are coloured red and blue and represent inspection and walking behaviours with additional letters corresponding to the position of the cyprid in the tracking tube.

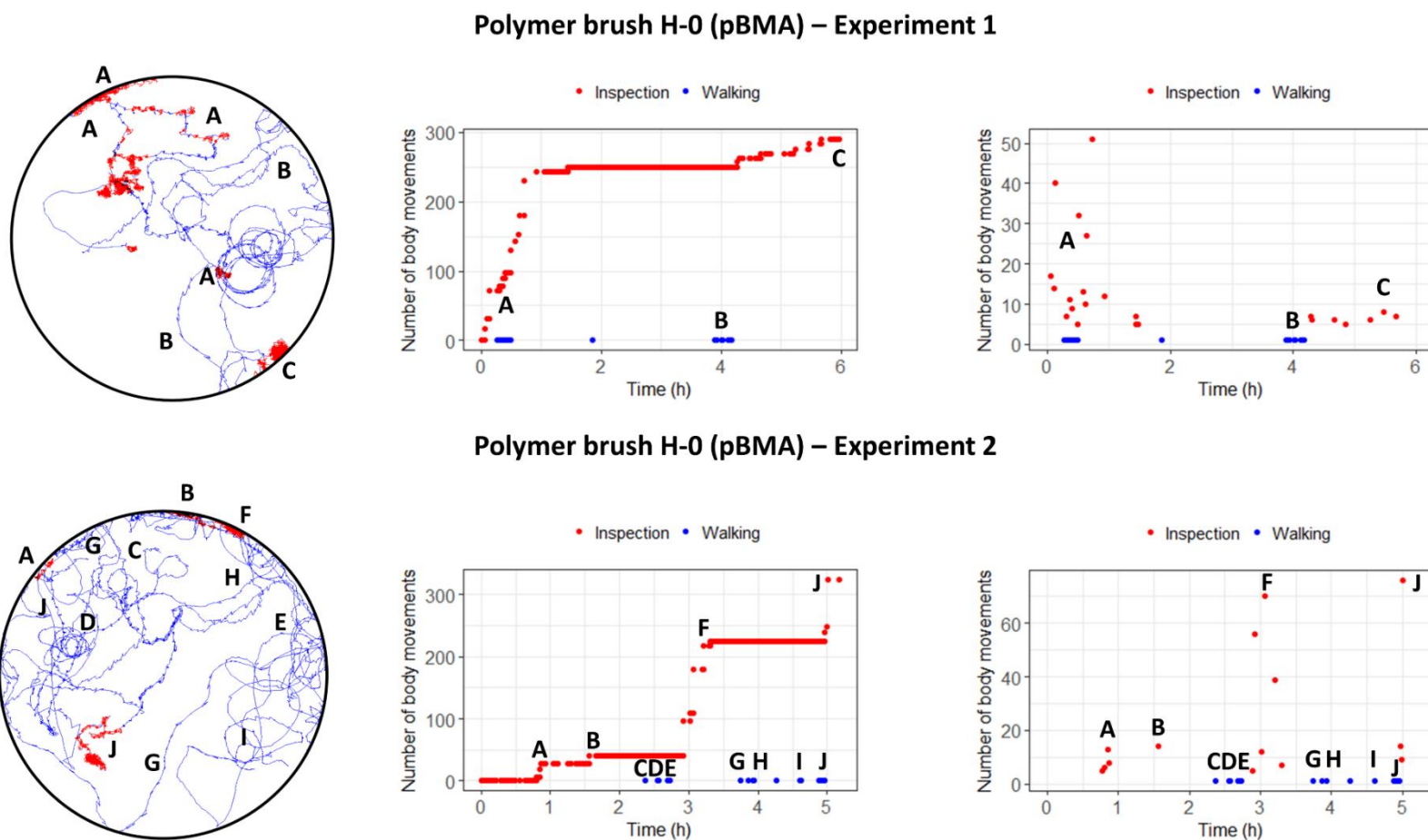
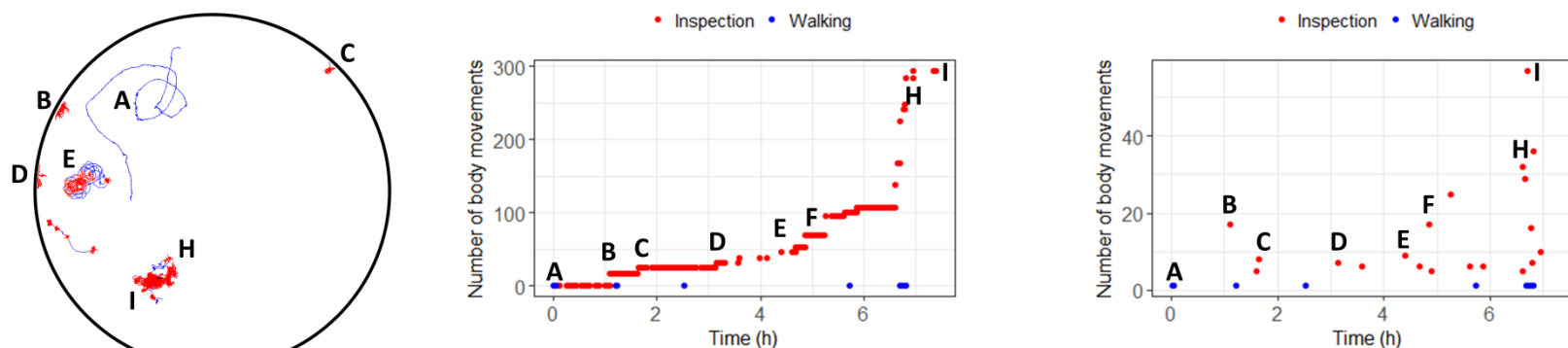


Figure K.1 Independent tracks of cyprid walking (blue) and inspection (red) behaviours in the polymer brush H-0 tracking tube. The cumulative inspection movements and walking stretches vs time are presented alongside, with letters corresponding to the cyprid trajectory in the tube.

Polymer brush E-L (pBMA-co-IBoMA-co-mPEG350MA) – Experiment 1



Polymer brush E-L (pBMA-co-IBoMA-co-mPEG350MA) – Experiment 2

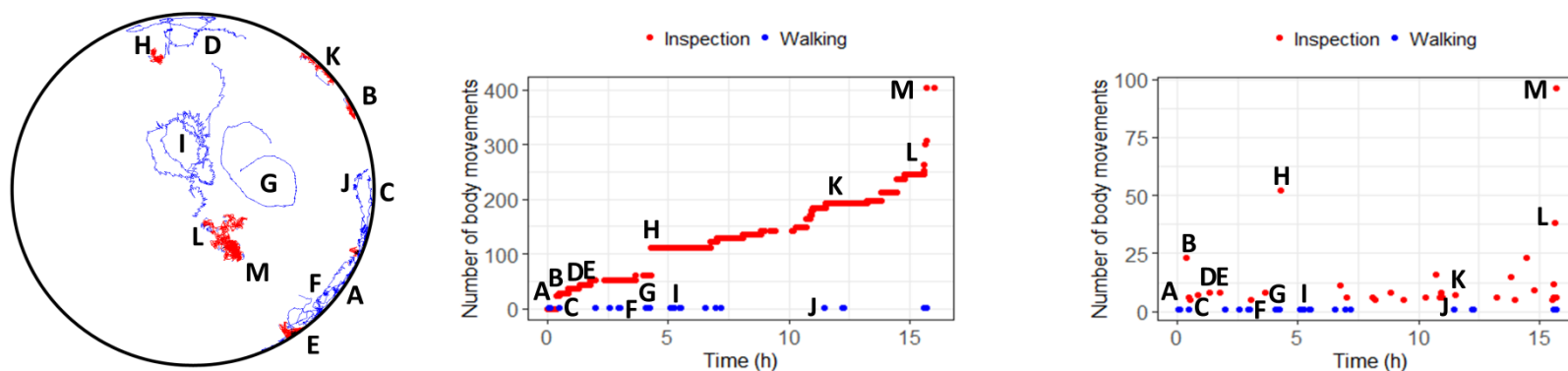


Figure K.2 Independent tracks of cyprid walking (blue) and inspection (red) behaviours in the polymer brush E-L tracking tube. The cumulative inspection movements and walking stretches vs time are presented alongside, with letters corresponding to the cyprid trajectory in the tube.

Polymer brush Z-L (pBMA-co-SBMA_{10mol%}) – Experiment 1



Polymer brush Z-L (pBMA-co-SBMA_{10mol%}) – Experiment 2

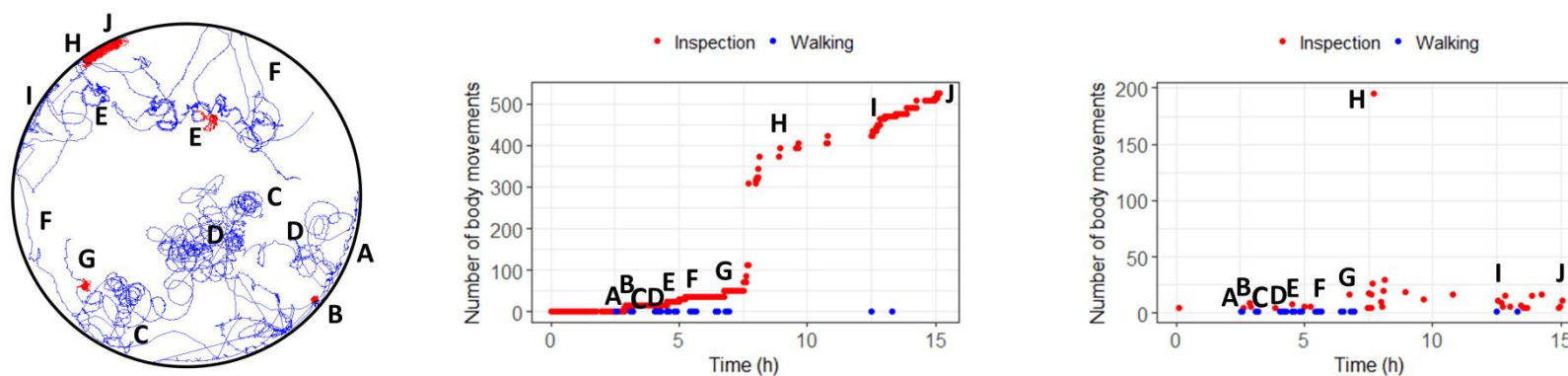


Figure K.3 Independent tracks of cyprid walking (blue) and inspection (red) behaviours in the polymer brush Z-L tracking tube. The cumulative inspection movements and walking stretches vs time are presented alongside, with letters corresponding to the cyprid trajectory in the tube.

Polymer brush A-L (pBMA-co-SPMA) – Experiment 1



Polymer brush A-L (pBMA-co-SPMA) – Experiment 2

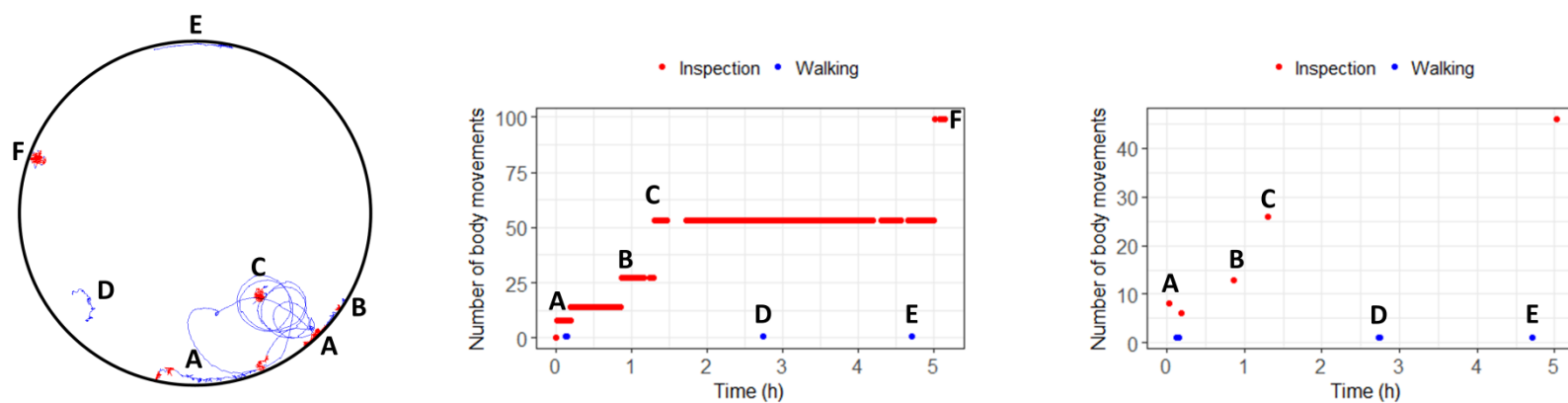
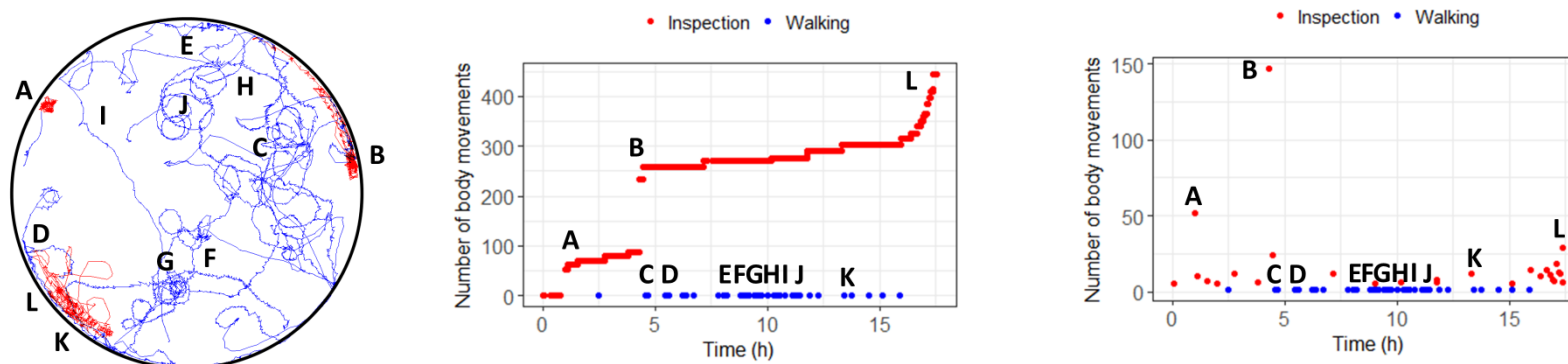


Figure K.4 Independent tracks of cyprid walking (blue) and inspection (red) behaviours in the polymer brush A-L tracking tube. The cumulative inspection movements and walking stretches vs time are presented alongside, with letters corresponding to the cyprid trajectory in the tube.

Polymer brush P-L10 (pBMA-*co*-SPMA_{5mol%}-*co*-METAC_{5mol%}) – Experiment 1



Polymer brush P-L10 (pBMA-*co*-SPMA_{5mol%}-*co*-METAC_{5mol%}) – Experiment 2

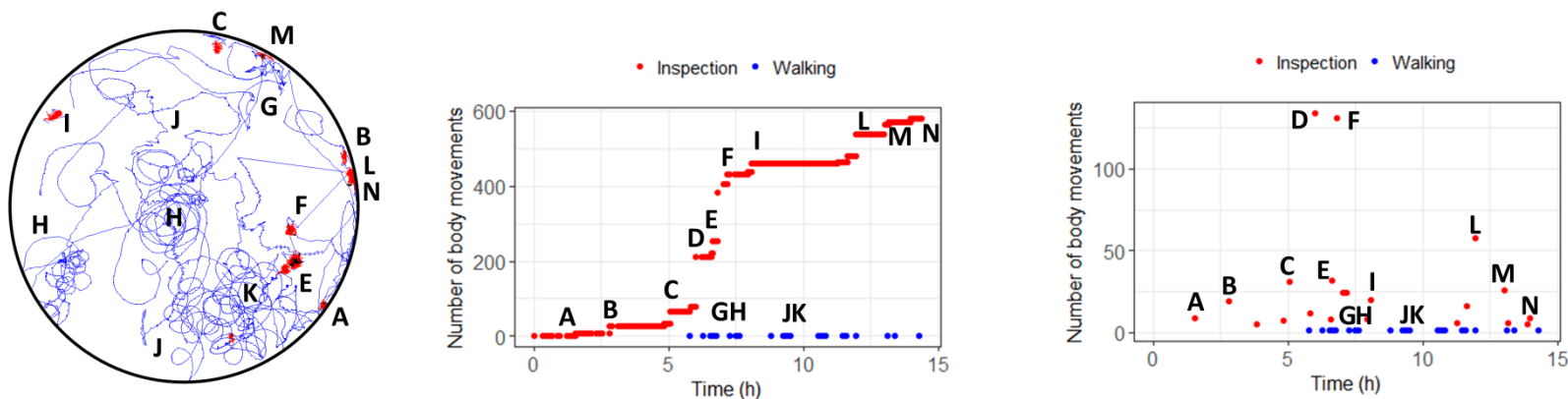


Figure K.5 Independent tracks of cyprid walking (blue) and inspection (red) behaviours in the polymer brush P-L10 tracking tube. The cumulative inspection movements and walking stretches vs time are presented alongside, with letters corresponding to the cyprid trajectory in the tube

References

- Aldred, N., Alsaab, A. and Clare, A.S. (2018) 'Quantitative analysis of the complete larval settlement process confirms Crisp's model of surface selectivity by barnacles', *Proceedings of the Royal Society B: Biological Sciences*, 285(1872).
- Aldred, N. and Clare, A.S. (2008) 'The adhesive strategies of cyprids and development of barnacle-resistant marine coatings', *Biofouling*, 24(5), pp. 351-363.
- Aldred, N. and Clare, A.S. (2014) 'Mini-review: Impact and dynamics of surface fouling by solitary and compound ascidians', *Biofouling*, 30(3), pp. 259-270.
- Aldred, N., Ekblad, T., Andersson, O., Liedberg, B. and Clare, A.S. (2011) 'Real-time quantification of microscale bioadhesion events in situ using imaging surface plasmon resonance (iSPR)', *ACS Applied Materials & Interfaces*, 3(6), pp. 2085-2091.
- Aldred, N., Gatley-Montross, C.M., Lang, M., Detty, M.R. and Clare, A.S. (2019) 'Correlative assays of barnacle cyprid behaviour for the laboratory evaluation of antifouling coatings: a study of surface energy components', *Biofouling*, 35(2), pp. 159-172.
- Aldred, N., Høeg, J.T., Maruzzo, D. and Clare, A.S. (2013) 'Analysis of the behaviours mediating barnacle cyprid reversible adhesion', *PLoS ONE*, 8(7), e68085.
- Aldred, N., Li, G., Gao, Y., Clare, A.S. and Jiang, S. (2010a) 'Modulation of barnacle (*Balanus amphitrite* Darwin) cyprid settlement behavior by sulfobetaine and carboxybetaine methacrylate polymer coatings', *Biofouling*, 26(6), pp. 673-683.
- Aldred, N., Scardino, A., Cavaco, A., de Nys, R. and Clare, A.S. (2010b) 'Attachment strength is a key factor in the selection of surfaces by barnacle cyprids (*Balanus amphitrite*) during settlement', *Biofouling*, 26(3), pp. 287-299.
- Almeida, E., Diamantino, T.C. and de Sousa, O. (2007) 'Marine paints: The particular case of antifouling paints', *Progress in Organic Coatings*, 59(1), pp. 2-20.
- Alsaab, A., Aldred, N. and Clare, A.S. (2017) 'Automated tracking and classification of the settlement behaviour of barnacle cyprids', *Journal of The Royal Society Interface*, 14(128).
- Alzieu, C. (1991) 'Environmental problems caused by TBT in France: Assessment, regulations, prospects', *Marine Environmental Research*, 32(1-4), pp. 7-17.

Alzieu, C., Sanjuan, J., Michel, P., Borel, M. and Dreno, J.P. (1989) 'Monitoring and Assessment of Butyltins in Atlantic Coastal Waters', *Marine Pollution Bulletin*, 20(1), pp. 22-26.

Anderson, C., Atlar, M., Callow, M.E., Candries, M., Milne, A. and Townsin, R.L. (2003) 'The development of foul-release coatings for seagoing vessels', *Journal of Marine Design and Operations*, 84, pp. 11-23.

Anderson, D.T. (1993) *Barnacles: structure, function, development and evolution*. London: Chapman & Hall.

Andersson, O., Ekblad, T., Aldred, N., Clare, A.S. and Liedberg, B. (2009) 'Novel application of imaging surface plasmon resonance for in situ studies of the surface exploration of marine organisms', *Biointerphases*, 4(4), pp. 65-68.

Andrade, J.D. (1973) 'Interfacial phenomena and biomaterials.', *Med. Instrum.*, 7(2), pp. 110-120.

Atlar, M. (2011) 'Recent upgrading of marine testing facilities at Newcastle University' *Proceedings of the Second International Conference on Advanced Model Measurement Technology for the EU Maritime Industry (AMT'11)*. Newcastle University, United Kingdom, April 4-6, 2011. Newcastle upon Tyne: School of Marine Science and Technology.

Azzaroni, O., Brown, A.A. and Huck, W.T.S. (2007) 'Tunable wettability by clicking counterions into polyelectrolyte brushes', *Advanced Materials*, 19(1), pp. 151-154.

Bauer, S., Alles, M., Arpa-Sancet, M.P., Ralston, E., Swain, G.W., Aldred, N., Clare, A.S., Finlay, J.A., Callow, M.E., Callow, J.A. and Rosenhahn, A. (2016a) 'Resistance of amphiphilic polysaccharides against marine fouling organisms', *Biomacromolecules*, 17(3), pp. 897-904.

Bauer, S., Arpa-Sancet, M.P., Finlay, J.A., Callow, M.E., Callow, J.A. and Rosenhahn, A. (2013) 'Adhesion of marine fouling organisms on hydrophilic and amphiphilic polysaccharides', *Langmuir*, 29(12), pp. 4039-4047.

Bauer, S., Finlay, J.A., Thomé, I., Nolte, K., Franco, S.C., Ralston, E., Swain, G.E., Clare, A.S. and Rosenhahn, A. (2016b) 'Attachment of algal cells to zwitterionic self-assembled monolayers comprised of different anionic compounds', *Langmuir*, 32(22), pp. 5663-5671.

Benschop, H.O.G., Guerin, A.J., Brinkmann, A., Dale, M.L., Finnie, A.A., Breugem, W.P., Clare, A.S., Stübing, D., Price, C. and Reynolds, K.J. (2018) 'Drag-reducing riblets with fouling-release properties: development and testing', *Biofouling*, 34(5), pp. 532-544.

Berendsen, A.M. (1989) *Marine Painting Manual*. Dordrecht: Springer-Science+Business Media, B.V.

Bodas, D. and Khan-Malek, C. (2007) 'Hydrophilization and hydrophobic recovery of PDMS by oxygen plasma and chemical treatment—An SEM investigation', *Sensors and Actuators B: Chemical*, 123(1), pp. 368-373.

Brady, R.F. (2000) 'Clean hulls without poisons: devising and testing nontoxic marine coatings', *Journal of Coatings Technology*, 72(900), pp. 45-56.

Brady, R.F. (2005) 'Fouling-release coatings for warships', *Defence Science Journal*, 55(1), p. 75-81.

Brancato, M.S. (1999) 'Riding the crest into the 21st century', *OCEANS'99 MTS/IEEE*, p. 676.

Bressy, C., Margailan, A., Fay, A., Linossier, I. and Rehel, K. (2009) 'Tin-free self-polishing marine antifouling coatings', in Hellio, C. and Yebra, D. (eds.) *Advances in Marine Antifouling Coatings and Technologies*. Cambridge: Woodhead Publishing, pp. 445-491.

Bretscher, M.S. and Raff, M.C. (1975) 'Mammalian plasma membranes', *Nature*, 258(5530), pp. 43-49.

Callow, J.A. and Callow, M.E. (2011) 'Trends in the development of environmentally friendly fouling-resistant marine coatings', *Nature Communications*, 2, p. 244-254.

Callow, M.E., Callow, J.A., Conlan, S.L., Clare, A.S. and Stafslie, S. (2014) 'Chapter 10, Efficacy testing of nonbiocidal and fouling-release coatings', in Dobretsov, S., Thomason, J. and Williams, D.N. (eds.) *Biofouling methods*. Chichester: Wiley Blackwell, pp. 291-316.

Callow, M.E., Callow, J.A., Ista, L.K., Coleman, S.E., Nolasco, A.C. and López, G.P. (2000) 'Use of self-assembled monolayers of different wettabilities to study surface selection and primary adhesion processes of green algal (*Enteromorpha*) zoospores', *Applied and Environmental Microbiology*, 66(8), pp. 3249-3254.

Callow, M.E., Callow, J.A., Pickett-Heaps, J.D. and Wetherbee, R. (1997) 'Primary adhesion of *Enteromorpha* (Chlorophyta, Ulvales) propagules: quantitative settlement studies and video microscopy', *Journal of Phycology*, 33(6), pp. 938-947.

Catli, C. (2016) *Novel synthetic approaches for fabrication of polymer brushes on gold surfaces via RAFT polymerization: a new era for gold modification*, PhD thesis, Georg-August-

Universität Göttingen, viewed 14 June 2018, <http://hdl.handle.net/11858/00-1735-0000-002E-E353-2>.

Chan, F.T., MacIsaac, H.J. and Bailey, S.A. (2015) 'Relative importance of vessel hull fouling and ballast water as transport vectors of nonindigenous species to the Canadian Arctic', *Canadian Journal of Fisheries and Aquatic Sciences*, 72(8), pp. 1230-1242.

Chen, S., Li, L., Zhao, C. and Zheng, J. (2010) 'Surface hydration: Principles and applications toward low-fouling/nonfouling biomaterials', *Polymer*, 51(23), pp. 5283-5293.

CIA (2005) *The World Factbook 2005*. Washington, DC: Central Intelligence Agency.

CIA (2010) *The World Factbook 2010*. Washington, DC: Central Intelligence Agency.

Clare, A., Thomas, R. and Rittschof, D. (1995) 'Evidence for the involvement of cyclic AMP in the pheromonal modulation of barnacle settlement', *The Journal of Experimental Biology*, 198(3), pp. 655-664.

Clare, A.S., Freet, R.K. and McClary, M. (1994) 'On the antennular secretion of the cyprid of *Balanus amphitrite amphitrite*, and its role as a settlement pheromone', *Journal of the Marine Biological Association of the United Kingdom*, 74(1), pp. 243-250.

Clare, A.S. and Matsumura, K. (2000) 'Nature and perception of barnacle settlement pheromones', *Biofouling*, 15(1-3), pp. 57-71.

Clare, A.S., Rittschof, D., Gerhart, D.J. and Maki, J.S. (1992) 'Molecular approaches to nontoxic antifouling', *Invertebrate Reproduction & Development*, 22(1-3), pp. 67-76.

Crisp, D.J. (1976) 'Settlement responses in marine organisms', in Newell, R.C. (ed.) *Adaptation to Environment: Essays on the Physiology of Marine Animals*. London: Butterworths, pp. 83-124.

Dai, L., StJohn, H.A.W., Bi, J., Zientek, P., Chatelier, R.C. and Griesser, H.J. (2000) 'Biomedical coatings by the covalent immobilization of polysaccharides onto gas-plasma-activated polymer surfaces', *Surface and Interface Analysis*, 29(1), pp. 46-55.

Davis, E.M. and Elabd, Y.A. (2013) 'Water clustering in glassy polymers', *The Journal of Physical Chemistry B*, 117(36), pp. 10629-10640.

De Vera, J.S., Venault, A., Chou, Y.-N., Tayo, L., Chiang, H.-C., Aimar, P. and Chang, Y. (2018) 'Self-cleaning interfaces of polydimethylsiloxane grafted with pH-responsive zwitterionic copolymers', *Langmuir*, 35(5), pp. 1357-1368.

Desai, D.V., Anil, A.C. and Venkat, K. (2006) 'Reproduction in *Balanus amphitrite* Darwin (Cirripedia: Thoracica): influence of temperature and food concentration', *Marine Biology*, 149(6), pp. 1431-1441.

Di Fino, A., Petrone, L., Aldred, N., Ederth, T., Liedberg, B. and Clare, A.S. (2014) 'Correlation between surface chemistry and settlement behaviour in barnacle cyprids (*Balanus improvisus*)', *Biofouling*, 30(2), pp. 143-152.

Dreanno, C., Kirby, R.R. and Clare, A.S. (2006) 'Smelly feet are not always a bad thing: the relationship between cyprid footprint protein and the barnacle settlement pheromone', *Biology Letters*, 2(3), pp. 423-425.

Drelich, J. and Chibowski, E. (2010) 'Superhydrophilic and superwetting surfaces: definition and mechanisms of control', *Langmuir*, 26(24), pp. 18621-18623.

Duwez, A.-S., Guillet, P., Colard, C., Gohy, J.-F. and Fustin, C.-A. (2006) 'Dithioesters and trithiocarbonates as anchoring groups for the “grafting-to” approach', *Macromolecules*, 39(8), pp. 2729-2731.

Ederth, T. and Ekblad, T. (2018) 'Swelling of thin poly(ethylene glycol)-containing hydrogel films in water vapor—a neutron reflectivity study', *Langmuir*, 34(19), pp. 5517-5526.

Ederth, T., Lerm, M., Orihuela, B. and Rittschof, D. (2019) 'Resistance of zwitterionic peptide monolayers to biofouling', *Langmuir*, 35(5), pp. 1818-1827.

Ekblad, T., Bergström, G., Ederth, T., Conlan, S.L., Mutton, R., Clare, A.S., Wang, S., Liu, Y., Zhao, Q., D'Souza, F., Donnelly, G.T., Willemsen, P.R., Pettitt, M.E., Callow, M.E., Callow, J.A. and Liedberg, B. (2008) 'Poly(ethylene glycol)-containing hydrogel surfaces for antifouling applications in marine and freshwater environments', *Biomacromolecules*, 9(10), pp. 2775-2783.

Estephan, Z.G., Schlenoff, P.S. and Schlenoff, J.B. (2011) 'Zwitteration as an alternative to PEGylation', *Langmuir*, 27(11), pp. 6794-6800.

Evans, S.M., Leksono, T. and McKinnell, P.D. (1995) 'Tributyltin pollution: A diminishing problem following legislation limiting the use of TBT-based anti-fouling paints', *Marine Pollution Bulletin*, 30(1), pp. 14-21.

Farrar, D. (2008) '9 - Modelling of the degradation process for bioresorbable polymers', in Buchanan, F. (ed.) *Degradation Rate of Bioresorbable Materials*. Cambridge England: Woodhead Publishing, pp. 183-206.

Finlay, J.A., Bennett, S.M., Brewer, L.H., Sokolova, A., Clay, G., Gunari, N., Meyer, A.E., Walker, G.C., Wendt, D.E., Callow, M.E., Callow, J.A. and Detty, M.R. (2010) 'Barnacle settlement and the adhesion of protein and diatom microfouling to xerogel films with varying surface energy and water wettability', *Biofouling*, 26(6), pp. 657-666.

Finlay, J.A., Callow, M.E., Ista, L.K., Lopez, G.P. and Callow, J.A. (2002) 'The influence of surface wettability on the adhesion strength of settled spores of the green alga *Enteromorpha* and the diatom *Amphora*', *Integrative and Comparative Biology*, 42(6), pp. 1116-1122.

Finlay, J.A., Fletcher, B.R., Callow, M.E. and Callow, J.A. (2008a) 'Effect of background colour on growth and adhesion strength of *Ulva* sporelings', *Biofouling*, 24(3), pp. 219-225.

Finlay, J.A., Krishnan, S., Callow, M.E., Callow, J.A., Dong, R., Asgill, N., Wong, K., Kramer, E.J. and Ober, C.K. (2008b) 'Settlement of *Ulva* zoospores on patterned fluorinated and PEGylated monolayer surfaces', *Langmuir*, 24(2), pp. 503-510.

Finlay, J.A., Schultz, M.P., Cone, G., Callow, M.E. and Callow, J.A. (2013) 'A novel biofilm channel for evaluating the adhesion of diatoms to non-biocidal coatings', *Biofouling*, 29(4), pp. 401-411.

Fowkes, F.M. (1964) 'Attractive forces at interfaces', *Industrial & Engineering Chemistry*, 56(12), pp. 40-52.

Geise, G.M., Paul, D.R. and Freeman, B.D. (2014) 'Fundamental water and salt transport properties of polymeric materials', *Progress in Polymer Science*, 39(1), pp. 1-42.

Gitlitz, M.H. (1981) 'Recent developments in marine antifouling coatings', *Journal of Coating Technology*, 53, pp. 46-52.

Goldberg, E.D. (1986) 'TBT: An environmental dilemma', *Environment: Science and Policy for Sustainable Development*, 28(8), pp. 17-44.

Göpferich, A. (1997) 'Polymer bulk erosion', *Macromolecules*, 30(9), pp. 2598-2604.

Grohens, Y., Ulvé, S., Vallée-Réhel, K., Péron, J.J. and Haras, D. (2003) 'Wettability of acrylate copolymer surfaces after ageing in water', *Macromolecular Symposia*, 203(1), pp. 271-276.

Gudipati, C.S., Finlay, J.A., Callow, J.A., Callow, M.E. and Wooley, K.L. (2005) 'The antifouling and fouling-release performance of hyperbranched fluoropolymer (HBFP)-poly(ethylene glycol) (PEG) composite coatings evaluated by adsorption of biomacromolecules and the green fouling alga *Ulva*', *Langmuir*, 21(7), pp. 3044-3053.

Guerin, A.J. and Clare, A.S. (2019) 'Mini-review: effect sizes and meta-analysis for antifouling research', *Biofouling*, 34(10), pp. 1185-1199.

Guo, S., Jańczewski, D., Zhu, X., Quintana, R., He, T. and Neoh, K.G. (2015) 'Surface charge control for zwitterionic polymer brushes: tailoring surface properties to antifouling applications', *Journal of Colloid and Interface Science*, 452, pp. 43-53.

Gurbuz, N., Demirci, S., Yavuz, S. and Caykara, T. (2011) 'Synthesis of cationic N-[3-(dimethylamino)propyl]methacrylamide brushes on silicon wafer via surface-initiated RAFT polymerization', *Journal of Polymer Science Part A: Polymer Chemistry*, 49(2), pp. 423-431.

Hamilton, W.C. (1972) 'A technique for the characterization of hydrophilic solid surfaces', *Journal of Colloid and Interface Science*, 40(2), pp. 219-222.

Harder, P., Grunze, M., Dahint, R., Whitesides, G.M. and Laibinis, P.E. (1998) 'Molecular conformation in oligo(ethylene glycol)-terminated self-assembled monolayers on gold and silver surfaces determines their ability to resist protein adsorption', *The Journal of Physical Chemistry B*, 102(2), pp. 426-436.

Harrell, M.L. and Bergbreiter, D.E. (2017) 'Using ^1H NMR spectra of polymers and polymer products to illustrate concepts in organic chemistry', *Journal of Chemical Education*, 94(11), pp. 1668-1673.

He, Y., Hower, J., Chen, S., Bernards, M.T., Chang, Y. and Jiang, S. (2008) 'Molecular simulation studies of protein interactions with zwitterionic phosphorylcholine self-assembled monolayers in the presence of water', *Langmuir*, 24(18), pp. 10358-10364.

Hoagland, K.D., Rosowski, J.R., Gretz, M.R. and Roemer, S.C. (1993) 'Diatom extracellular polymeric substances: function, fine structure, chemistry, and physiology', *Journal of Phycology*, 29(5), pp. 537-566.

Hogt, A.H., Gregonis, D.E., Andrade, J.D., Kim, S.W., Dankert, J. and Feijen, J. (1985) 'Wettability and ζ potentials of a series of methacrylate polymers and copolymers', *Journal of Colloid and Interface Science*, 106(2), pp. 289-298.

Holland, R., Dugdale, T.M., Wetherbee, R., Brennan, A.B., Finlay, J.A., Callow, J.A. and Callow, M.E. (2004) 'Adhesion and motility of fouling diatoms on a silicone elastomer', *Biofouling*, 20(6), pp. 323-329.

Holm, E.R. (1990) 'Attachment behavior in the barnacle *Balanus amphitrite amphitrite* (Darwin): genetic and environmental effects', *Journal of Experimental Marine Biology and Ecology*, 135(2), pp. 85-98.

Holm, E.R. (2012) 'Barnacles and biofouling', *Integrative and Comparative Biology*, 52(3), pp. 348-355.

Huang, W., Skanth, Baker, G.L. and Bruening, M.L. (2001) 'Surface-initiated thermal radical polymerization on gold', *Langmuir*, 17(5), pp. 1731-1736.

Jakobi, V., Schwarze, J., Finlay, J.A., Nolte, K.A., Spöllmann, S., Becker, H.-W., Clare, A.S. and Rosenhahn, A. (2018) 'Amphiphilic alginates for marine antifouling applications', *Biomacromolecules*, 19(2), pp. 402-408.

Jeon, S.I., Lee, J.H., Andrade, J.D. and De Gennes, P.G. (1991) 'Protein—surface interactions in the presence of polyethylene oxide', *Journal of Colloid and Interface Science*, 142(1), pp. 149-158.

Jhan, Y.-Y. and Tsay, R.-Y. (2014) 'Salt effects on the hydration behavior of zwitterionic poly(sulfobetaine methacrylate) aqueous solutions', *Journal of the Taiwan Institute of Chemical Engineers*, 45(6), pp. 3139-3145.

Kamino, K. (2013) 'Mini-review: barnacle adhesives and adhesion', *Biofouling*, 29(6), pp. 735-749.

Keefe, A.J., Brault, N.D. and Jiang, S. (2012) 'Suppressing surface reconstruction of superhydrophobic PDMS using a superhydrophilic zwitterionic polymer', *Biomacromolecules*, 13(5), pp. 1683-1687.

Kerckhof, F., Haelters, J. and Degraer, S. (2010) 'The barnacles *Chirona (Striatobalanus) amaryllis* (Darwin 1854) and *Megabalanus coccopoma* (Darwin 1854) (Crustacea, Cirripedia): two invasive species new to tropical West African waters', *African Journal of Marine Science*, 32(2), pp. 265-268.

Khandelwal, D., Hooda, S., Brar, A.S. and Shankar, R. (2011) '1D and 2D NMR studies of isobornyl acrylate – methyl methacrylate copolymers', *Journal of Molecular Structure*, 1004(1), pp. 121-130.

Khandeparker, L. and Anil, A.C. (2007) 'Underwater adhesion: The barnacle way', *International Journal of Adhesion and Adhesives*, 27(2), pp. 165-172.

Kiil, S., Weinell, C.E., Yebra, D.M. and Dam-Johansen, K. (2006) 'Chapter 7, Marine biofouling protection: design of controlled release antifouling paints', in Ng, K.M., Gani, R. and Dam-Johansen, K. (eds.) *Chemical Product Design: toward a perspective through case stories*. Amsterdam: Elsevier, pp. 181-239.

King, R.N., Andrade, J.D., Ma, S.M., Gregonis, D.E. and Brostrom, L.R. (1982) 'Interfacial tensions at acrylic hydrogel-water interfaces', *Journal of Colloid and Interface Science*, 103(1), pp. 62-75.

Koc, J., Schönemann, E., Amuthalingam, A., Clarke, J., Finlay, J.A., Clare, A.S., Laschewsky, A. and Rosenhahn, A. (2019a) 'Low-fouling thin hydrogel coatings made of photo-cross-linked polyzwitterions', *Langmuir*, 35(5), pp. 1552-1562.

Koc, J., Simovich, T., Schönemann, E., Chilkoti, A., Gardner, H., Swain, G.W., Hunsucker, K., Laschewsky, A. and Rosenhahn, A. (2019b) 'Sediment challenge to promising ultra-low fouling hydrophilic surfaces in the marine environment', *Biofouling*, 35(4), pp. 454-462.

Koehl, M.R.A. (2007) 'Mini review: Hydrodynamics of larval settlement into fouling communities', *Biofouling*, 23(5), pp. 357-368.

Kovach, K.M., Capadona, J.R., Gupta, A.S. and Potkay, J.A. (2014) 'The effects of PEG-based surface modification of PDMS microchannels on long-term hemocompatibility', *Journal of Biomedical Materials Research Part A*, 102(12), pp. 4195-4205.

Krishnan, S., Ayothi, R., Hexemer, A., Finlay, J.A., Sohn, K.E., Perry, R., Ober, C.K., Kramer, E.J., Callow, M.E., Callow, J.A. and Fischer, D.A. (2006) 'Anti-biofouling properties of comblike block copolymers with amphiphilic side chains', *Langmuir*, 22(11), pp. 5075-5086.

Lachnit, M., Buhmann, M.T., Klemm, J., Kröger, N. and Poulsen, N. (2019) 'Identification of proteins in the adhesive trails of the diatom *Amphora coffeaeformis*', *Philosophical Transactions of the Royal Society B: Biological Sciences*, 374(1784), 20190196.

Larsson, A.I., Granhag, L.M. and Jonsson, P.R. (2016) 'Instantaneous flow structures and opportunities for larval settlement: barnacle larvae swim to settle', *PLOS ONE* 11(7), e0158957.

Laschewsky, A. (2014) 'Structures and synthesis of zwitterionic polymers', *Polymers*, 6(5), pp. 1544-1601.

Laycock, B., Nikolić, M., Colwell, J.M., Gauthier, E., Halley, P., Bottle, S. and George, G. (2017) 'Lifetime prediction of biodegradable polymers', *Progress in Polymer Science*, 71, pp. 144-189.

Lee, H.-H., Ruželč, Ž., Malysheva, L., Onipko, A., Gutés, A., Björefors, F., Valiokas, R. and Liedberg, B. (2009) 'Long-chain alkylthiol assemblies containing buried in-plane stabilizing architectures', *Langmuir*, 25(24), pp. 13959-13971.

Lejars, M., Margaillan, A. and Bressy, C. (2012) 'Fouling release coatings: a nontoxic alternative to biocidal antifouling coatings', *Chemical Reviews*, 112(8), pp. 4347-4390.

Leng, C., Hung, H.-C., Sieggreen, O.A., Li, Y., Jiang, S. and Chen, Z. (2015) 'Probing the surface hydration of nonfouling zwitterionic and poly(ethylene glycol) materials with isotopic dilution spectroscopy', *The Journal of Physical Chemistry C*, 119(16), pp. 8775-8780.

Li, H.-X., Getzinger, G.J., Ferguson, P.L., Orihuela, B., Zhu, M. and Rittschof, D. (2016) 'Effects of toxic leachate from commercial plastics on larval survival and settlement of the barnacle *Amphibalanus amphitrite*', *Environmental Science & Technology*, 50(2), pp. 924-931.

Li, L., Chen, S. and Jiang, S. (2007) 'Protein interactions with oligo(ethylene glycol) (OEG) self-assembled monolayers: OEG stability, surface packing density and protein adsorption', *Journal of Biomaterials Science, Polymer Edition*, 18(11), pp. 1415-1427.

Li, L., Chen, S., Zheng, J., Ratner, B.D. and Jiang, S. (2005) 'Protein adsorption on oligo(ethylene glycol)-terminated alkanethiolate self-assembled monolayers: the molecular basis for nonfouling behavior', *The Journal of Physical Chemistry B*, 109(7), pp. 2934-2941.

Lindholdt, A., Dam-Johansen, K., Olsen, S.M., Yebra, D.M. and Kiil, S. (2015) 'Effects of biofouling development on drag forces of hull coatings for ocean-going ships: a review', *Journal of Coatings Technology and Research*, 12(3), pp. 415-444.

Liu, X., Sun, K., Wu, Z., Lu, J., Song, B., Tong, W., Shi, X. and Chen, H. (2012) 'Facile synthesis of thermally stable poly(N-vinylpyrrolidone)-modified gold surfaces by surface-initiated atom transfer radical polymerization', *Langmuir*, 28(25), pp. 9451-9459.

Longyear, J. (2014) 'Chapter 7, Section 2. Mixed population fermentor', in Dobretsov, S., Williams, D.N. and Thomason, J.C. (eds.) *Biofouling methods*. Oxford: John Wiley & Sons Ltd, pp. 214-219.

Lundberg, P., Bruin, A., Klijnsma, J.W., Nyström, A.M., Johansson, M., Malkoch, M. and Hult, A. (2010) 'Poly(ethylene glycol)-based thiol-ene hydrogel coatings—curing chemistry, aqueous

stability, and potential marine antifouling applications', *ACS Applied Materials & Interfaces*, 2(3), pp. 903-912.

Lyu, S., Sparer, R. and Untereker, D. (2005) 'Analytical solutions to mathematical models of the surface and bulk erosion of solid polymers', *Journal of Polymer Science Part B: Polymer Physics*, 43(4), pp. 383-397.

Makamba, H., Hsieh, Y.-Y., Sung, W.-C. and Chen, S.-H. (2005) 'Stable permanently hydrophilic protein-resistant thin-film coatings on poly(dimethylsiloxane) substrates by electrostatic self-assembly and chemical cross-linking', *Analytical Chemistry*, 77(13), pp. 3971-3978.

Maki, J.S. and Mitchell, R. (2002) 'Biofouling in the marine environment', in Bitton, G. (ed.) *Encyclopedia of Environmental Microbiology*. New York: John Wiley & Sons, pp. 610-619.

Maleschlijski, S., Bauer, S., Aldred, N., Clare, A.S. and Rosenhahn, A. (2015) 'Classification of the pre-settlement behaviour of barnacle cyprids', *Journal of The Royal Society Interface*, 12(102), 20141104.

Maleschlijski, S., Sendra, G.H., Di Fino, A., Leal-Taixé, L., Thome, I., Terfort, A., Aldred, N., Grunze, M., Clare, A.S., Rosenhahn, B. and Rosenhahn, A. (2012) 'Three dimensional tracking of exploratory behavior of barnacle cyprids using stereoscopy', *Biointerphases*, 7(1-4), 50.

MAN Diesel & Turbo (2011) *Basic Principles of Ship Propulsion*. Available at: <https://spain.mandieselturbo.com/docs/librariesprovider10/sistemas-propulsivos-marinos/basic-principles-of-ship-propulsion.pdf?sfvrsn=2> (Accessed: March 3, 2019).

Martinelli, E., Agostini, S., Galli, G., Chiellini, E., Glisenti, A., Pettitt, M.E., Callow, M.E., Callow, J.A., Graf, K. and Bartels, F.W. (2008) 'Nanostructured films of amphiphilic fluorinated block copolymers for fouling release application', *Langmuir*, 24(22), pp. 13138-13147.

Martinelli, E., Sarvothaman, M.K., Galli, G., Pettitt, M.E., Callow, M.E., Callow, J.A., Conlan, S.L., Clare, A.S., Sugiharto, A.B., Davies, C. and Williams, D. (2012) 'Poly(dimethyl siloxane) (PDMS) network blends of amphiphilic acrylic copolymers with poly(ethylene glycol)-fluoroalkyl side chains for fouling-release coatings. II. Laboratory assays and field immersion trials', *Biofouling*, 28(6), pp. 571-582.

Matsumura, K., Nagano, M. and Fusetani, N. (1998) 'Purification of a larval settlement-inducing protein complex (SIPC) of the barnacle, *Balanus amphitrite*', *Journal of Experimental Zoology*, 281(1), pp. 12-20.

Matthiessen, P., Reed, J. and Johnson, M. (1999) 'Sources and potential effects of copper and zinc concentrations in the estuarine waters of Essex and Suffolk, United Kingdom', *Marine Pollution Bulletin*, 38(10), pp. 908-920.

Mi, L. and Jiang, S. (2012) 'Synchronizing nonfouling and antimicrobial properties in a zwitterionic hydrogel', *Biomaterials*, 33(35), pp. 8928-8933.

Millichamp, I.S. (2017). *Method of Preparing a Zwitterionic Copolymer*. WO 2016/012472 A1.

Molino, P.J., Campbell, E. and Wetherbee, R. (2009) 'Development of the initial diatom microfouling layer on antifouling and fouling-release surfaces in temperate and tropical Australia', *Biofouling*, 25(8), pp. 685-694.

Molino, P.J. and Wetherbee, R. (2008) 'The biology of biofouling diatoms and their role in the development of microbial slimes', *Biofouling*, 24(5), pp. 365-379.

Morra, M. and Cassinelli, C. (1999) 'Surface studies on a model cell-resistant system', *Langmuir*, 15(13), pp. 4658-4663.

Murthy, N.S., Wang, W. and Kohn, J. (2010) 'Microphase separation in copolymers of hydrophilic PEG blocks and hydrophobic tyrosine-derived segments using simultaneous SAXS/WAXS/DSC', *Polymer*, 51(17), pp. 3978-3988.

Nott, J.A. (1969) 'Settlement of barnacle larvae: surface structure of the antennular attachment disc by scanning electron microscopy', *Marine Biology*, 2(3), pp. 248-251.

O'Connor, N.J. and Richardson, D.L. (1996) 'Effects of bacterial films on attachment of barnacle (*Balanus improvisus* Darwin) larvae: laboratory and field studies', *Journal of Experimental Marine Biology and Ecology*, 206(1-2), pp. 69-81.

Oláh, A., Hillborg, H. and Vancso, G.J. (2005) 'Hydrophobic recovery of UV/ozone treated poly(dimethylsiloxane): adhesion studies by contact mechanics and mechanism of surface modification', *Applied Surface Science*, 239(3-4), pp. 410-423.

Ombelli, M., Costello, L., Postle, C., Anantharaman, V., Meng, Q.C., Composto, R.J. and Eckmann, D.M. (2011) 'Competitive protein adsorption on polysaccharide and hyaluronate modified surfaces', *Biofouling*, 27(5), pp. 505-518.

Ostuni, E., Chapman, R.G., Holmlin, R.E., Takayama, S. and Whitesides, G.M. (2001a) 'A survey of structure–property relationships of surfaces that resist the adsorption of protein', *Langmuir*, 17(18), pp. 5605-5620.

Ostuni, E., Chapman, R.G., Liang, M.N., Meluleni, G., Pier, G., Ingber, D.E. and Whitesides, G.M. (2001b) 'Self-assembled monolayers that resist the adsorption of proteins and the adhesion of bacterial and mammalian cells', *Langmuir*, 17(20), pp. 6336-6343.

Owens, D.K. and Wendt, R.C. (1969) 'Estimation of the surface free energy of polymers', *Journal of Applied Polymer Science*, 13(8), pp. 1741-1747.

Peng, X., Zhao, L., Du, G., Wei, X., Guo, J., Wang, X., Guo, G. and Pu, Q. (2013) 'Charge tunable zwitterionic polyampholyte layers formed in cyclic olefin copolymer microchannels through photochemical graft polymerization', *ACS Applied Materials & Interfaces*, 5(3), pp. 1017-1023.

Petrone, L., Aldred, N., Emami, K., Enander, K., Ederth, T. and Clare Anthony, S. (2015) 'Chemistry-specific surface adsorption of the barnacle settlement-inducing protein complex', *Interface Focus*, 5(1), 20140047.

Petrone, L., Di Fino, A., Aldred, N., Sukkaew, P., Ederth, T., Clare, A.S. and Liedberg, B. (2011) 'Effects of surface charge and Gibbs surface energy on the settlement behaviour of barnacle cyprids (*Balanus amphitrite*)', *Biofouling*, 27(9), pp. 1043-1055.

Phang, I.Y., Aldred, N., Clare, A.S. and Vancso, G.J. (2008) 'Towards a nanomechanical basis for temporary adhesion in barnacle cyprids (*Semibalanus balanoides*)', *Journal of The Royal Society Interface*, 5(21), pp. 397-402.

Phang, I.Y., Aldred, N., Ling, X.Y., Tomczak, N., Huskens, J., Clare, A.S. and Vancso, G.J. (2009) 'Chemistry-specific interfacial forces between barnacle (*Semibalanus Balanoides*) cyprid footprint proteins and chemically functionalised AFM tips', *The Journal of Adhesion*, 85(9), pp. 616-630.

Ping, Z.H., Nguyen, Q.T., Chen, S.M., Zhou, J.Q. and Ding, Y.D. (2001) 'States of water in different hydrophilic polymers — DSC and FTIR studies', *Polymer*, 42(20), pp. 8461-8467.

Plegue, T.J., Kovach, K.M., Thompson, A.J. and Potkay, J.A. (2018) 'Stability of polyethylene glycol and zwitterionic surface modifications in PDMS microfluidic flow chambers', *Langmuir*, 34(1), pp. 492-502.

Poulsen, N., Kröger, N., Harrington, M.J., Brunner, E., Paasch, S. and Buhmann, M.T. (2014) 'Isolation and biochemical characterization of underwater adhesives from diatoms', *Biofouling*, 30(4), pp. 513-523.

Quintana, R., Gosa, M., Jańczewski, D., Kutnyanszky, E. and Vancso, G.J. (2013) 'Enhanced stability of low fouling zwitterionic polymer brushes in seawater with diblock architecture', *Langmuir*, 29(34), pp. 10859-10867.

Reise, K., Gollasch, S. and Wolff, W.J. (1998) 'Introduced marine species of the North Sea coasts', *Helgoländer Meeresuntersuchungen*, 52(3-4), pp. 219-234.

Rittschof, D. (2010) 'Chapter 27, Research on practical environmentally benign antifouling coatings', in Dürr, S. and Thomason, J.C. (eds.) *Biofouling*. Oxford: John Wiley & Sons Ltd, pp. 396-409.

Rosenhahn, A., Schilp, S., Kreuzer, H.J. and Grunze, M. (2010) 'The role of "inert" surface chemistry in marine biofouling prevention', *Physical Chemistry Chemical Physics*, 12(17), pp. 4275-4286.

Saha, S., Bruening, M.L. and Baker, G.L. (2011) 'Facile synthesis of thick films of poly(methyl methacrylate), poly(styrene), and poly(vinyl pyridine) from Au surfaces', *ACS Applied Materials & Interfaces*, 3(8), pp. 3042-3048.

Sahni, V., Blackledge, T.A. and Dhinojwala, A. (2011) 'A review on spider silk adhesion', *The Journal of Adhesion*, 87(6), pp. 595-614.

Scardino, A.J., Hudleston, D., Peng, Z., Paul, N.A. and de Nys, R. (2009) 'Biomimetic characterisation of key surface parameters for the development of fouling resistant materials', *Biofouling*, 25(1), pp. 83-93.

Schlenoff, J.B. (2014) 'Zwitteration: coating surfaces with zwitterionic functionality to reduce nonspecific adsorption', *Langmuir*, 30(32), pp. 9625-9636.

Schönemann, E., Laschewsky, A. and Rosenhahn, A. (2018) 'Exploring the long-term hydrolytic behavior of zwitterionic polymethacrylates and polymethacrylamides', *Polymers*, 10(6), 639.

Schultz, M.P. (2007) 'Effects of coating roughness and biofouling on ship resistance and powering', *Biofouling*, 23(5), pp. 331-341.

Schultz, M.P., Bendick, J.A., Holm, E.R. and Hertel, W.M. (2011) 'Economic impact of biofouling on a naval surface ship', *Biofouling*, 27(1), pp. 87-98.

Schultz, M.P., Finlay, J.A., Callow, M.E. and Callow, J.A. (2000) 'A turbulent channel flow apparatus for the determination of the adhesion strength of microfouling organisms', *Biofouling*, 15(4), pp. 243-251.

Schultz, M.P., Kavanagh, C.J. and Swain, G.W. (1999) 'Hydrodynamic forces on barnacles: implications on detachment from fouling-release surfaces', *Biofouling*, 13(4), pp. 323-335.

Schumacher, J.F., Aldred, N., Callow, M.E., Finlay, J.A., Callow, J.A., Clare, A.S. and Brennan, A.B. (2007) 'Species-specific engineered antifouling topographies: correlations between the settlement of algal zoospores and barnacle cyprids', *Biofouling*, 23(5), pp. 307-317.

Shao, Q., He, Y., White, A.D. and Jiang, S. (2010) 'Difference in hydration between carboxybetaine and sulfobetaine', *The Journal of Physical Chemistry B*, 114(49), pp. 16625-16631.

Shao, Q. and Jiang, S. (2013) 'Effect of carbon spacer length on zwitterionic carboxybetaines', *The Journal of Physical Chemistry B*, 117(5), pp. 1357-1366.

Shao, Q. and Jiang, S. (2014) 'Influence of charged groups on the properties of zwitterionic moieties: a molecular simulation study', *The Journal of Physical Chemistry B*, 118(27), pp. 7630-7637.

Shao, Q. and Jiang, S. (2015) 'Molecular understanding and design of zwitterionic materials', *Advanced Materials*, 27(1), pp. 15-26.

Shao, Q., Mi, L., Han, X., Bai, T., Liu, S., Li, Y. and Jiang, S. (2014) 'Differences in cationic and anionic charge densities dictate zwitterionic associations and stimuli responses', *The Journal of Physical Chemistry B*, 118(24), pp. 6956-6962.

Shivapooja, P., Yu, Q., Orihuela, B., Mays, R., Rittschof, D., Genzer, J. and López, G.P. (2015) 'Modification of silicone elastomer surfaces with zwitterionic polymers: short-term fouling resistance and triggered biofouling release', *ACS Applied Materials & Interfaces*, 7(46), pp. 25586-25591.

Smith, T.W.P., Jalkanen, J.P., Anderson, B.A., Corbett, J.J., Faber, J., Hanayama, S., O’Keeffe, E., Parker, S., Johansson, L., Aldous, L., Raucci, C., Traut, M., Ettinger, S., Nelissen, D., Lee, D.S., Ng, S., Agrawal, A., Winebrake, J.J., Hoen, M., Chesworth, S. and Pandey, A. (2015) *Third IMO GHG Study 2014*. London: International Maritime Organization (IMO).

Statz, A., Finlay, J., Dalsin, J., Callow, M., Callow, J.A. and Messersmith, P.B. (2006) 'Algal antifouling and fouling-release properties of metal surfaces coated with a polymer inspired by marine mussels', *Biofouling*, 22(6), pp. 391-399.

Stewart, R.J., Weaver, J.C., Morse, D.E. and Waite, J.H. (2004) 'The tube cement of *Phragmatopoma californica*: a solid foam', *Journal of Experimental Biology*, 207(26), pp. 4727-4734.

Strand, J. and Jacobsen, J.A. (2005) 'Accumulation and trophic transfer of organotins in a marine food web from the Danish coastal waters', *Science of The Total Environment*, 350(1–3), pp. 72-85.

Strehmel, V., Laschewsky, A. and Wetzel, H. 6 (2006) 'Homopolymerization of a highly polar zwitterionic methacrylate in ionic liquids and its copolymerization with a non-polar methacrylate' *e-Polymers*, 6(1), pp. 1-10.

Sundaram, H.S., Cho, Y., Dimitriou, M.D., Weinman, C.J., Finlay, J.A., Cone, G., Callow, M.E., Callow, J.A., Kramer, E.J. and Ober, C.K. (2011) 'Fluorine-free mixed amphiphilic polymers based on PDMS and PEG side chains for fouling release applications', *Biofouling*, 27(6), pp. 589-602.

Swain, G.W. and Schultz, M.P. (1996) 'The testing and evaluation of non-toxic antifouling coatings', *Biofouling*, 10(1-3), pp. 187-197.

Tanaka, M., Hayashi, T. and Morita, S. (2013) 'The roles of water molecules at the biointerface of medical polymers', *Polymer Journal*, 45, pp. 701-710.

Tanaka, M. and Mochizuki, A. (2004) 'Effect of water structure on blood compatibility—thermal analysis of water in poly(meth)acrylate', *Journal of Biomedical Materials Research Part A*, 68A(4), pp. 684-695.

Vallee-Rehel, K., Langlois, V. and Guerin, P. (1998) 'Contribution of pendant ester group hydrolysis to the erosion of acrylic polymers in binders aimed at organotin-free antifouling paints', *Journal of environmental polymer degradation*, 6(4), pp. 175-186.

van de Wetering, P., Zuidam, N.J., van Steenberg, M.J., van der Houwen, O.A.G.J., Underberg, W.J.M. and Hennink, W.E. (1998) 'A mechanistic study of the hydrolytic stability of poly(2-(dimethylamino)ethyl methacrylate)', *Macromolecules*, 31(23), pp. 8063-8068.

Ventura, C., Guerin, A.J., El-Zubir, O., Ruiz-Sanchez, A.J., Dixon, L.I., Reynolds, K.J., Dale, M.L., Ferguson, J., Houlton, A., Horrocks, B.R., Clare, A.S. and Fulton, D.A. (2017) 'Marine antifouling performance of polymer coatings incorporating zwitterions', *Biofouling*, 33(10), pp. 892-903.

Waite, J.H. (2017) 'Mussel adhesion – essential footwork', *The Journal of Experimental Biology*, 220, pp. 517-530.

Walker, G. and Yule, A.B. (1984) 'Temporary adhesion of the barnacle cyprid: the existence of an antennular adhesive secretion', *Journal of the Marine Biological Association of the United Kingdom*, 64(3), pp. 679-686.

Wan, F., Pei, X., Yu, B., Ye, Q., Zhou, F. and Xue, Q. (2012) 'Grafting polymer brushes on biomimetic structural surfaces for anti-algae fouling and foul release', *ACS Applied Materials & Interfaces*, 4(9), pp. 4557-4565.

Wang, J., Woodcock, S.E., Buck, S.M., Chen, C. and Chen, Z. (2001) 'Different surface-restructuring behaviors of poly(methacrylate)s detected by SFG in water', *Journal of the American Chemical Society*, 123(38), pp. 9470-9471.

Wang, R.L.C., Kreuzer, H.J. and Grunze, M. (1997) 'Molecular conformation and solvation of oligo(ethylene glycol)-terminated self-assembled monolayers and their resistance to protein adsorption', *The Journal of Physical Chemistry B*, 101(47), pp. 9767-9773.

Wang, Y., Pitet, L.M., Finlay, J.A., Brewer, L.H., Cone, G., Betts, D.E., Callow, M.E., Callow, J.A., Wendt, D.E., Hillmyer, M.A. and DeSimone, J.M. (2011) 'Investigation of the role of hydrophilic chain length in amphiphilic perfluoropolyether/poly(ethylene glycol) networks: towards high-performance antifouling coatings', *Biofouling*, 27(10), pp. 1139-1150.

Weinman, C.J., Finlay, J.A., Park, D., Paik, M.Y., Krishnan, S., Sundaram, H.S., Dimitriou, M., Sohn, K.E., Callow, M.E., Callow, J.A., Handlin, D.L., Willis, C.L., Kramer, E.J. and Ober, C.K. (2009) 'ABC triblock surface active block copolymer with grafted ethoxylated fluoroalkyl amphiphilic side chains for marine antifouling/fouling-release applications', *Langmuir*, 25(20), pp. 12266-12274.

Wetherbee, R., Lind, J.L., Burke, J. and Quatrano, R.S. (1998) 'Minireview—The first kiss: Establishment and control of initial adhesion by raphid diatoms', *Journal of Phycology*, 34(1), pp. 9-15.

Woods Hole Oceanographic Institution (WHOI) (1952) *Marine Fouling and its Prevention*, Annapolis: US Naval Institute.

Williams, S.L., Davidson, I.C., Pasari, J.R., Ashton, G.V., Carlton, J.T., Crafton, R.E., Fontana, R.E., Grosholz, E.D., Miller, A.W., Ruiz, G.M. and Zabin, C.J. (2013) 'Managing multiple vectors for marine invasions in an increasingly connected world', *BioScience*, 63(12), pp. 952-966.

Wu, D., Zhao, B., Dai, Z., Qin, J. and Lin, B. (2006) 'Grafting epoxy-modified hydrophilic polymers onto poly(dimethylsiloxane) microfluidic chip to resist nonspecific protein adsorption', *Lab on a Chip*, 6(7), pp. 942-947.

Wu, J., He, C., He, H., Cheng, C., Zhu, J., Xiao, Z., Zhang, H., Li, X., Zheng, J. and Xiao, J. (2017) 'Importance of zwitterionic incorporation into polymethacrylate-based hydrogels for simultaneously improving optical transparency, oxygen permeability, and antifouling properties', *Journal of Materials Chemistry B*, 5(24), pp. 4595-4606.

Wu, J., Lin, W., Wang, Z., Chen, S. and Chang, Y. (2012) 'Investigation of the hydration of nonfouling material poly(sulfobetaine methacrylate) by low-field nuclear magnetic resonance', *Langmuir*, 28(19), pp. 7436-7441.

Wu, S. (1971) 'Calculation of interfacial tension in polymer systems', *Journal of Polymer Science Part C: Polymer Symposia*, 34, pp. 19-30.

Xie, Q., Ma, C., Zhang, G. and Bressy, C. (2018a) 'Poly(ester)–poly(silyl methacrylate) copolymers: synthesis and hydrolytic degradation kinetics', *Polymer Chemistry*, 9(12), pp. 1448-1454.

Xie, Q., Xie, Q., Pan, J., Ma, C. and Zhang, G. (2018b) 'Biodegradable polymer with hydrolysis-induced zwitterions for antibiofouling', *ACS Applied Materials & Interfaces*, 10(13), pp. 11213-11220.

Yamaguchi, T., Prabowo, R.E., Ohshiro, Y., Shimono, T., Jones, D., Kawai, H., Otani, M., Oshino, A., Inagawa, S., Akaya, T. and Tamura, I. (2009) 'The introduction to Japan of the Titan barnacle, *Megabalanus coccopoma* (Darwin, 1854) (Cirripedia: Balanomorpha) and the role of shipping in its translocation', *Biofouling*, 25(4), pp. 325-333.

Yamauchi, T. and Tamai, N. (2003) 'A novel approach using differential scanning calorimetry to investigate the dissolved state in aqueous solutions of polymers used for papermaking', *Journal of Applied Polymer Science*, 89(10), pp. 2798-2807.

Yancey, P.H. (2005) 'Organic osmolytes as compatible, metabolic and counteracting cytoprotectants in high osmolarity and other stresses', *Journal of Experimental Biology*, 208, pp. 2819-2830.

Yandi, W., Mieszkin, S., Di Fino, A., Martin-Tanchereau, P., Callow, M.E., Callow, J.A., Tyson, L., Clare, A.S. and Ederth, T. (2016) 'Charged hydrophilic polymer brushes and their relevance for understanding marine biofouling', *Biofouling*, 32(6), pp. 609-625.

Yandi, W., Mieszkin, S., Martin-Tanchereau, P., Callow, M.E., Callow, J.A., Tyson, L., Liedberg, B. and Ederth, T. (2014) 'Hydration and chain entanglement determines the optimum thickness of poly(HEMA-co-PEG10MA) brushes for effective resistance to settlement and adhesion of marine fouling organisms', *ACS Applied Materials & Interfaces*, 6(14), pp. 11448-11458.

Yang, W., Chen, S., Cheng, G., Vaisocherová, H., Xue, H., Li, W., Zhang, J. and Jiang, S. (2008) 'Film thickness dependence of protein adsorption from blood serum and plasma onto poly(sulfobetaine)-grafted surfaces', *Langmuir*, 24(17), pp. 9211-9214.

Yang, W., Zhang, R., Wu, Y., Pei, X., Liu, Y. and Zhou, F. (2018) 'Enhancement of graft density and chain length of hydrophilic polymer brush for effective marine antifouling', *Journal of Applied Polymer Science*, 135(22), 46232

Yebra, D.M., Kiil, S. and Dam-Johansen, K. (2004) 'Antifouling technology—past, present and future steps towards efficient and environmentally friendly antifouling coatings', *Progress in Organic Coatings*, 50(2), pp. 75-104.

Yoshida, K., Yamaguchi, T., Adachi, T., Otomo, T., Matsuo, D., Takamuku, T. and Nishi, N. (2003) 'Structure and dynamics of hexafluoroisopropanol-water mixtures by x-ray diffraction, small-angle neutron scattering, NMR spectroscopy, and mass spectrometry', *The Journal of Chemical Physics*, 119(12), pp. 6132-6142.

Yule, A.B. and Walker, G. (1984) 'The temporary adhesion of barnacle cyprids: effects of some differing surface characteristics', *Journal of the Marine Biological Association of the United Kingdom*, 64(2), pp. 429-439.

Yule, A.B. and Walker, G. (1985) 'Settlement of *Balanus Balanoides*: the effect of cyprid antennular secretion', *Journal of the Marine Biological Association of the United Kingdom*, 65(3), pp. 707-712.

Yule, A.B. and Walker, G. (1987) 'Adhesion in barnacles', in Southward, A.J. (ed.) *Barnacle Biology*. Rotterdam: Balkema, pp. 389-402.

Zdyrko, B. and Luzinov, I. (2011) 'Polymer brushes by the “grafting to” method', *Macromolecular Rapid Communications*, 32(12), pp. 859-869.

Zhang, H. and Chiao, M. (2015) 'Anti-fouling coatings of poly(dimethylsiloxane) devices for biological and biomedical applications', *Journal of Medical and Biological Engineering*, 35(2), pp. 143-155.

Zhang, Z., Finlay, J.A., Wang, L., Gao, Y., Callow, J.A., Callow, M.E. and Jiang, S. (2009) 'Polysulfobetaine-grafted surfaces as environmentally benign ultralow fouling marine coatings', *Langmuir*, 25(23), pp. 13516-13521.

Zhao, W., Fonsny, P., FitzGerald, P., Warr, G.G. and Perrier, S. (2013) 'Unexpected behavior of polydimethylsiloxane/poly(2-(dimethylamino)ethyl acrylate) (charged) amphiphilic block copolymers in aqueous solution', *Polymer Chemistry*, 4(6), pp. 2140-2150.

Zhou, M., Pesika, N., Zeng, H., Tian, Y. and Israelachvili, J. (2013) 'Recent advances in gecko adhesion and friction mechanisms and development of gecko-inspired dry adhesive surfaces', *Friction*, 1(2), pp. 114-129.

Zhu, Y., Noy, J.-M., Lowe, A.B. and Roth, P.J. (2015) 'The synthesis and aqueous solution properties of sulfobutylbetaine (co)polymers: comparison of synthetic routes and tuneable upper critical solution temperatures', *Polymer Chemistry*, 6(31), pp. 5705-5718.